School of Mechanical, Materials and Manufacturing Engineering



University of Nottingham
UK | CHINA | MALAYSIA

# Machinability and surface integrity investigation of Ni-based aerospace superalloys based on energy thresholds investigation and innovative pendulum-based machining

By

**Dongdong XU**

May, 2019

Thesis submitted to the University of Nottingham for the degree of

Doctor of Philosophy

# Content

Abstract ..... V

Acknowledgements ..... VII

Publications ..... VIII

Nomenclature ..... IX

Acronyms ..... X

Chapter 1 ..... 1

Introduction ..... 1

1.1 Background ..... 1

1.2 Problem Overview ..... 4

1.3 Aims and Objectives ..... 4

1.4 Structure of thesis ..... 5

1.5 Highlights of Significant Thesis Contributions ..... 6

Chapter 2 ..... 8

Literature review ..... 8

2.1 Machining mechanism and principles in metal cutting ..... 8

2.1.1 Cutting mechanism and chip formation ..... 8

2.1.2 Metal cutting force and shear angle in metal cutting ..... 12

2.1.3 Geometries of cutting tool ..... 15

2.1.4 Heat generation in metal cutting ..... 16

2.2 Machined surface integrity of nickel-based workpiece ..... 18

2.2.1 Classification of machined surface anomalies ..... 19

2.2.2 Surface anomaly evaluation using optical and electron microscopy ..... 25

2.2.3 Residual stress measurement and X-ray diffraction ..... 28

2.2.4 EBSD and grain misorientation in machining ..... 31

2.2.5 Nano-indentation and hardness on machined surface ..... 37

2.3 Machinability investigation of nickel-based alloy ..... 42

2.3.1 Workpiece material machinability evaluation ..... 43
2.3.2 Machinability evaluation via status of cutting tool investigation ..... 44
2.3.3 Machinability evaluation regarding material deformation and surface integrity 47
2.4 Non-conventional methods for cutting performance evaluation ..... 51
2.4.1 Energy based research on machining ..... 51
2.4.2 Simulation and analytical method ..... 55
2.4.3 Modified pendulum method ..... 59
2.5 Current gaps in the research ..... 64
Chapter 3 ..... 69
Methodology ..... 69
3.1 Orthogonal cutting of Inconel 718 on pendulum-based machine ..... 69
3.1.1 Material and workpiece preparation ..... 69
3.1.2 Property instruction of used PBCT machine ..... 70
3.1.3 Cutting tools and wear measurement ..... 70
3.2 Cutting process monitoring and signals analysis ..... 72
3.2.1 Monitoring method and equipment ..... 72
3.2.2 Processing method for monitored signals ..... 74
3.3 Surface integrity and metallurgical inspection method ..... 77
3.3.1 Sample preparation for inspection ..... 77
3.3.2 Optical and SEM inspection of superficial surface ..... 79
3.3.3 EBSD evaluation of surface integrity ..... 82
3.3.4 Residual stress measurement of machined sample ..... 83
3.3.5 Nano-hardness investigation of superficial layer ..... 85
Chapter 4 ..... 87
Pendulum-based cutting test (PBCT) concept for surface integrity related machinability studies ..... 87
4.1 Illustration of PBCT principle ..... 87
4.1.1 Problem definitions ..... 87

4.1.2 Introduction of PBCT method ..... 88

4.1.3 Advantages of the PBCT method ..... 91

4.2 Surface integrity related machinability evaluation with energy concept ..... 92

4.2.1 Energy distribution in orthogonal cutting areas ..... 93

4.2.2 Energy calculation in different areas ..... 95

4.3 Design of the PBCT ..... 99

4.4.1 Main body design of PBCT ..... 100

4.4.2 Wet cutting condition design ..... 103

Chapter 5 ..... 106

Energy thresholds evaluation of workpiece surface damage in machining ..... 106

5.1 Introduction ..... 106

5.2 Research concept and PBCT design ..... 108

5.3 Design and research methodology ..... 109

5.3.1 Specialised setup for quick machining tests for energy evaluation ..... 109

5.3.2 Governing energy models ..... 111

5.4 Material and methods ..... 112

5.4.1 Equipment, specimen and cutting tools ..... 112

5.4.2 Experimental arrangements ..... 113

5.5 Results and discussion ..... 115

5.5.1 The relationship between energy distribution and surface integrity ..... 115

5.5.2 Energy thresholds for surface integrity with fresh tools ..... 122

5.5.3 Energy thresholds for surface integrity with worn tools ..... 129

5.5.4 Energy threshold for workpiece damage ..... 135

5.6 Conclusions ..... 137

Chapter 6 ..... 139

A novel method to continuously map the surface integrity and cutting performance transition in various cutting conditions ..... 139

6.1 Introduction ..... 139

6.2 Research methodology and experiment details ..... 143
6.2.1 Proposed concept ..... 143
6.2.2 Experiment setup ..... 144
6.3 Results and discussion ..... 145
6.3.1 Continuous varying cutting speeds in single test ..... 145
6.3.2 Energy consumption during cutting process ..... 148
6.3.3 Chip morphology variation for different cutting speeds in single test ..... 151
6.3.4 Surface integrity investigation with EBSD ..... 154
6.3.5 Residual stress analysis of machined surface integrity ..... 157
6.3.6 Superficial surface Nano-hardness investigation ..... 161
6.4 Conclusions ..... 163
Chapter 7 ..... 165
Discussion, conclusion and future Work ..... 165
7.1 Discussions ..... 165
7.2 Recommendation for Surface integrity related machinability evaluation ..... 172
7.3 Conclusion and key findings ..... 174
7.4 Completion of work from initial aims and objectives ..... 178
7.5 Future works ..... 179
Chapter 8 ..... 182
Reference ..... 182

## Abstract

Ni-based superalloys have been extensively used in high-value-added industries due to their excellent performance in extremely harsh environment, i.e. high strength at elevated temperature over the service life. However, their physical material properties also cause this class of materials difficult to be machined and yield to low surface integrity. Thus, the surface integrity related machinability evaluation of such kinds of superalloy is essential for safety critical components manufacturers (e.g. aerospace, nuclear, and marine) to increase their service life. However, the traditional evaluation methods are either time or money consuming as varieties of cutting experiments are needed to collect enough information. In addition, these methods could only assess a specific set of cutting parameters at a time. Therefore, with the varying combinations of cutting parameters, the test becomes complicated due to the fact that multiple factors need to be considered to establish the threshold of cutting parameters which ensure the compliance with required workpiece surface integrity. In particular, surface integrity related machinability is usually studied by conducting cutting tests on conventional machine tools by varying the cutting parameters and followed by part sectioning to analyse superficial layer damages, which is obviously time consuming and resourceful.

The research project in this thesis is related to Rolls Royce plc. and SECO Tools AB, aiming to develop a novel method that is able to evaluate the surface integrity related machinability of materials quickly with a limited volume of workpiece. A Pendulum-Based Cutting Test (PBCT) methodology is proposed which allows quick cutting tests for surface integrity evaluation along with providing cutting energies associated with particular levels of workpiece surface damage; this is supported by an unified cutting energy model that links level of machined surface with energy partition in the cutting areas. This method could rapidly define the energy consumed during the cutting process that result in particular magnitudes of surface damage without using conventional machine tools, while with the ability to monitor the cutting process in detail with only limited amount of materials required. The test results show that the level of surface damage could be related by the input energy, while given different cutting parameters that yield the same input energy, then result in the same level of surface damage. This gives the possibility to define energy thresholds for ensuring that particular levels of surface damage are not exceeded; hence, there is no need to test various cutting parameters. Therefore, this approach introduces an advantage for optimization and selection of cutting parameters for specific surface integrity by studying the

input energy levels of the cutting process rather than performing extensive machining trails with various cutting parameter combinations blindly.

Moreover, this research proposes an innovative concept which is able to generate machined surface that covers a wide range of cutting speeds continuously on a very limited geometry sample through a single test, thus to allow to continuously study the cutting performance transition of materials (e.g. Ni-based superalloy) at different cutting conditions. An obvious chip morphology variation, i.e. serrated chips at the start areas and smooth chips at the end of the chip, can be achieved, due to the decrease of cutting speed during cutting process. Coupled with energy-based surface integrity evaluation method, the consumed energy in different cutting areas (shear, friction and ploughing) at different cutting speeds could be evaluated and correlated with the continuous cutting mechanism transition along with various cutting conditions. To quantitatively study the plastic deformation of acquired machined surface, Electron Back Scattering Diffraction (EBSD) techniques has been employed. The experimental results showed that this research introduces an efficient way to carry out the surface integrity investigation of materials.

To conclude, a quick and simple method to evaluate the surface related machinability of materials in limited volume is of great interest for both academic and industrial areas. Therefore, as described above, the motivation of this thesis is to develop a new method to accomplish the anticipated ability. The innovative PBCT method supported by built energy evaluation model has been proposed to carry out the surface integrity related machinability evaluation tests for materials, while a quantitative method for surface damage level on machined components has been introduced to accurately identify the surface integrity. All of the demonstrations for the proposed concept and method are presented with Inconel 718 as examples, while detailed validation tests are discussed in this thesis.

## Acknowledgements

At first, I would like to express the greatest thanks to my main supervisor Professor Dragos Axinte for providing me the opportunity to pursue the PhD degree at the University of Nottingham (UoN). It will be impossible for my PhD research to achieve current stage without his invaluable guidance, generous support and sincere encouragement. His precious time spent on my PhD will be highly appreciated in the rest of my life and I am really grateful for his help outside the research field as well.

I have to thank to the support from Rolls-Royce Plc. and Seco Tools for providing the materials and tools used for my research. Particularly I would like to mention the valuable suggestion and help from Dr. Mark Hardy, Dr Andy Mantle of Rolls-Royce, Derby and Dr Rachid M'Saoubi of Seco Tools AB throughout my PhD research. In addition, I want to thank the generous financial and administration support from Institute of Aerospace Technology in UoN and Marie Sklodowska-Curie INNOVATIVE programme supported by European Commission.

My appreciation also has to be delivered to Dr Zhirong Liao, who works as the second supervisor, because of his kind help and training on my PhD. I am grateful for the technical and general engineering help provided by the technicians in the manufacturing department, especially Mr Mark Dain and Mr Ken Wilson. In addition, I would like to thank my colleagues who gave their kind knowledge support and brought the unforgettable happiness to me in Rolls-Royce UTC.

At the last but not least, I do want to express my great thanks to my family from the bottom of my heart for their generous love in my life and allowing me to pursue my wish freely. I will not be able to live happily without their strong mental support, no mention to pursue the PhD research. As another most important part, I want to thank my dear girlfriend, Yunhe Wang, for her endless love and understanding during my PhD period although most of the time we are in two countries away from almost 10,000 kilometres.

To conclude, I hereby want to sincerely express my thanks to all of the people who had provided any help on my PhD. Thanks!

Dongdong XU

5th, May, 2019

Nottingham, UK

## Publications

The research work in this thesis has contributed in part or full to the following publications and conference meetings:

Xu, Dongdong & Liao, Zhirong & Axinte, Dragos & Hardy, Mark. *A novelty method to continuously map the surface integrity and cutting performance transition in various cutting conditions*. International Journal of Machine Tools and Manufacture. (Submitting)

Xu, Dongdong & Liao, Zhirong & Axinte, Dragos & Hardy, Mark & M'Saoubi, Rachid. (2019). *A quick method for evaluating the thresholds of workpiece surface damage in machining*. CIRP Annals. 10.1016/j.cirp.2019.03.015.

Xu, Dongdong, *Innovative machinability evaluation method for nickel based superalloy*, Rolls Royce presentation talk, July 2018, Derby, United Kingdom

## Nomenclature

| | |
|---|---|
| $E$ | Total energy |
| $m$ | Mass of pendulum |
| $g$ | Gravity constant |
| $a$ | Pendulum release angle |
| $\beta$ | Pendulum final angle |
| $l$ | Pendulum arm length |
| $h$ | Pendulum maximum drop height |
| $v$ | Pendulum movement speed (cutting speed) |
| $E_s$ | Shear energy |
| $E_f$ | Friction energy |
| $E_p$ | Ploughing energy |
| $E_w$ | Worn energy |
| $\Theta$ | Stagnation angle |
| $\gamma$ | Clearance angle |
| $R$ | Tool radius |
| $F_t$ | Force in radial direction |
| $F_c$ | Force in cutting direction |
| $F_f$ | Friction force between tool rake face and chips |
| $F_w$ | Worn force between tool and surface |
| $F_s$ | Force in shear area |
| $F_p$ | Force caused by tool radius |
| $\Phi$ ($\varphi$) | Shear angle |
| $\gamma_s$ | Shear strain |
| $\alpha$ | Tool rake angle |
| $b$ | Cutting width |
| $t_{uc}$ | Uncut chip thickness |
| $t_c$ | Chip thickness |
| $\tau_s$ | Shear stress |
| $A$ | Shear area |
| $S$ | Chip teeth height |
| $h_p$ | Chip peak thickness |
| $h_v$ | Chip valley thickness |
| *AMIS* | Grain intragranular misorientation |
| $LC_{max}$ | Maximal peak half-width value |
| N | Newton (Force unit) |
| J | Joel (Energy unit) |
| m, mm | Meter, Millimetre (Length unit) |

## Acronyms

| | |
|---|---|
| PBCT | Pendulum Based Cutting Test |
| BSE | Back Scatter Electrons |
| BUE | Built-up Edge |
| EBSD | Electron Backscatter Detection |
| FCC | Face Centred Cubic |
| BCC | Body Centred Cubic |
| FIB | Focussed Ion Beam |
| SEM | Scanning electron microscope |
| TEM | Transmission Electron Microscope |
| XRD | X-Ray Diffraction |
| CBN | Cubic Boron Nitride |
| SE | Secondary Electrons |
| TET | Turbine Entry Temperature |
| SCC | Stress Corrosion Cracking |
| HE | Hydrogen Embrittlement |
| BCT | Body-Centred Tetragonal |
| BE | Backscattered Electron |
| EDM | Electrical Discharge Machining |
| EBSP | Electron Backscatter Patterns |
| SPS | Spark Plasma Sintering |
| LAM | Laser-Assisted Machining |
| FE | Finite Element |
| SHPB | Split-Hopkinson Pressure Bar |
| SC | Strain Contouring |
| AMIS | Average Intragrain Misorientation |

# Chapter 1

# Introduction

## 1.1 Background

The emergence of gas turbine engines around 75 years ago has enabled commercial flight to get into people's everyday life. As one of the most complex products, the aero-engine is comprised of more than 30,000 components and each one is essential to ensure full functionality at all times [1], [2]. Apart from the safety issues of the aero-engines, the performance efficiency and environmental issues/concerns are also in the minds of the designers and manufacturers. Fig.1-1 illustrates the turbine entry temperature (TET) increasing over the past decades. This gives a higher fuel efficiency of the turbines. To achieve the requirements of high temperature resistance and good performance, new materials are developed for more efficient blades in the critical regions of the engines. In addition, the other parts used in the aerospace or nuclear industry also require higher quality because of the increasing precision requirement and working environment.

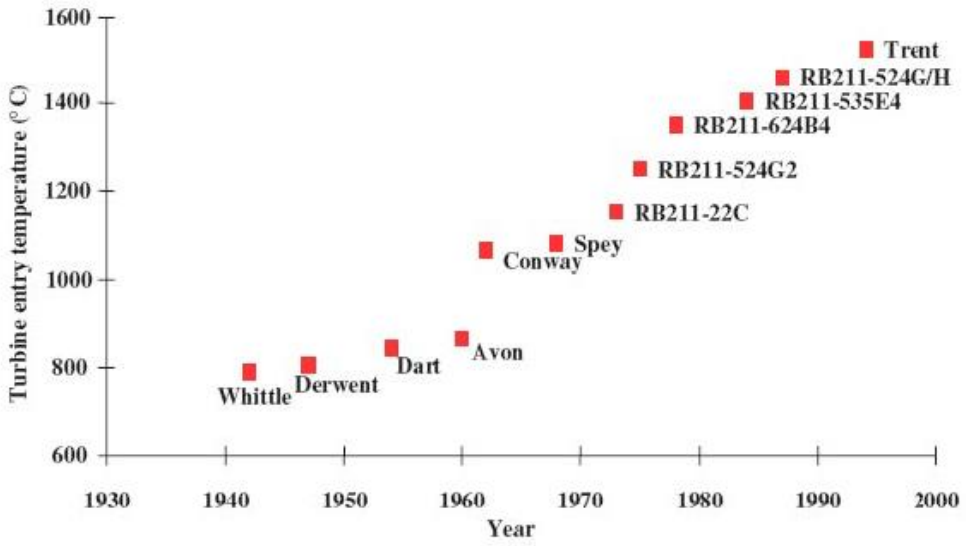



Fig.1-1 Increasing of turbine entry temperature (TET) over recent decades [1]

The TET is highly dependent on the properties of the materials used in the aero-engine blades and disks and design of the engine and corresponding cooling system. Titanium and nickel-based super alloys are the main materials in these kinds of parts and are widely used. In Fig.1-2, it can be seen that Ni-based superalloys are mainly used in the latter regions of the engine, where the temperature is the highest during operation. This highlights the capability of the

Ni-based superalloys to maintain their mechanical properties with increasing temperature when compared with the other materials available in the market now.

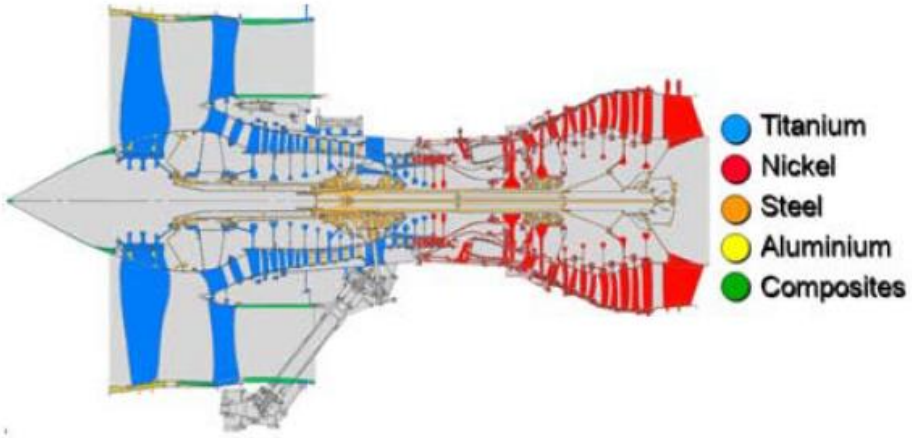



Fig.1-2 Material distribution of a Rolls Royce Trent engine [1]

Although manufactured part quality has increased with the development of modern manufacturing techniques, the failure rates of the aero-engine still must be considered as they are critical to the flight safety of air traffic. Therefore, most engine manufacturers including commercial and military applications have similar modes of failure predominately fatigue as could be seen in Table1-1 [3], [4]. The harsh environment in which the gas turbine works will cause the parts to be both mechanically and chemically damaged [5].

Table1-1, Frequency of failure mechanisms engineering and aircraft components [2]

| Failure method | Percentage of Failure [%] | |
|---|---|---|
| | Engineering components | Aircraft components |
| Corrosion | 29 | 16 |
| Fatigue | 25 | 55 |
| Brittle fracture | 16 | - |
| Overload | 11 | 14 |
| High temperature corrosion | 7 | 2 |
| Stress corrosion cracking (SCC) / Fatigue/ Hydrogen Embrittlement (HE) | 6 | 7 |
| Creep | 3 | - |
| Wear/ abrasion/ erosion | 3 | 6 |

Because of the high strength property and low thermal conductivity of these materials, they are regarded as "difficult to cut", when the designers and manufacturers want to process them. Surface defects and unfavourable residual stress distributions in the machined surface of superalloy parts contribute to the scrap rate, which is undesirable for manufacturers. Unfavourable tensile residual stresses are well known to impair the fatigue life of rotation components in the gas turbine [6]. However, it is essential to design and manufacture components which have high fatigue resistance, high strength at elevated temperatures and good creep resistance to improve aero-engine power and efficiency.

With the development of the aerospace industry, increasing numbers of superalloys are used to improve the performance of aerospace components and achieve the high quality standards required of aero parts. In this case, the machinability of superalloys is essential for aerospace manufacturers, such as Rolls Royce which is a leading company in aero engine manufacturing (Fig.1-3). The evaluation of cutting performance and post-machining surface integrity of these materials are valuable.




Fig.1-3 Rolls Royce Aero-engines (Trent series) [7]

## 1.2 Problem Overview

Superalloys are widely used in industry and new materials are continuously being developed. Their excellent properties allow high service performance, but it is difficult to be machined to desired parts from stock materials. For example, the Ni-based superalloys have been used extensively in the aerospace gas turbine industry in high pressure engine sections [8]. The aero engine manufacturers continue to spend time and money to understand the cutting performance of these materials. Apart from this, the manufacturers are still developing new materials with better properties to achieve higher performance of the aero engine.

Most researches in this field focus on the relationships between cutting tool wear, cutting force, cutting speed, chips formation and surface integrity. This type of research is usually resourceful to be applied to experimental scenarios with different cutting conditions. As the surface integrity is highly related to the machined components service performance, the manufacturers of safety critical industries (e.g. aerospace) are most interested in the surface integrity for machined parts. Currently, the aerospace industries, e.g. Rolls-Royce, have carried out thousands of cutting tests on target materials to understand their surface integrity of machined workpiece before choosing appropriate cutting parameters to machine industrial aero engine parts. In addition, for new materials which are still under development, it is impossible to carry out extensive testing as these methods need lots of stock materials while the materials under development exist in small quantities. Therefore, a new test method, with which it is easy and quick to carry out corresponding tests and is suitable for small amounts of material tests, is strongly demanded. Also, an in-depth understanding into the surface integrity and applicable evaluation method will be proposed.

## 1.3 Aims and Objectives

The aim of this study is to develop a simple and quick method for evaluating the surface integrity of difficult-to-cut materials in a limited volume. To achieve this goal, the project is broken down in the following objectives:

- Propose a quick method for evaluating the surface integrity related machinability of materials (e.g. Ni-based superalloy) with energy partitioning in cutting processes without using conventional machine tools. The corresponding theory of the adopted method, including its working mechanism and the energy model for surface evaluation will be presented and discussed in detail. The equipment will be designed, fabricated and

tested to show that it has the ability to carry out the anticipated cutting test reliably.

- Study the relationship among the used cutting parameters combinations, energy consumed during the cutting process and the generated surface damage level. This will be completed by carrying out validation tests to prove the proposed new method could be used to implement the cutting tests of materials in a different way and correlating the machined surface integrity to the energy consumed during the cutting process. By analysing the results based on several groups of cutting tests, the energy thresholds for specific surface damage level can be found.
- Continuously investigate the cutting performance transition between different cutting conditions and quantitatively evaluate the surface integrity. It will be accomplished by carrying out single tests on one limited volume sample to show the advantage of the proposed method which is able to capture multiple machined surface integrity at different cutting speeds, while the machined surface integrity will be studied quantitatively via EBSD, SEM and XRD, and they will be cross-checked in detail and presented as final results.

### 1.4 Structure of thesis

In Chapter 2, this thesis will provide an extensive literature review from different fields which includes the introduction of nickel based superalloys, their machining mechanisms and principles, surface integrity, machinability investigation, and current non-conventional methods used for evaluating the material machinability. At the end of this chapter, the current research gaps found based on the literature review will be presented as well. This will be followed by the proposed concept, basic principles and design within this research programme.

Chapter 3 will present the methodology to implement the above concept and the general arrangement for experiments, including the equipment and accessories used for tests, rigs and operation requirements for surface integrity inspection. The proposed concept of carrying out cutting experiments on limited geometry materials with Pendulum Based Cutting Machine (PBCT) will be illustrated in detail in chapter 4, which is one of the main topics of this research. Then an energy model used for studying the energy consumed in different cutting areas and their distribution will be proposed, which will be correlated with the PBCT method to establish a quick way to evaluate the surface integrity related machinability of the target materials.

In chapter 5 several groups of tests will be carried out to validate the proposed concept of testing materials in the PBCT machine. To attain this goal, the application for this specific Inconel 718 sample will be illustrated at first. Then the cutting test with a variety of cutting tools with different tool geometries will be used to validate the possibility of implementing cutting tests and explore the relationship between energy distributions and generated surface integrity. More test scenarios with different cutting conditions will be carried out to investigate the energy threshold for surface damage. With the analysis of machined surface integrity and the energy consumed in the cutting areas, the energy threshold for specific surface damage level will be identified. Both fresh tools and worn tools will be tested in this chapter.

In chapter 6, to investigate the machining mechanism transition continuously in different cutting conditions, a novel design will be introduced into the PBCT tests. This will allow the author to continuously capture the cutting process of Inconel 718 at different cutting conditions (cutting speed varying in the range of 150m/min to 30m/min). The continuous morphology variation of the generated chips and deformation variation on the machined surface caused by the cutting conditions changing will be able to be acquired. In addition, to establish the surface damage evaluation quantification standard, the analysis of EBSD results will be carried out in-depth, which will help to assess the surface integrity quantitatively.

To conclude, Chapter 7 will present the discussion and concluding remarks of this thesis. The recommendations for machinability evaluation and surface integrity inspection will be proposed based on the findings from the investigations in previous chapters. Plans for continuous research and possible future works inspired by this research will be discussed in the final section of this thesis.

## 1.5 Highlights of Significant Thesis Contributions

This thesis contains key findings regarding surface related machinability evaluation of hard-to-machine materials used in aero engine. The following section highlights these findings with a brief description:

1. Findings show that the developed pendulum based cutting machine is applicable to carry out quick cutting tests on small batch materials with accessory equipment to monitor the cutting process. It provides an alternative way to carry out cutting tests without extensive testing on CNC machine tools while it also gives the ability to test materials under development to accelerate the development progress.

2. It is found that the machined surface integrity of superalloys (e.g. Inconel 718) strongly relates to the energy input and distribution in cutting areas during the cutting process. Different energy input and distribution (Shear, Friction, Ploughing and Worn energy) in the cutting area will lead to various cut surface integrity (depth of grain deformation). This implies that the machined surface integrity could be predicted by controlling the energy input into the cutting process rather than the practical observation on the machined sample.
3. The test results for both fresh and worn tools showed that similar energy input and distribution in the cutting areas have been identified and they would lead to similar surface integrity even if the cutting conditions were completely different. This proves that the proposed method does not rely on the testing of various cutting parameters but goes into the basis of them directly, i.e. the energy consumed for generating the surface. In addition, the shear energy and worn energy (energy consumed between tool flank face and machine surface because of the tool wear) are the main factors affecting the surface integrity during the cutting process. An energy threshold for a specific machined surface damage level of Inconel 718 has been identified. It gives the perspective that a specific surface damage level could be controlled if the level of input energy keeps "constant" irrespective the cutting parameters combination used.
4. A novel design is introduced to acquire the machined surfaces at continuously decreasing speeds in a single sample through one test. This allows avoiding multiple time-consuming cutting tests. The machined surface integrity of the material at different cutting speeds is able to be studied on the single sample to allow rapid understanding of the cutting performance.
5. Machined surface integrity is analysed with different measurement methods (SEM, EBSD, and XRD). A correlation between different measurement results of machined surfaces has been carried out to quantify the superficial layer deformation after machining. The EBSD results show clear relationships with SEM and XRD results and specific figures could be used to quantify the deformation instead of using only the surface picture. The quantified method employed can help to identify the machined surface damage level in a more accurate way rather than empirical evaluation.

# Chapter 2

# Literature review

In this chapter, a literature review of superalloy machining and its surface integrity evaluation methods will be discussed in relation to both academic and industrial fields. The properties of superalloys, especially the nickel-based alloys that are mainly used in aero engines, will be included. The information of alloys machining including basic cutting mechanism, machinability and material response to different cutting conditions will be considered. The properties of surface integrity of the machined workpiece (especially nickel-based alloy) were investigated and state-of–the-art evaluation methods will be presented. At the end of this chapter, the research gaps, on which the present research is based on will be summarized.

## 2.1 Machining mechanism and principles in metal cutting

Metal cutting is the description of wide range of processes to remove material and obtain designed geometries with different tools. Normally, the machining process concerns the interaction between cutting tool and target materials, including the machined surface and formed chips. There are different standards to classify the machining processes and traditionally they are divided into turning, milling, grinding, broaching, and drilling. However, the machining principles of most of these processes are carried out based on the orthogonal cutting or oblique cutting which is the fundamental principle. Therefore, in this part, the cutting related factors relating to orthogonal and oblique cutting including forces, chip formation, cutting tool geometry and heat generation will be briefly reported.

### 2.1.1 Cutting mechanism and chip formation

Orthogonal cutting (Fig.2-1) is used to explain the basic principles of material shear and removal phenomenon during cutting operations. Normally, material ahead of the cutting tool is removed by the cutting edge where the shearing mechanism is defined by the shear angle. Then, the deformed material is removed by the cutting tool, becoming a chip which slides along the tool rake face and is ejected [9]–[11]. As a basic theory to illustrate metal cutting, there are several assumptions [12] in the present orthogonal cutting model. Such an ideal two dimensional cutting operation is referred to as orthogonal cutting.

1) The cutting tool is perfectly sharp and there is no contraction along the clearance face;

2) The shear surface is the plane extending upward from the cutting edge;

3) The cutting edge is a straight line extending perpendicular to the direction of motion and generated as a plane surface as the work moves past it;

4) The chip does not flow to the other side (plane strain);

5) The depth of cut is constant;

6) The width of the tool is greater than that of the workpiece;

7) The work moves relative to the tool with uniform velocity;

8) A continuous chip is produced with no built-up edge (BUE);

9) The shear and normal stresses along shear plane and tool are uniform.

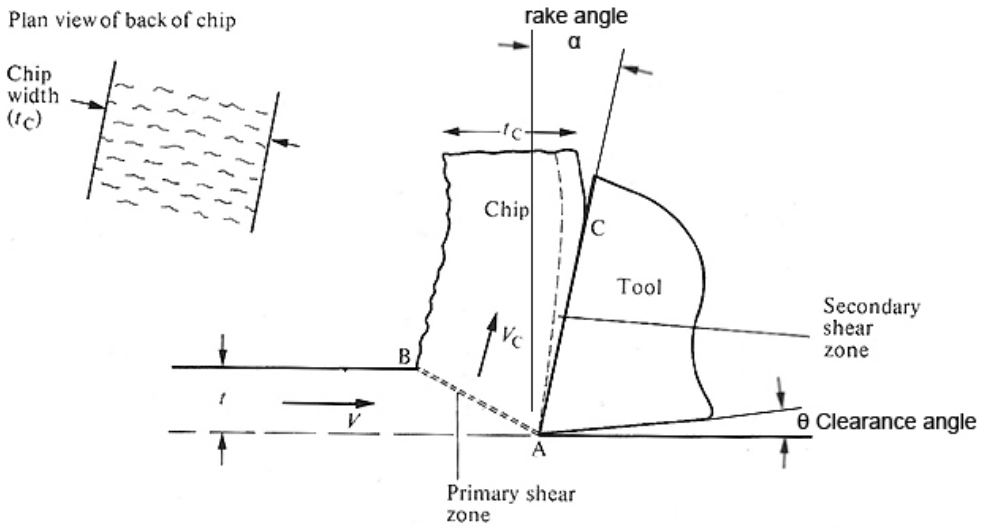
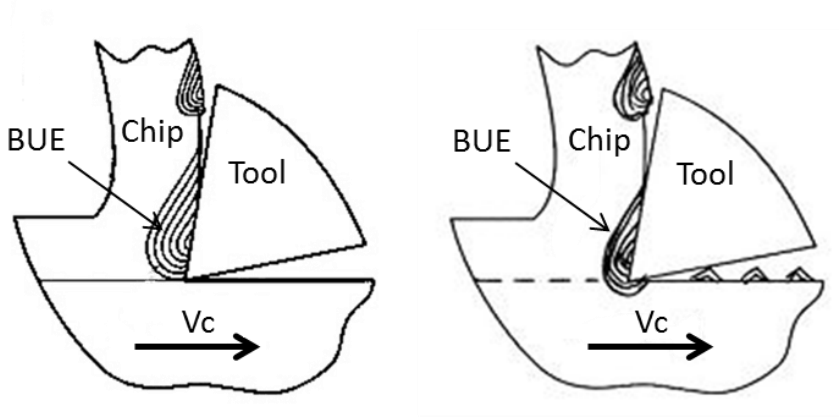



Fig.2-1 Illustration diagram of orthogonal cutting operation [12]

To describe in a better way, some parameters are explained. The shear angle $\varphi$ is defined as the deviation between the shear plane and the direction of the cutting speed. Also, the rake angle $\alpha$ of the tool can be measured. It is also known that the normal stress and shear stress are considered constant [13].

In practical orthogonal cutting, a built-up edge will form before the cutting tool, as illustrated in Fig.2-2a, at several cutting scenarios. Fracture may occur within the chip along the approximately right angles to the shear plane when the cutting temperature within the tool-chip interaction area is relatively low. Thereby, a portion of the chip will be left on the tool rake face and then the generated BUE will act as the cutting edge and grow in size until it reaches the limit to pass off

with the chip. At the same time, this cyclic variation of the BUE will have a direct influence on the cutting depth and the machined surface roughness as shown in Fig.2-2b. Normally, the BUE effect is avoided by improving the cutting speed to lead to higher temperatures in the cutting area, which therefore softens the material.




a) b)

Fig.2-2 Influence of built-up edge (BUE) during orthogonal cutting proecss. a) Formation of BUE by shear fracture with chip and b) Detrimental surface roughness due to BUE [14]

As said, the present orthognal cutting model considers the metal cutting as an ideal model, however the cutting chips vary when the cutting parameters or conditions change, and can even sometimes change when constant. Uncontrollable variation to chip form is caused by [14]:

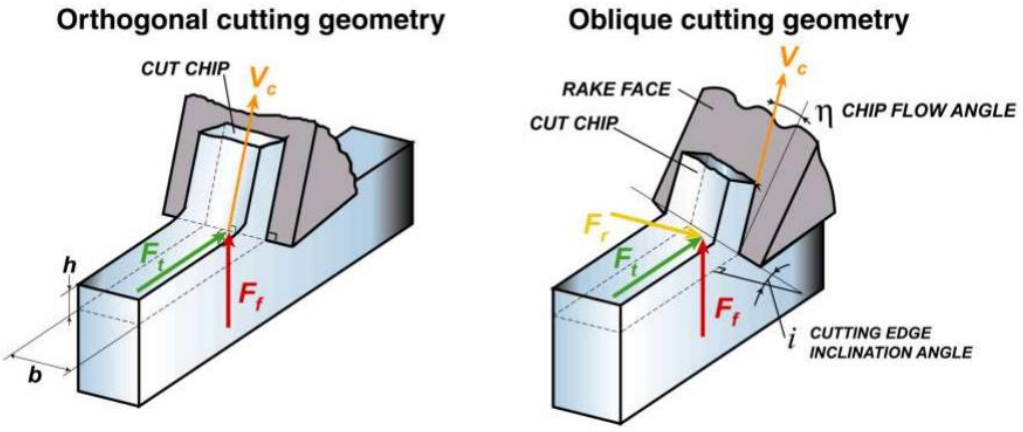
1) Variation of the force acting on the chip: the weight of the chip will increase and the center of gravity varies following the progress of cutting. In addition, the chips gathered before the cutting tool will act as an obstacle to chip flow thefore increasing the resistance force to the chip. In additon, the direction of maxmium shear stress and strain will be influenced by the root of the chip, which is in a plastic state. Therefore, different mophology chips are generated.

2) Transient phenomena in the intial stage of the cutting: the cuttting process may vary because of the lubricants or absorbed layers of oxide or other foreign material that only exist at the very early stage of the cutting. Then the friction coefficient, chip thickness and radius of the upward curvature increase gradually.

3) Variation of tool geometry: evidently the cutting tool will become worn after a long cutting times, therefore leading to a variation of the tool geometry, which affects the cutting mechanism as well the formation of chips.

4) Non-uniformity of the work material: normally, the material is considered as homogeneous when studying the cutting mechanism. However, it is impossible to achieve ideal materials even after production in the same condition (e.g. heat treatment, composition). The shear angle and the formation of chips is influenced by the non-uniformity of the material. Also, the machined layers are normally affected by the former cutting process and hence influence the succeeding cutting process.

As seen in orthogonal cutitng, the angle between tool cutting dege and cutting direction is 90°which is a particular case in the practical turning. Different from the orthogonal cutting, most of the turning process are carried out with oblique cutting, where the inclination angle (Fig.2-3b) between cutting edge and cutting direction is not pependicular. Then an additional force component can be resolved from the force acting on the edge comparing with orthogonal cutting.



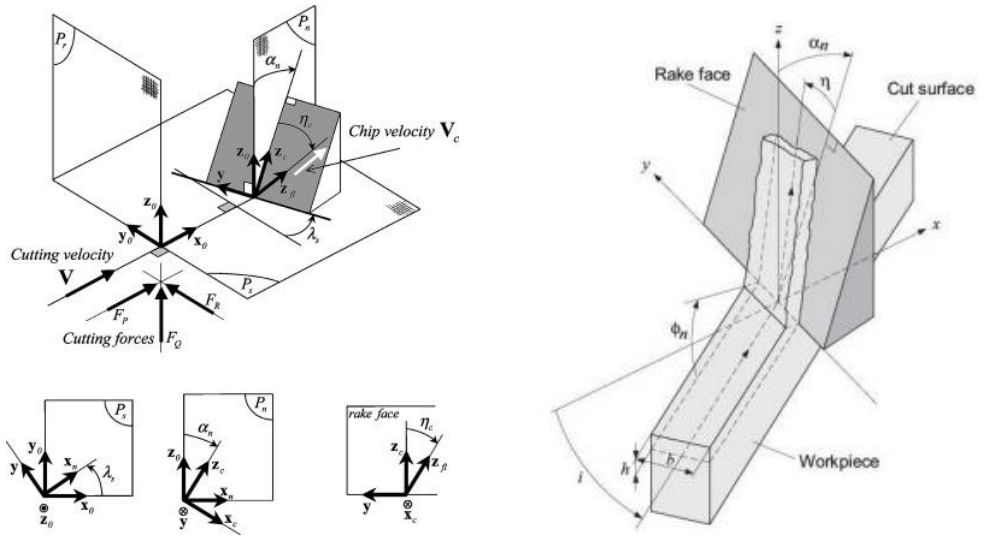

a) b)

Fig.2-3 Basic cutting operations. a) Orthogonal cutting and b) Oblique cutting [13]

The information of geometrical parameters associated to the oblique cutting is illustrated in the Fig.2-4 where the inclination of the cutting edge could be clearly seen in the 3-D illustration. With oblique cutting introduced, the chips flow directions show an angle to the cutting direction, making the mean rake angle increased, thereby leading to the decrease of cutting resistant force and a better machined surface integrity. To describe the oblique cutting (three-dimensional

cutting), it must be described on the basis of the effective rake angles in the direction of chip flow.

In this thesis, it is supposed to propose a simple and quick method for carrying out cutting tests, thefore the orthogonal cutting which is often chosen for analytical and academic study will be used to carry out the analysis and validation.




a) b)

Fig.2-4 Geometrical characteristic parameters associated to oblique cutting. a) The detail characteristic of oblique cutting in three dimensional coordinate and b) Geometry of oblique cutting and chips illustration [15]

### 2.1.2 Metal cutting force and shear angle in metal cutting

As one of the most important components of metal cutting, the cutting force must be considered as shown in Fig.2-5 (orthogonal cutting). *R* represents the force between cutting tool face and generated chip, while the *R'* is the force between the workpiece and chip along the shear plane. If they were plotted at the tool tip point, it could be illustrated as a circular force, shown in Fig.2-5b. The forces R and R' are equal and parallel where it forms the diameter of the force circle and the lines that connect with the circle represent the practical right angle of the force, which will allow the R to be solved graphically into orthogonal cutting process in desired directions, as suggested by Merchant [12], [16]. With the help of the force circle to explain the force system in orthogonal cutting, the Merchant shear angle solution, well known as Emst and Merchant, theory is illustrated.

$$R = \sqrt{{F_P}^2 + {F_Q}^2} \tag{2-1}$$

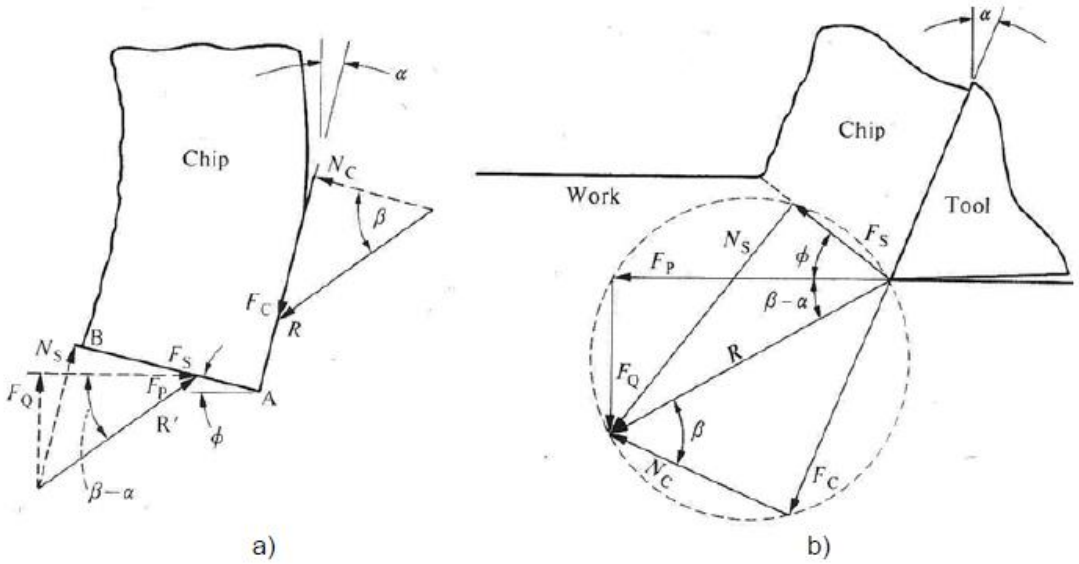



Fig.2-5 The illustration of cutting diagram in orthogonal cutting. a) Free body diagram of a chip and b) Composite cutting force circle for orthogonal cutting [12].

$$\phi = \tan^{-1}\left(\frac{r \cdot \cos(\alpha)}{1 - r \cdot \sin(\alpha)}\right) \tag{2-2}$$

Where $\varphi$ is shear angle; $a$ is rake angle; $r$ is cutting ration which is the uncut chip thickness/chip thickness.

It has been presented that in the machining process, material is removed and forms chips. These chips sharply change the flow direction from the main cutting direction and move along the tool rake face. The chips are formed by shear deformation, slip, or lamellar sliding along a plane, called a shear plane as shown in Fig.2-6.

The shear plane is a plane that separates work material layer, in the form of a chip, from the bulk material due to shear along that plane. The shear angle is the angle of inclination between the shear plane and the direction of cutting velocity. As shown, the value of the shear angle depends on the chip thickness before and after cutting and the tool rake angle (orthogonal cutting). Normally, the shear angle decreases and has an inverse relationship with an increasing of rate of chip thickness/cutting depth. In addition, the shear angle will increase with increasing tool rake angles, indicating that a more favourable machining condition requires less energy. The shear strain is developed along the shear plane due to the machining action, and the cutting strain explanation is found in Fig.2-7.

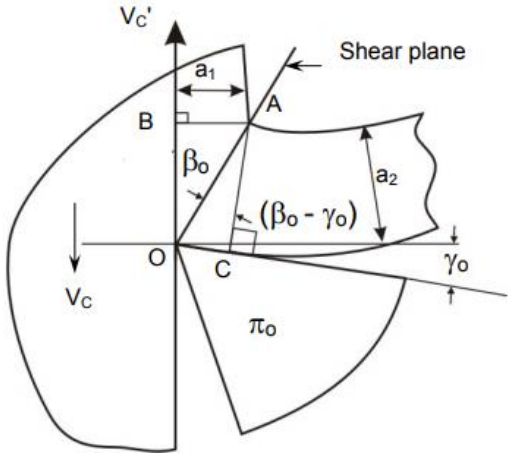



Fig.2-6 Shear plane and shear angle in chip formation for orthogonal cutting [17]

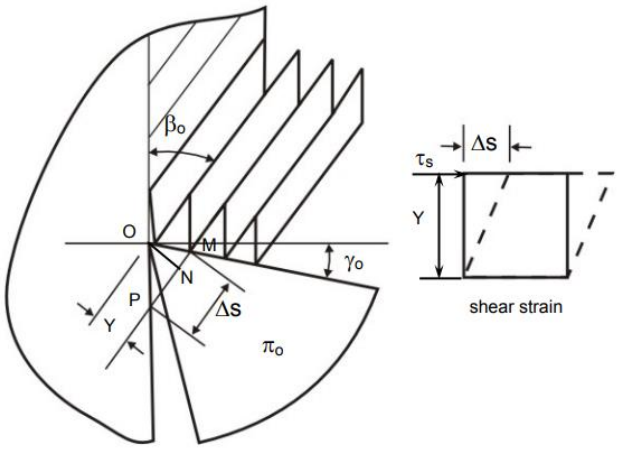



Fig.2-7 Cutting strain explanation in the orthogonal cutting process [17]

Regarding the oblique cutting process, there is an inclination angle ($\lambda_s$ and $i$) between the cutting speed direction and cutting edge direction as shown in Fig.2-4.It could be considered that the mechanics of oblique cutting in the normal please are equivalent to the orthogonal cutting with a projection depending in the inclination angle. The normal shear angle ($\varphi_n$) is the angel between the shear and horizon plane ($P_s$). The sheared chips flow over the rake face with an angle called chip flow angle ($\eta$), normal to the cutting edge and it is known to lie on the normal plane ($P_n$). The normal rake angle ($\alpha_n$) is the angle between the Z axis and the normal vector on the rake face.

The normal shear angle $\varphi_n$ in the normal plane $P_n$ can be given as:

$$\tan\varphi_n = \frac{r\cos\alpha_n}{1-r\sin\alpha_n} = \frac{r_l(\cos\eta/\cos\lambda_s)\cos\alpha_n}{1-r_l(\cos\eta/\cos\lambda_s)\sin\alpha_n} \tag{2-3}$$

Where $r$ and $r_l$ is are the chip thickness and chip length ratios; $\alpha_n$ is the normal rake angle; $\eta$ is the chip flow angle.

### 2.1.3 Geometries of cutting tool

Generally two kinds of tool geometry standards exist, ISO [18] and ANSI standard [19] (mainly used in North American). The ISO standard is more advanced as it is clearer and contains more functional definitions. In addition, it explains the geometry of different types of cutting tools well, showing them in multiple examples, while the ANSI can only explain single-point cutting tools.

As the cutting process is strongly related to the geometry, the precise definition of the tool geometry is often essential. A system of tool angles is presented as shown in Fig.2-8, which is known as the tool-in-hand system (T-hand-S) [9]. The rake, wedge, and flank angles are illustrated as γ, β and α, respectively while further subscript of plane of consideration is used to identify them.

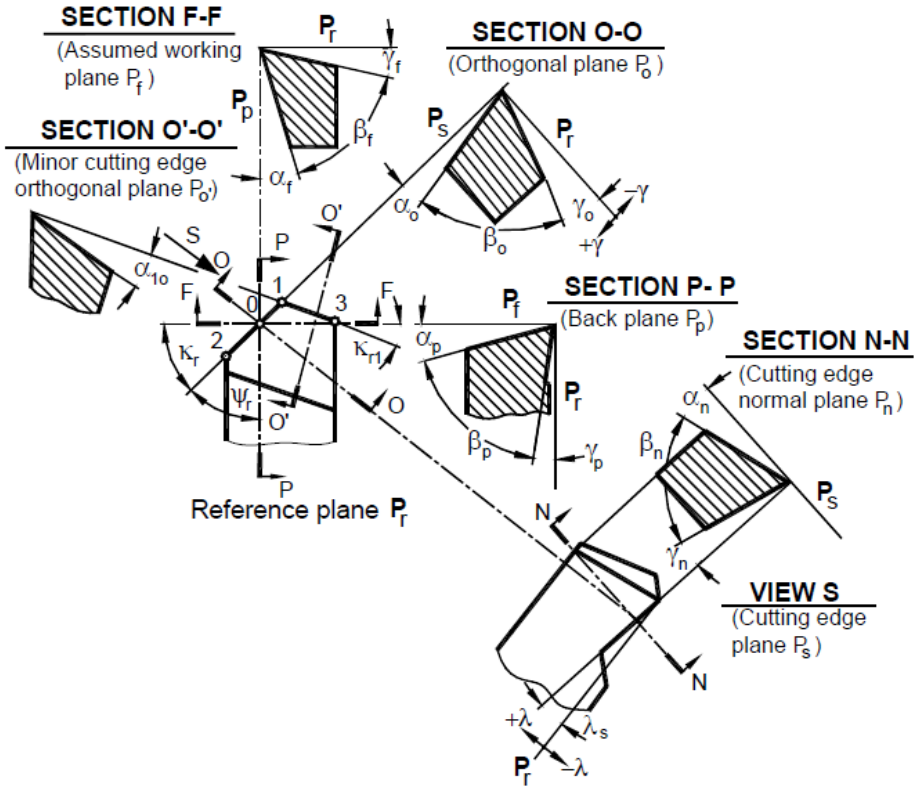



Fig.2-8 System of tool angles in the defined planes in T-hand-S (after Astakhov [20])

When the cutting tool is presented to the workpiece, the rake angle is the effective angle on which the generated chips flow away. There are three categories of rake

angles: positive, neutral and negative as illustrated in Fig.2-9. Tools with positive rake angles are generally used for cutting low strength materials such as aluminium or plastics, while the neutral rake angle tools are normally for cutting stronger materials like low carbon and normalized alloy steels. For the cutting of strongest materials like heated steels, the negative tools are more suitable. Stainless steels or aerospace alloys (e.g. nickel-based alloys, or titanium) are normally cut using positive rake angle tools with honed top-edges, to enable easy material removal and retain the tool strength at the same time.

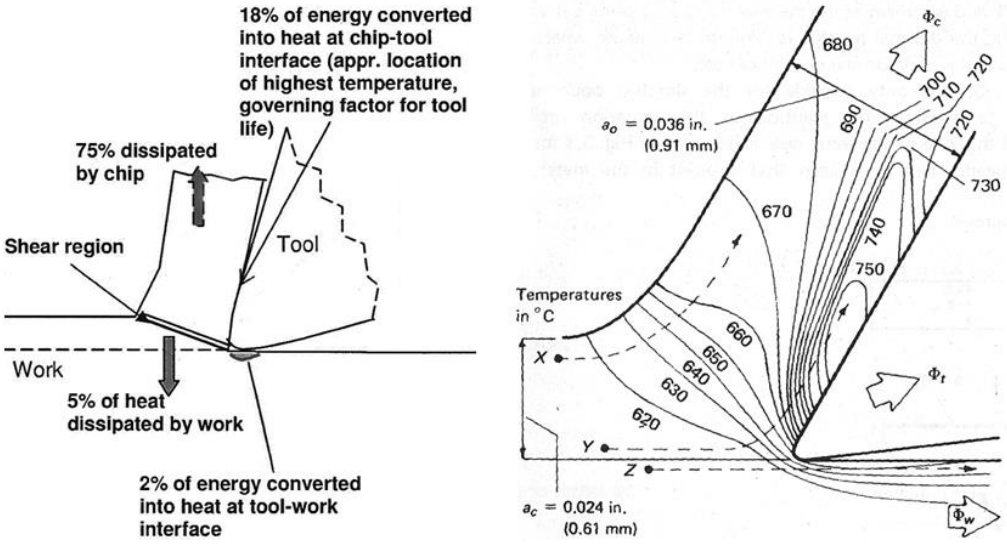


a) b) c)

Fig.2-9 Turing operation by using cutting tools with different rake angles [21]

### 2.1.4 Heat generation in metal cutting

With the deformation of material from bulk material to chips, part of the cutting energy input into the cutting area is converted to heat. Normally, the heat is generated from the process of chip deformation (shear area) and the friction between chips and tool rake face, which leads to high temperatures in the deformation zones and surrounding regions of the chip[11], [22], [23]. The dissipation principles of generated heat in the cutting areas are shown in Fig.2-10 a). It is important to study the influence of heat on the both the cutting tool and the machined surface as around 25% of the energy generated during the cutting process is converted into heat. As seen in Fig.2-10 b), the highest temperature appears at the rake face of the tool, which will significantly affect the cutting process (including tool life, softening the material, increasing tool wear rates or deforming the cutting tool) [11]. It will become more important when machining nickel-based alloys, which have high resistance and low thermal conductivity properties. The effect of temperature on residual stress should be also considered as the residual stress is also an important factor in evaluating the machined surface integrity [24], [25].




a) b)

Fig.2-10 Example of heat generation during the orthogonal cutting process. a) Typical energy distribution in metal cutting at conventional speed [23] and b) Temperature distribution in workpiece and chip during orthogonal cutting for mild steel [22].

An exemplar temperature distribution when cutting mild steel is presented in Fig.2-10. In the cutting process, the traveling path of point X is tracked, showing that X moves towards the cutting tool, passing via the primary shear zone whilst heated, until it flows away as a chip. The Y point passes through both the primary and secondary shear zones, where it is cooled as heat is conducted into the body of the cutting tool. Then it is found that the maximum temperature is located in the chip area that has a distance from the tool rake face, while the chips finally achieve an almost uniform temperature. The point positioned under the maximum cutting depth is retained on the machined surface and the temperature at this point mainly conducts from the primary shear zone and partly from the secondary shear zone, from the body of the cutting tool. The heat generated in the cutting area could be summarised by the following equation [22]:

$$P_m=\Phi_c+\Phi_w+\Phi_t \tag{2-4}$$

Where $P_m$ is the total rate of heat generation; $\Phi_c$ is the rate of heat transportation by the chip; $\Phi_w$ is the rate of heat conduction into the workpiece; $\Phi_t$ is the rate of heat conduction into the tool.

It is worth noting that most of the heat generated is conducted away by the flowing chips as they have a relatively high moving speed, while only a small portion of heat ($\Phi_t$) is transferred to the tool and may can be neglected in some cases [22].

## 2.2 Machined surface integrity of nickel-based workpiece

Surface integrity refers to metallurgical or chemical property variation of the machined workpiece surface after material removal from the bulk by manufacturing. A significant decrease in component quality and service performance, such as fatigue failure, could be caused if the surface damage exceeds particular limits, which are normally defined by individual aerospace manufacturers.

Surface integrity is essential for safety critical components working in harsh environments such as gas turbine blades in aero engine or nuclear plants. To ensure the component operation over the service life and to improve the cost effectiveness, surface integrity requires much attention and must be kept to the highest achievable quality. Theoretically, any material removal from the bulk will lead to some degree of deformation of the generated surface when using conventional shear-based removal methods, which will influence the workpiece performance and ultimately affect the fatigue life of the machined components. In terms of the alterations to the machined surface, these include both geometric and non-geometric aspects, while enabling crack initiation and propagation to some extent. The service time before failure is normally determined by the rate at which a crack develops to the critical length after which the component does not work properly. Apart from deformation in the superficial surface and the morphology of the surface, residual stresses at the machined surface influence the fatigue life as well. Therefore, it is also considered as one aspect of surface integrity in this thesis.

Strict surface quality inspection methods have been implemented on the important components, such as turbine blades, to help maximise the service life and minimise premature failures. As discovered, the most common failure mode of aero-engines is due to fatigue failure [3], [4], [26]. However, obvious cracks or defects on the components will dramatically decrease the service life of the machine [27]. In addition, severe deformation on many machined surfaces, recognised as the white layer, is known to have adverse effects to the surface, regarding corrosion and wear resistance, which is not favourable in aerospace applications. Therefore, the generation of the surface and its integrity should be investigated carefully and fully understood.

### 2.2.1 Classification of machined surface anomalies

Surface anomalies are normally referred to the micro/marco differences from the bulk material in terms of geometrical/metallurgical aspects. Evidently, these deviations are detrimental to the performance of the machined components, thereby safety critical component manufacturers have established tight procedures to evaluate surface integrity. According to the exist industrial standards [28], classified geometrical and non-geometrical surface anomalies are listed in Table 2-1. In practical machining, these will not be the only types of surface anomaly found on the machined surface. In this subchapter, several representative surface anomalies will be presented and discussed in detail to help the understanding of their generation and influence.

Table2-1 Catalogue of surface anomalies in both geometrical and non-geometrical aspect

| **Geometrical Surface Anomalies** | **Non-Geometrical Surface anomalies** |
|---|---|
| Surface roughness | Residual stress |
| Chatter marks | Changes in the hardness of the surface layer due to work-hardening |
| Lapping | Micro and macro cracking |
| Plucking | Material drag/ plastic deformations |
| Scores/ Scratches | White/ recast layer |
| | Foreign material |

1) Surface roughness

Due to the inherent action of the machining process, the machined surface consists of the fine irregularities that are called roughness. This includes the feed marks and any other irregularities caused by machining process within a limit length of the cutting on the sample. Clearly, the surface roughness is highly affected by the interaction between the cutting tool and the machined sample. Therefore, the cutting speed, federate and chattering of the tool will significantly influence its value. Also, the BUE generated by several cutting conditions will affect the surface roughness, especially when the size of the BUE has a high variability [10]. Normally, a rough surface will have higher friction coefficients and will wear more quickly compared to a smoother one. It has been often used as a predictor for mechanical properties as the cracks or corrosion will always appear at these nucleation sites on an irregular surface. To quantify the value of surface roughness and evaluate it, several terminologies are used to measure the surface roughness [28], [29].

$R_a$ is the widely adopted indicator in the industrial areas to describe the surface roughness. It is reported that the level of consistency decreases significantly for the machining of nickel-based alloy components, when using worn tools and the measured surface roughness values are much higher, leading to low workpiece reliability [30]. More importantly for the safety critical industries (aerospace, nuclear, medical etc.), high surface roughness is well understood to lead to poor fatigue performance [31]–[33]. Therefore, it is beneficial to keep a low $R_a$ value and small variation during cutting process and then to acquire a better finished surface, for example, reaming and plunge milling is reported that have the ability to improve surface roughness of a drilled hole [30], [34].

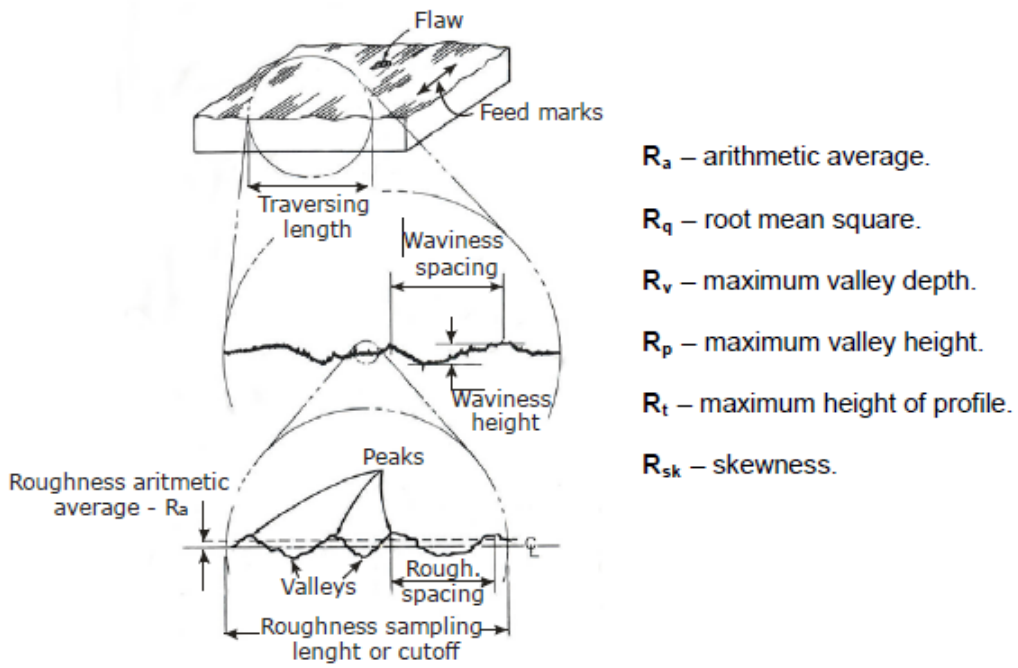
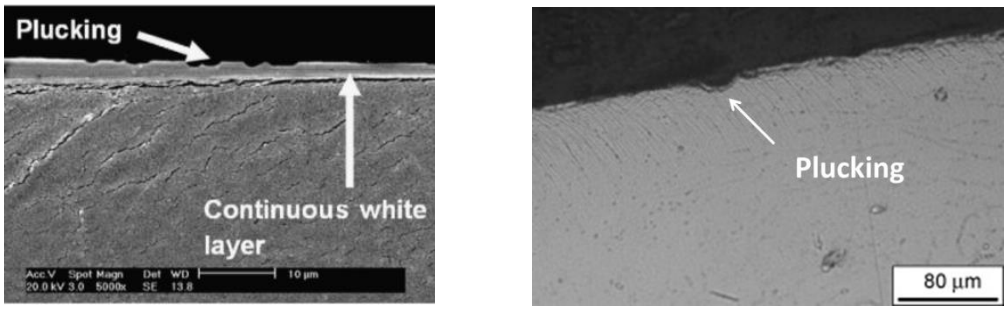



Fig.2-11 Characteristic examples on machined surface. a) Uni-directionally surface characteristics based on ANSI 846.1-1978 [28]; b) Terminology for surface roughness measurements

2) Plucking

In the machined surface, there will be small holes or pockets caused by the mechanical removal of small particles (e.g. grains and particulates) as shown in Fig.2-12. These surface defects appear due to different reasons, such as damaged cutting edges, excessive cutting depth, or scarf entrapment.

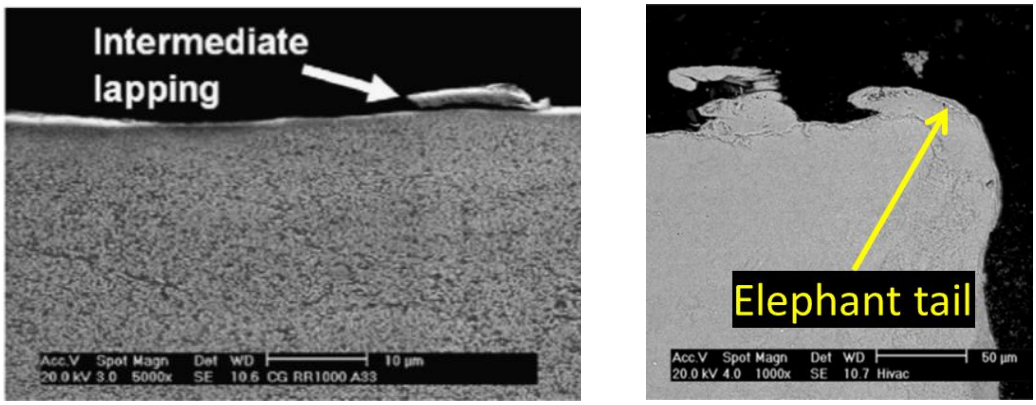



a) b)

Fig.2-12 Examples of plucking phenomenon on machined surface. a) Observed plucking in a white layer generated from abusive drilling of CG RR1000 [35]; b) Plucking following a turning operation in nickel-based superalloy [36].

3) Lapping

Lapping is the phenomenon when plastic deformation of material causes a fold in the machined surface region, as shown in Fig.2-13. The plucked material as mentioned above sometimes can be folded back onto the machined surface with a subsequent manufacturing process, which then leads to a lapping phenomenon. Also, the materials from a sharp corner or burred edge could generate some fold materials at the surface called 'elephant tails' during some processes, such as shot peening [28], [37].

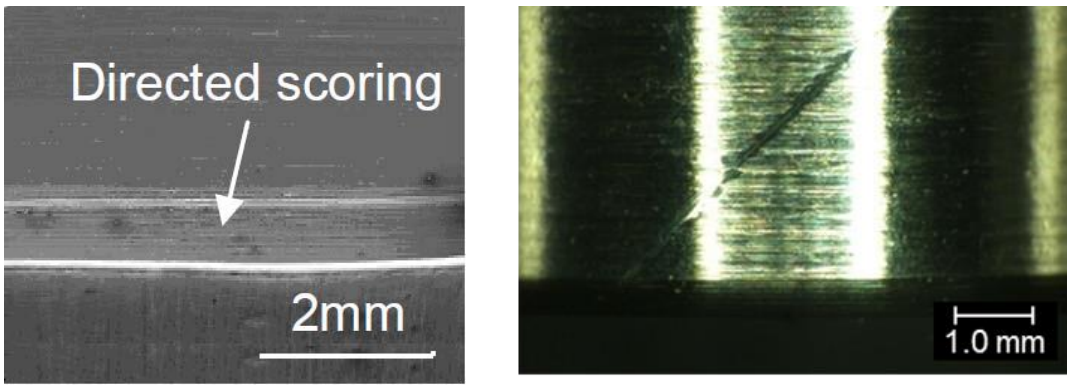



a) b)

Fig.2-13 Examples of lapping phenomenon on machined surface. a) Cross-section of laps found in the drilling of CG RR1000 [35]; b) Elephant tail type lap generated following shot peening.

4) Scores or scratches

Generally when cutting tools are retracted following a machining process, they may have several contact interactions with the machined surface, or generated chips may be inducted into the space between tool and machined surface, both of which lead to scores or scratches on the machined surface if the interaction force exceeds the limits. Of course, a third party body may be introduced as well and could cause the scratches by linear contact or impact [37]. Regarding the generated scratches, the shapes vary depending on the causes and they can either be smooth with a rounded base or deep V-type notches, which are normally shallow.

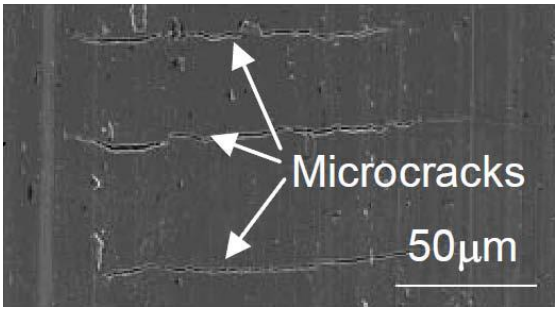



a) b)

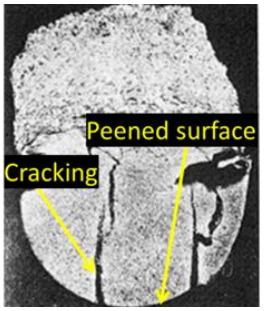
Fig.2-14 Images of scratches and scores of machined surface by a) Broaching [38] and b) Drilling operation

5) Cracks

The cracks are defined as the narrow ruptures or separations that alter the continuity of the machined surface [28]. Normally, they are generated by excessive deformation of the machined surface because of overheating, or strain introduced by the cutting edges, during the cutting process (Fig.2-15 a). In addition, subsequent processing may also lead to cracks (Fig.2-15 b).




a)

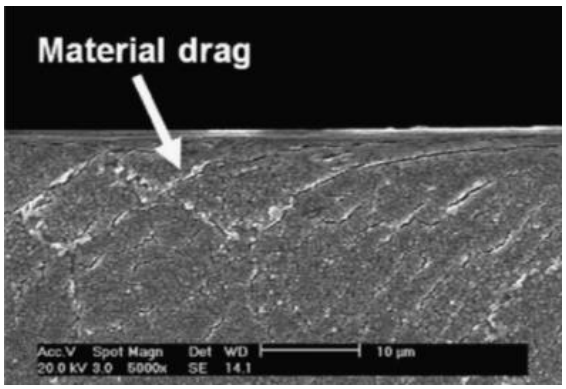



b)

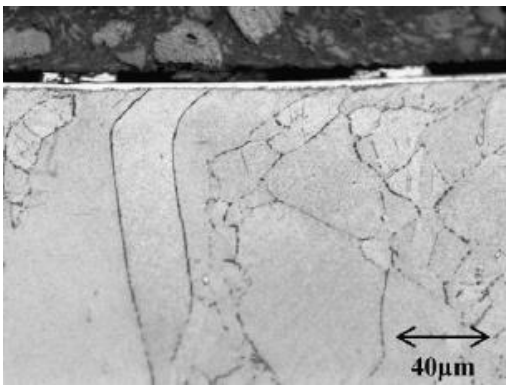
Fig.2-15 Cracks phenomenon on machined surface. a) Micro-cracks found in abused broaching [37] and b) Cracking from the hole surface into bulk material from the white layer

6) Material drag or plastic deformation

When the material is removed, normally it is sheared by the cutting tool edge and severe plastic deformation is generated on both sides of the separated area (chips and generated surface). In addition, the contact between the tool flank surface and machined surface will contribute to surface deformation as well. Therefore, plastic deformation (also called material drag) (Fig.2-16) often appears when the workpiece material exceeds the yield stress with loading during machining. Generally, the deformation direction (grain or grain boundary bent direction) follows the loading direction (cutting direction, speed or feed rate).




a)

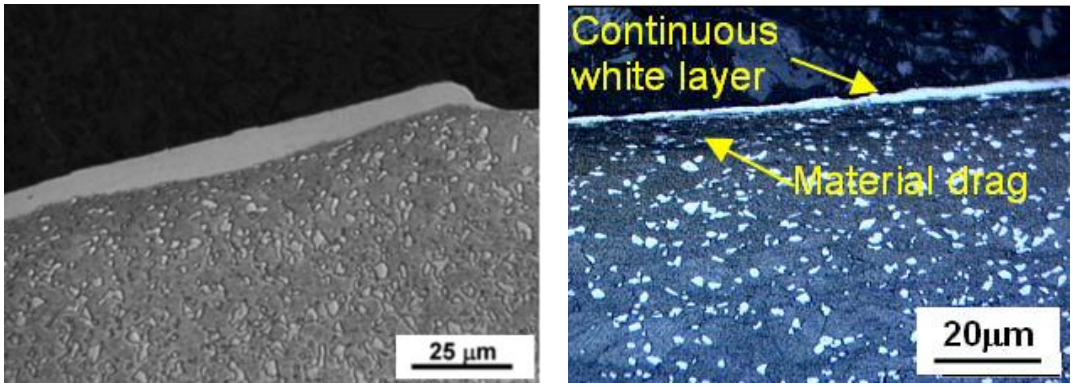



b)

Fig.2-16 Material drag phenomenon on machined surface. a) Material drag in hoop direction for drilling on CG RR1000 [35] ; b) Deformation in grain and boundaries of Inconel 718

7) White layer, re-cast layer or severely plastically deformed layer

At some machining conditions, a special layer, which has noticeably different properties from the bulk material will be found at the machined surface. As it appears white during observation with optical or electron microscopy, it is called a white layer (Fig.2-17). Normally it is caused by a shear transformation resulting from excessive thermos-mechanical loading conditions. For example machining with abusive cutting parameters, such as excessive feed rates or speeds, severely worn tools and dry cutting [37] could lead to overheating and the generation of obvious white layer at the machined surface.

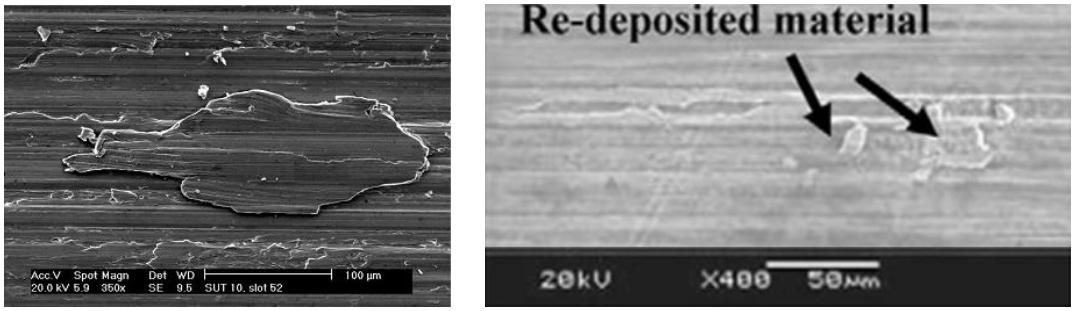



a) b)

Fig.2-17 Examples of generated white layer on machined surface. a) White layer generated on FG Inconel 100 in milling [39]; b) White layer found in drilling of RR1000

8) Re-deposited material

Often, discrete particles randomly dispersed on the machined surface can be found and sometimes these particles are only observable after etching the surface (Fig.2-18). These are caused by small volumes of sheared material from the cutting tool, which did not flow away with the chips and were left at the surface, after which they will be re-deposited. Some of the folded back materials (laps) appear as re-deposited materials as well.




a) b)

Fig.2-18 Examples of re-deposited materials left on machined surface. a) Re-deposited material found on surfaces after drilling in RR1000; b) Re-deposited material left on the surface after end milling [40]

Apart from these defects, there are many other types of surface anomalies in different materials, or after different processes, but the above descriptions present most of the major typical surface anomalies in the machining of nickel-based alloys. In addition, the above anomalies at the machined surface are not entirely unacceptable. Some may be post-processed to yield a finer surface finish, or they do not affect the rough manufacturing process.

### 2.2.2 Surface anomaly evaluation using optical and electron microscopy

To investigate the surface integrity, e.g. the surface morphology and superficial surface deformation, optical microscopy and SEM (scanning electron microscope) techniques are normally adopted. Although both optical and SEM can be used to study surface integrity, the latter one is more powerful due to its higher achievable magnification, as many surface anomalies are at micron length scales. However, optical techniques are still used widely as they are much easier to apply compared with SEM, allowing the possibility to analysis large surface areas. In addition, the optical microscope only need limited training before use, which is more acceptable for industrial application.

1) Sample preparation

To carry out the surface analysis under the microscope, the specimen should be prepared carefully. Typically, a procedure of cutting, mounting and polishing is used to get a high quality, artefact-free sample while the machined surface should not be damaged. Regarding the details of sample preparation, it will be described in Chapter 3. To minimize the induced mechanical and thermal alterations when

sectioning the samples, a precision cut-off machine should be used. Although the microscope will help to observe the surface defects, it will be hard to distinguish and extract the information between phases at the surface. Therefore, etching techniques are employed to reveal the microstructures [41] on the surface and the subsurface when using optical microscopy or SEM.

Optical microscopes cannot be used to analyse microstructural variation as the contrast differences are not clearly revealed by human eyes. However, optical contrast enhancement is achievable by etching, due to the different dissolution rates of the polished surface. Normally, there are two kinds of etching methods including chemical and electrolytic etching [28] for revealing the microstructure.

2) Optical microscope

The optical microscope mainly contains a lens system to magnify images and lights to illuminate the sample. It is widely used in both industrial area and laboratories for surface integrity inspection, which will allows the users to quickly evaluate the surface. An example of the optical microscop illustration has been shown in Fig.2-19.

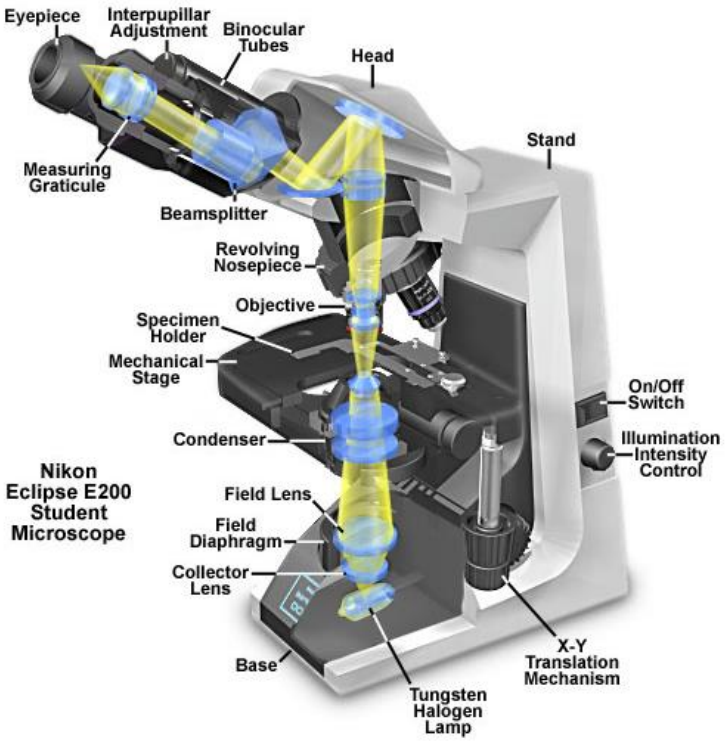



Fig.2-19 Illustration of the structure of an example optical microscope [42]

3) Scanning Electron Microscope

Compared with optical microscopy, the scanning election microscope (SEM) has lots of advantages, such as higher achievable magnifications and the possibility to carry out measurement for greater depth of field. The principle of SEM operation uses the primary electron beam, with a diameter of circa around 10 to 100nm (normally from a heated tungsten cathode), to scan the machined surface [41]. The corresponding voltage needed to acquire images generally ranges between 1 to 50kv, while the current is in the order of 10pA. However, different electrons and X-rays, having various depths of penetration will be released, when the primary electron beam excites different electrons in the specimen (Fig.2-20).

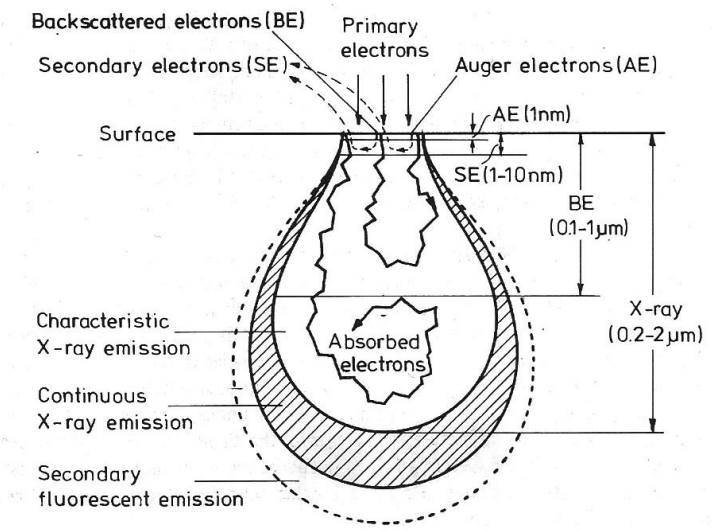



Fig.2-20 Types of electron beam excited electrons and radiation corresponding to different penetration depth in SEM [41]

Therefore, to acquire images on the video display unit, special detectors should be chosen and aligned for collecting the specific emitted electrons from the target surface. The secondary mode (SE), which is widely used, requires an Everhart-Thornley [43]. The electrons which are detected by the SE method are ejected from the k-orbitals of the specimen atoms by inelastic scattering interactions with the primary beam electrons. These are efficient for revealing surface topography, with high resolution due to escape from small depths below the surface. Apart from this, the backscattered electron mode (BE) is another widely used method for surface integrity analysis, but its depth is higher penetration into the surface and it requires a high-energy electrons originating from the cathode beam and reflected from the specimen by elastic scattering. BE mode has advantages, for example analysing areas with different chemical compositions, as higher atomic number elements scatter more electrons, leading to brighter images, showing mass contrast.

### 2.2.3 Residual stress measurement and X-ray diffraction

The stress existing in the materials while no external force applied is regarded as residual stress, which could be induced at any stage of component creation. It can have a significant influence on the life of the component [6], [44] and as such needs to be fully understood. Generally, compressive stress are advantageous for improving fatigue life because they help close cracks upon initiation and thereby delay crack propagation. Conversely, tensile stresses are treated as detrimental as they have the opposite effect on the cracks, encouraging faster crack development, deeper into the material [6], [45]. Many post-machining operations (e.g. shot peening) are used to induce the compressive residual stresses on the machined components to improve the performance of parts in service [45], [46]. Therefore it is important to investigate the residual stresses on the machined workpiece, and normally the produced stress by inhomogeneous deformation will be the opposite of the plastic deformation [24], [47]. Residual stress is considered as elastic stress, thereby the maximum value will be determined by the elastic limit of the material. Plastic deformation will occur if the stress exceeds the elastic limit of the material, until the yield stress of the materials if reached [48].

1) Classification of residual stress

Typically the residual stress could be divided into three groups: first order residual stress (σ'), second order residual stress (σ'') and third order residual stress (σ''') based on the scale of the constant stress, while it is related to the microstructure of the crystalline materials [49]–[52] at the same time (Fig.2-21).

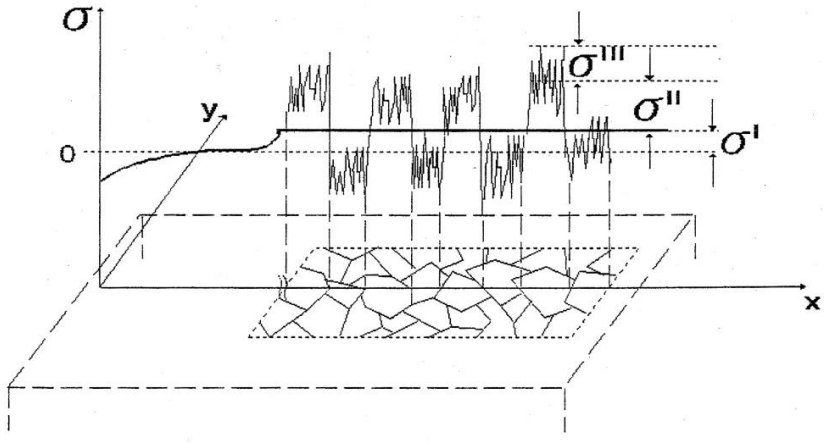
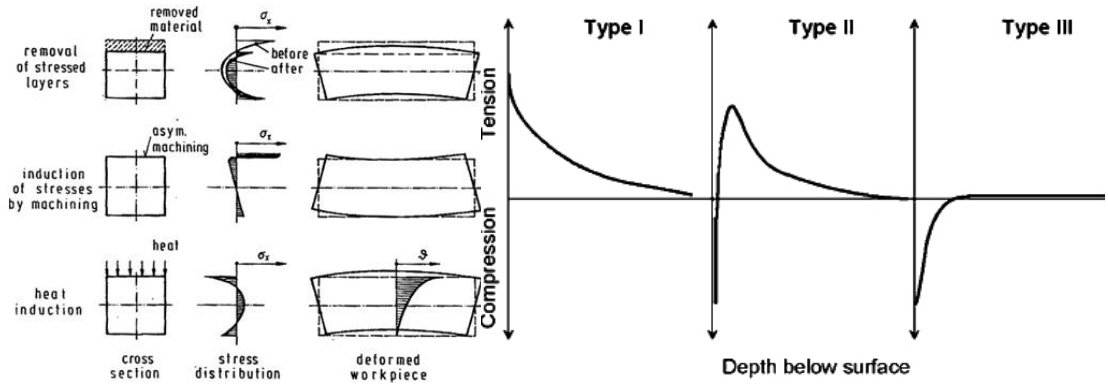



Fig.2-21 Definition of first, second and third order residual stress in polycrystalline materials [52]

Normally first order residual stress (σ') refers to the residual stress which is constant over a large bulk of material and can be classified as a macro stress. The second order residual stress (σ'') is generally defined as the stress over grains or intergranular scales. The third order residual stress (σ'''), refers to the stress at the atomic scale and normally within a single grain or inside one crystallite. As described, the second and third order residual stresses are on the microscale, and both can be measured by X-ray diffraction.

2) Machining induced residual stress distribution

Residual stresses in machining processes are normally induced because of plastic deformation at high strain rates [53]–[55], or a metallurgical transformation during the cutting process [55]. Generally, the machining will introduce the residual stress into the depth at several hundred microns, which will significantly affect the deformation and geometry of a thin workpiece. At the same time, extensive heat will be generated in most of the machining process (exceeding 700℃, [56], [57]), which will obviously influence the residual stress distribution and lead to tensile surface stresses on after cooling because of the thermal contraction. The influence of machining induced residual stress is shown in Fig.2-22 a) and three kinds of typical residual stress distributions are presented in Fig.2-22 b).




a) b)

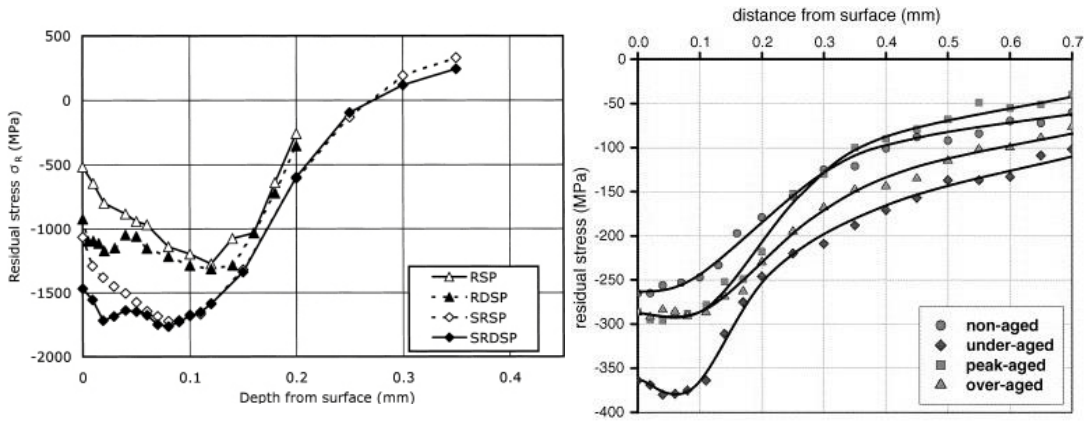
Fig.2-22 Examples of residual stress related phenomenon. a) Machining induced deformation because of residual stress [55]; b) Different types of machining induced stress distribution [58]

Type I residual stresses are normally found on surfaces machined by a hard-turning with extremely worn tools, because of excessive friction heat generated during cutting. This distribution is the worst one as tensile stresses are found in

both the surface and the superficial surface. The second kind of residual stress distribution (Type II) is the most common one corresponding to normal machining processes, where both the heat and plastic deformation significantly contribute to the profile of the residual stress. The favourable residual stress is Type III, in which only compressive stress is found, when the surface is normally machined by completely new tooling and no heat is introduced. Although the residual stress left on the surface are influenced by many factors such as cutting speeds, federate, depth of cut, tool wear and coolant condition etc., they can be generally separated into two groups: mechanical induced stress and thermal induced stress [55], [59], [60].

3) Mechanical and thermal influence on residual stress

As known, most of the material removal machining processes include both thermal and mechanical behaviours. Therefore it is difficult to separate the generated residual stresses. However, a typical example of a mainly mechanical influenced process is shot peening, which is commonly applied to introduce compressive stress at the machined surface [45], [46], [61] as shown in Fig.2-23 a). The rolling process [55],[62] will also introduce compressive stress into the workpiece surface (Fig.2-23b), which has a preferential machining direction, while shot peening does not have this property.

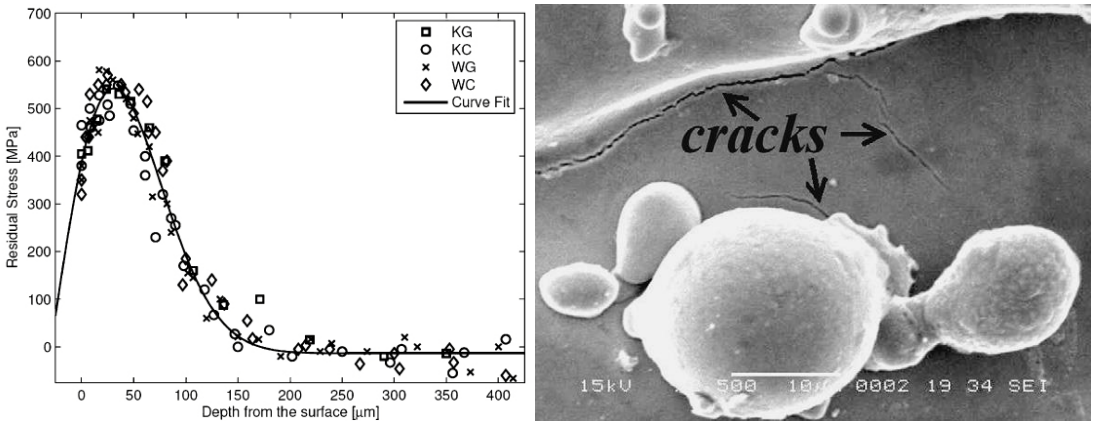



a) b)

Fig.2-23 Residual stress profiles for different processes. a) Shot peening [55]; b) Deep rolling [62].

The thermal influenced stress is mostly caused by the differential cooling rates of the workpiece in different sections and thermally induced residual stress are prone to occur on non-uniform bodies in the unbalanced cooling areas [24]. Although

the final residual stress state is determined by the interaction of all the related factors, the thermal factors are treated as the most damaging to the surface integrity because of the generated tensile stress [63]. A typical example of mainly thermally induced residual stress profile (Fig.2-24) is found in the electrical discharge machining (EDM) process [27] where micro-cracks are found due to the tensile stress release [27], [55], [63].




a) b)

Fig.2-24 Example of tensile stress and its influence. a) Tensile stress generated by EDM and b) Micro-cracks found on the surface because of tensile release [27]

### 2.2.4 EBSD and grain misorientation in machining

The above illustration presented the optical microscope, SEM and residual stress measurements to study the integrity of machined surfaces. They allow the researcher and manufacturers to evaluate the surface integrity at micro level and improve product quality. With the development of new techniques and the increasing of quality requirement, the above methods are unable to study the superficial surface properties after machining in a material perspective. Therefore electron backscatter diffraction (EBSD) is introduced to study the surface integrity at the grain scale. With EBSD, it is possible to identify the variation of specific grains on the machined surface and their properties, which could be linked to the surface integrity and component service performance.

1) Work principle illustration of EBSD

The EBSD is a microstructural-crystallographic characterisation method for the investigation of crystalline materials [64]. Normally, this method is used to study the microstructure, texture, defects, grain morphology and deformation of the

materials. Combined with SEM techniques, it can be used for phase discrimination between crystalline materials. Here, the principle of EBSD is presented as follow.

As known, primary beam electrons can be diffracted by the target material atomic planes if it is crystalline property. The diffracted electrons can be captured on a phosphor screen as they are impinged. Then, visible lines called Kikuchi bands (also known as electron backscatter patterns, EBSP) are generated. These bands are the effective projection of the lattice planes of the crystals, which express information about crystal structure, grain orientation etc. from which the bands originate. By correlating this information with a database that includes the basic crystallographic structure and phase information, the phases of crystalline materials can be identified using software. EBSD gives the ability to perform microstructural analysis on polycrystalline materials (grain structure, orientation, boundary characteristics, macro & micro texture, phase discrimination and deformation).

To carry out EBSD, the polished sample is placed in the SEM at a tilt angle of approximately 70° relative to the normal incidence of the electron beam (Fig.2-25). Diffracted electrons are captured by a camera with a phosphor integrated digital frame grabber, then the Kikuchi pattern shown on the phosphor screen can be digitized (Fig.2-26). Then these data can be studied to carry out the microstructural analysis of the sample, such as systematic textural relations between phases or grains etc.

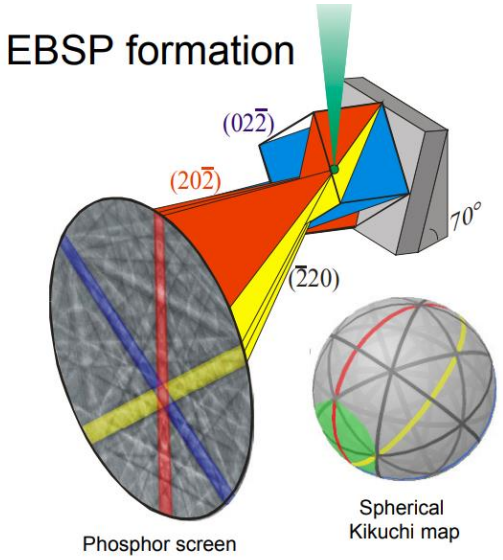
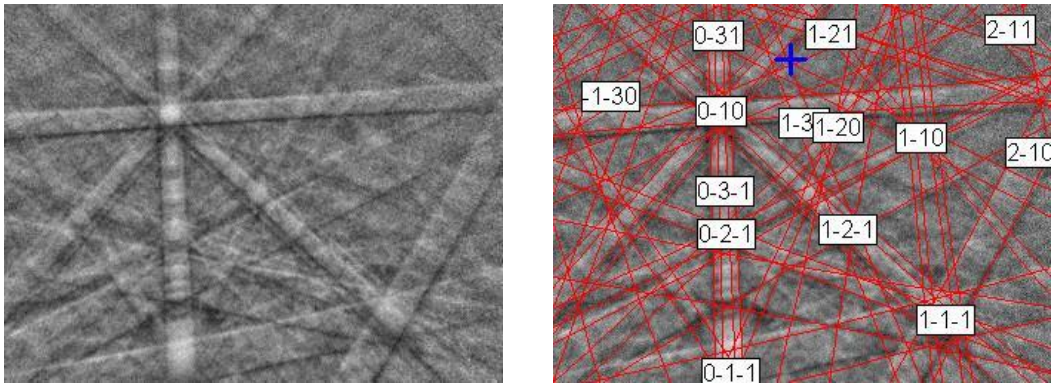



Fig.2-25 EBSP information illustration [65]




a) b)

Fig.2-26 Kikuchi patterns on the phosphor screen and its recognition. a) Acquired patterns and b) Recognised bands by software [65]

By comparing and indexing the acquired data from EBSD (with Hough transform technique), crystal orientations in the material can be identified. Thus, a microstructural map (Fig.2-27) of the measured grain orientation and structure can be built if a prescribed area is measured. These maps spatially describe the properties of crystalline materials that are interrogated. With orientation data, parent phase texture at elevated temperature, residual deformation in mechanical testing, precipitates and grain boundary variation can be revealed.

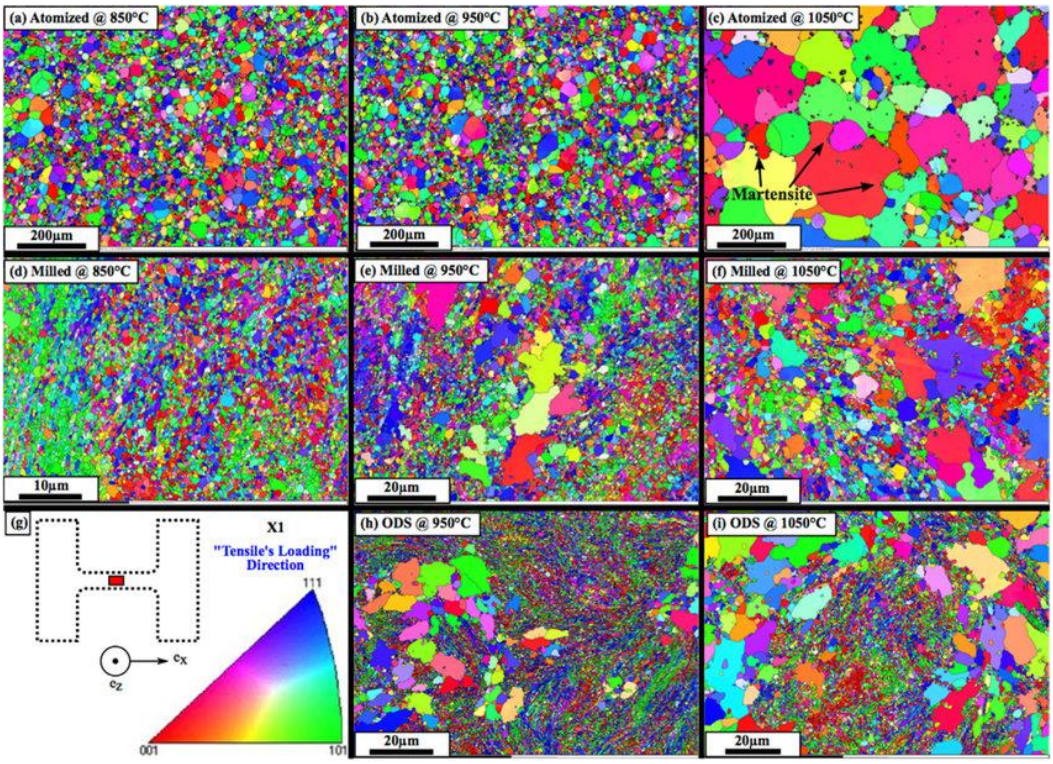
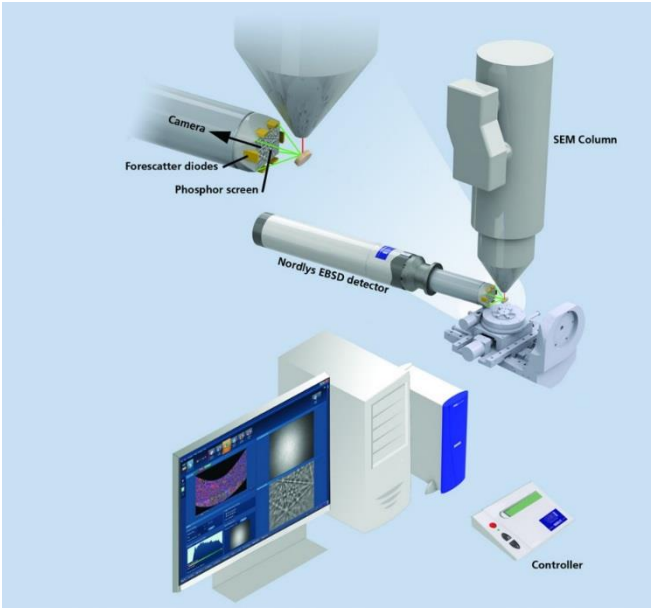


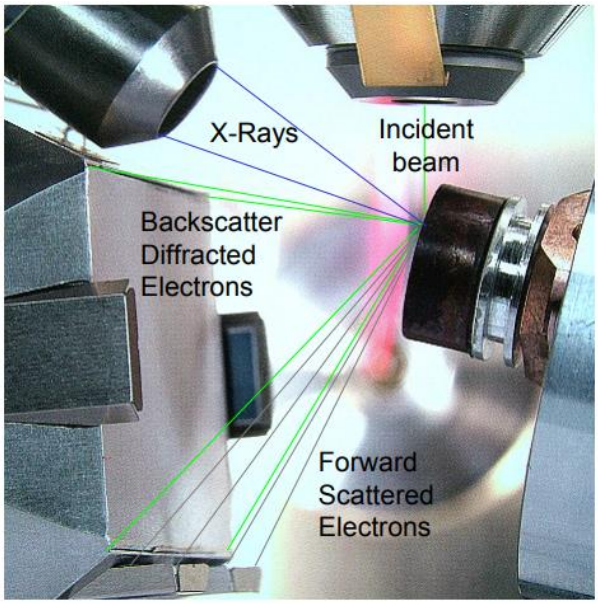

Fig.2-27 EBSD orientation map of 8 SPS (Spark Plasma Sintering) compacts showing various metallurgical states [66]

2) EBSD equipment and setups

Fig.2-28 presents the main components of an EBSD system, containing the primary electron beam, sample movement stage, forward scatter & backscatter diffracted electron detectors, phosphor screen, camera and the digital signal process unit (for control and data acquisition).




a)




b)

Fig.2-28 Illustration of typical EBSD setups. a) The composition of example EBSD system; b) The physical component of the EBSD in a practical measuring scenario [65]

A typical EBSD detector design is shown in Fig.2-29. The projection generated on the phosphor screen by the crystal target material is transferred to the CCD (charge coupled device) camera after transmittance through the leaded glass window and lens. At this stage, the characteristic material data has already been captured by the camera. A head amplifier is then used to enhance signal strength for transfer to the data processing system (including storage and analysis). It is worth noting that the length of the tube will not affect the efficiency of the EBSD as the image and information already been acquired at the front part of the detector as described above (Fig.2-29).

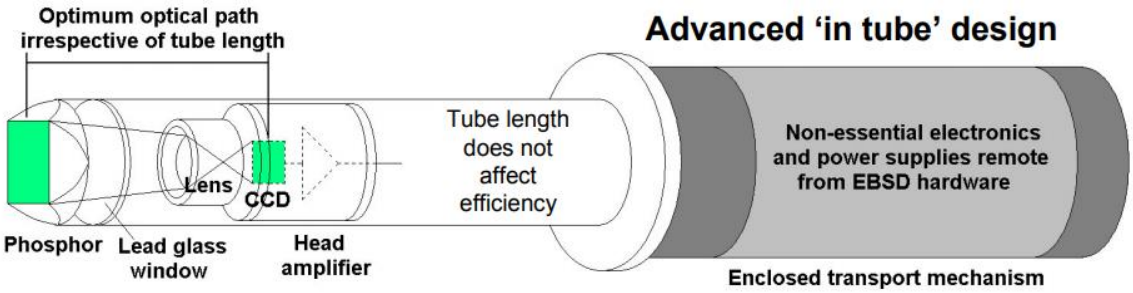



Fig.2-29 Example hardware design of EBSD detector [65]

3) EBSD application on surface integrity analysis

As described, EBSD is a powerful tool for material structure determination, therefore it has been applied towards studying material property variation by mapping the extent of plastic deformation under machined surface.

Initially, researchers used both EBSD and X-ray diffraction analysis to study the differences in crystallographic texture for turned single crystal aluminium [67]. A lattice rotation on the machined surface caused by the shearing along the cutting direction was found in a separate grooving experiment. Regarding surface analysis with EBSD, Yamamoto et.al studied the superficial ground surface finding many slip bands and small angle grain boundaries (Fig.2-30) in the affected region (around 25 μm depth) [68].

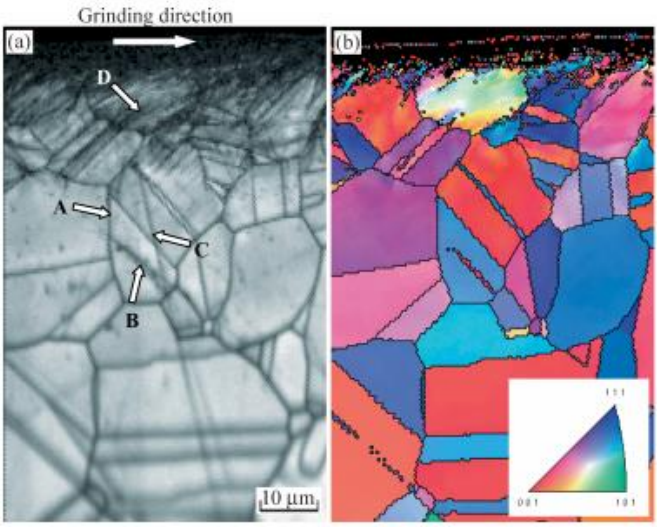



Fig.2-30 EBSD map of superficial surface on machined workpiece. a) IQ (image quality) maps and b) IPF (Inverse pole figure) maps of the perpendicular cross section [68]

Apart from subsurface inspection after machining, Rachid [69] applied the EBSD method to investigate deformation zones in metal cutting based on steel turning operations. The plastic deformation zones in the chip root specimen and surface, in the case of single and two-phase steels have been reported (Fig.2-31).

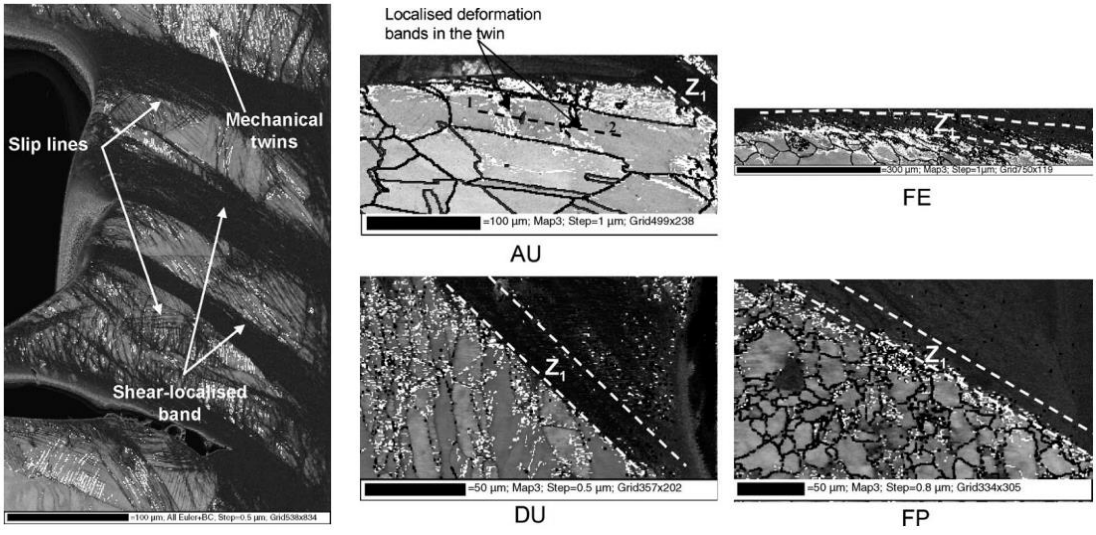



Fig.2-31 EBSD analysis of a) The chip and b) Deformation zone ahead of the tool tip [69]

EBSD has now been widely applied to inspect the crystal orientation variation and grain misorientation in the near machined surface area. Rachid et. al attempted

to study the strain distribution beneath the machined surface on an Inconel 718 sample processed by turning. The difference in the strain map distribution is clearly distinguished between different cutting conditions, showing surface integrity variation (Fig.2-32) [70].

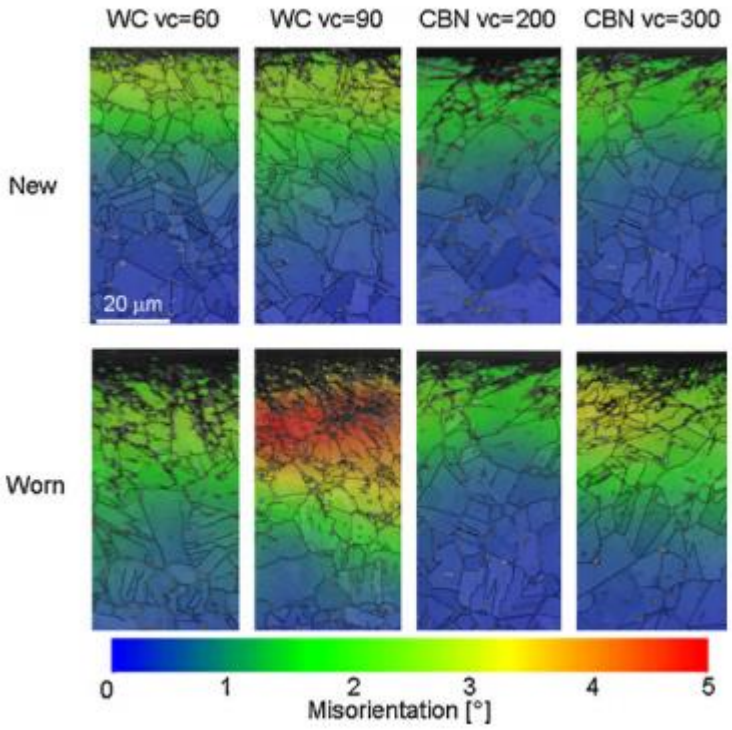



Fig.2-32 The strain contour maps obtained from EBSD measurement for machined surface in different cutting conditions [70]

### 2.2.5 Nano-indentation and hardness on machined surface

Hardness is another factor used to evaluate the machined surface properties in practical industrial application and is normally accomplished by carrying out indentation hardness tests. To some extent, it reflects the mechanical properties of the material after machining. However, conventional macroscale testing, is able to assess local material properties, but in the millimetre scale. It is difficult to capture hardness information when the material grain or the deformation region is in microscale or nanoscale. Therefore, a nano-indentation device is introduced to locally explore the mechanical properties at these smaller scales.

1) Theory of hardness measurement in indentation

For both macro and nano-indentation, the basic principle is that a hard tip with known properties and made of hard materials (normally diamond) is pressed into the sample. With the penetration depth of the tip increasing into the material, the

loading on the tip will increase to achieve a pre-defined value. In addition, the loading maybe kept constant for a period or removed immediately at the defined value. Then the deformation areas caused by the indentation on the sample can be measured and the hardness *H* can be acquired, which is normally defined as:

$$H = \frac{P_{max}}{A_r} \tag{2-5}$$

Where *H* is the measured hardness; $P_{max}$ is the maximum loading; and $A_r$ is the residual indentation area.

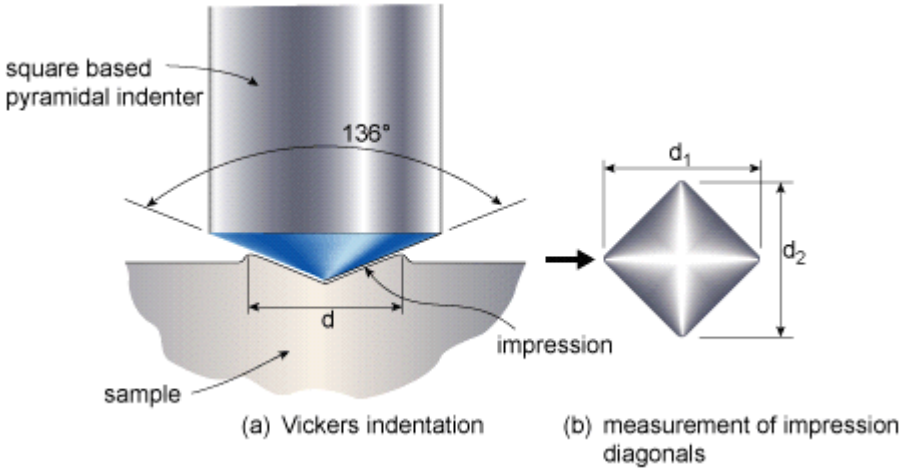



Fig. 2-33 Illustration of an example Vickers hardness test [71]

With the indentation test, the hardness of the sample surface can be quantified. It can give an approximate hardness value for homogeneous materials and minor variation surfaces. However, the size of the indentation tip will bring variation in application regarding microscale and macroscale. The traditional indentation, stated above, is limited to the tip size and shape, and is not able to have good spatial resolution on the sample. To achieve this, indentation techniques that can be accurately carried over areas of a few square micrometres or even nanometres are required. To achieve this, an indenter with known high precision geometry, such as Berkovich tip, was developed allowing the investigation of samples at micro and nanoscale. The penetration depth of the indent can be measured and then the indent area could be calculated based on the know geometry tip.to give information of the hardness of specific area.

2) Nano-hardness measurement and advantages

Compared with conventional indentation, the biggest difference of Nano-indentation is that the microscale indentation tip gives the possibility to focus on

specific small areas. An in-depth investigation of the local area properties of the materials can be carried out in detail, which is important to understand the material performance.

During the nano-indentation test, the corresponding parameters including load, depth of penetration depth versus time are recordable and can be plotted on to illustrate the propagation process as shown in Fig.2-34 [72]. The mechanical properties of the target material can be extracted from the plotted load-displacement curve.

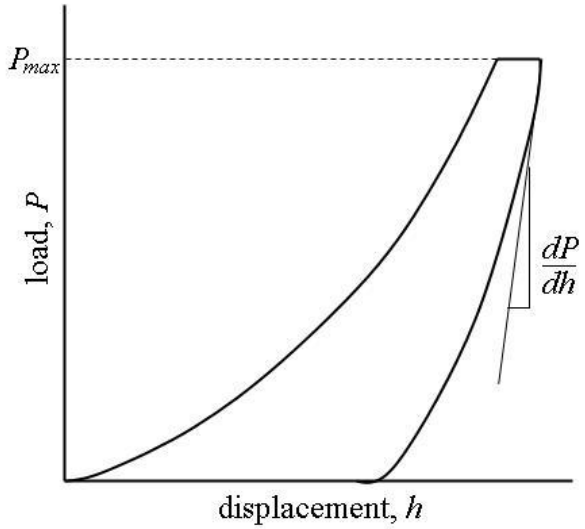



Fig.2-34 Schematic of load-displacement curve for an instrumented nano-indentation test [72]

To calculate the reduced Young's modulus ($E_r$) and the hardness ($H$) from the above curve, the Oliver and Pharr method [73], [74] can be applied. The load-displacement relationship can be conveniently written as:

$$P = \alpha h^m \tag{2-6}$$

where $P$ is the indenter load, $h$ is the elastic displacement of indenter, and $a$ and $m$ are constants depending on the experiment situation ranging from 1 to 2.

Regarding the Young's modulus ($E_r$), it could be expressed as:

$$\frac{1}{E_r} = \frac{(1-v^2)}{E} + \frac{(1-v_i^2)}{E_i} \tag{2-7}$$

where $E$ and $v$ are the Young's modulus and Poisson's ratio for the specimen and $E_i$ and $V_i$ are the same parameters for the indenter.

The loading and displacement data shown in Fig.2-34 can be analysed according to the following equation:

$$S = \frac{dP}{dh} = \frac{2}{\sqrt{\pi}} E_r \sqrt{A} \tag{2-8}$$

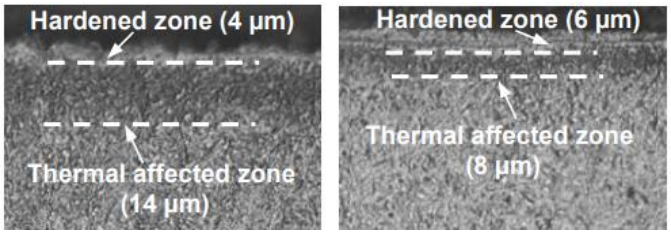
Here, the *dP*/*dh* is the experimental measured stiffness of the upper portion of the unloading data. And *A* is the projected area of the elastic contact area.

With the contact area at peak load A, the nano-hardness $H_N$ can be calculated as follows:

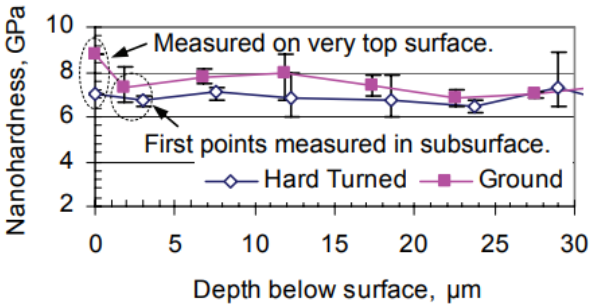
$$H_N = \frac{P_{max}}{A} \tag{2-9}$$

3) Nano-indentation application in surface integrity evaluation

As stated, the surface integrity of manufactured parts is critical for their application and the fatigue life of the corresponding machine, where the mechanical properties of the subsurface contribute significantly to the component performance. Nano-indentation is capable of studying local area properties of the materials while avoiding edge effects during the measurement [75]. As shown in Fig.2-35, the nano-hardness of the materials in the depth of 30 μm can be acquired and multiple points can be measured, giving the possibility to study the local area material properties that are very important for aerospace manufacturers.



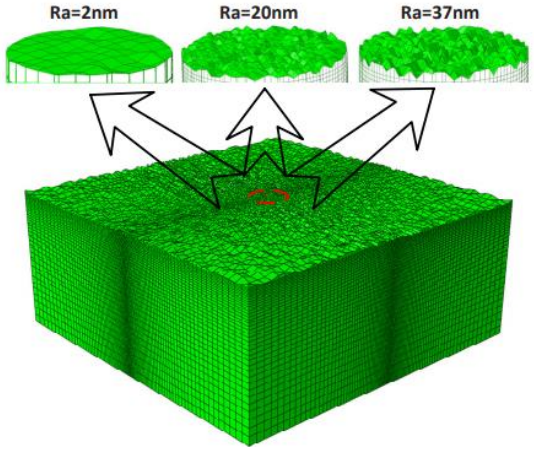

a)



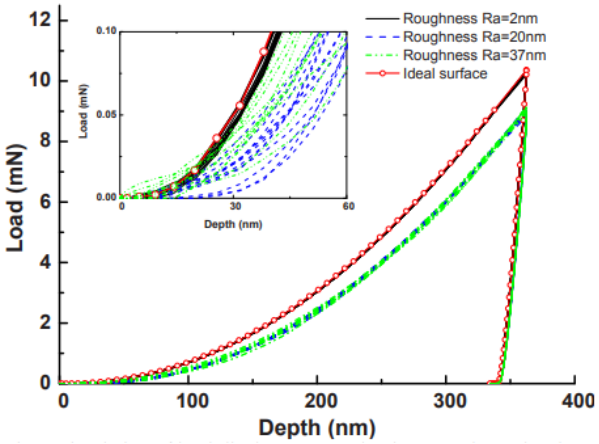

b)

Fig.2-35 Example of nano-hardness measurement for subsurface on machined component. a) Microstructures at different cutting conditions and b) Corresponding measured Nano-hardness [76]

Apart from superficial layer investigation of the machined surface, the machined surface roughness can also be investigated via nano-indentation techniques (Fig.2-36). This is impossible to be carried out using conventional hardness testers as the indentation tip is too big to recognise differences arising from differential surface roughness.




a)




b)

Fig.2-36 Investigation of surface roughness on the indentation tests. a) 3D FE roughness model; b) Load-displacement curves with different surface roughnesses [77]

To conclude, nano-indentation testing is a robust method for investigations of local mechanical properties of the superficial layer in the machined surface, which is of great interest to high quality component manufacturers. Therefore, nano-indentation can be used for investigating not only homogeneous materials, but

heterogeneous materials as well [78]. Because of the reduction in tip size requirements in nano-indentation, this technique can be used across different areas, where the target sample does not present enough material for conventional hardness testing.

### 2.3 Machinability investigation of nickel-based alloy

With the application of high performance superalloys (e.g. nickel-based alloy, titanium alloys) employed, more efficient and advanced parts have been manufactured and introduced into harsh operational environments (such as aerospace, nuclear, medical and marine etc.) [79] because of their superior properties (fatigue strength, thermal stability and corrosion resistance). These however, make them difficult to machine. Strict surface integrity checks are applied to these machined safety critical components as they are directly related to the service performance of generated products [2]. Thus, studies on the cutting performance of these materials and the surface integrity analysed method have been the subject of considerable research [80]–[83].

Regarding machinability, there are no specific standards. Actually, machinability is defined in many ways. According to [84], it is mainly divided into two catalogues: machining specific horsepower and tool life comparison. Machining specific horsepower is based on the power required for specific material removal. The tool life comparison indicates that a material that can be machined faster at equal tool life has a better machinability. In addition, ease of chip formation, and surface integrity are being regarded as evaluation factors as well.

To conclude, machinability can be defined as the ease (or difficulty) with which a material can be machined under a given set of operating conditions including cutting speed, feed rate, and depth of cut etc. [85]. An example of machinability comparison of different materials is shown in Fig.2-37, highlighting the difficulty of machining Inconel 718. Many factors are used to evaluate the machinability, such as component cutting force, chip shapes, tool life, and surface integrity etc. as stated in the reference.

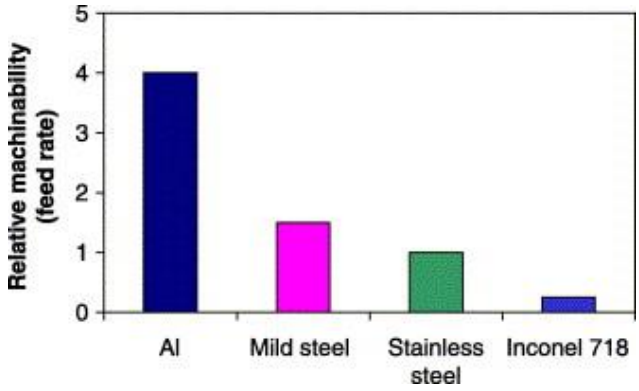



Fig. 2-37 Comparison of relative ease of machining among various alloys [85]

### 2.3.1 Workpiece material machinability evaluation

As described, nickel-based alloys are widely used in safety critical areas such as aerospace, nuclear and medical industries. They have austenitic matrix, and like stainless steels, work harden rapidly during machining and tend to generate high temperatures. Although they have great performance in high temperature working environments because of their excellent properties, this introduces high temperatures (>1000℃) and stresses (>3450MPa) in the cutting zone, challenging machinability [86]. Since the nickel-based alloy was developed in the 1940s, it has developed into different families with different chemical composition and microstructures [87]. Apart from nickel-based alloys, titanium, aluminium are widely used in the aerospace industry as well. Material differences will lead to variation in the machinability evaluation results. For superalloys, machinability is impaired mainly due to inherent characteristics including the following [85]:

1) High hot hardness and strength causing deformation of the cutting tool during machining.

2) High dynamic shear strength during cutting, resulting in localisation of shear stress and the production of abrasive saw-tooth edges, which encourages notching of cutting tools when machining titanium alloys.

3) The austenitic matrix of nickel-based alloys causes rapid work hardening during machining. This is one of the major causes of severe wear at the depth of cut line.

4) Presence of hard abrasive carbides (i.e. MC, M23C6) in the microstructure of nickel-based alloys encourages abrasion related tool failure.

5) Low thermal diffusivity, leading to localisation of cutting temperatures (≥1000 °C) at the tool tips, leading to high thermal gradients.

6) Welding of the workpiece to the tool cutting edge forming unstable built-up edges, which deteriorate machined surfaces as well as worsening components integrity.

8) Titanium alloy reaction with most tool materials at elevated temperatures, resulting in accelerated tool wear.

For example, Nouari [87]investigated the effect of workpiece microstructure on the machinability, taking tool wear as the main factor for machinability evaluation (Fig.2-38).

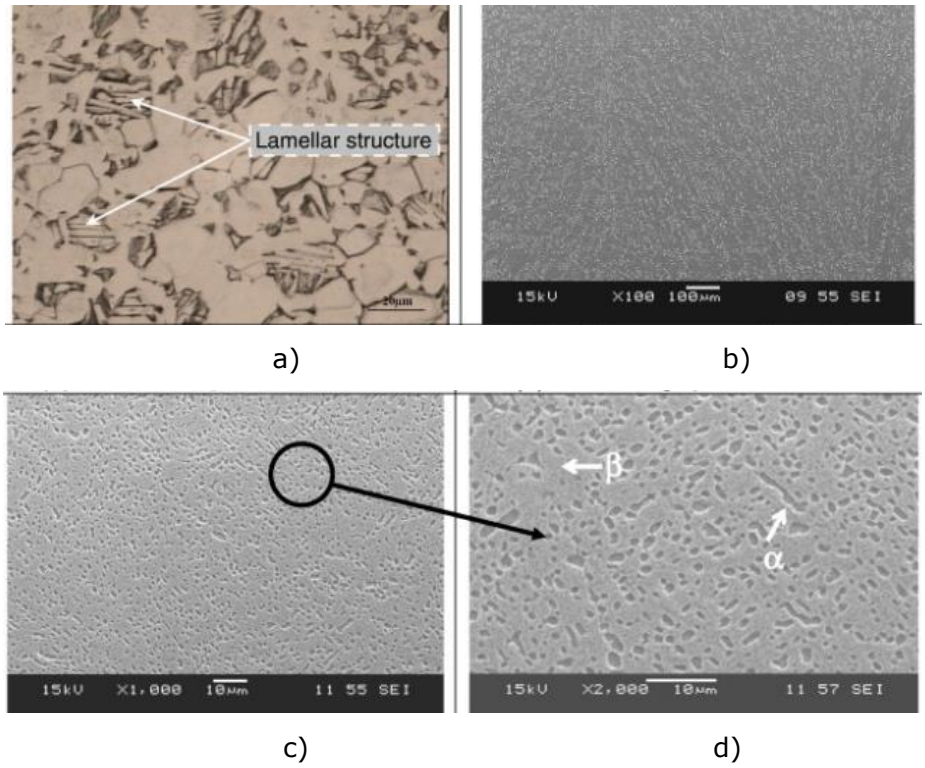



Fig. 2-38 Microstructure of different titanium superalloys. a) Optical micrograph of Ti-6Al-4V, b) SEM micrograph of Ti-6Al-4V, c) SEM micrograph of Ti-555 and d) High magnification of SEM micrograph of Ti-555 [88]

### 2.3.2 Machinability evaluation via status of cutting tool investigation

Conventional machining methods are based on material removal by tools to generate a desired surface and geometry. Therefore, cutting tools are one of most important factors involved in cutting processes, and have been used as an indicator for machinability evaluation. Different cutting tool factors in cutting processes, such as the tool life for specific materials at same cutting condition,

tool wear at same cutting time period, etc. have been used to assess the machinability.

As reported, the poor machinability of superalloys subjects the cutting tool materials to extreme thermal and mechanical stresses close to the cutting edge, which will lead to plastic deformation and accelerated tool wear [85]. The normal failure modes found when machining aeroengine materials are: notching at the nose, flank wear, crater wear, chipping and catastrophic tool failure. The materials used for cutting tools should be able to withstand the elevated temperatures generated in cutting conditions, thereby increasing the edge strength and reducing the tool wear. An example list of softening points of commercially available tool materials is shown in Table 2-5 and the Fig.2-39 illustrates the hardness variation of tools upon temperature elevation [85].

Table 2-5 Softening points of tool materials [89]

| Tool materials | Softening point temperature (°C) |
|---|---|
| High speed steel | 600 |
| WC | 1100 |
| Al2O3 | 1400 |
| CBN | 1500 |
| Diamond | 1500 |

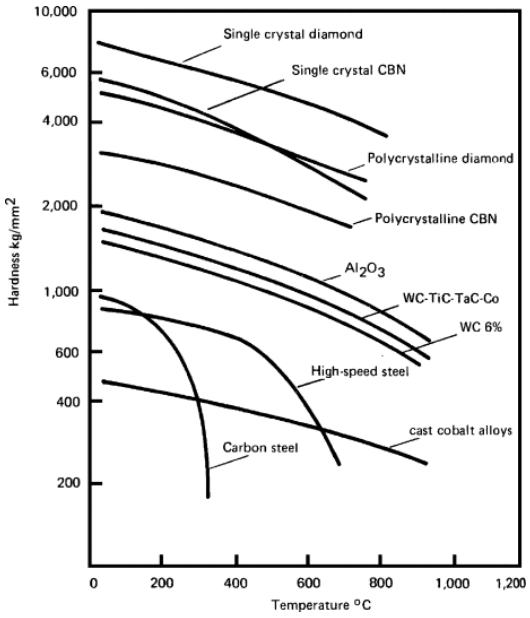



Fig.2-39 Typical hot hardness of several different tool materials [90]

Many researchers have tried to investigate the machinability by studying the tool conditions after cutting. For example, Shintani et al. studied the cutting performance of CBN tools when machining nickel-based alloys by investigating tool tip wear and the reaction between workpiece and tool materials [88]. Ezugwu presented an overview of machinability of aero engine alloys, mainly studying nickel and titanium-based alloys because of their dominance in a typical engine [89]. The research mainly considered the cutting performance of different material cutting tools during machining nickel and titanium alloys (Fig.2-40). Coolant method to improve machinability of alloys was also investigated, but surface integrity was not reported (Fig.2-41).

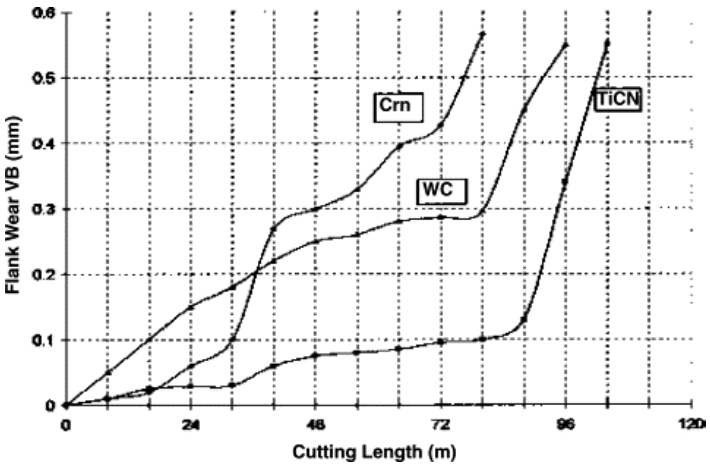



Fig. 2-40 Flank wear curves when machining titanium-based superalloys [85]

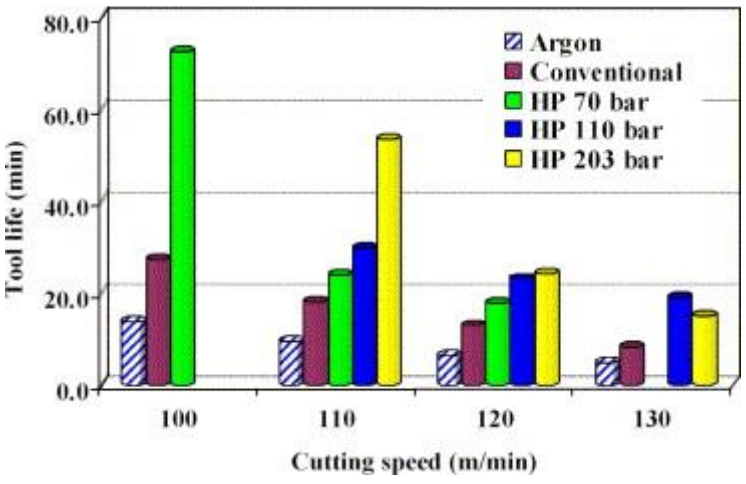



Fig.2-41 Tool life comparison when machining titanium alloy as various coolant pressure [91]

Bushlya presented research regarding the effect of cutting conditions on the machinability of Inconel 718 [90]. Cutting force, tool life and wear morphology

with coated and uncoated PCBN tools were studied and the surface stress of machined surface was compared as well (Fig.2-42).

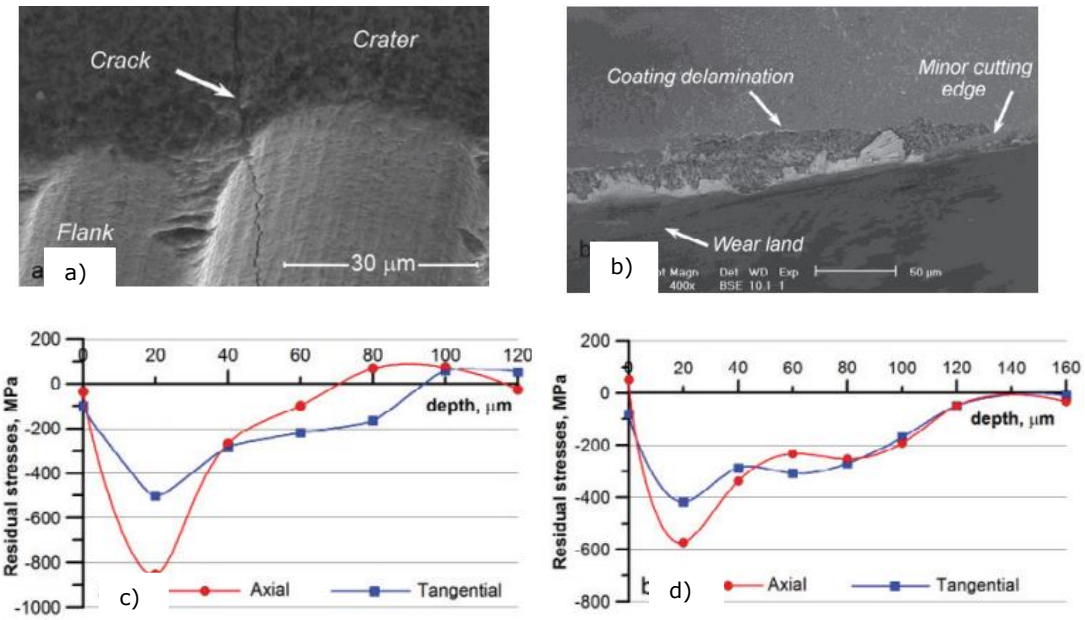



Fig.2-42 Tool cracking after machining Inconel 718 and surface residual stresses. a) Thermal cracking on tools, b) Coating delamination on the minor cutting edge, c) Residual stress profile for uncoated tools, and d) Residual stress for coated tools (cutting speed: 300m/min, feed rate: 0.1mm/rev, new tool) [82]

### 2.3.3 Machinability evaluation regarding material deformation and surface integrity

In addition to cutting tools, another factor directly relating to the cutting process is material deformation, mainly including shear phenomenon, material deformation force, the chip morphology and the heat generated.

The measurement of cutting force is essential for material cutting performance evaluation. It provides the basis for the selection of cutting tools, cutting parameters to minimize production costs and time, while maintaining acceptable machined surface integrity. Fig.2-43 illustrates the influence of material properties on the cutting force in the same cutting conditions [88].

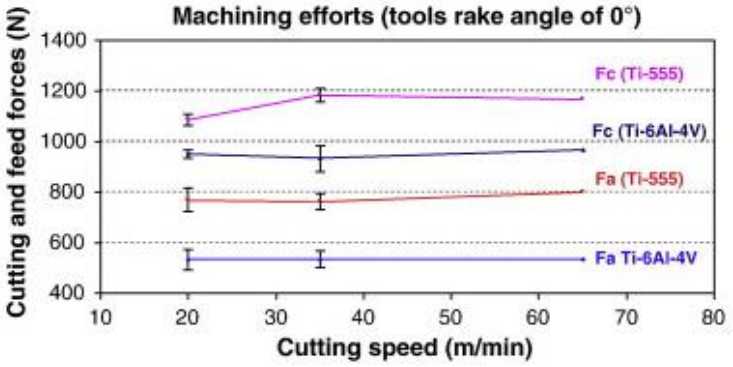



Fig.2-43 Comparison between cutting forces obtained for Ti-6Al-4V and Ti-555 with a cutting tool rake angle of 0° [88]

Regarding the chip formation, Arrazola mainly studied the chip morphology and tool wear to evaluate machinability of Ti6Al4V and Ti555.3 (Fig.2-44) [81]. Dandekar attempted to improve the machinability of Ti6Al4V using laser-assisted machining (LAM) and hybrid machining, where the cutting force is obviously reduced. In this study, cutting speeds, tool wear and specific cutting energy were used to evaluate the machinability of target materials as well [85].

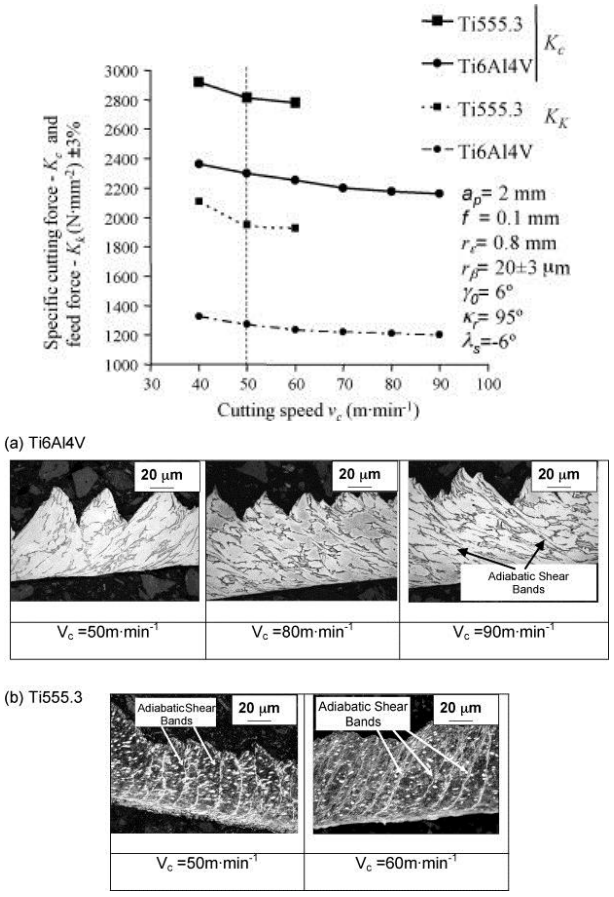



Fig. 2-44 Example of specific cutting force and chip morphology [92]

Due to its high importance, machined surface integrity remains the most interesting subject for manufacturers. As stated, techniques to reveal surface integrity include optical microscopy, SEM, XRD etc. Significant research has been carried out to study the machinability of materials in the respect of surface integrity. For example, Ulutan [82], presented a review, focussing on the machined surface integrity of titanium and nickel alloys, widely applied in aerospace. Common surface defects (Fig.2-45) and their causes, the effect of surface integrity on functional performance of component, and surface integrity evaluation methods were discussed in the review. In addition, some the analysis methods of machined surface integrity are also presented (Fig.2-46). Jawahir et al. [93] gave a comprehensive description of the development of surface integrity and state of art technology in materials processing. The surface integrity evaluation method was described in detail and composite materials were also considered. Surface integrity research is also a main factor when considering the machinability of materials, as the final purpose of machining is to provide an appropriate quality component.

To conclude, many factors contribute to cutting processes and can be used to evaluate the machinability of materials individually or together, e.g. Luca carried out a synthetic evaluation method to assess the machinability of titanium by considering different factors (Fig.2-47) [94], although the process still requires many cutting tests.

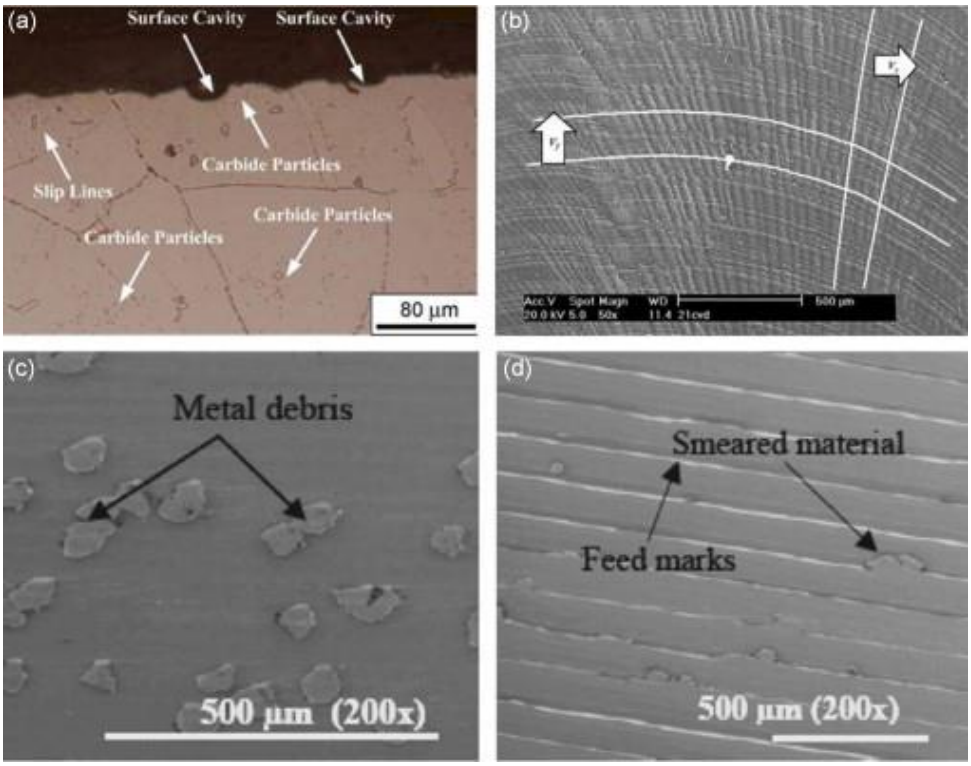



Fig. 2-45 Common surface defects in machining of nickel based alloys. a) Metallographical microstructure of NiCr20TiAl after turning at V=60 m/min, f=0.15 mm/rev and DoC=1 mm, b) Lay pattern after dry milling Ti-6242S at V=125 m/min, f=0.2 mm/tooth, DoC=2.5 mm, c) Metal debris after turning IN-718 at V=125 m/min, f=0.05 mm/rev, and DoC=0.5 mm, and d) Smeared material and feed marks after turning IN-718 at V=125 m/min, f=0.1 mm/rev, and DoC=0.75 mm [82]

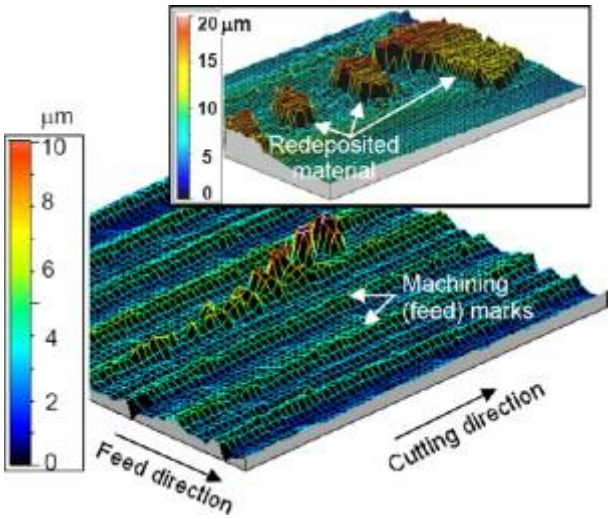



Fig. 2-46 3D profile of machined surface geometry [93]

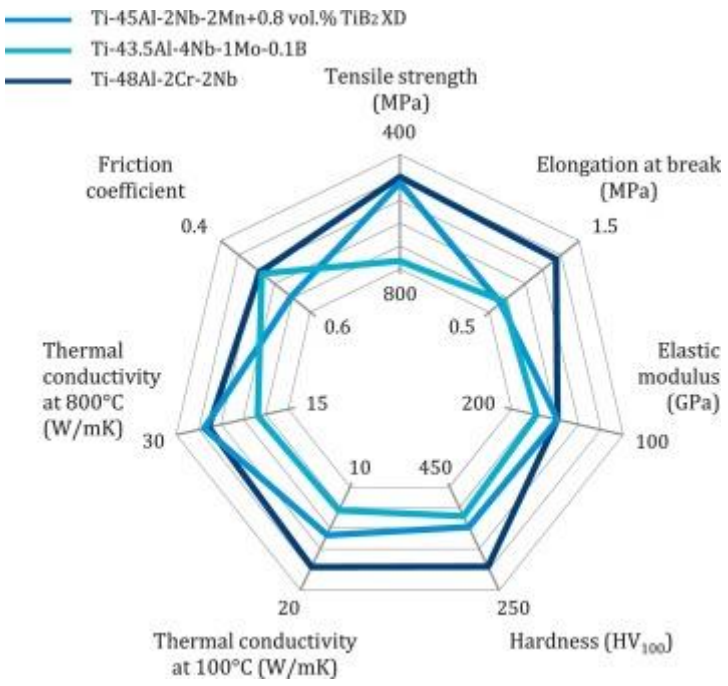



Fig.2-47 Comparison of machinability based on different evaluation factors [94]

## 2.4 Non-conventional methods for cutting performance evaluation

Surface integrity, as a main aspect of machinability evaluation, has been widely studied. However, up to now the evaluation method is generally based on tool wear analysis, cutting force, chip morphology, cutting temperature etc. at specific cutting conditions, with many variables (including tool geometry, cutting speeds, depth, width etc.) [81], [82], [85], [88], [91]–[93], [95]–[97] that effect the evaluation of cutting performance in materials, complicating evaluation processes. As seen, machinability and surface integrity analyses of materials are traditionally studied with many cutting tests on machine tools to obtain the cutting force, chip morphology, tool wear and cutting speeds etc. Practical cutting tests require large amounts of material, for variation of cutting parameters. In addition, cutting tests are followed by part sectioning to analyse surface integrity that effects component functional performance. To explore alternative methods of machinability investigation, non-conventional methods that either do not rely on machine tools or do not come from the cutting process directly have been introduced.

### 2.4.1 Energy based research on machining

The energy consumed in cutting processes, which is related to different cutting conditions, is also treated as an evaluation factor for mechanical machining processes, regardless of the process methods. Most studies focus on the electric energy or power consumed by machine tools to understand the cutting process

indirectly. For example, Timothy et al. [98] reported on the specific electrical energy consumed for different manufacturing process rates (Fig.2-48). This presented an approximate evaluation of energy consumption for different machining methods as a function of material removal rates.

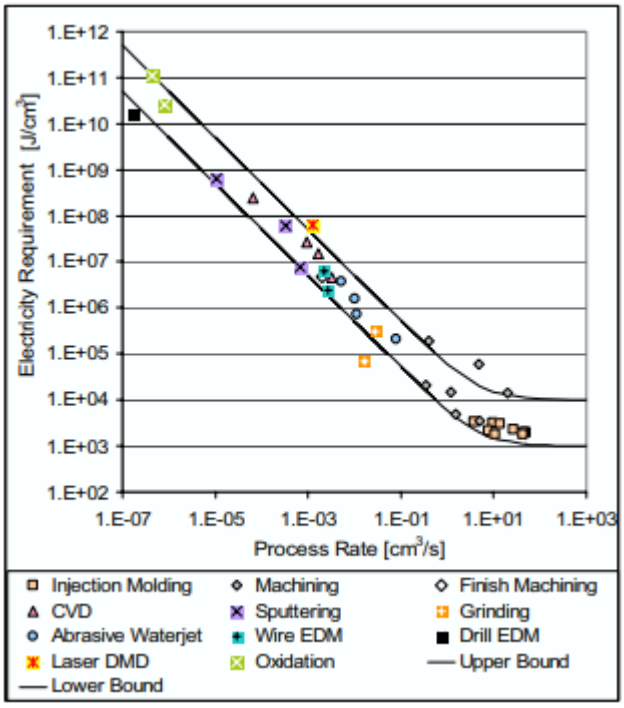



Fig. 2-48 Specific electricity requirements for various manufacturing processes as a function of the material processing rate [98]

Regarding energy consumption for different materials, Balogun et al. machined three kinds of material, mainly considering the relationship between un-deformed chip thickness and specific cutting energy [99]. As an example in Fig.2-49, the power state of the machine tool in different stages of one cutting process were reported, where it was found that the power consumption of the cutting state is significantly greater than the ready state and basic state. The difference could be theoretically used for the investigation of machinability of different materials or process.

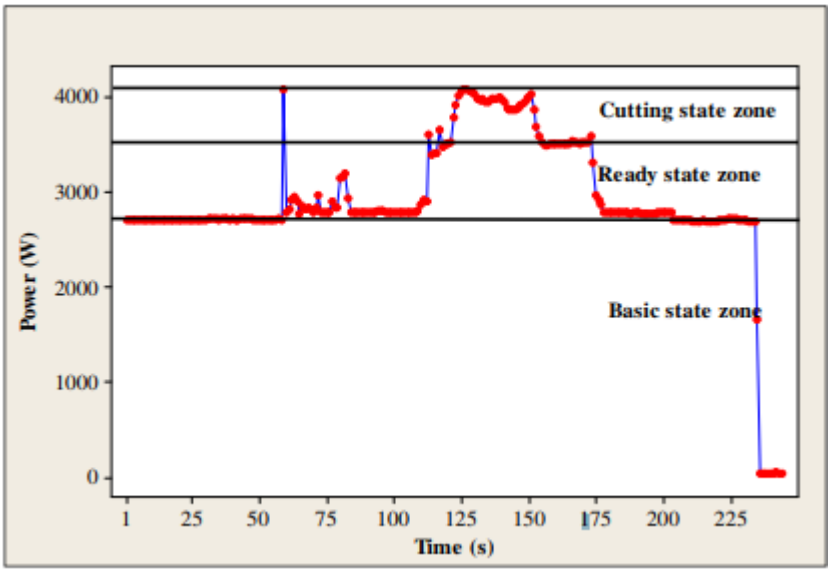



Fig.2-49 Total power consumption trend for machining toolpaths [99]

Sealy et al. considered cutting power as the signature for evaluation of surface integrity [100]. They distinguished the differential between energy consumed in different states, and were therefore able to study and correlate energy with the cutting process (Fig.2-40). They correlated the consuemd net cutting energy, spindle specific energy and total specific energy to the machined surface roughness (Fig.2-51), microhardness and residual stress seperately. This shows the possibility of using the energy to evaluate machinability in cutting processes, while the comparision for worn tools was also considered (Fig.2-52).

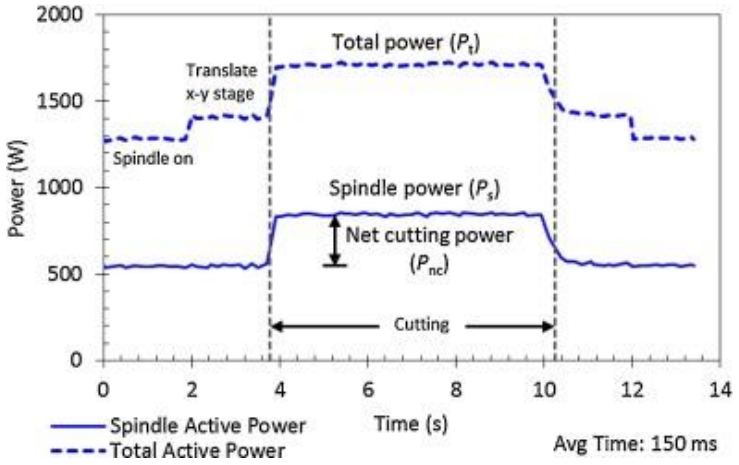



Fig.2-50 Representative total and spindle active power curves measured during milling of AISI H13 tool steel [100]

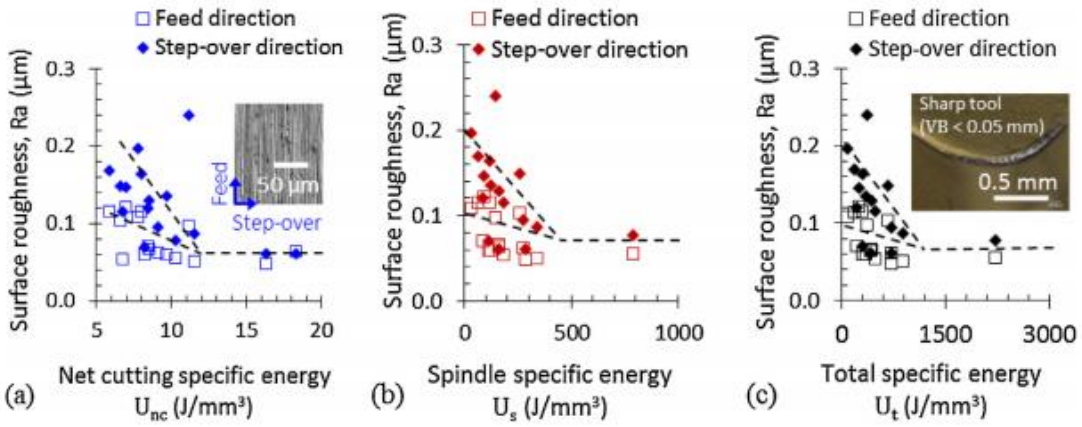



Fig.2-51 Coherence of surface roughness with (a) Net cutting, (b) Spindle, and (c) Total specific energy by milling with a sharp tool [100].

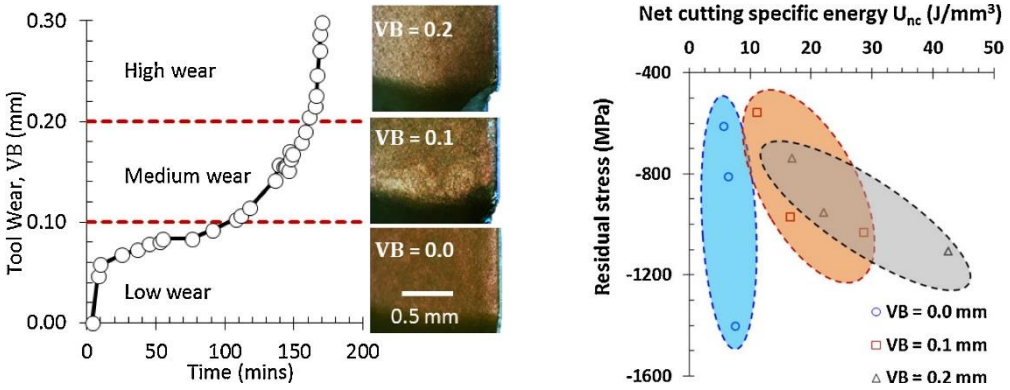



Fig.2-52 Tool wear condition and the coherence between residual stress and cutting specific enregy [100]

In addition, Sarwar et al. studied the specific cutting energy consumed during machining of three different materials with a band saw and correlated this to tool wear (Fig. 2-53) [101]. In Dandekar's study [96], aside from tool wear, total specific cutting energy was used to evaluate the machinability of titanium, making a simple correlation between this and surface roughness (Fig.2-54), although is the study was mainly concerned with the comparison between Laser assisted and conventional machining. Other researchers have carried out similar studies to use energy for cutting process evaluation [98], [102], [103]. However, the concept is similar and fewer of them are concerned with superalloy machining, therefore no effective and proper method is proposed. Nerveless, these studies imply that the energy method could be used to estimate machinability of target materials.

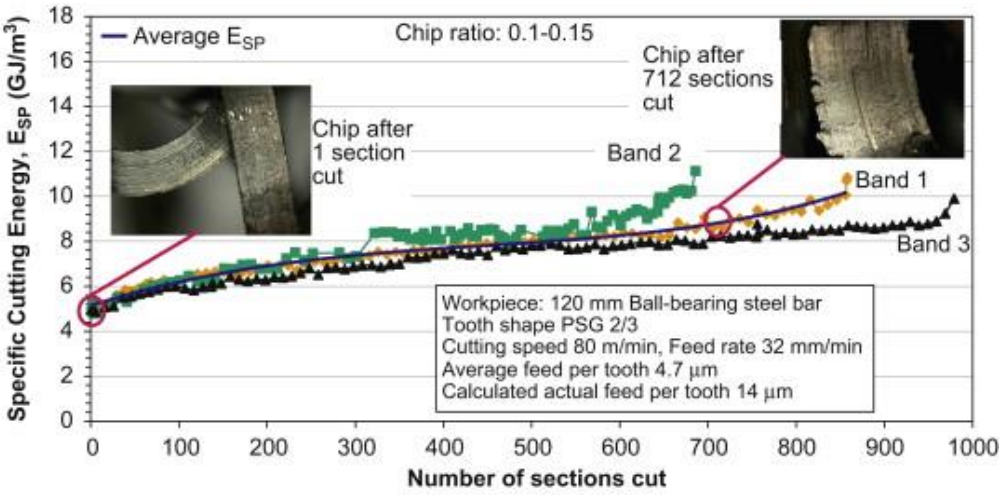



Fig. 2-53 Specific cutting energy during band sawing [101]

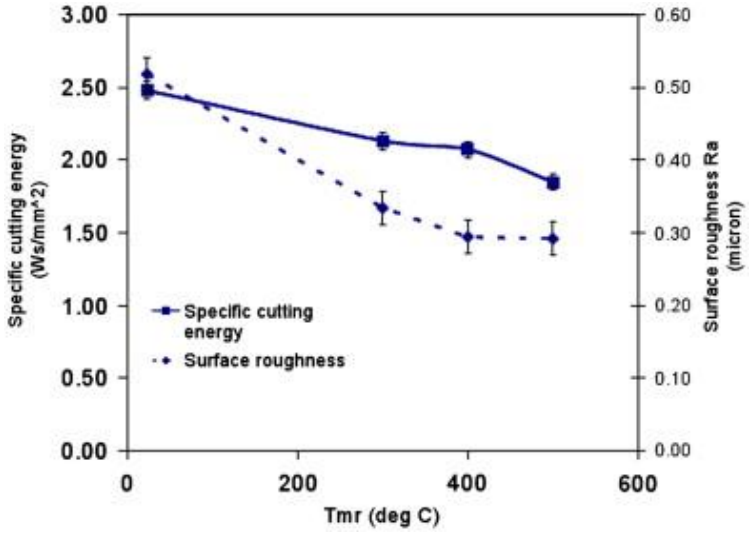



Fig.2-54 Surface roughness and specific cutting energy consumed during cutting [108]

### 2.4.2 Simulation and analytical method

As a result of the drawbacks of machinability testing using conventional machine tools, such as large cutting tests, resource consumption etc., researchers have attempted to apply the finite element (FE) method and analytical mathematical methods to study the cutting process. Following the increase in computational power, it has become possible to calculate materials with smaller meshes and more detail to define boundaries approaching practical cutting processes. With the help of this technique, many cutting process and fundamental research have been studied.

Regarding the simulation and analytical method for evaluating materials processing, the material constitutive model is the most important in terms of accuracy of results [104]. The identification of the material property is the crucial step for this simulation. Generally, Johnson-cook's (*J-C*) constitute equation (Eq.2-10) is used to establish the model for simulating workpiece material behaviour [105], [106].

$$\sigma = (A + B\varepsilon^n)\left(1 + C\ln\left(\frac{\dot{\varepsilon}}{\dot{\varepsilon_0}}\right)\right)\left(1 - \left(\frac{T - T_{room}}{T_{melt} - T_{room}}\right)^m\right) \quad (2\text{-}10)$$

where $\sigma$ is the flow stress, $\varepsilon$ the plastic strain, $\dot{\varepsilon_0}$ is the reference plastic strain rate ($s^{-1}$), $\dot{\varepsilon}$ the strain rate ($s^{-1}$), T (°*C*) is the workpiece temperature, $T_{\text{melt}}$ is the melting temperature of the workpiece material (1300 °C for Inconel 718), and $T_{\text{room}}$ is room temperature (25 °C). *A*, *B*, *C*, *n*, and *m* are the *J–C* constants where *A* (MPa) is the yield strength, *B* is (MPa) the hardening modulus, *n* is the hardening coefficient, *C* is the strain rate sensitivity coefficient, and *m* is the thermal softening coefficient. In fact the first, second and third bracket in *J–C* equation are taken into account for the strain hardening, strain-rate hardening, and thermal softening effect, respectively [104]. Researchers then use different methods to identify the above corresponding parameters in the equation, normally from Split-Hopkinson pressure bar (SHPB) tests [104], [107], [116], [117], [108]–[115].

Subsequently, Lorentzon et al. [113] developed a new *J-C* material model considering the thermal softening effect in the equation [112]. With the modified *J-C* equation (Eq.2-11), the effect of temperature-dependent flow softening was also included [114]–[117].

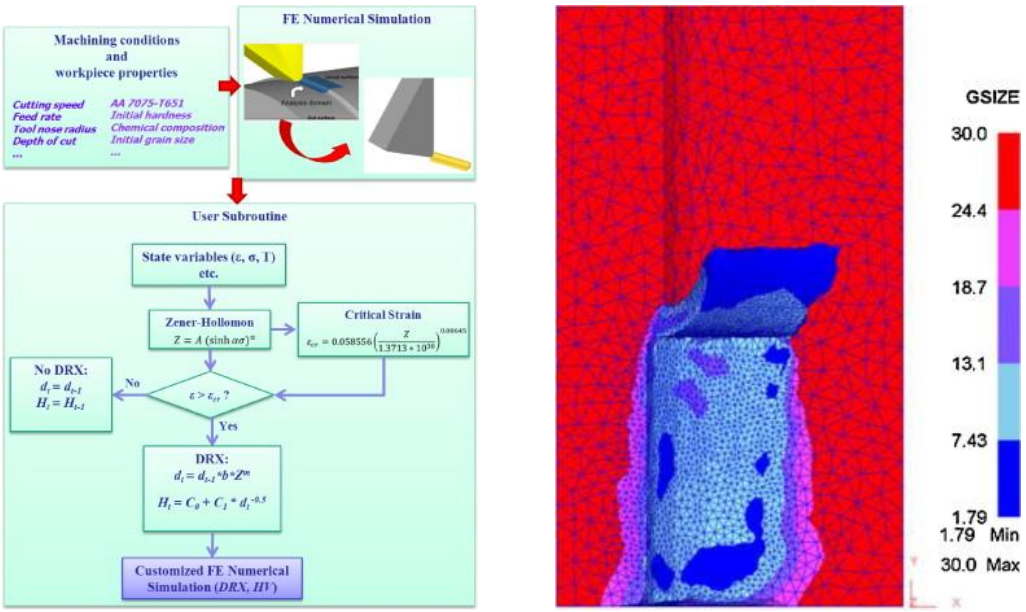
$$\sigma = (A + B\varepsilon^n)\left(1 + C\ln\left(\frac{\dot{\varepsilon}}{\dot{\varepsilon}_0}\right)\right)\left(1 - \left(\frac{T - T_{room}}{T_{melt} - T_{room}}\right)^m\right)\left[D + (1 - D)\left[\tan h\left(\frac{1}{(\varepsilon + S)^r}\right)\right]^{\dot{s}}\right] \quad (2\text{-}11)$$

where *A*, *B*, *C*, *n*, and *m* are the *J–C* parameters used in the Lorentzon's model [113] while *D*, *S*, and *r* were introduced to take into account the dynamic behaviour of Inconel 718.

Furthermore, an inverse methodology was applied, based on FE simulation and the response surface methodology, to build a new J-C constitutive equation (Eq.2-12), where the initial workpiece hardness was included, by adding the functions, F and G [116], [117].

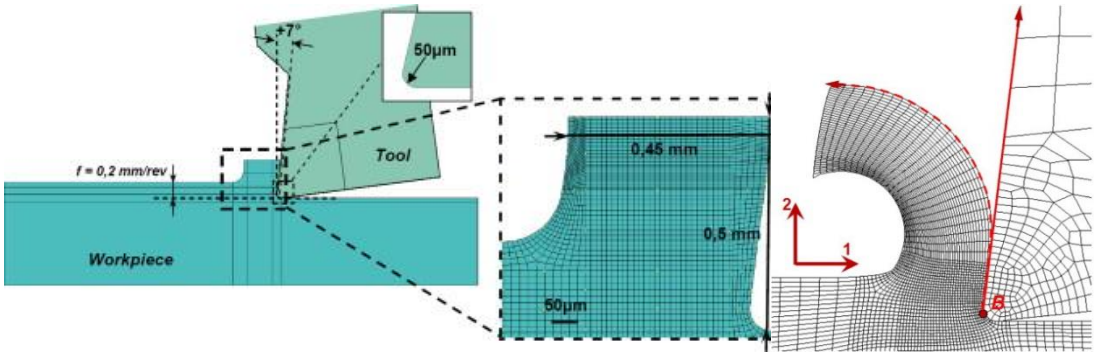
$$\sigma = (A + (F + 200) + G\varepsilon + B\varepsilon^n)\left(1 + C\ln\left(\frac{\dot{\varepsilon}}{\dot{\varepsilon_0}}\right)\right)\left(1 - \left(\frac{T - T_{room}}{T_{melt} - T_{room}}\right)^m\right) \quad (2\text{-}12)$$

Regarding the application of the simulation, an example of simulation for predicting the grain size and hardness is presented in Fig.2-55 a) [105]. With the help of the simulation, the grain size variation caused by the mechanical machining of the surface is presented in Fig.2-55 b). Courbon et al. applied the simulation method (Fig.2-56) to study the turning of Inconel 718 with a high pressure jet included in the cutting process [106], widely expanding the application. To improve simulation accuracy, many studies have attempted to identify input parameters for the simulation based on previous experiments. For example, Chandrasekaran carried out a simulation for cutting based on data extracted from SHPB tests rather than assumption (Fig.2-57) [118].




a) b)

Fig.2-55 Example of simulation process for grain size and hardness prediction. a) Structure of the user routine for predicting the grainsize and hardness, and b) Predicted grain size (μm) [105]




a) b)

Fig.2-56 Simulation of turing Inconel 718 with a high pressure jet included. a) Build simulation model of the workpiece and cutting tool and b) Summary of the extraction lines during the cutting process [106]

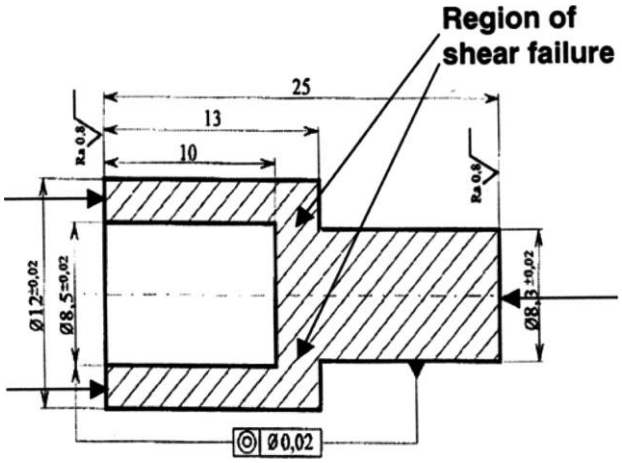



Fig.2-57 Geometry of the 'hat' shaped specimens for SHPB test to extract shear related data for simulation [118]

To conclude, the simulation and numerical method for studying cutting processes or material deformation provides a powerful tool for cutting performance investigation, reducing work compared with practical experiments. However, the major disadvantage for these methods the number of assumptions, as the material properties and contact boundary cannot be fully understood and clearly defined. Despite significant progress, such as using input data based on practical experiments to minimize errors, it still cannot be used for the prediction of practical machining especially in safety critical areas.

### 2.4.3 Modified pendulum method

Machinability and cutting tests of materials, as reported, are normally undertaken on machine tools, which consumes time and money. Therefore, effective test methods to reduce these costs have been the subject of different studies. Several methods without using machined machine tools, but still able to assess cutting processes, have been reported.

Eyma modified the dynamic pendulum, based on the Chardin's machine, which is similar to Charpy's pendulum (Fig.2-58). Cutting force is acquired experimentally and compared with the test results significantly. Later, Pfeiffer [119] used the modified machine [120], based on Chardin's pendulum [121], to study chip formation mechanisms in wood. The chip deformation process is captured with a camera and their properties have been analysed in detail. Chardin [121] reported the dynamometric pendulum method to study the sawing process of wood in 1958 (Fig.2-59).

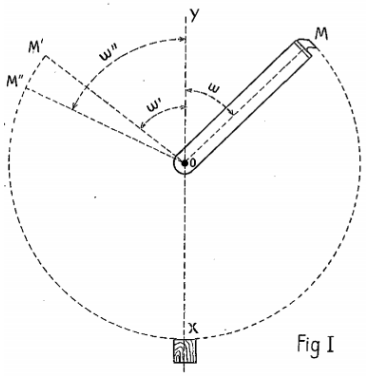



Fig.2-58 Principle of Chardin's dynamic pendulum [121]

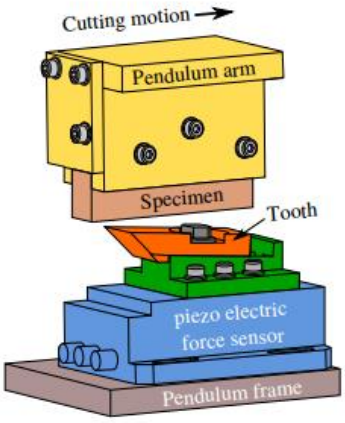



Fig.2-59 Modified dynamic machine for wood cutting study [119]

Although there is no comprehensive description of this method from the aforementioned studies, they introduced the possibility to use the pendulum method to study cutting processes. To apply this method to metal cutting, several attempts were carried out. Vingsbo [122] studied the dynamic micro mechanism and chip deformation during cutting via the pendulum technique. He proposed use of a pendulum, shown in Fig.2-60, to carry out cutting. A quick stop part was designed as well to study the chip formation. Using this machine, small specimen cutting tests can be undertaken and the chip extrusion captured (Fig.2-61). In addition, the specific grooving energy was considered to describe deformation in the grinding process. Although no machinability conclusion was drawn from this study, it described cutting performance study without using machine tools, paying attention to cutting area in energy view. With a customized cutting tool fixed on modified Charpy machine (Fig.2-62), Bergman et al. studied the tool wear phenomena when cutting metal matrix composites.

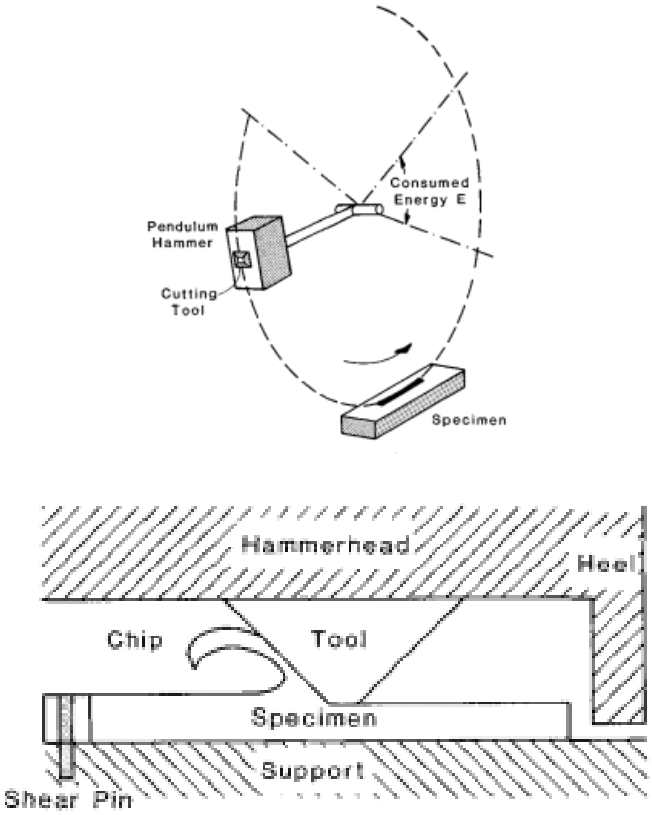



Fig.2-60 Proposed pendulum technique [122]

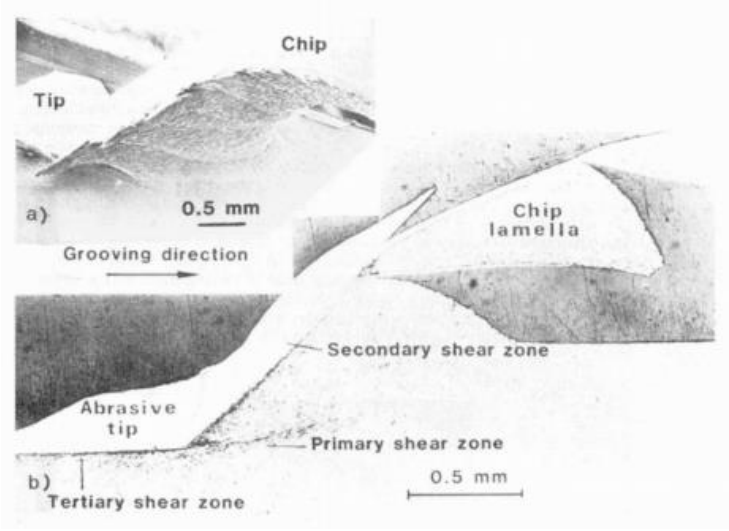
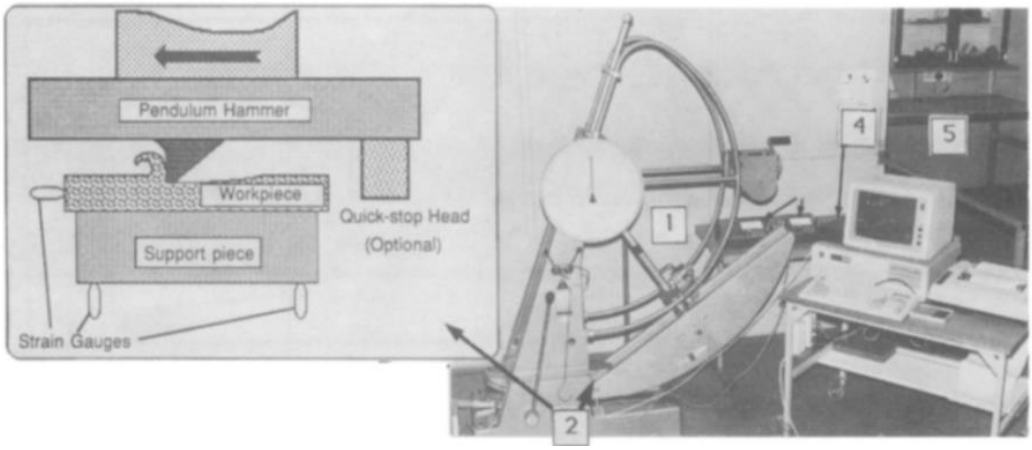



Fig.2-61 Scanned picture of chip formation [122]



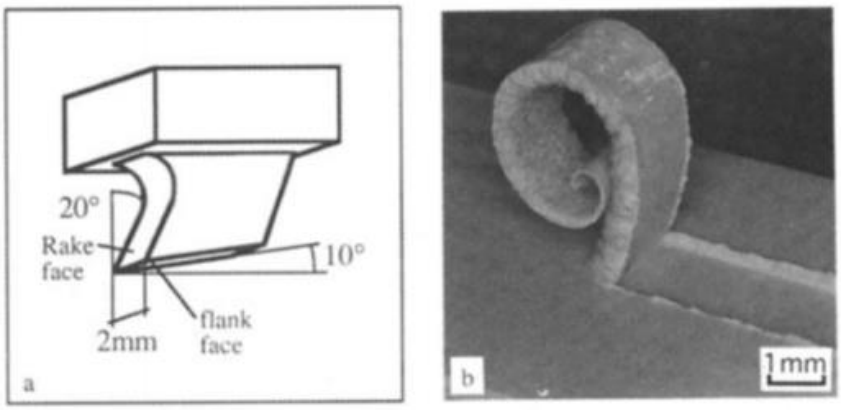




Fig. 2-62 Geometry of cutting edge and the workpiece material after a quick-stop cutting based on modified Charpy machine [123]

To study the chip formation, Rodrigues [124] modified the Charpy machine (Fig.2-63), which is similar to the pendulum method mentioned above. However, the experimental arrangement and proposal are more practical and give a simple but clear method to evaluate the consumed total. Different to the pendulum cutting concept, Stefan applied a rotary test station (Fig.2-64), which was a combination of rotational and linear motion to carry out cutting operations in food engineering, where gum was treated as the cutting target. High speed cutting was claimed in this study and the generated sample surfaces were compared to investigate performance under different cutting conditions.

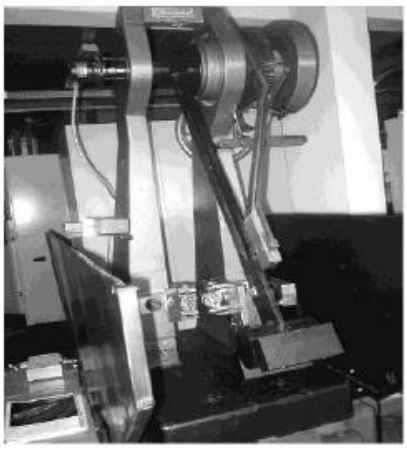


Fig.2-63 Schematic of modified Charpy machine [124]

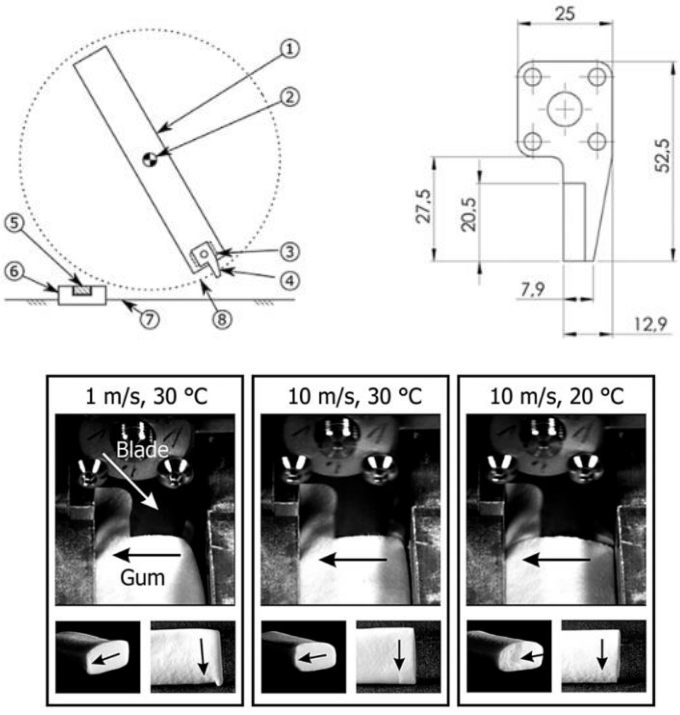



Fig.2-64 Illustration of proposed rotor test station and representative photographs of cut process for gum in food engineering [125]

Apart from the pendulum-based method and the liner motor design, an impact machine (Fig.2-65) consisting of a falling instrument, falling passage, cutting instrument and supporting legs was proposed to undertake cutting for mineral specimens [126]. A defined weight is released from the top of the impact blade in a designed distance by a noose the hook, and energy transferred during falling is transferred to the blade by impacting, cutting the rock specimen. A detailed illustration of the cutting area is shown in Fig.2-66.

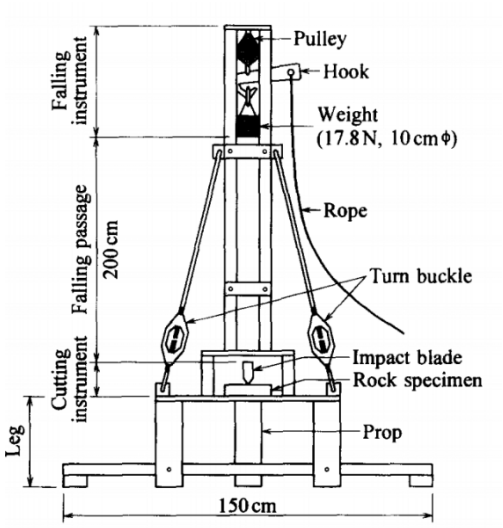



Fig. 2-65 Impact test apparatus for rock cutting [126]

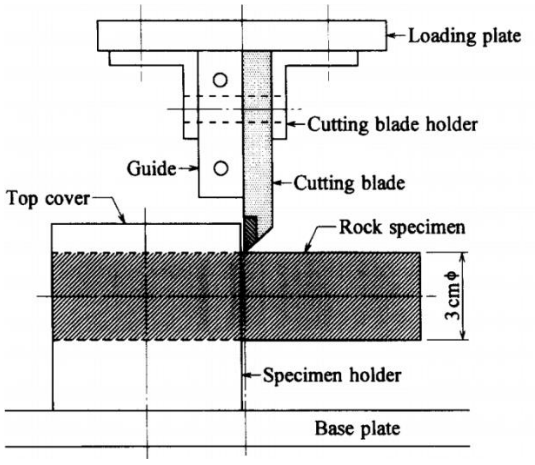



Fig.2-66 Cutting instrument for impact shear tests [126]

To conclude, although most of the studies focus on soft materials (comparing with the superalloys used in the aero-engine) or chip formation, it has been shown that the modified pendulum method was able to carry out cutting tests. Limited consideration is given to the cutting energy and the detailed mechanism in the cutting area, which means that the input cutting energy, surface integrity and

variation of cutting speeds have not been studied. Although there are already some studies investigating the cutting process based on a modified pendulum, the advantages have not been investigated and explored in detail. Based on this review, more advantages such as the ability to test small material volumes and monitor the cutting process, etc. could be accomplished with the pendulum-based cutting, which will be described in detail later. These will bring significant benefits to the study of material machinability.

In this research, we will develop a pendulum based cutting test machine, which has a moving pendulum fixed with target material and stationary cutting tool to carry out the cutting tests. Different from the above mentioned research in literatures which just use the machine to generative grooves or quick stop investigations or studying soft materials, this research will establish a comprehensive machinability study method based on orthogonal machining with proper monitored. The machining chips, generated surface and cutting process information (including force, evolution process) could be collected. Although the wet cutting condition will be developed and included in this research, thus gives the PBCT method the ability to investigate cutting performance in wet cutting and the properties of coolants. Apart from this, an energy based surface integrity evaluation methodology will be included and it will introduce another surface integrity investigation path by studying the energy input the cutting areas directly. As a conclusion, this PBCT method will establish a comprehensive research method of cutting performance and surface integrity of machining rapidly rather than simple trial tests. The energy based thresholds for surface integrity prediction will improve the process of cutting parameters selection and optimization.

## 2.5 Current gaps in the research

Seen from the above extensive literature review, it is evident that the surface integrity related machinability investigation of superalloys, such as the nickel based (Inconel 718), are significant and challenging for materials application in the safety critical areas (aerospace, nuclear, medical etc.). This is mainly caused by the inherent material properties including high material strength at elevated temperatures, low thermal conductivity leading to increased cutting forces and temperatures at tool point/rake face [12], [34], [91], [127]–[129]. While the surface integrity is well known to be crucial for the fatigue life of manufactured components [6], [44], [85], [130], [131], the surface anomalies should be minimised to prevent potential failure in services. More importantly, new materials with higher strength and unique capabilities are under development because of

the increasing of design requirements. Their surface integrity related machinability investigation will be obvious challenges because of the limited volume in the developing stage.

Although lots of work have been done to study the surface integrity related machinability, such as massive cutting tests, analytical models and simulation, not too much findings have been reported to change the experimental implementation methods that carry out cutting tests. Experiments on the machine tools are still the main methods to study the surface integrity related machinability of materials practically, which is obviously resourceful as stated above. It must be also noted that the current published information is restricted to a relatively narrow window of machining parameters and conditions. This is mainly because of the massive work required for even few cutting parameter combinations. To understand the full material response on a wider spectrum of cutting parameter combinations, simple and rapid methods need to be developed and proposed. To avoid the countless procedures for surface observation and evaluation, an energy concept has been proposed but they are mainly focusing on the electrical energy consumed which could not be directly correlated to the surface damage level. Regarding the surface damage evaluation standard, current methods are normally based on the empirical observation which is qualitative based. In respect of the components with higher surface integrity standards, current methods may be not enough to have an accurate evaluation of its service performance. Therefore, a quantify-based surface damage degree evaluation method that could give the measured surface damage quantitatively is beneficial.

**Academic Challenge 1:** New surface related machinability evaluation methods must be investigated to cope with the challenges that massive resources are using to carry out cutting performance research on machine tools. Because the current methods are consuming a lot of resources to carry out even only few couples of cutting parameters combinations. Also, the materials in limited volume or developing period need to be considered as well to get the understanding of its surface integrity related machinability. In addition, it is not able to study the continuous machining mechanism transition following the cutting conditions variation. To make full understanding of the machining mechanism and surface integrity related machinability of target materials, novel testing method are needed.

**Industrial Benefit 1:** Due to the heavy work needed for surface integrity related machinability evaluation with even several cutting parameter combinations, the

selection of appropriate machining cutting parameters combinations for higher efficiency production will be difficult. Therefore, further research is required to enhance the understanding of material manufacturing processes. The understanding of the material surface integrity related machinability properties could be transferred to deliver machining strategies to improve production and surface quality on machined components. Also it could improve the understanding of how these cutting parameters influence the life of components comprehensively. In addition, the proposed rapid method will help the material developing companies to have pre-understanding of not only the material property itself, but the relationship with cutting performance as well. In this case, it will significantly reduce the time of material developing cycle and helps to develop better and more practical materials for specific applications.

**Academic challenge 2:** Better understanding and higher requirement of the machined surface integrity generated from the machining process are popular academic interests especially for the safety critical components (such as those in aerospace, nuclear, medical etc.). Currently the cutting tests could normally just get one specific kind of machined surface at one time, which means that the cutting parameter is directly correlated to the machined surface integrity. Although electrical energy was introduced to study the machining process, it has not been correlated to the material properties and the machined surface integrity. A general method which could directly investigate the relationship between energy inputs to the cutting areas and machined surface damage level regardless of the cutting parameters used is anticipated and beneficial. In this way, the relationship between energy consumed and the machined surface damage level could be built. Therefore the machined surface integrity could be investigated by studying the energy.

**Industrial benefit 2:** The surface defects could be found on almost all on the machined components even if the parameters and conditions are optimised, with tool failures or wear leading to damages on the workpiece. Understanding the effects of these surface defects on the performance life of the component will help the manufacturers understand whether the tight machining regulations they have in place are correct or if the standard needs to be updated or could be considerably optimized. As the energy based method could correlate the energy input into the cutting areas and the machined surface integrity directly while it does not rely on specific cutting parameter combination, the surface integrity could be directly evaluated by studying the energy consumed in different areas after correlation benchmark established. In this way, the manufacturers could monitor the

corresponding signals that linked to the energy calculation during the cutting process, then the surface integrity could be acquired rather than sectioning and observation every time. In other words, an alternative non-destructive surface integrity evaluation method could be established.

**Academic challenge 3:** As known, the surface integrity related machinability of materials depends on the practical machining tests on the machined tools with specific cutting parameters combinations. Therefore, only limited cutting conditions could be evaluated which makes the evaluation of the materials cutting performance localization. It is necessary to investigate the cutting mechanism and performance variation continuously following the cutting condition changing. However, these are no such kind of techniques applied for material surface integrity related machinability investigation as far as the author knows.

**Industrial benefit 3:** Massive cutting tests are carried out in different manufacturing companies to find the best cutting parameters combinations for higher production and better surface integrity on components. Even if these tests have been carried as much as possible, they still only cover limited cutting conditions considering the numerous cutting parameters combination. The method proposed in the thesis will be able to continuously capture the cutting conditions variation in a single test and on limited volume of materials as well. This will significantly reduce the work load needed and the manufacturers could study the cutting conditions various continuously on both the generated chips and the machined surface integrity, thereby the optimal process parameters could be acquired with wider cutting parameters combinations.

**Academic challenge 4:** The surface integrity is a wide definition for the machined components including material drags, residual stress and hardness variation etc. An important and popular method to inspect the surface integrity is the observation of superficial surface after the component sectioning. However, currently it mainly depends on the empirical observation to provide the information qualitatively, for example the material drag depth, while it is the main aspect that is investigated in this thesis. To establish a scientific and quantitative method to identify the surface integrity of the machined components is definitely necessary and will be beneficial for predicting the service performance accurately.

**Industrial benefit 4:** The investigation of above quantitative method will allow the manufacturers to evaluate the surface integrity of components accurately and scientifically rather than current qualitative method. A standardised procedure could be established. It will be helpful as well for studying the inherent effects of

the deformation in superficial surface on the component performance. Therefore, deeper understanding of the material properties and its cutting performance even the service performance could be gotten.

# Chapter 3

# Methodology

To give a comprehensive understanding of the experimental method in this thesis, the equipment, setups and approaches will be presented in detail in this chapter. At first, the equipment, including the mentioned pendulum-based cutting machine, accessories for cutting process monitoring, will be illustrated. Then the properties of materials used and the sample preparation procedure is explained, while the employed machines are also included. The techniques and equipment needed for surface integrity analysis (such as SEM, EBSD, XRD, Nano-hardness etc.) are shown at the end of this chapter.

## 3.1 Orthogonal cutting of Inconel 718 on pendulum-based machine

To study the cutting performance of materials, the basic orthogonal cutting is carried out on the PBCT machine to validate the concept of surface integrity related machinability evaluation with energy based method. Different cutting parameters and cutting tools will be used to investigate the affection of different cutting conditions and prove the robustness of the proposed method.

### 3.1.1 Material and workpiece preparation

The widely used Ni-based superalloy, Inconel 718, was used as the test material, supplied by Rolls-Royce plc with a chemical composition of 18.5% Cr, 5.0% Nb, 3.0% Mo, 0.8% Ti, 0.5% Al, 0.05% C, 0.07% Si, 0.04% Mn, 18.0% Fe and balance Ni. Two sample shapes are designed for different study objectives. Both are 1 mm thick flat sheet (20 mm×25 mm) in rectangular shape but different in cutting length and cut out of the bar using electrical discharge machining (EDM). While the top surface of the sample with 20 mm×1 mm dimension is used to clamp into the pendulum on the PBCT machine. The bottom of the sample is the designed cutting area which include a cutting length at 10mm and another sample has a cutting length at 20mm (Fig.3-1).

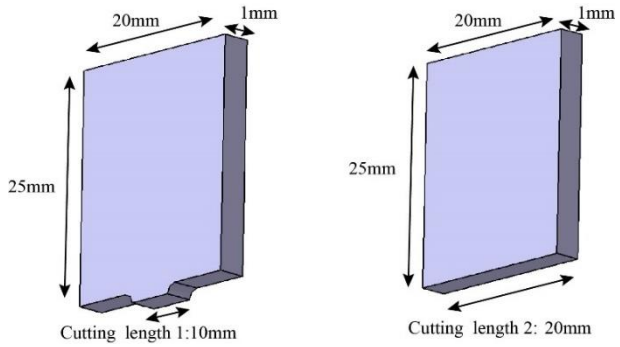



Fig.3-1 Geometry and dimension of the designed sample. a) Sample with 10mm applicable cutting length, and b) Sample with 20mm cutting length

### 3.1.2 Property instruction of used PBCT machine

The used Pendulum Based Cutting Test (PBCT) machine is shown in Fig.3-2, in which a dial is used to record the release angle and end angle of the pendulum. As described, with the weight of pendulum, the energy consumed during a single test can be calculated. The cutting sample is fixed to the movable pendulum and the cutting tool is positioned on the base consisting of tool holders, cutting tools, wedge lever, dynamometer etc.

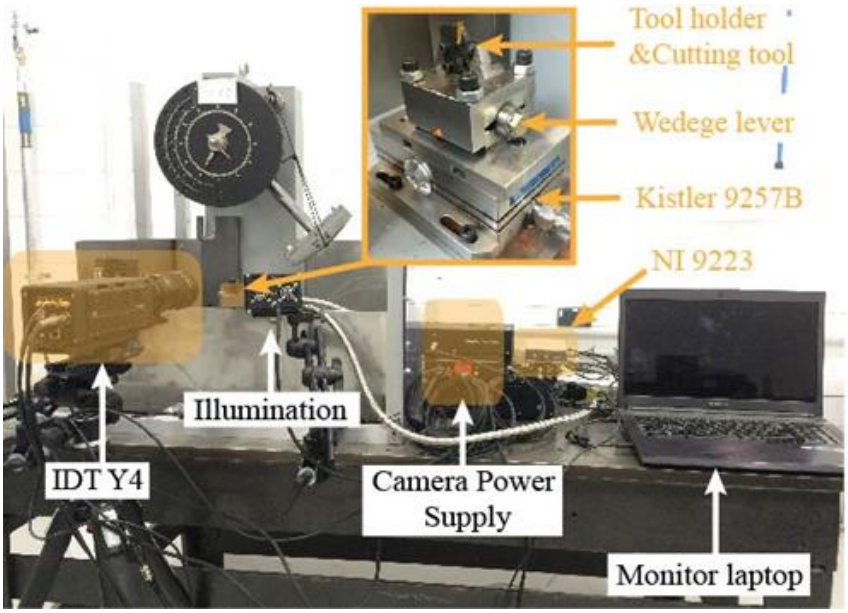



Fig.3-2 Photograph of designed Pendulum Based Cutting Test (PBCT) machine

### 3.1.3 Cutting tools and wear measurement

The cutting tools used for the tests in this thesis were provided by SECO Tool AB in Sweden. There are different cutting conditions (dry and wet cutting) designed

in this research. Therefore, different cutting tools for dry and wet cutting condition are employed correspondingly.

For the dry cutting condition, cutting tools (LCGN160400-CP500) with customized geometry were provided, shown in Fig.3-3. Considering the validation requirement of the proposed PBCT method, tools with different rake angles (-10°, 0° and 20°) but same clearance angle (5°) and tool radius (5 μm and 50 μm) are used as an example in Fig.3-4.

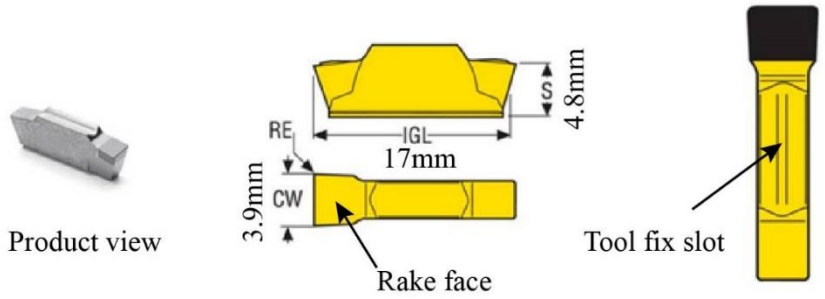
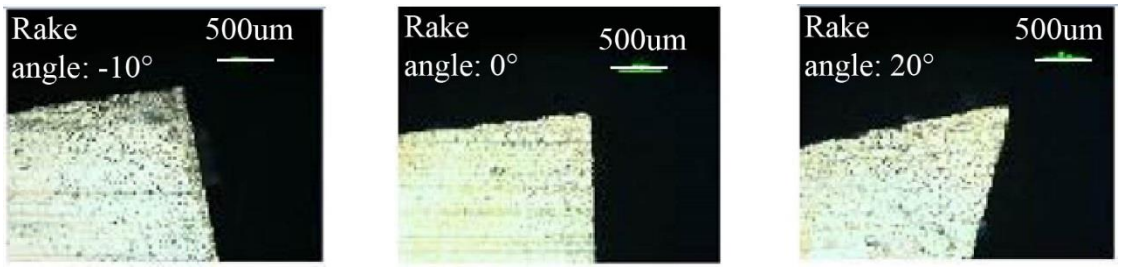



Fig.3-3 Main geometry of used customized tools for dry cutting




a) b) c)

Fig.3-4 Example of tools with different rake angles. a) Negative tool, b) Neutral tool, and c) Positive tool

As well as tooling for dry cutting, Fig.3-5 shows the cutting tool geometry provided for wet cutting conditions. Tools with different rake angles and tool radii are also used. It is worth noting that the tools are customized and the tool rake face is neutral to eliminate effects from rake face geometry variation while studying the energy distribution of cutting. Therefore, the practical rake face is different from the example in Fig.3-5. To investigate the cutting process when the tools are worn, cutting tools with different wear length in the flank face are prepared (as example in Fig.3-6) and measured in microscope. The wear on the tools are ground with sickles at first to get anticipated length and later applied in the practical turning machining to make worn approaching the practical worn in machining.

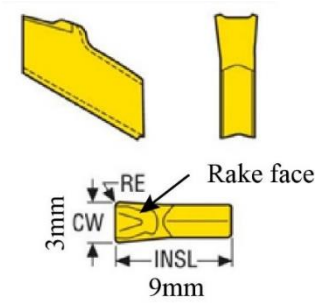
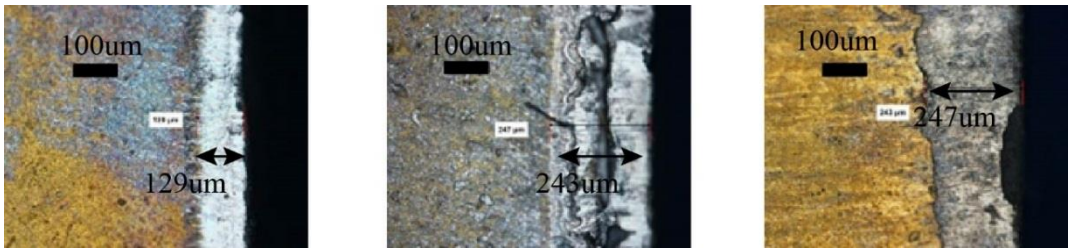



Fig. 3-5 Main dimensions of used tools for wet cutting




a) b) c)

Fig.3-6 Example of tools with different wear length on flank face. (Wear length: a) 129μm, b) 243μm and c) 247μm)

### 3.2 Cutting process monitoring and signals analysis

As one of the advantages of this proposed method, it is easy to monitor the cutting process in detail thereby providing enough information for in-depth analysis of the cutting performance. The corresponding cutting force of the cutting process is measured with dynamometer. A high speed camera is employed to monitor the chip formation process and the interaction between cutting tool and workpiece materials. Corresponding signal and data processing methods are used to analyse the acquired information.

#### 3.2.1 Monitoring method and equipment

To acquire the cutting force during processing, a Kistler dynamometer (9257A) was chosen and installed. The dynamometer is equipped with a water resistant cable enabling working in wet cutting. As the designed cutting sample has lengths of 10 mm or 20 mm, the cutting process time will be around $10^{-2}$ s even with low cutting speeds such as 30 m/min. Therefore, a very high data acquisition rate is needed to capture the cutting force over the very short cutting times. Therefore, a corresponding amplifier was used to amplify signal exported from dynamometer and NI 9223 data acquisition is used (Fig.3-7). This model has the sample rate up to 1 MHz, which will provide the ability to monitor detailed force variation.

Also, high speed camera (IDT Y4-S2) was used and real-time cutting speed was derived from the videos to acquire cutting process videos in detail for validating the proposed PBCT method. The camera has a maximum frame rate of 5100 fps at the full resolution (1024x1024), giving the possibility to capture the cutting process over both cutting lengths (10mm and 20mm). High density lux light is used to illuminate the objective as required for high speed cinematography. Accessories such as light power, camera power, clamp arms and tripod are used as well. A full list of equipment for monitoring the cutting process is provided in Table 3-1.




Fig 3-7 Equipment used for force monitoring. (Dynamometer, charge amplifer and data acquisition)

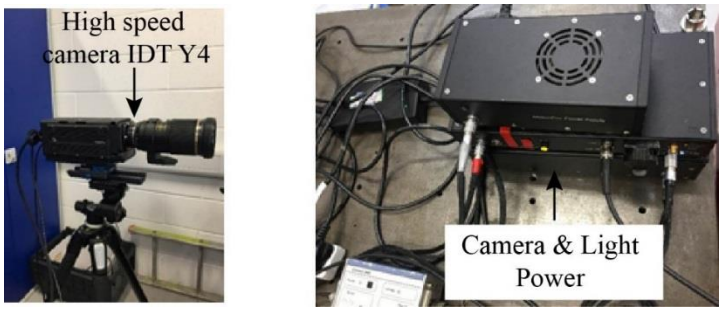



Fig.3-8 High speed camera and accessories for cutting process monitoring

Table 3-1 List of equipment used in PBCT

| Number | Name | Type |
|---|---|---|
| 1 | PBCT machine | Designed |
| 2 | Dynamometer | Kistler 9257A |
| 3 | Amplifier | Kistler |
| 4 | Data acquisition | NI 9233 |
| 5 | High speed camera | IDT motion studio |
| 6 | Monitor computer | Thinkpad X260 |

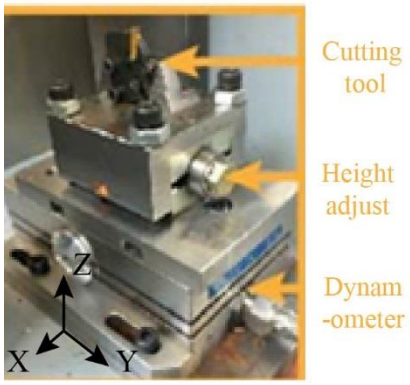
### 3.2.2 Processing method for monitored signals

Multiple types of monitoring equipment were used to capture information (force and video) during cutting processes. To acquire useful data for analysis, the raw data needed to be processed with corresponding techniques.

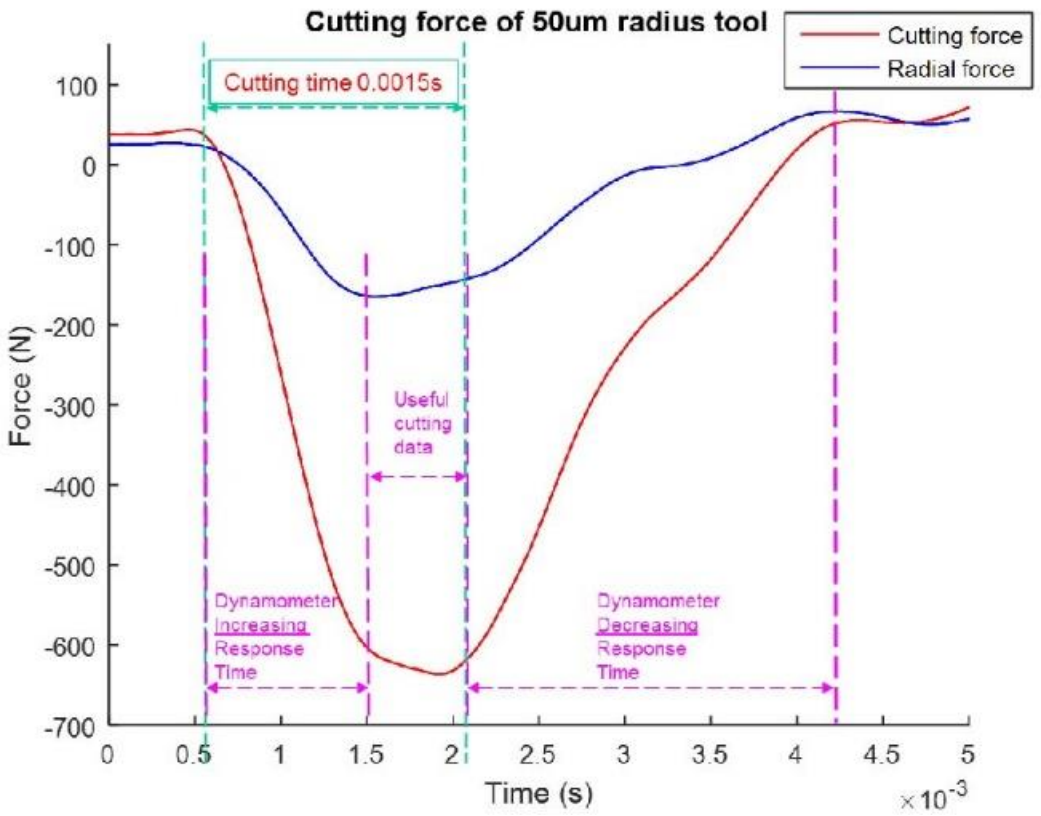
1) Signal processing for cutting force

As described above, the cutting force signal can be acquired via the dynamometer, and the processing method for these signals will be discussed here. The signal generated in the dynamometer by the cutting force in both the cutting and radial direction (y and z direction in Fig.3-9) are acquired with Labview Signalexpress software. The dynamometer is placed on the bottom with y and z direction used corresponding to the 2-D orthogonal cutting.

The designed samples have small geometry (10 mm to 20 mm), while practical cutting speeds were chosen (e.g. 50 m/min). In this case, the cutting time will be very short, in the level of $10^{-4}$ s for all total cutting processes. To capture the detailed variation during cutting processes, a sample rate of 500 kHz per channel was chosen to capture many sample points for analysis. The acquired voltage signals were transferred to a charge amplifier as described. Then, the voltage signals in TDMS format is transferred into a text file for analysis in Matlab. A plotted example of monitored cutting force for 5 mm cutting length sample is shown in Fig.3-9, where it is found that the total cutting time is around $1.5^{-3}$s in the cutting speed of around 200 m/min. As the cutting process is short, the response time of the dynamometer can be identified at the start and end of the cutting process (rise time).




a)




b)

Fig.3-9 Cutting force monitoring system. a) Cutting tools fixed on dynamometer, and b) Example of acquired cutting force

2) Video processing techniques

A high speed camera was used to monitor the cutting process, while the video was processed by Motion Studio software. An exemplar video frame during cutting is shown in Fig.3-10, where the sample (5 mm length) is processed by the cutting tools and chips are generated. As a high frame rate was used, the cutting process could be followed in detail. The cutting speed can be calculated from the movement of the target in each acquired frame, as the time between two frames is constant (as long as the frame rate is known). With the tracking function of Studio, the movement of tracked points in different frames can be acquired and corresponding cutting speeds and acceleration can be calculated (Fig.3-11). Therefore, the cutting speed variation is identified for the following analysis. As the cutting force is monitored at the same time, the cutting speed and force could be correlated together thereby the main properties of cutting process are comprehensively monitored.

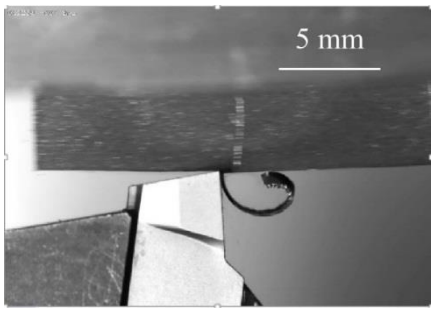



Fig.3-10 Example monitored video of cutting process. (Rake angle: 0°; tool radius: 50μm; cutting depth: 0.1mm; cutting width: 1mm; cutting speed: variation)

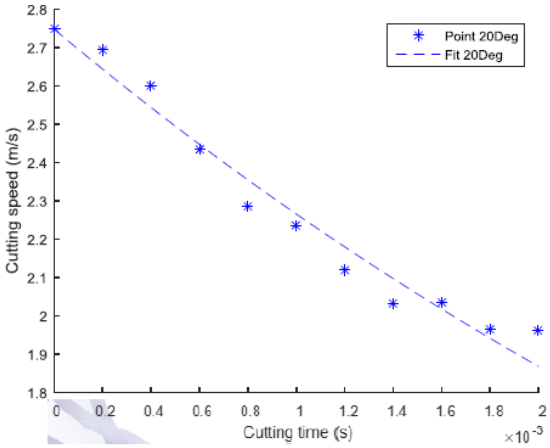
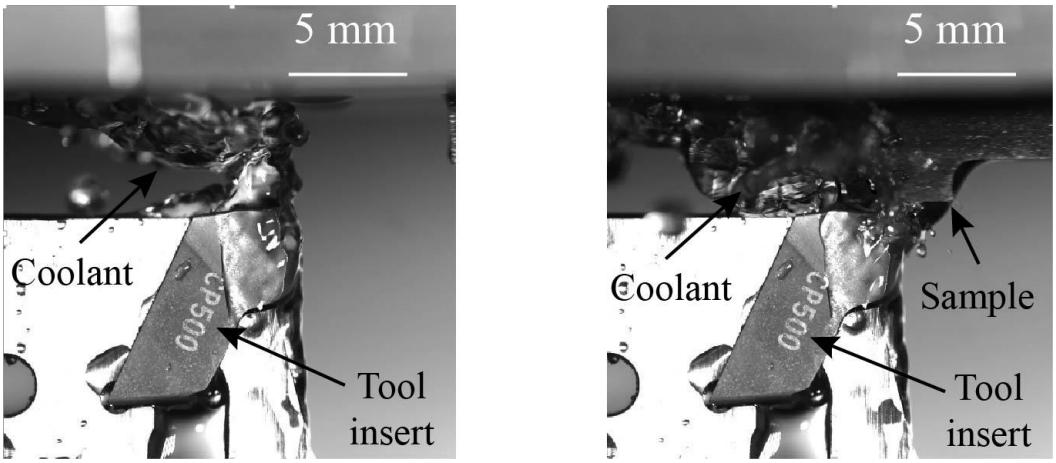



Fig.3-11 Example of tracked speed points for cutting process and fitted line. (Rake angle: 20°; tool radius: 50μm; cutting depth: 0.1mm; cutting width: 1mm)

Regarding the wet cutting process, liquids are delivered via the internal coolant channels in the tool holder. An example illustration of the coolant process is presented in Fig.3-12 with water. There is coolant liquid passing on the rake and clear surface of the cutting tool, meaning that the coolant liquid can be jetted into the cutting centre to achieve the maximum cooling efficiency. The movement of the sample passing the cutting area shows that the wet cutting design could act as coolant during the cutting process and it could simulate the practical turning coolant situation.




a) b)

Fig.3-12 Wet cutting condition with internal coolant tool. a) Coolant free flow scenario and b) The moment of machining sample

### 3.3 Surface integrity and metallurgical inspection method

With the proposed PBCT method, the orthogonal cutting process can be carried out without using conventional machine tools. To investigate the cutting performance of materials with PBCT method, the machined surface integrity must be evaluated to determine the quality in the machined state. The adopted method, procedure and criteria will be presented as follows. It mainly includes the sample preparation, optical and SEM study methods, EBSD investigation of machined surface, residual stress and nano-hardness of the superficial surface.

#### 3.3.1 Sample preparation for inspection

The superficial surface quality of machined Inconel 718 samples will be studied to validate the possibility of evaluating material cutting performance with the PBCT method. Also, surface integrity is regarded as the evaluation target with the energy based method. To allow the full surface integrity analysis at microscales with optical or SEM techniques, the specimen must be prepared properly.

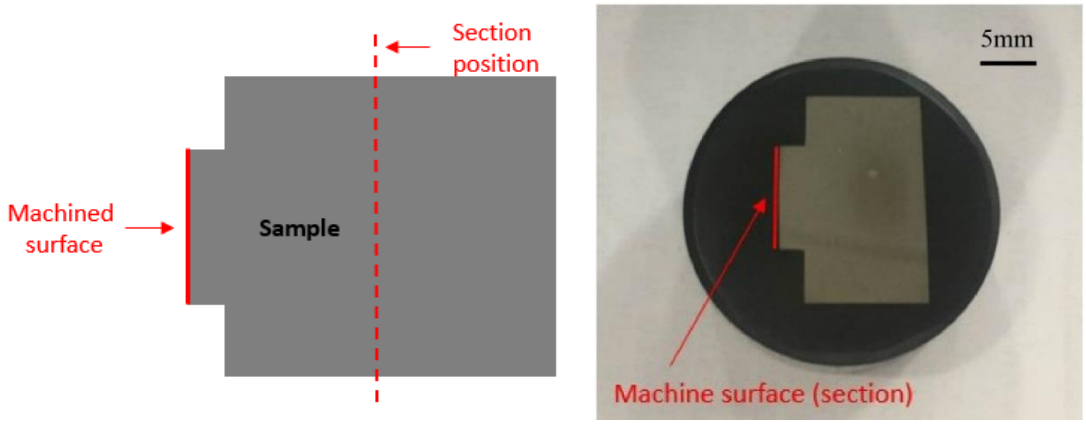
Due to the mounting machine size requirements (Fig.3-13a), samples are cut into small pieces to adapt to the maximum 30 mm diameter in the machine. To achieve this, a cutting machine (BRILLANT 220) (Fig.3-13b) with an Acu-thin abrasive wheel was used to cut the workpiece. As the material (Inconel 718) is hard to machine, a low feed rate of 0.1 mm/min and water based coolant were used to minimise both mechanical and thermal alterations. Illustration of the cutting section and geometry of the sample are presented in Fig.3-14, where the excess

part of the sample is removed. Once the workpiece samples are sectioned, they were positioned into the mounting machine to be covered by conductive Bakelite as shown in Fig.3-14.




a) b)

Fig.3-13 Machine used for sample preparation. a) Conductive resin mounting machine and b) Cutting machining for sectioning samples




a) b)

Fig.3-14 Sample preparation explanation. a) Section illustration of machined workpiece and b) Example of mounted sample

As described, the machined chip dimensions and properties are included in the analysis of material cutting performance, therefore they are collected after machining, although they are very small (length of 10mm and rolled up). Similarly, they need to be mounted for analysing and measuring accurately, but the hardness and strength of the chips are relatively weak after machining, such that they are unsuitable to be mounted with the pressure mounting machine. Chemical transparent mounting with epoxy resin was instead used to mount the chips.

The directly mounted sample requires a series of polishing operations before precise observation and evaluation. Samples were ground using silicon carbide paper through to 2400 grit, and then polished to a 1μm finish on DUR (6 μm) and NAP (1 μm) cloths as seen. While these procedures are the common preparation routine for the following observations, there are additional requirements for optical and SEM or EBSD inspection methods accordingly.

### 3.3.2 Optical and SEM inspection of superficial surface

The machined surface integrity can be revealed by the direct material drag and deformation under the machined surface, which can be a direct reflection of the surface properties. Therefore, optical and SEM observations can be used to determine the surface integrity qualitatively.

1) Optical microscope

An optical microscope (Fig.3-15: Nikon) was used to evaluate the machined surface by observing the morphology and the deformation of the sub-grains with magnification from X5 –X100 was used.

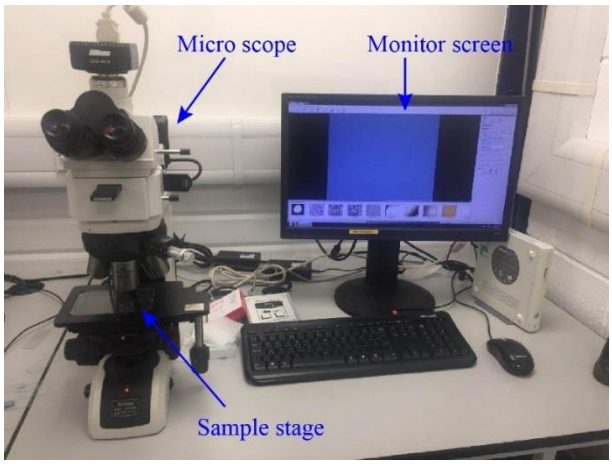



Fig.3-15 Used microscope for preliminary superficial surface deformation observation

As mentioned, the sample is mounted in resin before measurement. However the surface directly after mounting is not suitable for inspecting the in-depth deformation of the sample. Electrical etching is therefore adopted to make the contrast between boundaries in microstructure clear for observing. As seen in Fig.3-16, the etching was carried out with 10% orthophosphoric acid in distilled water using a current of 2-3A with stainless steel wires as the anode and cathode.

It gives the ability to investigate the material drag and grain deformation in the superficial layer of the machined surface (Fig.3-17) as well as the mounted chips.

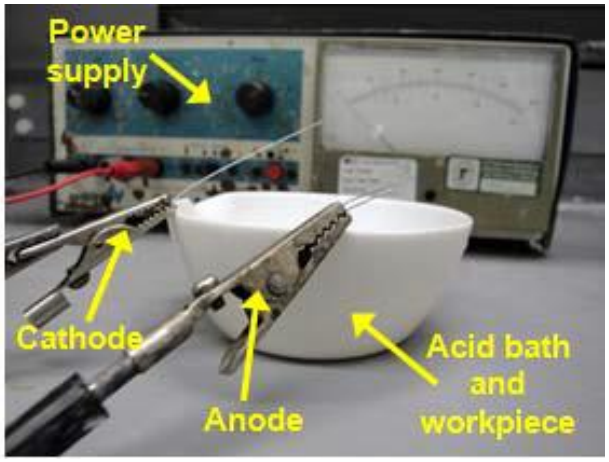
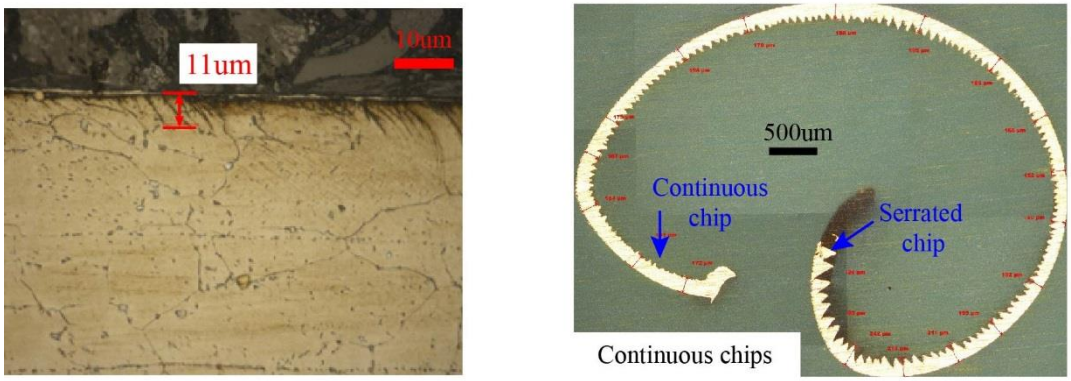



Fig.3-16 Equipment used for carrying out electrolytic etching on samples for optical and SEM observation




a) b)

Fig.3-17 Examples of microscope pictures of superficial layer and chips. a) Example superficial surface deformation (material drag) and b) Generated long chips with morphology variation at start and end

2) Scanning Electron Microscope (SEM) operation

The surface defects (e.g. anomalies) are probably generated in the machining of Ni-based superalloys with inappropriate cutting parameters or conditions. Normally, these kinds of anomalies, such as micro cracks or plastic deformation, are in the level of 10 μm or less, in which case the optical microscope can not capture the information in enough detail. To overcome this drawback, SEM is employed to get high quality images with magnification from 1X to 100,000X.

Similar to optical microscope measurements, samples require electrical etching before observation in the SEM. The sample of interest is placed into the vacuum chamber, and properly fixed on the work stage with a sample holder, as shown in Fig.3-18. The sample is aligned with the electron detectors once the chamber is closed. The chamber must be evacuated before the electron beam (spot size of 3 with 15 kV voltage) can be launched. Once the electron beam is activated, an image of the target will be displayed on the screen. A standard procedure of focusing, stigmatism correction and brightness or contrast adjusting need to be carried out to achieve an optimal image. However, there are two modes, secondary electron (SE) and backscatter electron mode (BSE), which can be selected for the SEM imaging.

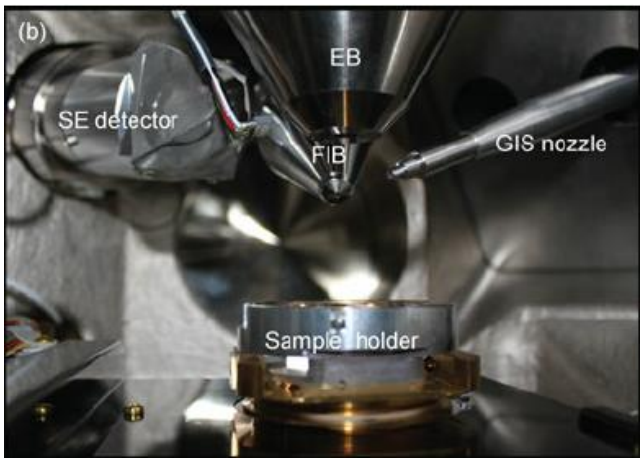



Fig.3-18 Example of working stage in a JEOL 6490LV SEM machine

The ejected electrons from the k-orbital of the specimen atom by inelastic scattering interactions with beam are detected by Everhard-Thornley detector in the secondary election mode. With this mode, only the surface and several nanometers depth properties can be revealed because of the low energies of k-orbital electrons. In contrast, the backscatter electron mode uses high-energy electrons originating from the election beam, which are reflected or back-scattered from the specimen interaction volume by elastic scattering interactions with specimen atoms. The BSE mode is used to detect contrast between areas with different chemical compositions as the heavy elements (high atomic number) backscatter electrons are stronger than the light elements (low atomic number), thus to appear brighter in the images. For the investigation of machined surface analysis, the SE models are often used to highlight the defects on the near surface of the workpiece materials, in which case normally no exotic chemical elements are introduced.

### 3.3.3 EBSD evaluation of surface integrity

With the increasing surface integrity requirements of machined workpiece components, defects left on the machined surface and their effects are becoming more important than ever. The results obtained from optical and SEM investigations are not enough to support the discussion. Therefore EBSD, which is able to provide in-depth information at the grain level of the material to understand workpiece deformation and variation after machining, is introduced. Accordingly, a FEGSEM (field emission gun scanning electron microscope) Jeol 7100F machine (Fig.3-19) is used to carry out the EBSD measurement.

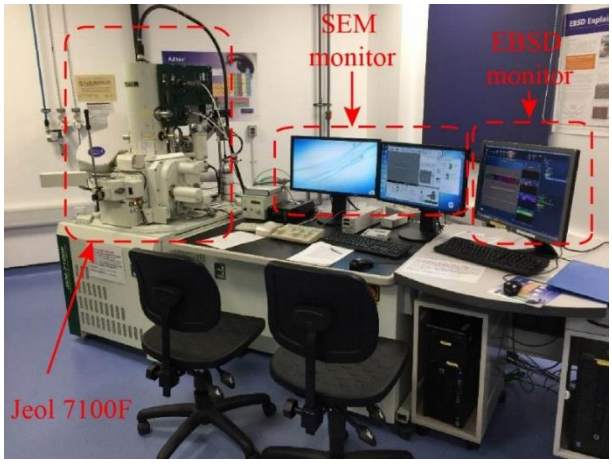



Fig.3-19 Used Jeol 7100F machine for EBSD measurement on superficial surface on machined workpiece

By using the EBSD detector, signals of different grains can be collected for the following analysis. To process large amounts of signal data and information acquired, Aztec software (Fig.3-20) is used to properly set the measurement condition and make the signal viewable. Their standard procedure to adjust the setting conditions to get better signal for measurement is used.

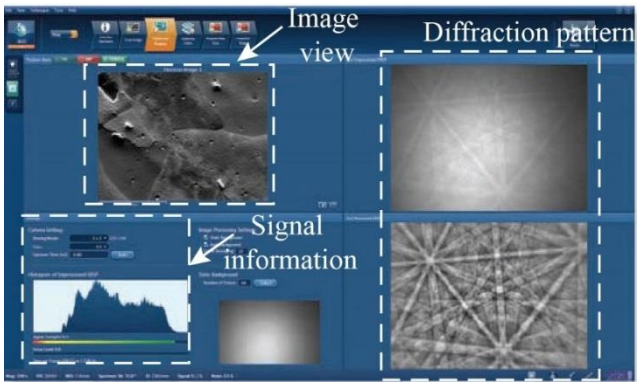



Fig.3-20 Example view of Aztec software during the EBSD measurement

Regarding sample preparation for EBSD measurement, the procedure for SEM is not enough. Therefore additional steps are required to acquire clear and strong signals. The general rules for sample preparation are still used until the final polishing stage without any deviation from the normal route employed. Subsequently, polishing with additional colloidal silica on cloth pads (Fig.3-21) is a necessary step for the Inconel 718 sample preparation to get a suitable finish for EBSD.

At several stages, samples polished with silica are still not good enough to get the signals or better images with the signals. To improve the surface finish further, a Vibropolisher (Buehler) machine (Fig.3-21) was used to prepare higher quality polished surfaces for EBSD. The 7200 cycles per minute horizontal motion produces a very effective polishing action, providing superior results, exceptional flatness and less deformation on the section surface therefore suitable for EBSD observation. The vibratory polisher removes minor deformation remaining after mechanical preparation, revealing the stress-free surface without need for the hazardous electrolytes required by electro-polishers.




a) b)

Fig.3-21 Machine used for high quality surface finishes sample preparation. a) Polishing machine will silica liquid and b) Vibropolisher-VibroMet2 (Buehler)

### 3.3.4 Residual stress measurement of machined sample

Residual stress states are critical for the workpiece service performance and fatigue life, therefore, it is necessary to examine it after the machining process. Here a Proto iXRD (Fig.3-22) is used to carry out the residual stress measurement on the machined sample. As the sample is small in geometry, no sectioning is needed for residual stress measurement on this machine. The residual stresses in two directions (axial and orthogonal) are measured to fully understand its distribution on the measured surface as shown in Fig.3-23.

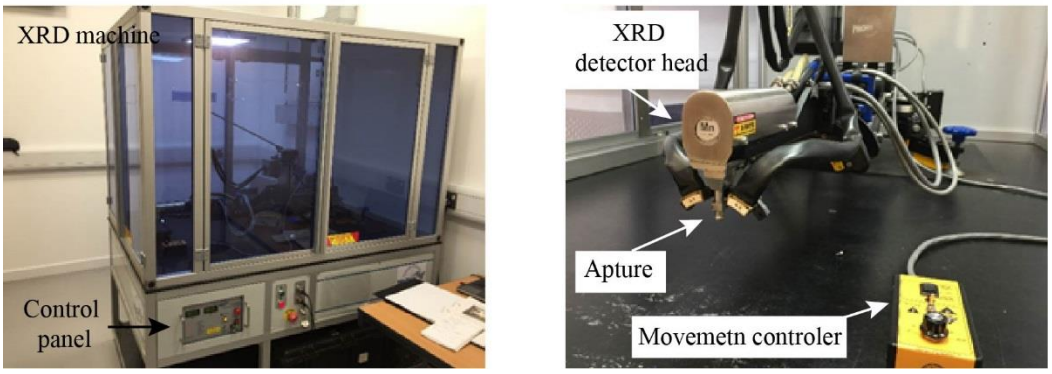
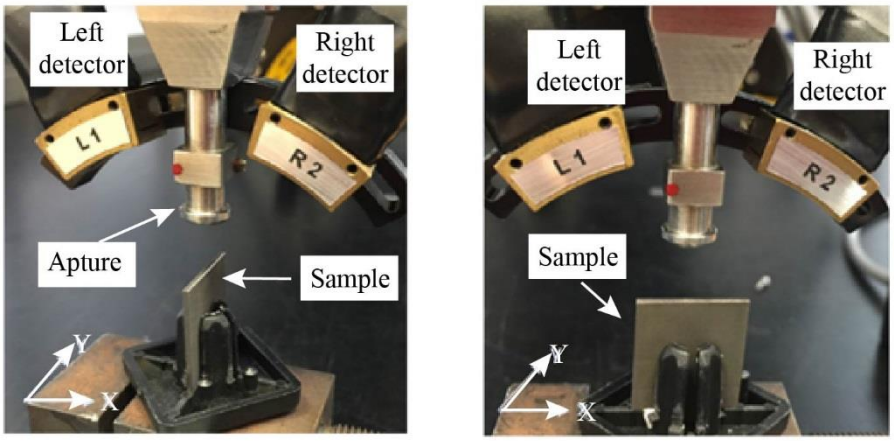



Fig.3-22 The XRD equipment used for residual stress measurement of the machined sample




a) b)

Fig.3-23 Illustration of measurement scenario of target sample with XRD machine in both a) Hoop direction and b) Cutting direction

To explore the residual stress in the superficial layer of the machined surface, its values at different depths from the surface are tested with the help of electro-polishing techniques. The corresponding electro-polish machine (PROTO Electrolytic Polisher Model 8818-V3) is used to carry out electrolytic polishing (Fig.3-24). The electrolytic polishing is a process where a metal sample is the anode in an electrolytic cell. Material is removed by electrolytic action in such a manner that the surface irregularities are removed and the surface finish will become smooth and bright. As seen in Fig.3-24, with electro-polishing, a potential difference exists between the matrix and secondary phases. The anode film controls the rate at which the dissolution products can diffuse away from the anode. Since there is a difference in concentration gradient, preferential dissolution occurs at the asperities and the surface becomes "smoothed". The existence of such a surface layer could also explain the difference between etching and polishing

conditions. Etching will occur if the electrolyte has free access to the anode surface since anodic dissolution occurs preferentially at the sites of high energy. Different polishing depth under the machined surface (Fig.3-25) can be achieved by controlling the polishing time.

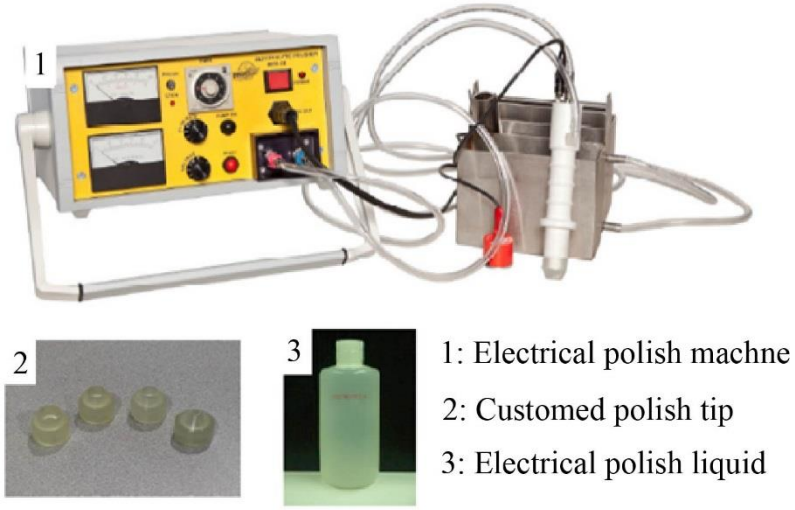
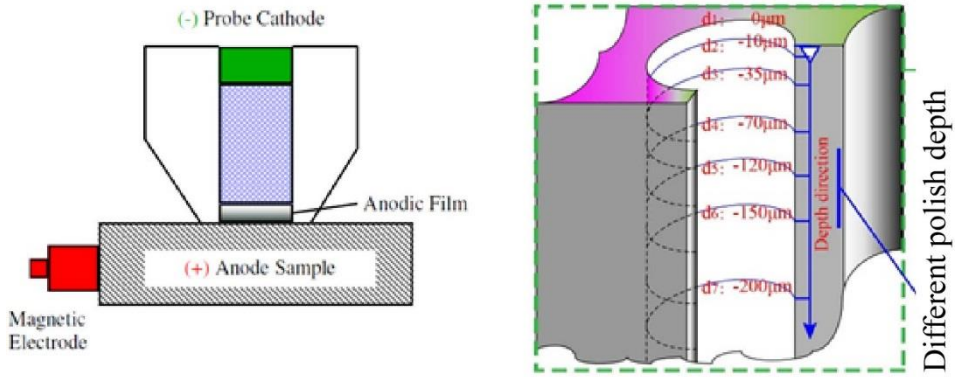



Fig.3-24 Package of Proto Electrolytic Polisher including machine, tips and polishing liquid




a) b)

Fig.3-25 Electrolytic polishing principle illustration. a) Electrical polishing theory and b) Different polishing depth achieved with electrical polishing

### 3.3.5 Nano-hardness investigation of superficial layer

To explore the mechanical properties of layers as thin as 20 nm, nano-indentation measurement is introduced to study the hardness, modulus, thin film adhesion and toughness. Here, a MicroMaterials Ltd Nanotest Platform 3 macnine (Fig.3-26) is used to test the nano-hardness of the superficial surface layer.

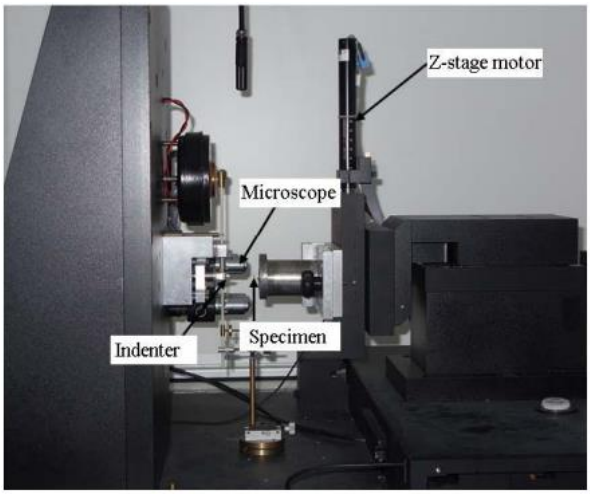



Fig.3-26 The Nano-test platform used for Nano-hardness measurement [132]

The machined sample is firstly mounted into resin, followed by polishing in the sectioned surface as shown in Fig.3-27. The indentation is carried out at the superficial surface layer (see sectioned area) in different positions to a depth of around 30 μm. Several tests will be implemented in this area to present the material property variation under the machined surface as a function of distance to surface. Hardness is regarded as the main factor here to present the surface integrity and will be discussed in the following chapters.

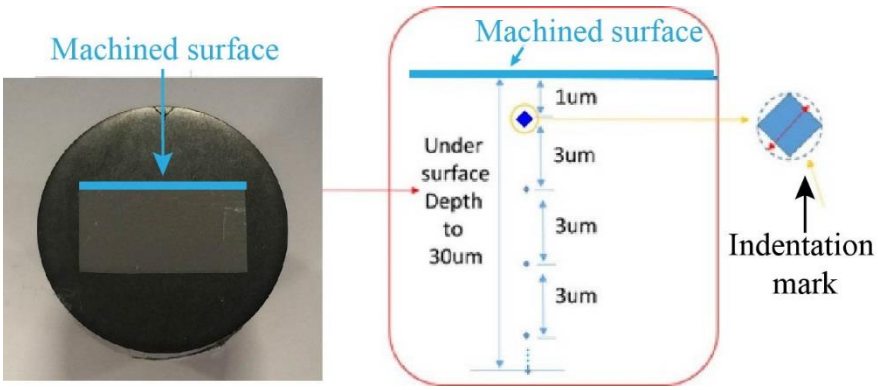



Fig.3-27 Illustration of indentation position in superficial surface of the measured sample.

# Chapter 4

# Pendulum-based cutting test (PBCT) concept for surface integrity related machinability studies

In this chapter, the pendulum-based cutting test (PBCT) method, which can be used to undertake machining experiments instead of machine tools will be presented. The novel concept of evaluating material machinability and surface integrity via inspecting the consumed specific energy in cutting process is illustrated as well. Firstly, the principle of the PBCT machine and energy evaluation concept will be discussed. Then, the energy calculation process and detailed design of proposed PBCT machine will be shown. In addition, the wet cutting conditions for the proposed PBCT machine will also be designed and presented.

## 4.1 Illustration of PBCT principle

### 4.1.1 Problem definitions

Superalloys are widely used in the aerospace industry and new types of superalloys are also being developed due to their excellent performance in extremely harsh environments. However, they are difficult to be manufactured into desired geometries because of their high strength and heat resistance. The surface integrity related machinability evaluation of such kinds of superalloys is essential for aerospace manufacturers.

As discussed in the literature review, many studies have investigated the machining performance and surface integrity of difficult-to-machine materials. Most of the research is carried out separately for several specific factors. However, there are too many relating factors, including tool geometry, tool materials, cutting speed, and temperature etc., that affect material machinability. Therefore, normally the test results cannot be transferred into other cutting conditions as every single test is unique to a specific cutting condition. As a result, researchers are studying cutting performance via energy based methods, which treat the specific cutting energy as the evaluation factor.

There are a limited number of studies concentrating on machining process energy, and most of these do not provide a clear correlation between machined surface integrity and consumed energy. A simple and effective experimental method to achieve this will significantly improve research progress. . As presented in Chapter 2, most of the existing machinability evaluation methods are based on practical

machining tests in CNC machine tools with variation of cutting parameters, requiring large amounts of bulk material. Practical processes therefore consume time and money, especially for expensive metals (nickel-based alloys, titanium alloys, etc.).

While considering such materials under laboratory conditions, it is impossible to undertake large machining tests on machine tools using traditional testing methods, when only small volumes can be used. Traditional methods may delay the development of new materials as researchers have no intermediate knowledge on new material machinability leading to inherent drawbacks in efficiency, as well as post-machining surface integrity.

### 4.1.2 Introduction of PBCT method

A Charpy machine (Fig.4-1) (also known as the Charpy impact machine), is commonly used to test material toughness. It is a standardized high strain rate test, where strain rates are similar to cutting processes, and measures the amount of energy absorbed by target material during fracture to determine material toughness.

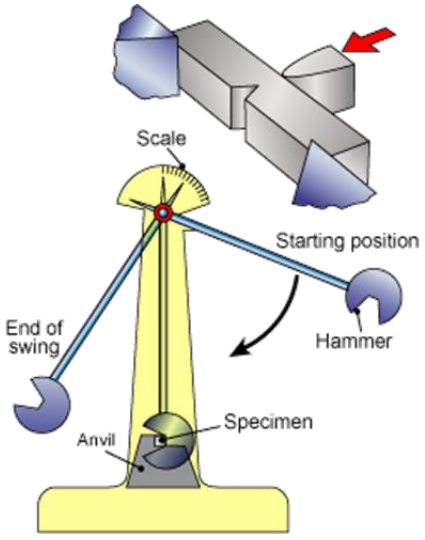



Fig.4-1 Schematic of a standard Charpy machine for materials toughness test

Inspired by the charpy test machine used for material toughness, an orthogonal cutting test method is proposed in Fig.4-2. The cutting tool can be fixed to the tool holder which is kept stationary on the base. The target cutting sample is fixed on the bottom of the pendulum and moves freely with the pendulum. Cutting speed is acquired from gravity during the forward (downwards) swing of the moving pendulum. When the pendulum is lifted to an angle and released, the pendulum

accelerates, achieving the highest speed at the lowest point of the moving cycle, where the cutting process occurs. The relative movement between the stationary cutting tool and the moving sample provides the cutting speed and can be controlled by adjusting the release angle of the pendulum. In this way, samples can be machined at predetermined cutting speeds and orthogonal cutting tests can be implemented as shown in Fig.4-3.

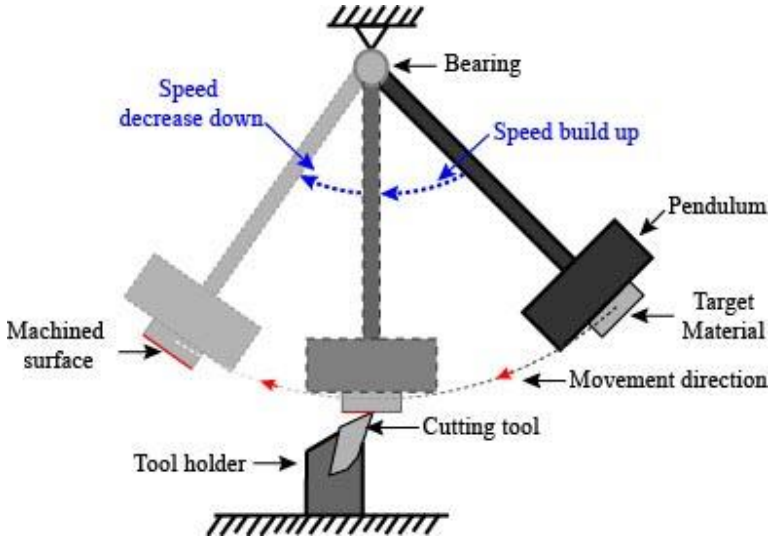



Fig.4-2 Principle of orthogonal cutting in proposed PBCT concept

For the cutting process calculation, an example is presented in (Fig.4-3). The pendulum is released from the start position with an $\alpha$ angle to the vertical direction. When the pendulum passes the lowest position, the sample will be machined by the cutting tool fixed to the base. After the cutting process completion, the pendulum will rise and arrive at the final position, $\beta$ angle to vertical direction, which is less than $\alpha$ as energy is transferred in cutting the sample.

If the mass of the pendulum, $m$, and the arm length, $r$, are known, the energy consumed during cutting can be expressed as

$$E = mgr(1-\cos\alpha) - mgr(1-\cos\beta) = mgr(\cos\beta - \cos\alpha) \quad (4\text{-}1)$$

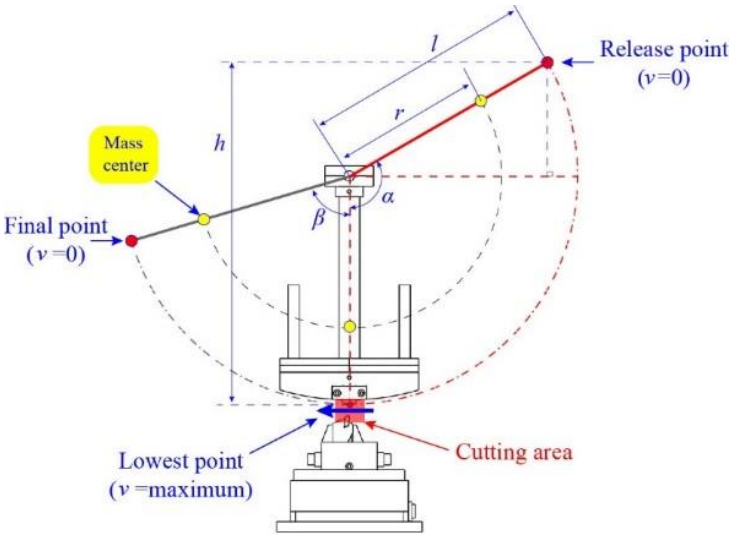



Fig.4-3 Principle of implemented orthogonal cutting process in the proposed PBCT machine

The cutting speed at the lowest point of the swing (the start point of the machining) can be calculated according the energy conservation theory with following the equation:

$$\frac{mv^2}{2} = mgh \tag{4-2}$$

where $h = l \times (1 + \sin\alpha)$, then the corresponding cutting speed will be

$$v = \sqrt{2 \times g \times l \times (1 + \sin\alpha)} \tag{4-3}$$

where v is the calculated cutting speed; *g* is the standard gravity factor; *l* is the pendulum arm length as shown in previous figure; and *α* is the releasing angle.

With the proposed pendulum method, it is possible to replicate the orthogonal cutting process without using machine tools. The cutting area during the cutting process is shown in Fig.4-4, where the sample is machined by the fixed cutting tool and a chip can be generated. The cutting condition, which is defined by cutting depth, cutting width, tool rake angle, tool tip radius and clear angle is shown in the Fig.4-4. It is evident that this modified machine can be used to simulate orthogonal cutting processes instead of testing using machine tools.

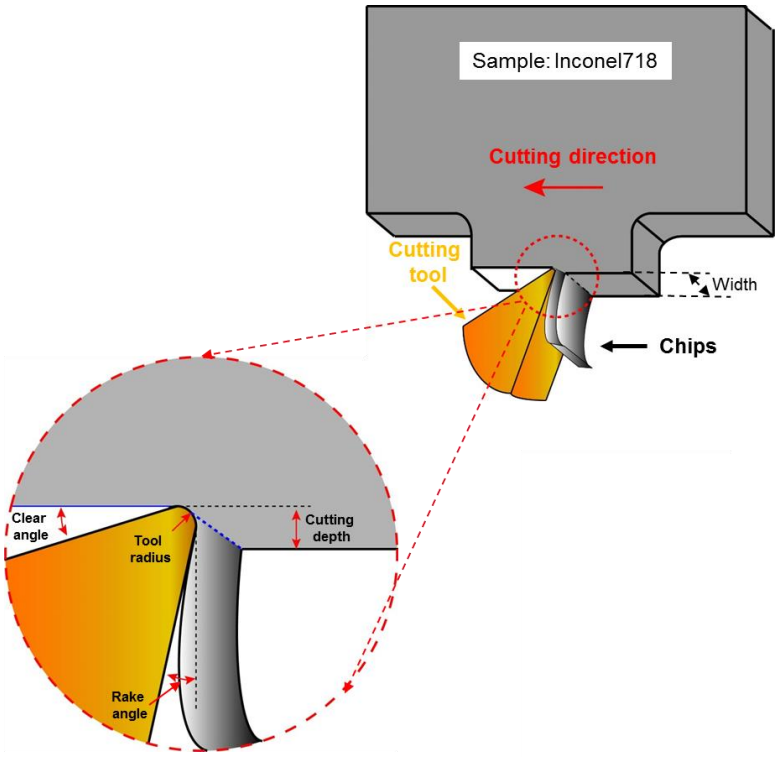



Fig.4-4 Illustration of cutting characteristics in the cutting areas during the cutting process on PBCT machine

### 4.1.3 Advantages of the PBCT method

Compared to conventional methods where material surface integrity related machinability evaluation is based on various machining tests using machine tools, which is time and money consuming, the proposed PBCT method is advantageous.

The greatest advantage of PBCT is that it can replicate orthogonal cutting conditions, allowing the evaluation of surface integrity related machinability, without expensive setups or large test workpiece requirements. Therefore, it is possible to study material surface integrity related machinability without carrying out tests using machine tools. As there is no continuous energy input during testing, the cutting speed will continuously decrease from the start of cutting, meaning that the speed over a single test is constantly changing. With appropriate cutting parameters choice, the cutting performance of a target material at different cutting speeds can be studied in a single test, significantly reducing the testing time and amounts of materials.

Sample geometry using this method is flexible requiring small amounts of material, allowing the method to test expensive materials or small batches. Considering new materials, which need to be machined into various parts for many industries such

as automotive, nuclear, medicine and chemical industries etc., it is challenging to study their cutting performance with conventional methods, so a new method is demanded. PBCT will give an approximate evaluation of material cutting performance before it is put into industrial production, thereby improving the efficiency of materials development and reducing the risk of failure.

In addition, this design has the ability to carry out thermal investigations in cutting performance. As the cutting length in this method is restricted to very short timescales, cutting temperature elevation in these tests will be less, meaning that this method is temperature independent. In addition, fewer thermal effects mean that with appropriate design, wet cutting conditions can be introduced into the method, therefore enabling investigation of coolant lubrication performance.

Although this method is initially proposed for surface integrity related machinability investigations of superalloys, it may also be used to study cutting performance of other metal materials and non-metal materials, such as 3-D print materials, plastic materials and composite materials etc. The only modification required is the change in target material, which in this method is easy to replace and flexible in geometry.

Apart from the above advantages, the cutting performance and wear mechanism of cutting tools can also be studied with this method using a high speed camera. Oblique cutting can be achieved with modification of the tool holder angles in horizontal direction on the base. In addition, instead of using quick-stop devices in the machine tools, which is complicated and not safe, this method could be used as a quick stop equipment as well with little materials by appropriate modification.

## 4.2 Surface integrity related machinability evaluation with energy concept

With the increasing quality requirement of components in application, the evaluation of surface integrity has become critical to processing. Traditionally, surface integrity is evaluated by carrying out serial measurements on cutting chips, cutting force, tool condition etc. and there is no standard evaluation process for these kinds of tests. As known, the surface integrity is affected by variation in cutting parameters. However, no method to transfer this knowledge from one process to another is applicable as there is no unified approach for relating the appearance of particular surface defects at particular thresholds of process parameters/measurements so far. To make the evaluation process simpler and quicker, an energy aspect method is proposed. As all cutting processes are

completed by the energy loaded on the cutting tools, the machined surface may be evaluated based on the input energy to damage and form new surface during cutting processes, therefore not relying on a specific cutting process.

### 4.2.1 Energy distribution in orthogonal cutting areas

To study the cutting performance via investigating energy consumed during the cutting process, the energy distribution in different areas during orthogonal cutting is treated as an example. A simple and novel method which is based on the calculation of energy consumed in machining and corresponding area (shear, friction and ploughing) to evaluate the surface integrity related machinability of materials is proposed. The relationship between energy consumed in different cutting areas and corresponding surface integrity can be studied.

As shown in Fig.4-5, the total energy input for orthogonal cutting is used to remove materials in front of the cutting tool and form a new machined surface. Overall, the input energy is used to form chips, consumed by friction between chip and the tool and the friction between the tool and the surface. Specifically, the energy consumed by tool-surface friction can be divided into the ploughing energy caused by the cutting tool radius and the worn energy caused by interaction between the worn cutting tool and machined surface. It is worth noting that there is no worn energy for fresh tools, therefore this factor can be neglected for these tools.

It is clear that the generated machined surface is strongly related to material deformation in the cutting areas (shear, friction, ploughing and worn). In this case, the machined surface integrity can be related to the energy input to activate the corresponding deformation and form the surface by the cutting tool. After the energy consumed during the cutting process is evaluated, the machined surface integrity can be predicted without carrying out measurement on machined components. Then, an energy table of thresholds for different machined surfaces could be built. Taking the orthogonal cutting experiment as an example (Fig.4-6), material is removed by the cutting tool with relative rotation movement, where energy input to accomplish this process is divided into the four different parts (neglecting worn energy for fresh tools), and these energy determine the properties of the machined surface integrity.

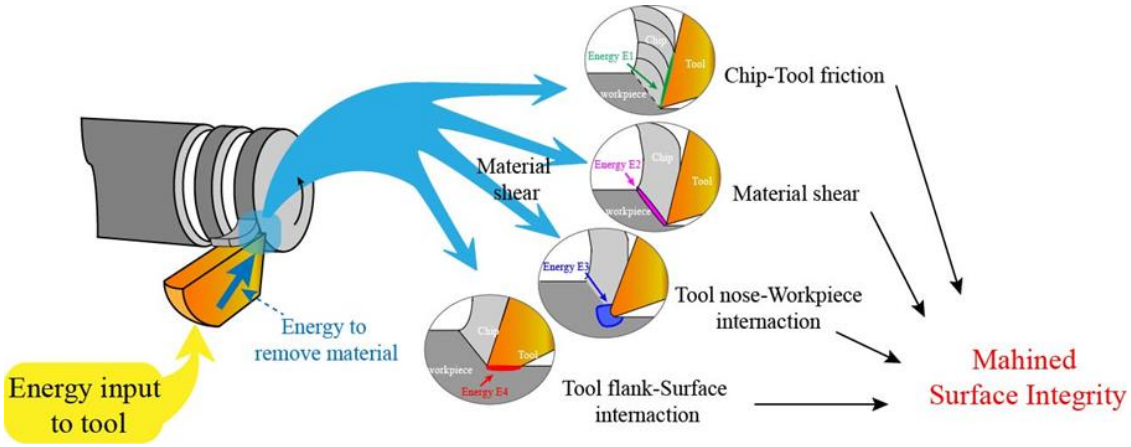
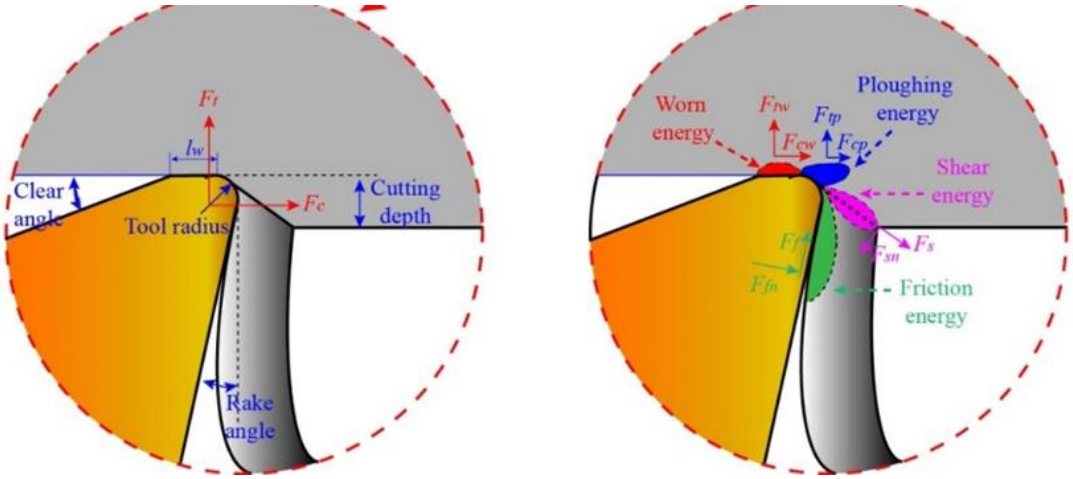



Fig.4-5 Energy distribution figure for different areas in orthogonal cutting

The cutting process during testing with the PBCT machine, when the tool encounters the sample is shown in Fig.4-6 a). Target material is removed by the cutting tool and a chip is generated with cutting parameters defined accordingly. It shows good coherence with the orthogonal cutting process, which validated the applicability of the concept. The cutting energy in different parts (shear energy, friction energy, ploughing energy and worn energy (energy consumed between tool flank face and machine surface because of the tool wear) in the cutting area is presented in Fig.4-6 b). These energies can be calculated based on the analysis of the cutting force and collected experimental data, which has be described in detail in Chapter 3.




a) b)

Fig.4-6 Cutting area and energy distribution. a) Corresponding cutting parameter; b) Energy distribution in cutting area

The energy distribution in PBCT is the same as the one mentioned in Fig.4-5 as it is also orthogonal cutting. As shown in Fig.4-6, the consumed energy is divided into four main parts and the corresponding forces in different areas are presented as well. $F_c$ is the cutting force in cutting direction and $F_r$ is the force in vertical direction. $R$ is the resistance force. $F_s$, $F_f$ and $F_p$ are shear force, friction force and ploughing force accordingly. Then, the energy consumed during cutting can be expressed as:

$$E = E_s + E_c + E_p + E_w \tag{4-4}$$

where $E$ is the total energy transferred, $P_s$ is shear energy, $P_p$ is ploughing energy, $P_c$ is friction energy and $P_w$ is worn energy (energy consumed between tool flank face and machine surface because of the tool wear).

### 4.2.2 Energy calculation in different areas

To study the energy quantitatively and build the relationship between consumed energy and surface integrity, the energy transferred in different areas in the cutting process should be calculated and analysed. As described, these energies can be acquired by using the following equations and the measured experimental data.

1) The calculation of shear energy ($E_s$) [12]

According the illustration of shear energy by Shaw [12], energy for the shear portion can be calculated following the next steps.

The cutting ratio ($r$), which is used to describe the deformation of chip thickness can be expressed as:

$$r = \frac{t_{uc}}{t_c} \tag{4-5}$$

where $t_{uc}$ is the uncut chip thickness and $t_c$ is the chip thickness.

The shear angle ($\phi$) during cutting can be calculated as:

$$\phi = \tan^{-1}\left(\frac{r \cdot \cos(\alpha)}{1 - r \cdot \sin(\alpha)}\right) \tag{4-6}$$

where $\alpha$ is tool rake angle.

Then the shear strain ( $\gamma_s$ ) during cutting is shown as:

$$\gamma_s = \frac{\cos(\alpha)}{\sin(\phi)\cdot\cos(\phi-\alpha)} \tag{4-7}$$

Based on the force acquired from the dynamometer, shear force ($F_s$) on the shear plane can be expressed as:

$$F_S = F_r \cdot \cos\phi - F_c \cdot \sin\phi \tag{4-8}$$

where $F_c$ is the cutting force in the cutting direction, and $F_r$ is the force in the vertical direction.

The shear area ($A_s$) in orthogonal cutting is:

$$A_S = b \cdot \frac{t_{uc}}{\sin\phi} \tag{4-9}$$

where $b$ is the cutting width and $t_{uc}$ is the uncut chip thickness.

Therefore the shear stress ( $\tau_S$ ) during cutting can be expressed as:

$$\tau_S = \frac{F_S}{A_S} \tag{4-10}$$

Finally, the shear energy is calculated as:

$$E_S = \tau_s \cdot \gamma_s \tag{4-11}$$

2) Calculation of friction energy ($E_f$) [12]

Regarding friction energy, it is similar to shear energy and can be calculated following Shaw's theory.

The friction force ($F_f$) during cutting is:

$$F_f = F_r \cdot \sin\alpha + F_c \cdot \cos\alpha \tag{4-12}$$

Correspondingly, the friction energy is given as:

$$E_f = \frac{F_f \cdot r}{b \cdot t} \tag{4-13}$$

3) Calculation of ploughing energy ($E_p$) [133]

Contact length:

$$l_f = l_1 + l_2 + l_3 \tag{4-14}$$

where,

$$l_1 = \theta \cdot r \tag{4-15}$$

$$l_2 = \gamma \cdot r \tag{4-16}$$

$$l_3 = r \cdot \frac{\cos\gamma - \cos\theta}{\sin\gamma} \tag{4-17}$$

and where $\theta$ is the stagnation angle, $\gamma$ is the clearance angle, $r$ is the cutting edge radius and $l_1$, $l_2$ and $l_3$ are the contact lengths in Fig.4-7.

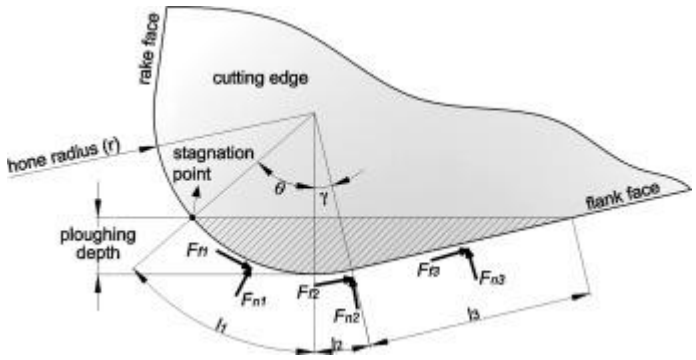



Fig.4-7 Cutting edge illustration for ploughing phenomenon

Pressure distribution on flank face is calculated as:

$$P(x) = a \cdot x^2 + b \cdot x + c \tag{4-18}$$

where

$$a = \frac{P_0}{2 \cdot l_f \cdot l_3 - l_f^2} \tag{4-19}$$

$$b = -2 \cdot a \cdot l_1 \tag{4-20}$$

$$c = P_0 \tag{4-21}$$

where $P_0$ is the normal pressure

Normal force in the deformation area is:

$$F_{Ni} = -\int_{l_i}^{l_i + l_{i+1}} w \cdot P(x) \cdot O(x) dx \tag{4-22}$$

where $w$ is depth of cut. $O(x)$ is direction function, which can be acquired from literature [133].

Friction force in the deformation area is calculated as:

$$F_{Fi} = \int_{l_i}^{l_i + l_{i+1}} \tau_1 \cdot P(x) \cdot O(x) dx \tag{4-23}$$

where $\tau_1$ is the shear stress.

Ploughing force in tangential direction and feed direction:

$$F_{te} = \sum_{i=1}^{3} F_{Nix} + \sum_{i=1}^{3} F_{Fix} \tag{4-24}$$

$$F_{fe} = \sum_{i=1}^{3} F_{Niy} + \sum_{i=1}^{3} F_{Fiy} \tag{4-25}$$

Ploughing force is:

$$F_p = F_{fe} \cdot \cos\phi + F_{te} \cdot \sin\phi \tag{4-26}$$

Ploughing energy is therefore calculated as:

$$E_p = \frac{F_p \cdot V_s}{t \cdot b \cdot V_c} \tag{4-27}$$

4) Calculation of worn energy

For worn tools, worn energy also contributes and the corresponding worn force can be acquired from the literature [134].

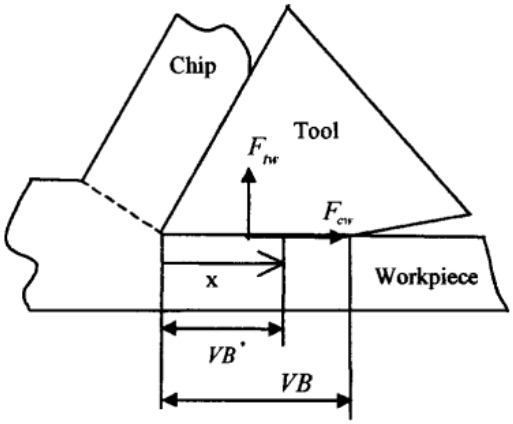



Fig.4-8 Force due to flank wear in orthogonal cutting [134]

The worn force in the normal direction is:

$$F_{tw} = w \cdot \int_0^{VB} \sigma_w(x)dx \tag{4-28}$$

While the worn force in the cutting direction is:

$$F_{cw} = w \cdot \int_0^{VB} \tau_w(x)dx \tag{4-29}$$

where $\sigma_w$ is normal stress, $\tau_w$ is shear stress, and w is the width of cut.

The worn energy is expressed as:

$$E_w = \frac{F_{cw} \cdot r}{b \cdot t} \tag{4-30}$$

Where $F_{cw}$ is calculated based on the calculation of the force on the wear length [134].

### 4.3 Design of the PBCT

The previous chapters have shown the advantages of the proposed PBCT concept and the corresponding energy based method to evaluate the cutting performance of materials. Therefore, the proposed PBCT method will be validated using the designed pendulum machine presented in detail in this chapter. The designed

pendulum based cutting machine is based on a standard Charpy machine (Fig.4-9), utilising the main body.

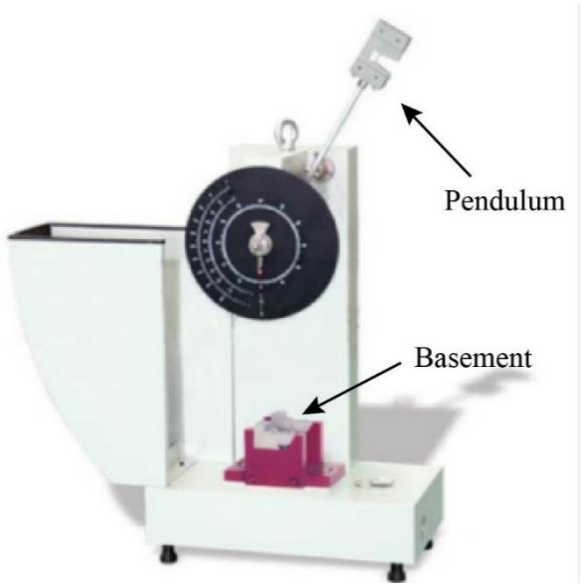



Fig.4-9 Standard Charpy machine. (DW5415C)

### 4.4.1 Main body design of PBCT

Apart from the PBCT, other parts have been designed to fix the base onto the dynamometer. A drawing of designed PBCT is shown in Fig.4-10. The detailed dimensions and geometry of the designed parts can be found in the Appendix A.

The hammer is replaced by a customized pendulum, while the sample is fixed at the bottom of the pendulum. The base of the standard Charpy machine was replaced with a new base composed of fixed tools, tool holders, adjustable module and a dynamometer was installed. The CAD model of main parts of the designed PBCT machine is shown in Fig.4-11. Several main properties of the machine, including impact energy ranges, cutting speed ranges, main dimensions are shown in Table 4-1.

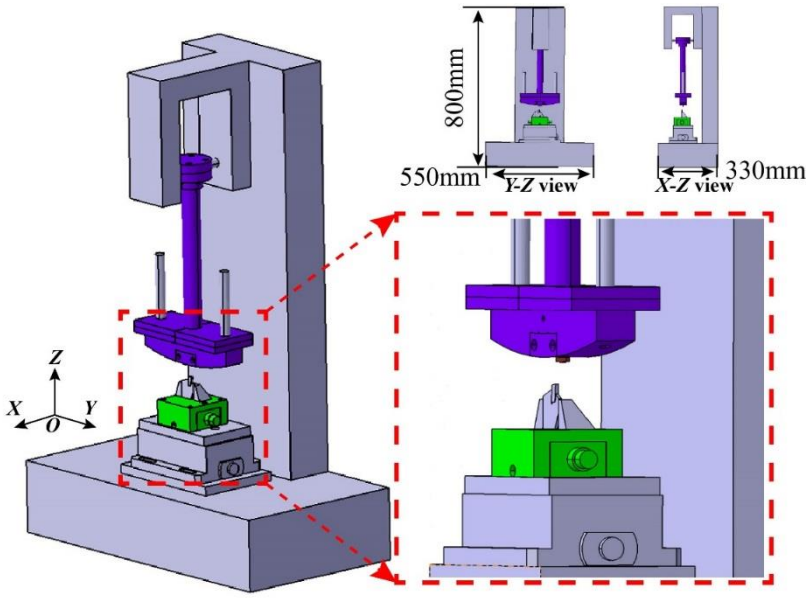



Fig.4-10 CAD model of main parts of the proposed PBCT machine

Table 4-1 Properties of proposed PBCT machine

| | |
|---|---|
| Impact energy range: | 0 to 60 J |
| Impact velocity: | 0 to 210 m/min |
| Impact centre distance: | 350 mm |
| Pre-elevation of pendulum: | 150° |
| Display mode: | dial type |
| Dimension (Approx.) | 550 mm×300 mm×890 mm |

A schematic of the designed parts for the modified pendulum machine is shown in Fig.4-11, where the new pendulum, sample, cutting tool and corresponding base are illustrated. As seen, a new pendulum arm is designed with which the mass can be adjusted by adding or removing mass blocks attached to the pendulum. The arm is fixed on the cylinder, supported by the bearing in the Charpy body, similar to the previous Charpy arm (Fig.4-11). At the bottom of the designed pendulum arm, a target sample is designed and fixed to it by pressing using a sample pressing part and two screws.

A tool holder, provided by SECO tools (Fig.4-12) for cutting off was modified and fixed to the designed part, which is designed to position and hold the tool holder. To fix the tool holder on the base and achieve the objective of adjusting the height of the work-stage, a part with screw holes and position holes was designed. An edge lever, used to adjust the height of the work-stage is employed and the dimensions for fitting to the part are shown in Fig.4-13. The rotation of the screw

on the wedge lever can adjust the movement of Block 1, thereby causing the movement of Block 2. As the cutting tools are fixed on the top of Block 2, the movement of Block 2 will cause the movement of cutting tools in the vertical direction, therefore adjusting the cutting depth.

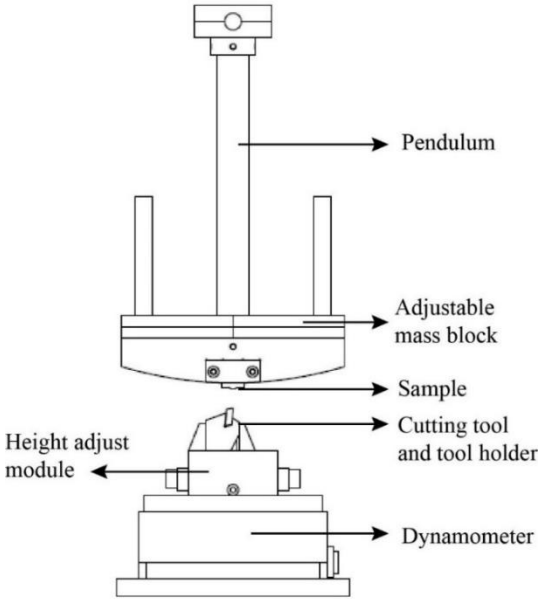



Fig.4-11 Assembled PBCT machine illustration with dominant parts

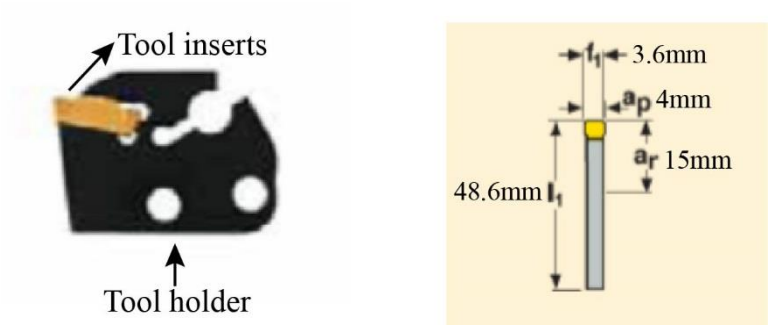



Fig.4-12 Tool holder and inserts for dry cutting tests

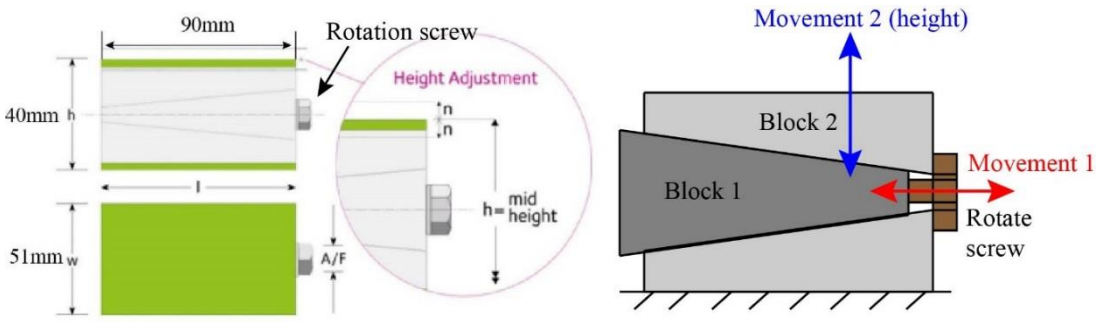



Fig.4-13 Illustration of the wedge lever used for work stage height (cutting depth) adjustment

### 4.4.2 Wet cutting condition design

Normally, lots of heat will be generated during superalloy machining because of its high strength and heat resistance. To protect the cutting tool and retain the required machined surface integrity, coolant will always be introduced into the cutting process. Therefore it is necessary to understand the cutting performance of materials in coolant conditions.

For the PBCT machine test method, coolant condition is also considered and the corresponding required parts are designed. With the development of coolant technology, internal coolant (Fig.4-14), which is more efficient and environmental, has been developed and applied widely in industry. Here, wet cutting is designed, based on a commercial internal coolant turning tool holder provided by SECO tool. An internal coolant parting-off tool holder (SECO, L150.10-1616-15JETI (Fig.4-15)) is modified to adapt to the PBCT base. Customized carbide inserts (CP500) with designed geometry fitting the holder were provided by SECO and used as the cutting tool.

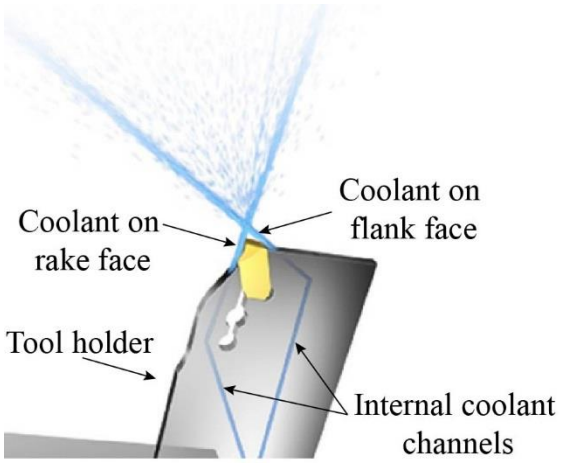



Fig.4-14 Working principle and flow channels of internal coolant tool

The tool holder in Fig.4-15 is modified to adapt to the designed PBCT machine as is shown in Fig.4-16. The modified tool holder can be fixed to the base of the Charpy machine with the designed fixed part and coolant liquid can be supplied from the connecter indicated by green arrow.

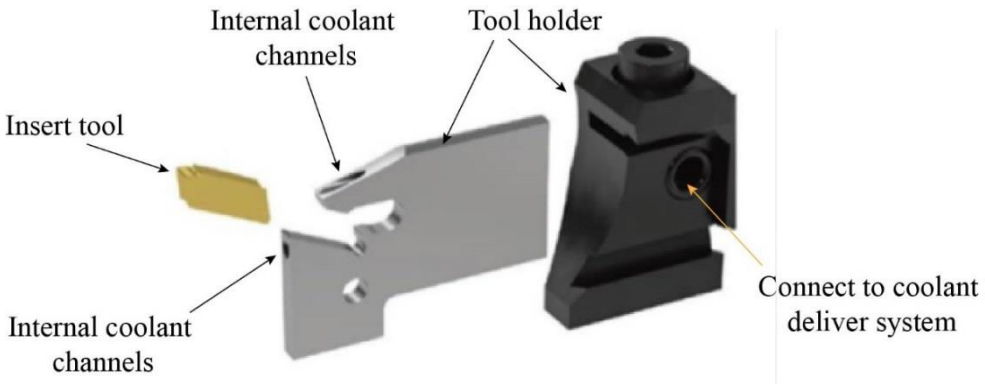



Fig.4-15 Internal coolant tool with corresponding holder and connection

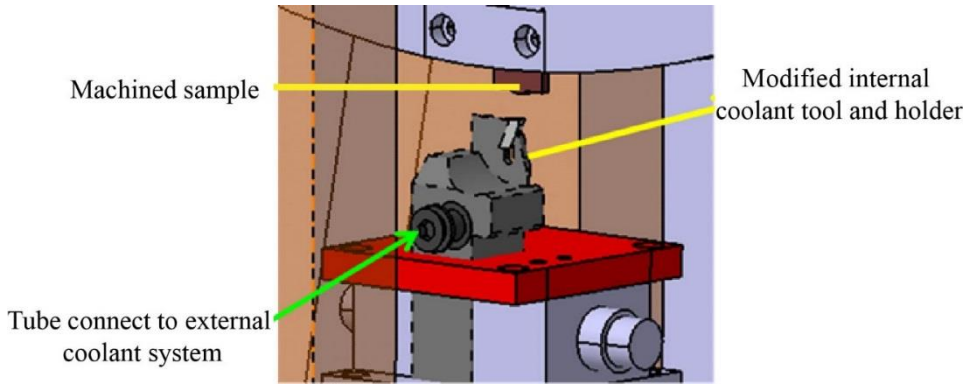



Fig.4-16 Modified coolant holder on the proposed PBCT machine base

With an appropriate pump and connector, the wet cutting tool can be set down. The flow of coolant liquid can be controlled by a valve to adjust the coolant condition. The designed PBCT machine with the coolant cutting condition accessory is shown in Fig.4-17. A steel tray is used to collect liquid after cooling and for recycling back into the coolant tank with a tube. As shown, the coolant liquid can be jetted from the tool holder coolant holes on both the rake face and flank face of the cutting tool.

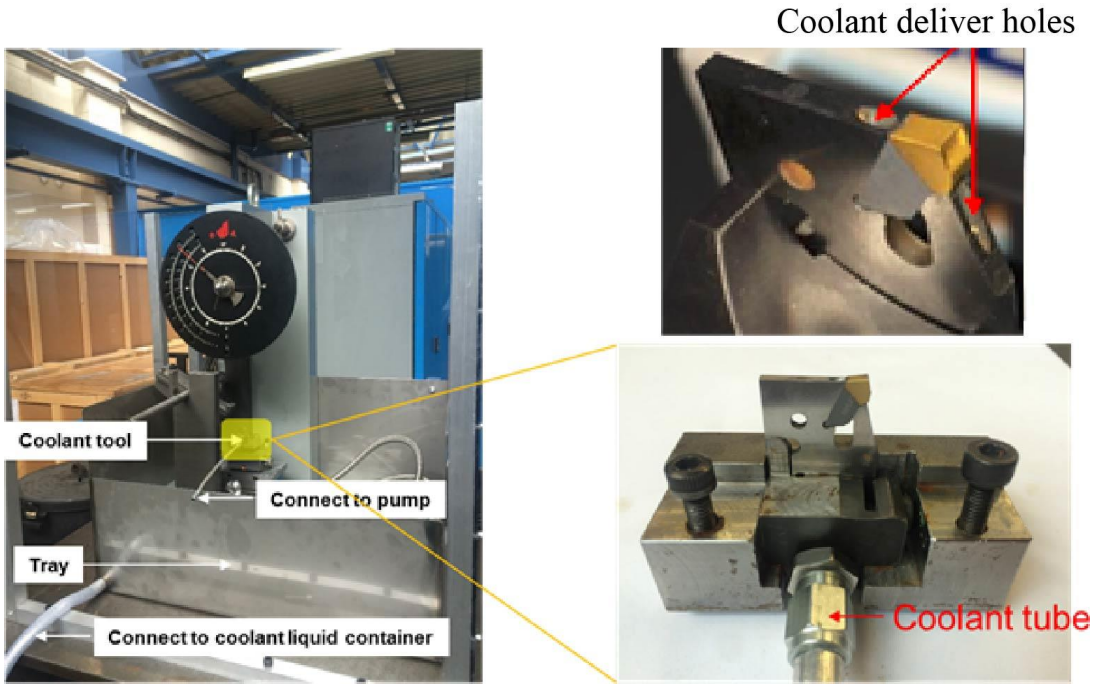



Fig. 4-17 Designed PBCT machine with wet cutting accessory

# Chapter 5

# Energy thresholds evaluation of workpiece surface damage in machining

In high-value-added and safety critical industries, such as nuclear and aerospace, surface integrity of machined components is critical. To evaluate the effects of cutting conditions on the workpiece surface integrity, traditional machining test methods usually require significant time and materials investment. This often represents a problem during the material development stage, as only little volume of testing material can be provided. In this chapter, a Pendulum-Based Cutting Test (PBCT) methodology is presented, which could allow quick performance of cutting tests for surface integrity evaluation while providing threshold values of cutting energies that are associated with particular levels of workpiece surface damage. This method gives the ability to rapidly evaluate the energy consumption of a particular machined surface without the need for using machine tools, and properly monitor the process with only a small amount of material. A unified cutting energy evaluation model is developed to monitor energy input and output during the cutting test that allows linking damage levels of machined surfaces with the energy distribution in specific cutting areas. Cutting tests with different cutting parameters, tool wear and geometries are employed to validate the proposed PBCT evaluation methodology on limited dimension material samples, which are usually difficult to test with traditional cutting tests using machine tools. Interestingly, results show that the surface integrity is highly based on the input energy and energy distribution during the cutting process. Different levels of surface damages are obtained with different energy distribution consumption during the cutting process and similar levels of surface integrity are found when the energy input and distribution are similar even if the cutting parameters are completely different. An energy threshold for a specific surface integrity of tested material (i.e. Inconel718) is presented to validate the proposed methodology which allows the evaluation of cutting performance based on an energy approach.

## 5.1 Introduction

The machinability of high strength aerospace materials (e.g. Nickel-based alloy) decreases significantly with the increase of their strength at elevated temperatures; this becomes a challenge when ever-stronger new materials are developed. Surface integrity, as one of the critical aspects associated with machinability evaluation, is related to a number of different process parameters (e.g. tool

geometry, cutting speed, depth of cut). Due to the high number of possible combinations of different cutting parameters, surface integrity related machinability tests become complicated, due to the interactions between multiple factors that need to be considered simultaneously in order to establish the threshold of cutting parameters that ensure the compliance with required workpiece surface integrity industrial standards. In particular, machinability vs. surface integrity is usually studied by conducting cutting tests on conventional machine tools by varying of cutting parameters followed by part sectioning to analyse superficial layer damage, which is time consuming and requiring significant volume of testing material. This problem is aggravated when testing those experimental materials which can only be acquired in small batches.

One way to address the problem of performing extensive cutting tests is to define a particular "agent" which could map the surface integrity while reflecting the differences induced by various combinations of cutting parameters. Cutting energy, which is one of the features that reflect the phenomenon of machining process, has the potential to be employed as the "agent" for surface integrity. However, most researches focused on the study of consumed energy by the machine tools, which could, indirectly, reflect the cutting conditions but the information of specific damage on workpiece superficial layers has not been put in evidence.

To capture the consumed cutting energy in the cutting areas, a novel pendulum-based method is proposed in this thesis in which the specific energies in different cutting zones could be evaluated thus, to enable the mapping of the workpiece surface integrity and establish the corresponding energy thresholds to ensure "damage-controlled" machined surfaces. This is in contrast to the pendulum grooving technique and Split-Hopkinson Pressure Bar tests that have been previously used only determining material properties (e.g. flow stress for modelling) or chip formation process rather than machinability evaluation and quick workpiece surface integrity evaluation as we propose here.

With the proposed pendulum-based cutting energy evaluation method, the machined surface integrity can be acquired and evaluated quickly by mapping the corresponding cutting energy against levels of workpiece damage rather than performing extensive tests with different cutting parameters on machine tools. The proposed PBCT method is quick and requires very limited amounts of testing material while allowing the cutting process to be monitored in detail for deeper process understanding. To validate the proposed method, different cutting tool geometries are employed, while the consumed energy (shear, friction and

ploughing energy) and corresponding surface integrity (by Scanning Electron Microscope-SEM, X-ray diffraction-XRD) are studied to allow the correlation between energy thresholds and levels of workpiece surface damages.

## 5.2 Research concept and PBCT design

The cutting energy evaluation model that calculates the consumed energy and energy distribution in cutting areas (shear, friction, ploughing and worn energy) during the cutting process is developed and presented in section 3.2. Fig.5-1 b) shows the energy distribution during orthogonal cutting which is used to remove material in front of the cutting tool and form new machined surfaces. Overall, the input energy is consumed by forming chips, friction on chips-tool interaction and the friction in tool-surface interaction. To be specific, the energy consumed during tool-surface could be divided into the ploughing energy caused by the cutting tool radius and the worn energy caused by interaction between the worn area of cutting tool and machined surface. It is however worth saying that there is no worn energy for fresh tools as there is no wear for such kinds of tools, therefore this fraction of energy can be neglected for surface generation. Along with the calculated energy that is required to generate and damage the machined surface, the relationship between surface integrity and consumed energy in cutting areas can be revealed, and an energy table for different damage levels of machined surface can be built.

The PBCT machine design concept shown in Fig.5-1 (a) is inspired by the pendulum test and charpy test machine generally used for material toughness testing. A custom-made hammer, with adjustable mass, is added as a pendulum, with the target testing material sample is fixed on the tip, while the cutting tool is kept stationary and fixed on the base. During the cutting process, the hammer is released from an elevated position, and allowed to freely swing, gaining momentum, which reaches the maximum during the impact with the cutting tool at the lowest position. The relative motion between the stationary cutting tool and moving sample works is equivalent to the cutting speed used during conventional machining. In this way, the sample can be machined in a specific direction with specific cutting speeds and the orthogonal cutting test can be completed on a small material sample as is shown in Fig.1 (a), while the consumed energy can be calculated by knowledge of the initial and final position of the hammer. The cutting parameters of desired orthogonal cutting test can be designed freely depending on requirements and a detail description will be presented in the following sections. Thanks to the flexibility of the proposed PBCT machine, different cutting parameters can be assessed, and in combination with the energy evaluation

method, it will allow the evaluation and prediction of the surface integrity via the study of the corresponding consumed energy inputted during cutting with limited amounts of tests and materials.

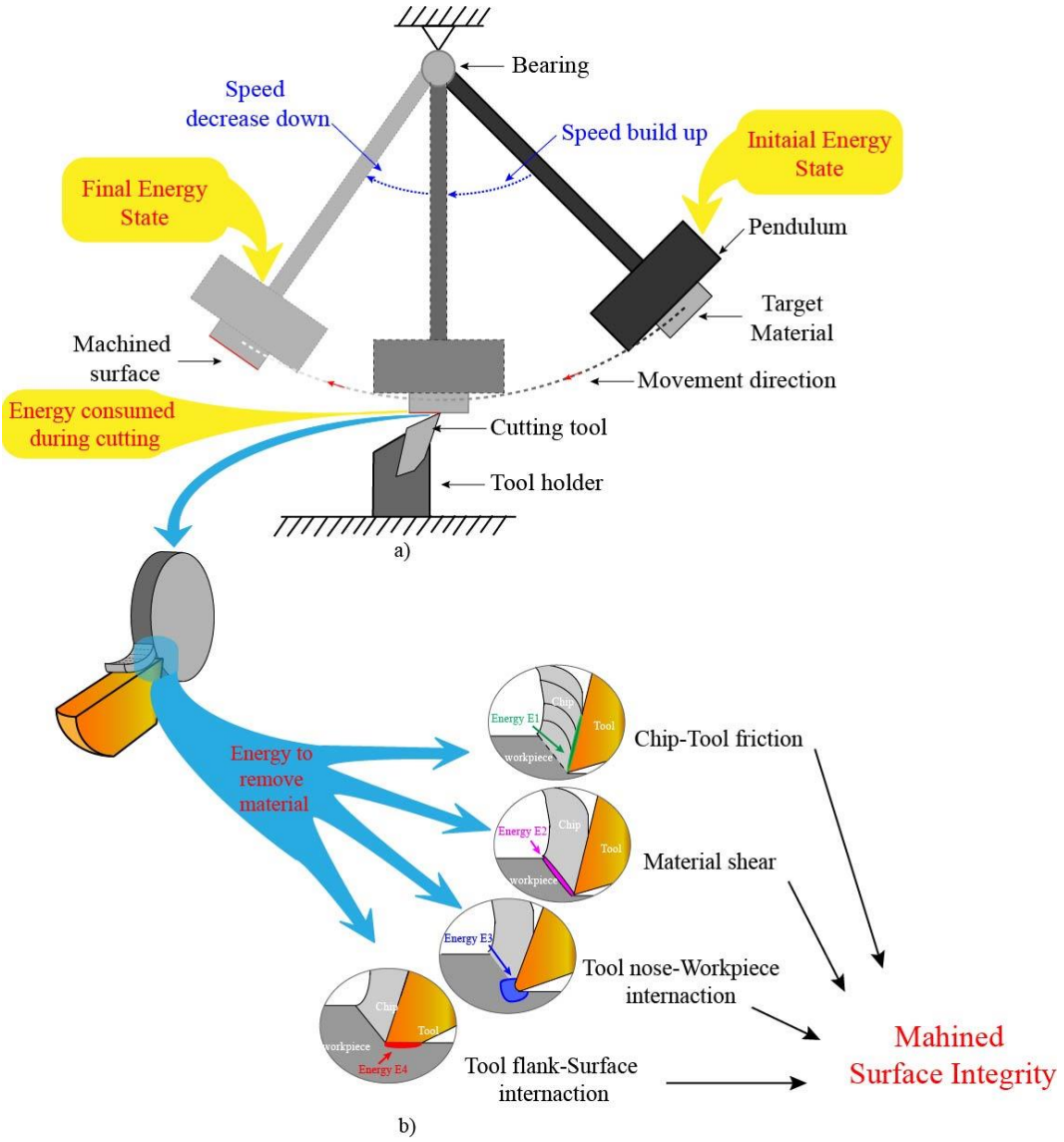



Fig.5-1 Principle of cutting test in proposed method and energy footprint in cutting process. a) Illustration of cutting process in PBCT machine and b) Energy distribution in cutting areas

## 5.3 Design and research methodology

### 5.3.1 Specialised setup for quick machining tests for energy evaluation

As previously mentioned, a PBCT machine has been designed from a standard charpy machine on which the swing pendulum is replaced by a custom made hammer, with the workpiece sample to be cut fixed in the bottom of the pendulum,

as seen in the CAD model in Fig.5-2 (a) & (b). The base of the PBCT machine includes the cutting tool (in a fixed position), a dynamometer, a wedge lever and other various accessories to allow the close observation of the chip formation and capturing the cutting process with high speed camera. The wedge lever is used to adjust the height of cutting tool so as to control the cutting depth and a dynamometer used to monitor and acquire the cutting force during tests.

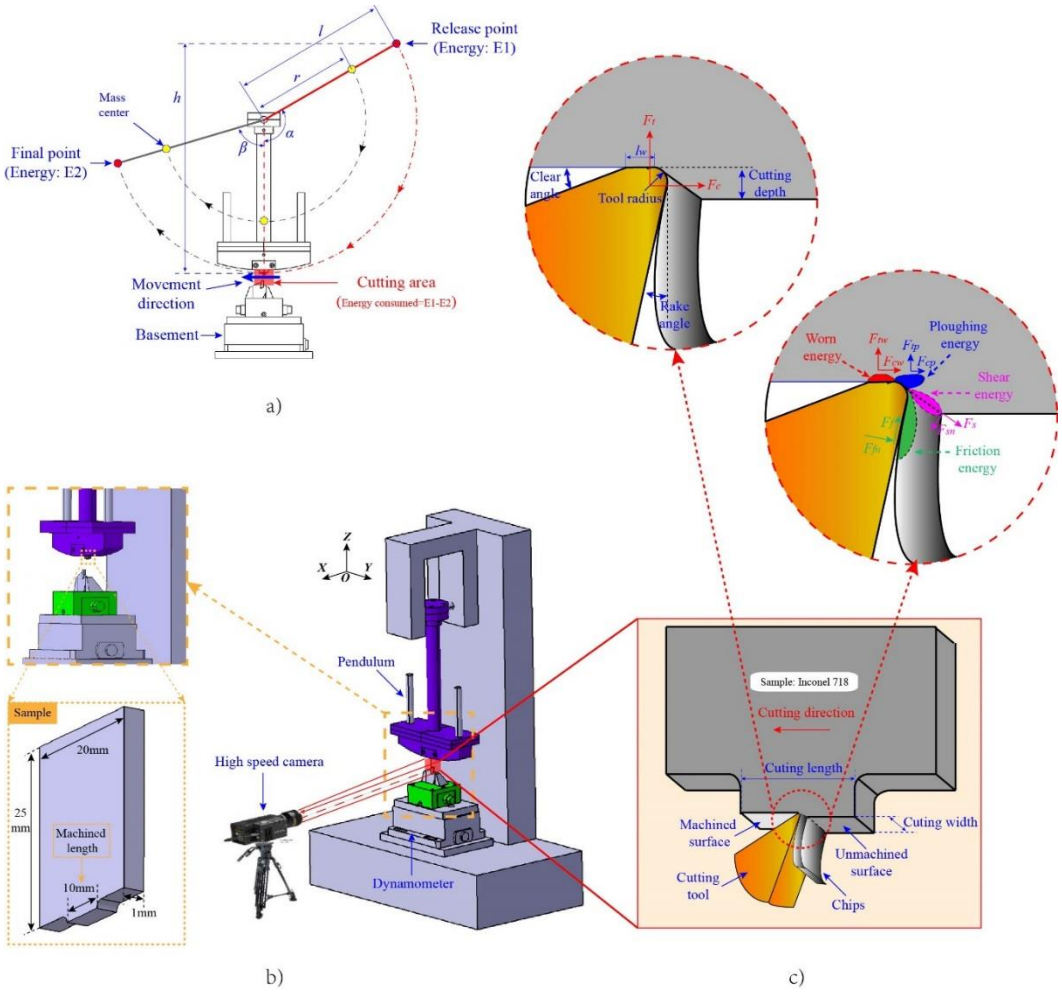



Fig.5-2 Schematic and illustration of designed PBCT machine. a) Principle of pendulum based cutting; b) Example of cutting scenario in PBCT machine; c) Explanation of cutting areas and energy distribution

As can be seen from the working principle of the designed machine in Fig.5-2 (a), the cutting sample is fixed in the tip of pendulum and it is released from an elevated starting position, with an angle α to the vertical direction and energy E1. After releasing, it arrives at the final position with an angle β to vertical direction an energy E2. This allows to know the total consumed total energy to be known by a simple subtraction. The cutting speed during the cutting process at the

bottom of the PBCT machine could be decided based on the release angle and the properties of the pendulum. It could be expressed as follows.

$$v = \sqrt{2 \cdot g \cdot r \cdot (1 + \cos \alpha)} \tag{5-1}$$

where r is the radius of pendulum form the gravity centre to rotary centre; a is the release angle; and g is the gravity accelerometer.

The cutting condition which is defined by cutting depth, cutting width and tool geometry is presented and could be seen clearly (Fig.5-2 c) while the interaction between cutting tool and designed sample is illustrated as well. As there is no continuous energy input during the cutting process, the cutting speeds will decrease during the cutting because it will need energy to remove the materials and generate a new surface but we could capture this with the help of high speed camera. A dynamometer is used and installed in the basement of the machine to monitor the cutting force in both cutting and radial directions for orthogonal cutting. To be specific, both the cutting forces in cutting direction and radial direction are combined by the following forces: shear force, friction force on rake face, worn force at flank face of tool and the ploughing force caused by tool radius. These forces have been illustrated (Fig.5-2 c) and the corresponding energy partition, which these forces contribute to, is presented in the different cutting areas as well.

### 5.3.2 Governing energy models

To study the surface integrity from an energy point of view, the specific energy distribution in different cutting areas needs to be explored in which case the function of each part of the energy could be found. Generally the energy consumed during cutting is known as specific cutting energy and this can be divided into several main components: shear energy, friction energy, ploughing energy (and worn energy only for worn tools) as seen in the orthogonal cutting illustration in Fig.5-2 (c). $F_c$ is the cutting force in cutting direction and $F_t$ is the force in vertical direction while R is the resistance force. $F_s$, $F_f$ and $F_p$ are shear force, friction force and ploughing force correspondingly and worn force $F_w$ is introduced to describe the interaction between the flank face of cutting tools and machined surface if the cutting tool is in worn condition. The energy consumed in every portion can be calculated based on the cutting force.

The total energy consumed during cutting:

$$E = E_s + E_f + E_p + E_w \tag{5-2}$$

where $P_s$ is shear energy, $P_p$ is ploughing energy, $P_c$ is friction energy and $P_w$ is worn energy. It is worth noting that the formulas used to calculate the corresponding energies are cited form literatures as indicated below.

The cutting force and parameters needed to calculate the energy distribution shown above can be acquired from the experimental testing results presented below. Following above equations, energy consumed in different parts in the cutting areas will be correlated to the machined surface and compared among different tests. Then the required energy levels for generating specific damage depth surface could be found in which chase the energy threshold for specific surface integrity will be able to be decided.

## 5.4 Material and methods

### 5.4.1 Equipment, specimen and cutting tools

Apart from the PBCT machine proposed and designed above, accessory equipment is used as well to carry out the cutting tests properly. To acquire the cutting force during process, a kistler dynamometer 9257A and corresponding amplifier are used when NI 9223 data acquisition is chosen to transfer and record the signal in monitor computer. In addition, as the designed cutting sample is 10mm in length, the time of the cutting process will be in the level of $10^{-2}$s even with low cutting speed such as 30m/min. This in turn translates to a very short cutting time; therefore the data acquiring sample rate needs to be high enough to capture the process with a sufficient resolution. For most tests, this has been set as 1 MHz to capture the cutting force. High speed camera (IDT Y4) is used to visually monitor the cutting process and allow calculation of the real-time cutting speed. Cutting chips will be collected and measured for energy calculation. Surface integrity will be studied with SEM. The experimental rig could be seen in Fig.3-2.

Solid carbide cutting tools with different geometry conditions are used in the following tests. As is seen in Fig.5-3, three groups of cutting tools have been presented and the three-dimensional geometry of cutting edges, including tool radius, for the cutting tools have been measured with Alicona machine. Tools in group A are those with around 5μm tool radius and with different tool rake angles (-10°, 0°and 20°) while tools in B groups have three kinds of tool rake angles as well but with around 50μm tool radii. Worn tools with around 50μm tool radius and the same three rake angles are presented in Group C and the flank face worn

length of cutting tools with -10°, 0°and 20° rake angles are 129μm, 247μm and 243μm respectively.

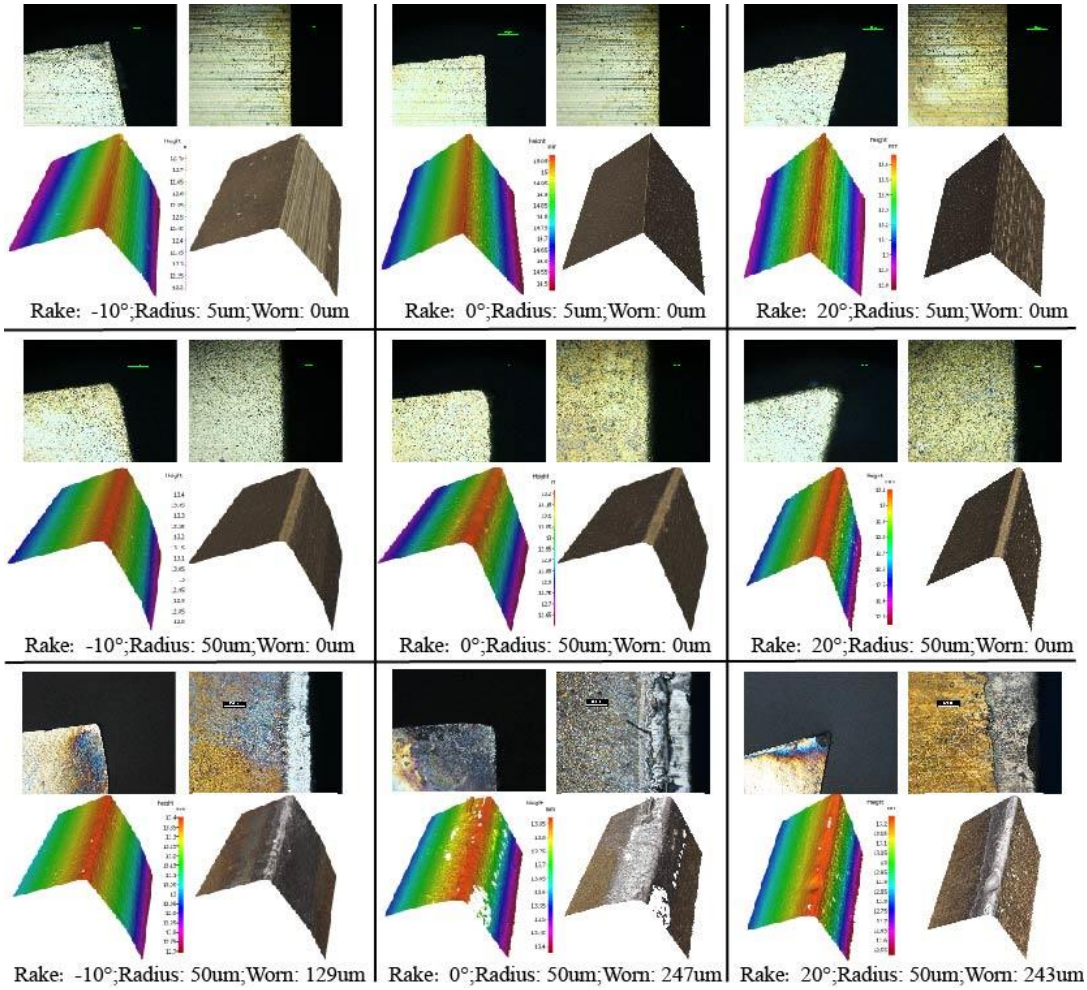



Fig.5-3 Geometry and condition of cutting tools used in tests

### 5.4.2 Experimental arrangements

To validate the concept of carrying out orthogonal cutting tests on the PBCT machine and evaluating machine performance from an energy point of view, three groups of experiments have been carried out to understand the following: 1) The relationship between energy distribution and surface integrity; 2) Energy thresholds for surface integrity with fresh tool; 3) Energy thresholds for surface integrity with worn tool.

In the first test group, six kinds of different cutting tools but same cutting depth and width are chosen to achieve the purpose of comparing machined surfaces with different cutting conditions which means different energy input. The cutting depth, cutting length and cutting width in these tests are the same and they are 0.1mm,

10mm and 1mm correspondingly. The rest of the detailed cutting conditions and parameters are listed in the Table 5-1. All of the tools used in this test group are fresh tools without worn.

Table 5-1 Cutting conditions to study relationship between energy distribution and surface

| Test No. | No.1 | No.2 | No.3 | No.4 | No.5 | No.6 |
|---|---|---|---|---|---|---|
| Tool radius (μm) | 50 | 50 | 50 | 5 | 5 | 5 |
| Rake angle (°) | 20 | 0 | -10 | 20 | 0 | -10 |
| Tool worn length (mm) | 0 | | | | | |

Three couples of tests are designed and compared in the second test group. The cutting depth and speeds are different in the first couples of tests while the second couple has different tool rake angles and cutting speeds. The third couple selects a larger cutting depth with different tool rake angles and cutting speeds. The tool radius, cutting length and cutting width in these tests are the same and they are 50μm, 10mm and 1mm correspondingly. The rest of the detailed cutting conditions and parameters are listed in the Table 5-2.

Table 5-2 Cutting conditions to test energy thresholds for fresh tools

| | Case 1 | | Case 2 | | Case 3 | |
|---|---|---|---|---|---|---|
| Test No. | 1 | 2 | 3 | 4 | 5 | 6 |
| Cutting depth (mm) | 0.05 | 0.05 | 0.2 | 0.1 | 0.15 | 0.15 |
| Rake angle (°) | 0 | -10 | 20 | 20 | -10 | 0 |
| Tool worn length (mm) | 0 | | | | | |

To validate the robustness and adaptability of this proposed method, another test group with worn tools is proposed. The aim of this test group is similar to the second test group but another cutting parameter, worn length, is introduced, which means that worn energy (energy consumed between tool flank face and machine surface because of the tool wear) will be included and should be considered during the evaluation of surface integrity. The tool radius, cutting length and cutting width in these tests are the same and they are 50μm, 10mm

and 1mm. The rest of the detailed cutting conditions and parameters are listed in the Table 5-3.

Table 5-3 Cutting conditions to test energy thresholds for worn tools

| | Case 1 | | Case 2 | | Case 3 | |
|---|---|---|---|---|---|---|
| Test No. | 1 | 2 | 3 | 4 | 5 | 6 |
| Cutting depth (mm) | 0.05 | 0.05 | 0.05 | 0.1 | 0.1 | 0.1 |
| Rake angle (°) | -10 | 20 | 0 | 20 | -10 | 0 |
| Tool worn length (mm) | 129 | 243 | 247 | 243 | 129 | 247 |

## 5.5 Results and discussion

### 5.5.1 The relationship between energy distribution and surface integrity

As mentioned above, the cutting process is monitored by high speed camera, with single frames shown in Fig.5-4. With the help of video process software MotionPro, the cutting speeds of every frame of the video could be tracked. Then the cutting speeds of whole process for these tests could be acquired and they are shown in Fig.5-5.

The captured cutting speed points and fitted curves for tools with 50 μm tip radius are presented in Fig.5-5a. Cutting speeds start from around 70m/min and decrease to 39m/min, 33m/min and 28m/min for 20 degree, 0 degree and -10 degree tool rake angle respectively. The reason for the speed decrease is due to a lack of continuous energy input during the cutting process, which means that the cutting speed will start to decrease once the energy is consumed to remove materials, leading to the cutting speed at final point being different (i.e. smaller) from the cutting speed at the start point. In addition, it is clear that there are differences among the decrease trend for these three curves which is because different tools will consume different energies to remove the same volume of material. Tools with negative rake angle (-10) will consume more energy, so the cutting speed downtrend is more pronounced compared with 0 degree and 20 degree.

Fig.5-5(b) presents similar information as what shown above, for different tools with 5μm tip radius. A similar trend of cutting speeds decrease during the cutting

process is shown to the trend in Fig.5-5(a). The cutting speed starts from 70m/min and decreases to 45m/min, 41m/min and 36m/min. The difference is that the cutting speeds at the final points in Fig.5-5(b) are a little larger than the corresponding ones in Fig.5-5a. This is because tools with smaller tool tip radius (5μm) will consume less energy during cutting compared with tools with larger tool tip radius (50μm).

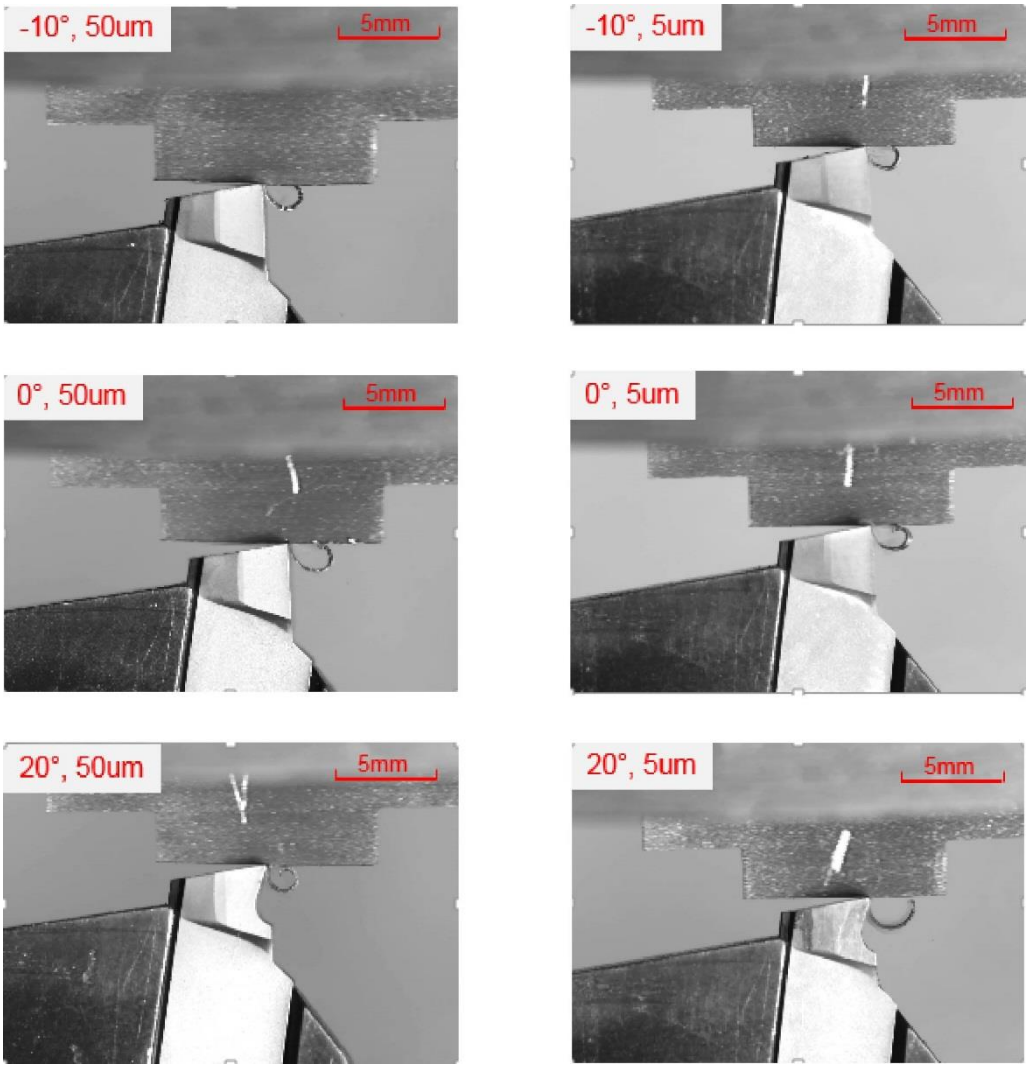



Fig.5-4 Monitoring videos for cutting process of different cutting tools

The cutting speeds at 50m/min for different cutting tools could be frozen on Fig.5-5(a) & (b) and corresponding times during the whole cutting process could be captured as well. The movement distance from the start point could be calculated based the acquired data following equation (5-8), which means that the machined surface at 50m/min can be positioned on the machined sample.

$$l = \int_0^x v dt \tag{5-8}$$

where *x* is the time when the cutting speed approach target speed.

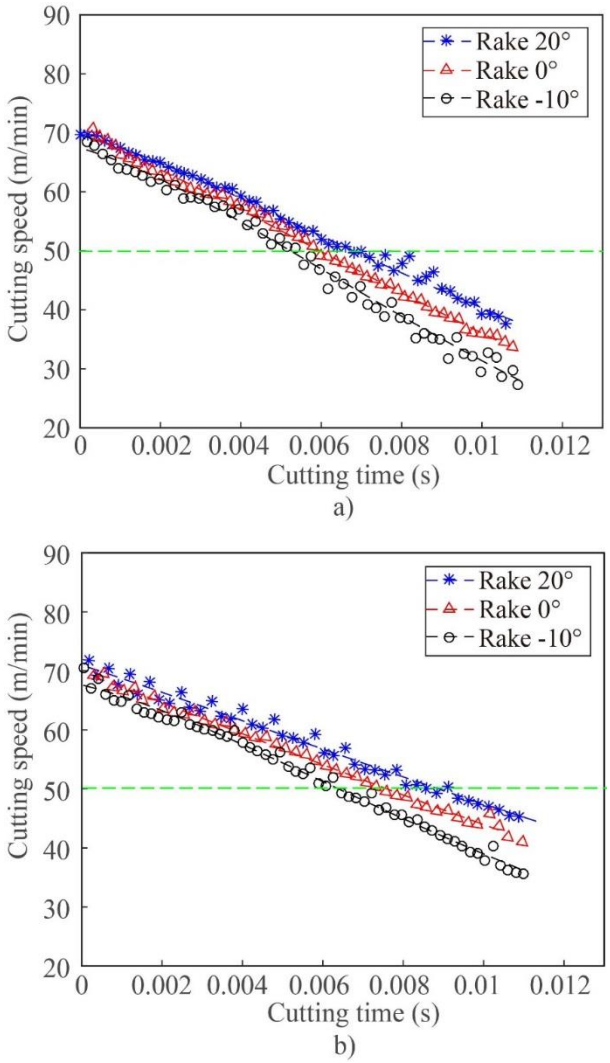



Fig.5-5 Cutting speed variation during cutting process. a) Results for 50μm radius tool; b) Results 5μm radius tool

Apart from the cutting speeds for every test, the cutting force is captured as well and shown in Fig.5-6 (a) and (b). There is a clear slope at the start and end point of every force curve. The reason is that the cutting process is very short (around 0.01s), so the dynamometer response time appear clearly on the measured force signal and as a slope. The specific cutting force remains stable after the response time of the dynamometer and another slope is observed because of the force unloading on dynamometer. The force is different in these six tests as the cutting conditions are different. Seen from the figure for cutting speeds (Fig.5-5 a & b), the time when the cutting is 50m/min could be determined and the corresponding cutting force could be identified in Fig.5-6. The specific cutting force for 50μm tip radius tool is around 3980N/mm$^2$, 2790 N/mm$^2$ and 2330 N/mm$^2$ correspond to

the rake angles -10 degree, 0 degree and 20degree respectively. For 5μm tip radius tool, the corresponding forces are 3130 N/mm$^2$, 2400 N/mm$^2$ and 1910 N/mm$^2$. The specific cutting force in the radial direction can be obtained in the same method.

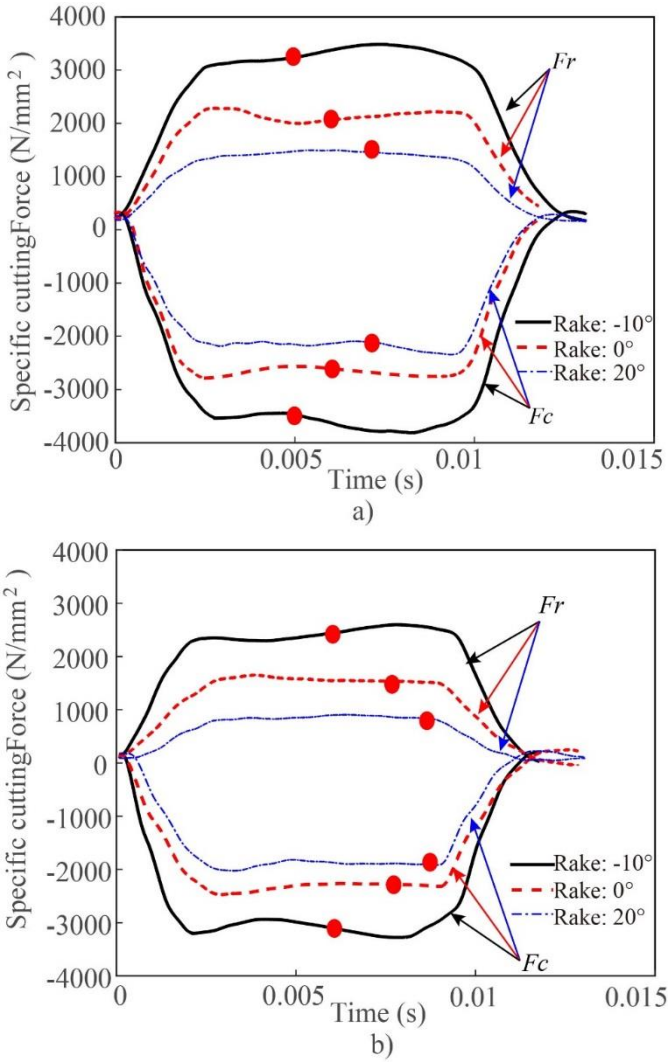



Fig.5-6 Cutting force variation during cutting process. a) Results for 50μm radius tool; b) Results for 5μm radius tool.

An overview of the test results for test group 1 is shown in Table 5-3. With the test result data and energy calculation method mentioned above, the energy consumed during cutting is calculated and shown in Table 4 as well. The calculated energy results include total energy (Total energy used to remove material), shear energy (energy consumed in shear part), friction energy (energy consumed because of the friction between chips and tool rake face) and ploughing energy (energy consumed because of the ploughing phenomenon between cutting tool

and machined surface caused by tool radius). Worn energy is not considered here as all the tools used in this test group are fresh tools without wear.

Table 5-4 Test condition and energy calculation result for test group 1

| Test No. | 1 | 2 | 3 | 4 | 5 | 6 |
|---|---|---|---|---|---|---|
| Tool radius (μm) | 50 | 50 | 50 | 5 | 5 | 5 |
| Rake angle (°) | -10 | 0 | 20 | -10 | 0 | 20 |
| Cutting speed (m/min) | 50 | 50 | 50 | 50 | 50 | 50 |
| Specific cutting force ($N/mm^2$) | 3980 | 2790 | 2330 | 3130 | 2400 | 1910 |
| Specific radial force ($N/mm^2$) | 3500 | 2200 | 1300 | 2700 | 1750 | 920 |
| Total energy per volume ($J/mm^3$) | 3.98 | 2.79 | 2.33 | 3.13 | 2.40 | 1.91 |
| Shear energy per volume ($J/mm^3$) | 2.21 | 1.40 | 1.07 | 1.87 | 1.36 | 1.01 |
| Friction energy per volume ($J/mm^3$) | 1.59 | 1.26 | 1.12 | 1.24 | 1.02 | 0.88 |
| Ploughing energy per volume ($J/mm^3$) | 0.23 | 0.16 | 0.14 | 0.018 | 0.015 | 0.012 |

It can clearly be seen that the energy spent in different cutting conditions is different and the energy distribution partition in different parts for different cutting tools is presented in Fig.5-7. For the test with a negative rake angle (-10 degree) and 50μm tip radius tool, the shear energy occupies 55% of the total energy and friction energy takes 39% while the rest 6% is ploughing energy. The shear and friction energy take the most part of the energy and ploughing energy represents a small part. With the increasing of tool rake angle (from -10 degree to 0 degree and then 20 degree), the portion of shear energy in total energy starts to decrease and friction energy has an increasing trend at the same time while ploughing energy keeps almost constant during this period. The same phenomenon could be found for the tools with 5μm tip radius. However, the ploughing energy takes only less than 1% of the total energy for the tools with small tool radius. It means that the tool radius has a significant influence on the ploughing energy and the tool rake angle affects the energy distribution greatly.

Apart from the energy distribution studied above, the absolute value of the corresponding energy is presented in Fig.5-8 as well (the detail calculation process of presented energy partition could refer to section 4.2.2). For example, the total energy consumed is 3.98J/mm$^3$ during the cutting process when using the negative (-10degree) rake angle and 50μm tip radius tool. The shear energy, friction energy and ploughing energy are 2.21J/mm$^3$, 1.59J/ mm$^3$ and 0.23J/mm$^3$ respectively. The total energy is decreasing while the tool rake angle increasing for both 50μm and 5μm tool tip radius and the same trend is found for shear energy, friction energy and ploughing energy. In Fig.5-7, the partition of friction energy is increasing with tool rake angle increasing, which is not the same as the trend in Fig.5-8. It is because Fig.5-8 presents the absolute energy value and Fig.5-7 shows the portion of every part energy in total energy. Although the partition is increasing, the absolute energy is decreasing actually.

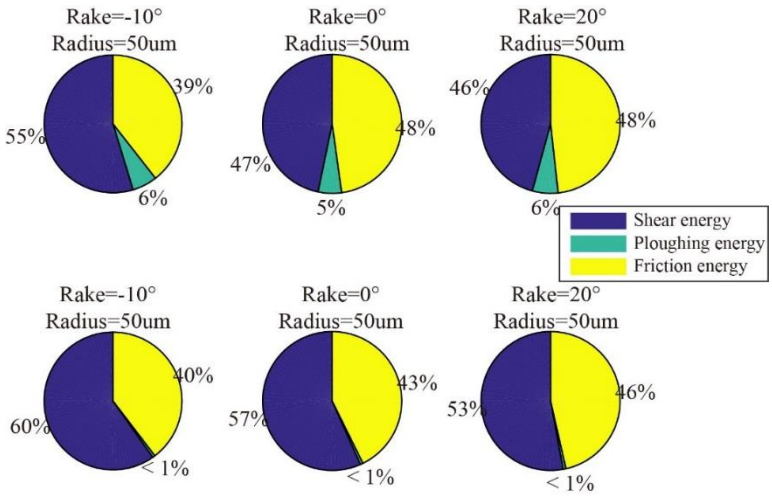



Fig.5-7 Energy partition with different energy input during cutting process

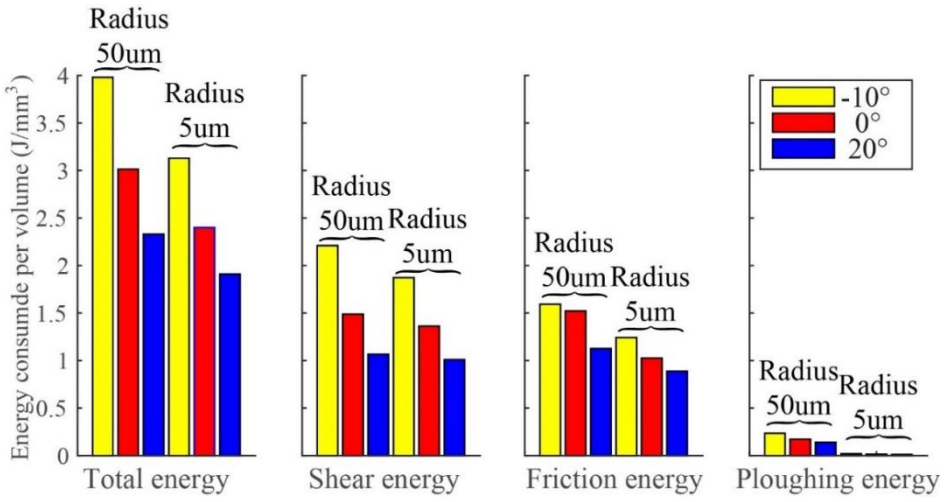



Fig.5-8 Absolute energy distribution during cutting process for different cutting conditions

Machined surface integrity of the tested samples is studied with Scanning Electron Microscope (SEM). All of the samples are mounted in resin and properly polished and etched. Following the position in equation (5-7), the machined surface at the cutting speed of 50m/min could be positioned. Material deformation is found in the SEM pictures and material deformation depth is chosen as the main factor to evaluate the surface integrity.

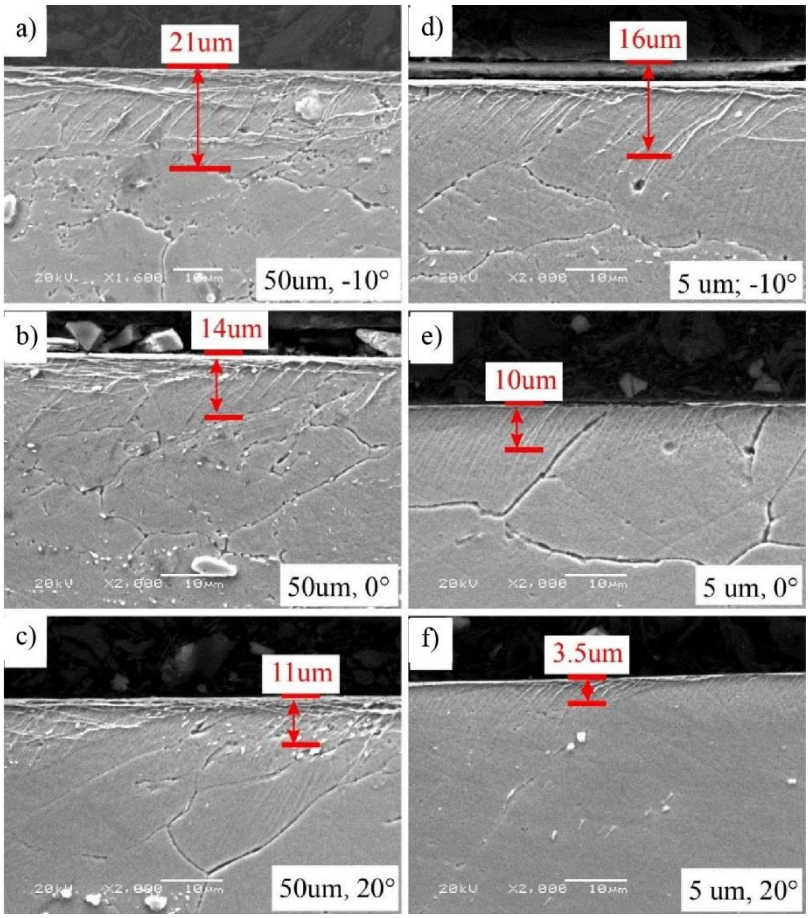



Fig.5-9 Surface integrity acquired with different energy input during cutting process

The material under the machined surface is dragged when the material is removed by the cutting tool. The deformation depth is marked by a clear dragging in the grains. In Fig.5-9-(a), the surface machined with 50μm tool tip radius and negative tool rake angle (-10degree) and the deformation depth is around 21μm (indicated by red arrow lines in the picture). For the tools with 50um tip radius, the deformation depth is 14μm and 11μm for tools with 0 and 20 degree rake angle correspondingly (Fig.5-9-(b) and (c)). As is seen in Fig.5-9-(d) to (f), the material deformation depths for 5μm tool tip radius are 16μm, 10μm and 3.5μm

correspondingly with the tool rake angle changing from -10 degree to 0 degree and 20 degree finally.

The deformation depth decreases when the consumed total energy decreases for both tools with 50μm and 5μm tip radius. As the friction energy describes the energy consumed between chips and tool rake face, it does not contribute to the machined surface integrity. The shear energy and ploughing energy are considered to be the main parts to determine the integrity of machined surface. During this changing process, it could be seen that the deformation depth decreases quickly from 21μm to 11μm for the tools with radius (50μm). The shear energy decreases more obviously while the ploughing energy does not change significantly, which means that the deformation is mainly influenced by the decreasing of shear energy as is seen in Fig.5-9-(a) to (c). The same phenomenon can be found for 5μm tip radius tool. When comparing Fig.5-9-(b) and (e), they have similar shear energy but the ploughing energy is completely different. The difference in material deformation depth is supposed to be caused by the difference in ploughing energy, which means the ploughing energy contributes to material deformation as well. Seen from these results, both shear energy and ploughing energy will have influence on the machined surface integrity and the energy consumed during cutting can be a characterization method and used to evaluate the machined surface integrity.

### 5.5.2 Energy thresholds for surface integrity with fresh tools

The above tests for different cutting tools have demonstrated that it is possible to study the orthogonal cutting and cutting performance of materials with this proposed PBCT method. To continue the investigation, and validate the relationship between consumed energy and surface integrity different cutting parameters, the test results are compared to check that whether similar surface integrity can be acquired if the energy distribution is similar during the cutting process. Three cases of tests are carried out and the cutting parameters could be seen in Table 5-2.

In this group, three cases are carried out and there are two tests in each case. Similarly, the cutting speed varies in each test with this method. With the same method used above, the specific cutting force and cutting speed variation are captured and presented in Fig.5-10, Fig.5-11 and Fig.5-12. The tools used for Case 1 are the same and the chosen tool had the properties of 50μm tip radius and 20 degree rake angle and the measurement results are presented in Fig.5-10. For test No.1, it decreases from 157m/min to 144m/min and tool rake angle is 0°

while the cutting speed is varying from 68m/min to 42m/min and tool rake angle is -10° for test No.2. Both of the specific cutting force in the cutting direction and radial direction are acquired. As the cutting speed for test No.1 is higher compared with test No.2, the cutting time is shorter for test No.1 and this could be seen from the force figure (Fig.5-10b) as well. The specific cutting force and radial force for test No.1 is higher than those in test No.1 and they have a good correlation with the cutting speeds on time scale.

Another validation test case is carried out with different cutting tools and different cutting parameters. The tools tip radius (50μm) used in this case are the same as the first case but their cutting depths are 0.2mm and 0.1mm for test No.3 and test No.4 respectively. The speed variation and cutting force during the cutting process are collected and presented in Fig.5-11. The cutting speed decreases from 89m/min to 40 m/min for test No.3 and from 158m/min to 138m/min for test No.4. Cutting force and radial force for these two tests in Case 2 are different as well because of the different cutting parameters.

The third cutting test case selects a larger cutting depth, compared with the previous two Cases, and higher cutting speeds. As is shown in Fig.5-12, the cutting speeds and cutting force are presented in the similar way at the previous ones.

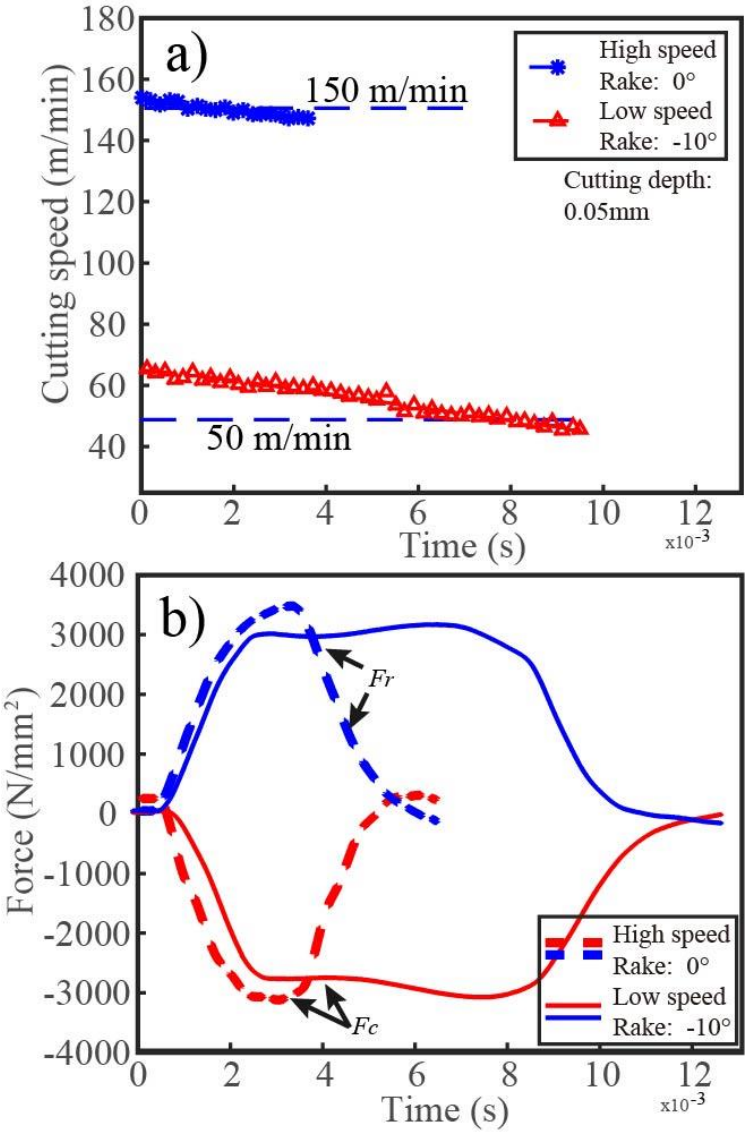



Fig.5-10 Cutting force and speeds for fresh tools group for Case 1.

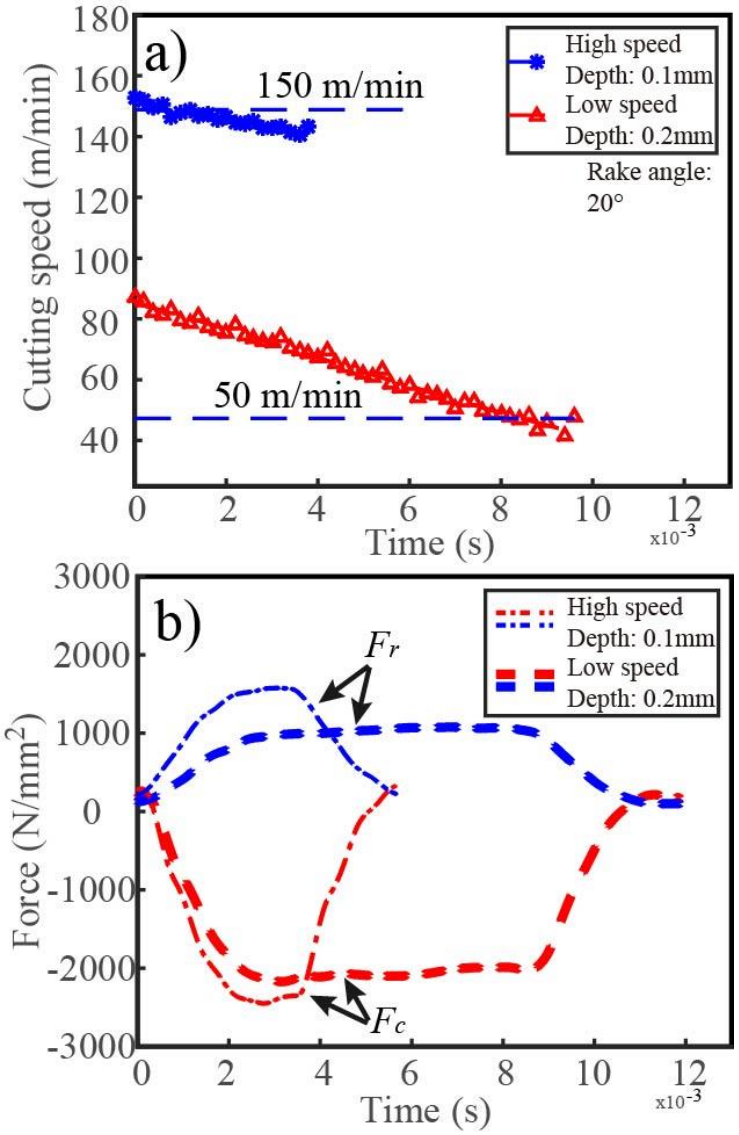



Fig.5-11 Cutting force and speeds for fresh tools group for Case 2.

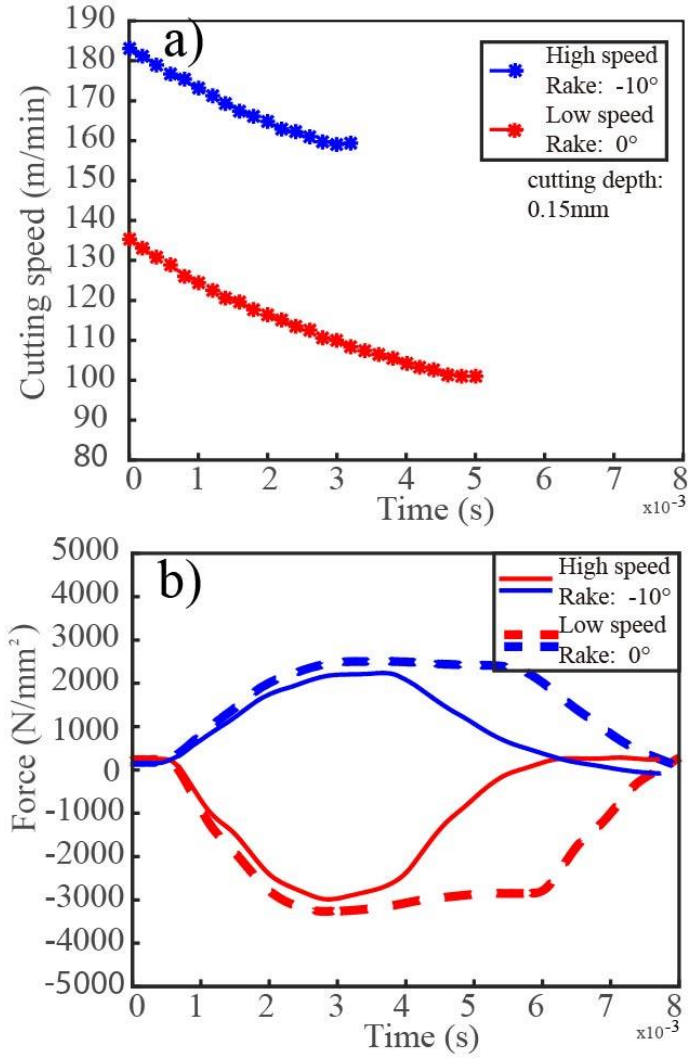



Fig.5-12 Cutting force and speeds for fresh tools group for Case 3.

Based on the testing data acquired and the energy model proposed above, the energy consumed in every test at the specific selected points are calculated and shown in Table 5-5. To be clearer they are shown in Fig.5-13 as bar charts. Seen from the bar, the value of the total energy and the energy in every part are similar for both of the tests in Case 1. The energy distribution in every part are similar as well. SEM pictures of the machined surface for those two tests in Case 1 are presented in Fig.5-13. It can be found that the material deformation depth is 10.5μm for test No.1 and 11μm for test No.2. If considering the measuring error, the deformation depth can be treated as the same deformation for these two tests with different cutting conditions in case1. Although these two surfaces are machined in different cutting conditions, the deformation depths of them are similar while the energy distribution is similar at the same time. It gives the message that similar surface integrity can be acquired while the energy consumed and distribution is similar. With the same analysis process and method in Case 1,

similar energy distribution is found for the rest of the two cases in specific different cutting conditions (Fig.5-13). SEM pictures were acquired from the machined surfaces for these tests. As is shown in Fig.5-13, it is found that the deformation depth for test No.3 are 21.5μm and 20μm for test No.4 when the energy distribution for test No.3 and test No.4 are similar. In Case 3, the difference is that white layer is found with this fresh tool. The deformation depth for test No.5 is 16μm with around 2μm white layer and it is 14.5μm deformation depth and around 2μm white layer for test No.6. The machined surfaces are still similar while the energy distribution in every part is similar for Case 3. The phenomenon that similar energy distribution during cutting leads to similar machined surface even when the cutting condition is completely different is found for the fresh tools.

Table 5-5 Test results and energy partition for fresh tools (Edge radius: 50um)

| | Case 1 | | Case 2 | | Case 3 | |
|---|---|---|---|---|---|---|
| Test No. | 1 | 2 | 3 | 4 | 5 | 6 |
| Rake angle (°) | 0 | -10 | 20 | 20 | -10 | 0 |
| Cutting speed (m/min) | 150 | 50 | 50 | 150 | 110 | 170 |
| Cutting depth (mm) | 0.05 | 0.05 | 0.2 | 0.1 | 0.15 | 0.15 |
| Specific cutting force ($N/mm^2$) | 2980 | 3020 | 2100 | 2420 | 3700 | 1550 |
| Specific radial force ($N/mm^2$) | 3620 | 3380 | 1055 | 1570 | 4530 | 2225 |
| Total energy per volume ($J/mm^3$) | 2.4833 | 2.5176 | 2.8800 | 2.8700 | 3.0200 | 2.9667 |
| Shear energy per volume ($J/mm^3$) | 1.0346 | 1.0483 | 1.4989 | 1.4805 | 1.8398 | 1.8174 |
| Friction energy per volume ($J/mm^3$) | 1.3043 | 1.3221 | 1.2741 | 1.2150 | 1.0838 | 1.0445 |
| Ploughing energy per volume ($J/mm^3$) | 0.1670 | 0.1809 | 0.1101 | 0.1745 | 0.1260 | 0.1246 |

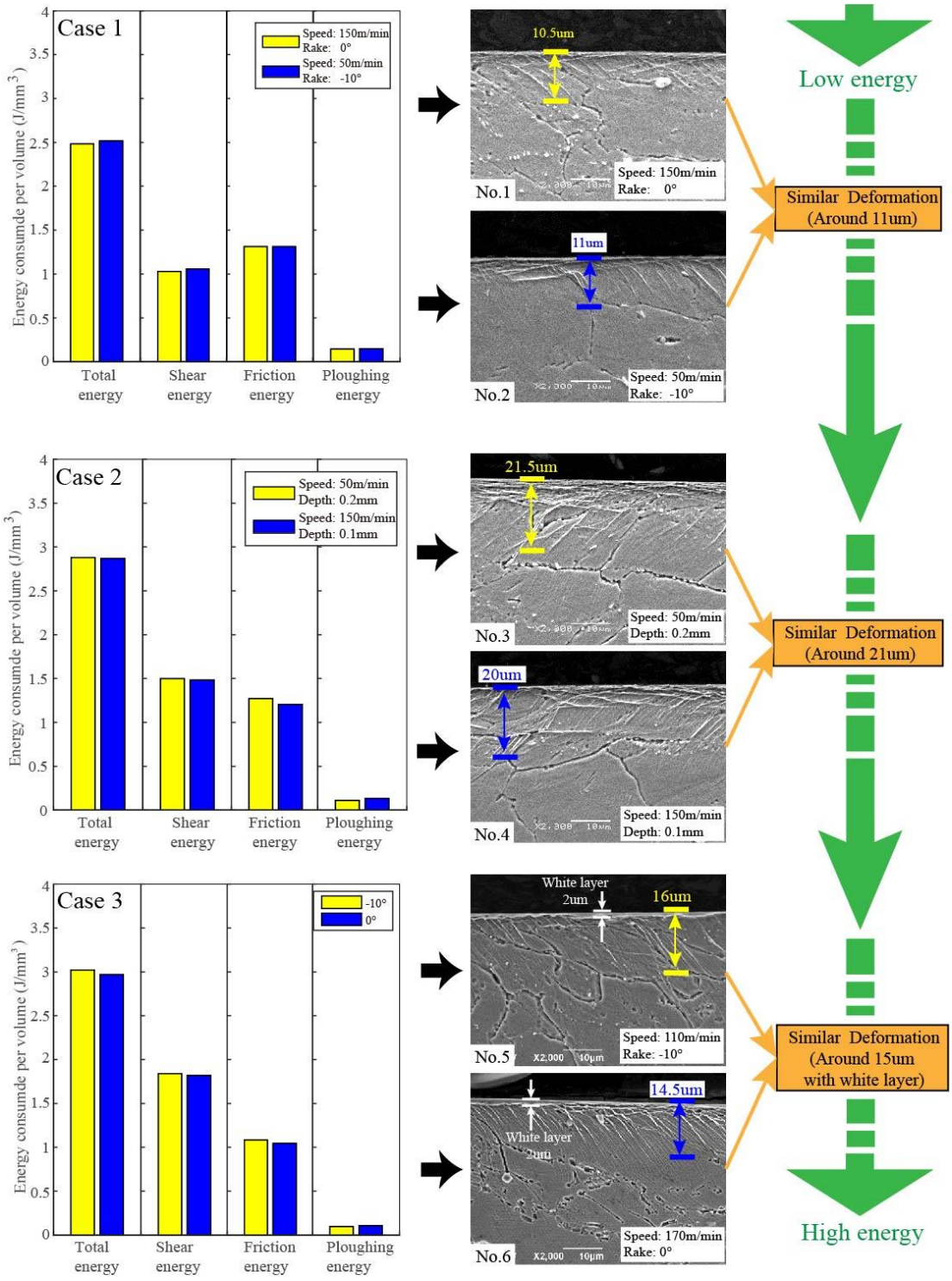



Fig.5-13 Energy distribution and corresponding machined surface for fresh tools (radius: 50um) test group.

Comparing the machined surface of three cases, the deformation depths of the machined surface are different and the energy distribution is different as well. From Case 1 to Case 3, the deformation depth increases when it could be seen

from the energy distribution that there is an increase in the total energy and the shear energy increase as well. However the ploughing energy remains not large changing during this time. The friction energy has no contribution to the machined surface integrity as the friction energy is the energy consumed on the tool rake face. The results show that the shear energy plays a main role in determining the machined surface integrity during cutting process. For this material, the machined surface will be unacceptable while the total energy goes higher than 2.9667J/mm^2 and the shear energy increase over the energy limit of 1.8174J/mm^2 and the ploughing energy keeps at the level of 0.12J/mm^2. It gives an indication of machined surface integrity in the energy view as is seen in Fig.5-13. The machined surface integrity for the fresh tool will be able to be analysed from the energy consumed during the cutting process.

### 5.5.3 Energy thresholds for surface integrity with worn tools

In the practical machining process, tools will always become worn after several cutting times especially for suprealloy machining. To make the validation tests practical and check the effectiveness of the proposed method, another series test of cases for worn tools are carried out and the test method is similar to the tests for fresh tools. The test arrangements have been shown in Table 5-3. Three cases including 6 tests with different cutting conditions (cutting tool geometry and cutting parameters) are studied.

The cutting force and speeds during cutting process are collected and presented in Fig.5-14. For test No.1 in Case1, the rake angle of the cutting tool is -10° and a worn length of 129μm is found while the rake angle for test No.2 is 20° with a worn length of 243μm. The cutting speed decreases from 102m/min to 83m/min for test No.1 and from 103m/min to 90m/min for test No.2. The cutting time for test No.2 is shorter because the radial force and cutting force for test No.1 is smaller which will consume less energy and the decrease in speed will be slower. The cutting force could be seen in Fig.5-14b and it gives the same information of the cutting process in the time scale. The test results for Case 2 and Case 3 are dealt with using the same method and give a the similar information of the cutting process as shown in Fig.5-15 and Fig.5-16.

Energy consumed in different parts in the cutting area during the cutting process could be calculated based on the energy model proposed in the previous chapter and they are shown in Table 5-6. The energy distribution for different cutting tests for every case is shown in Fig.5-17. As worn tools are used, worn energy (energy consumed between tool flank face and machine surface because of the tool wear)

are clearly found in the energy distribution bar because of the wear in the flank face of the cutting tool.

Table 5-6 Test results and energy distribution for worn tools

| | Case 1 | | Case 2 | | Case 3 | |
|---|---|---|---|---|---|---|
| Test No. | 1 | 2 | 3 | 4 | 5 | 6 |
| Rake angle (°) | -10 | 20 | 0 | 20 | -10 | 0 |
| Cutting speed (m/min) | 101 | 95 | 108 | 100 | 107 | 113 |
| Cutting depth (mm) | 0.05 | 0.05 | 0.05 | 0.1 | 0.1 | 0.1 |
| Specific cutting force ($N/mm^2$) | 2820 | 2740 | 2720 | 2670 | 3090 | 3156 |
| Specific radial force ($N/mm^2$) | 4860 | 3580 | 4380 | 2360 | 3090 | 3401 |
| Total energy | 2.72 | 2.68 | 2.79 | 2.74 | 3.0909 | 3.1500 |
| Shear energy | 0.5317 | 0.4163 | 0.5972 | 0.7956 | 1.5151 | 1.3168 |
| Friction energy | 1.8778 | 1.7534 | 1.3924 | 1.3548 | 1.0880 | 1.0907 |
| Ploughing energy | 0.0891 | 0.0744 | 0.1115 | 0.0830 | 0.1091 | 0.1133 |
| Worn energy | 0.3214 | 0.4959 | 0.6188 | 0.4403 | 0.3787 | 0.6292 |

For test Case 1, the worn length of cutting tools and tool rake angles are completely different while the cutting speeds are different as well. However, the energy distribution at specific points during these two cutting conditions are similar and the machined surface at these points is shown in Fig.5-17 in which the deformation depths could be found to be similar (around 4.5μm) as well. For Case 2, the energy distribution is similar in the two different cutting condition tests and gives a similar machined surface deformation as well. The deformation depths for test No.3 and test No.4 are around 7μm and with a clear white layer near the

machined surface. A similar phenomenon is found for Case 3 and the deformation depth for both of the tests are around 11μm but with a thicker white layer (around 2μm). The test results give an indication that the similar energy distribution during cutting process will lead to a similar machined surface for both fresh tools and worn tools.

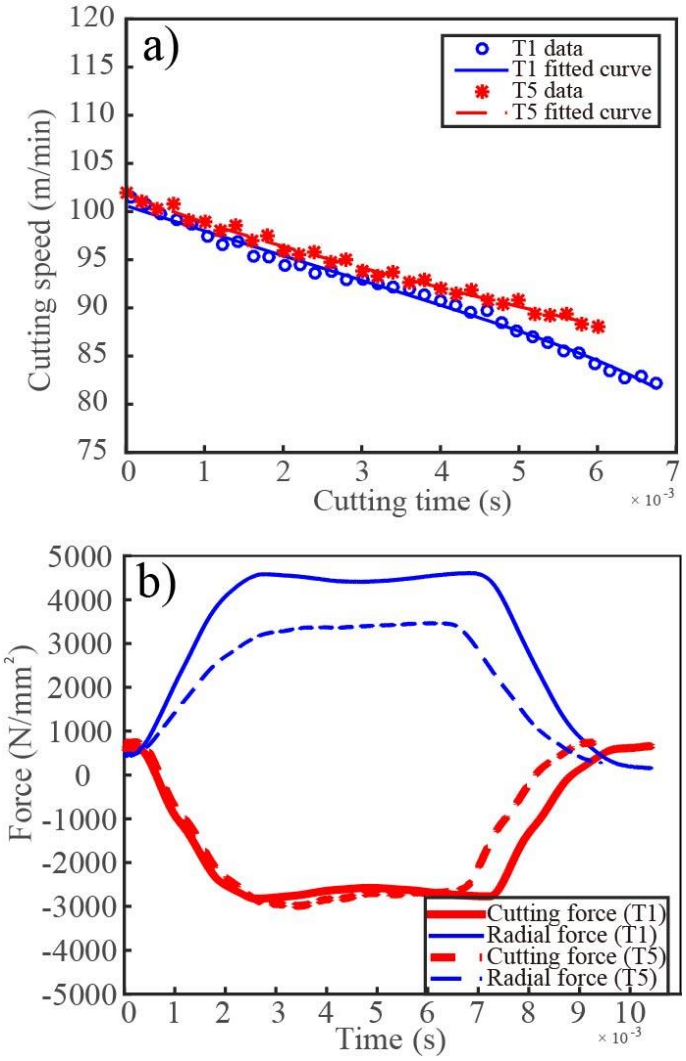



Fig.5-14 Cutting force and speeds for worn tools group Case 1. a) cutting speeds; b) Specific cutting force.

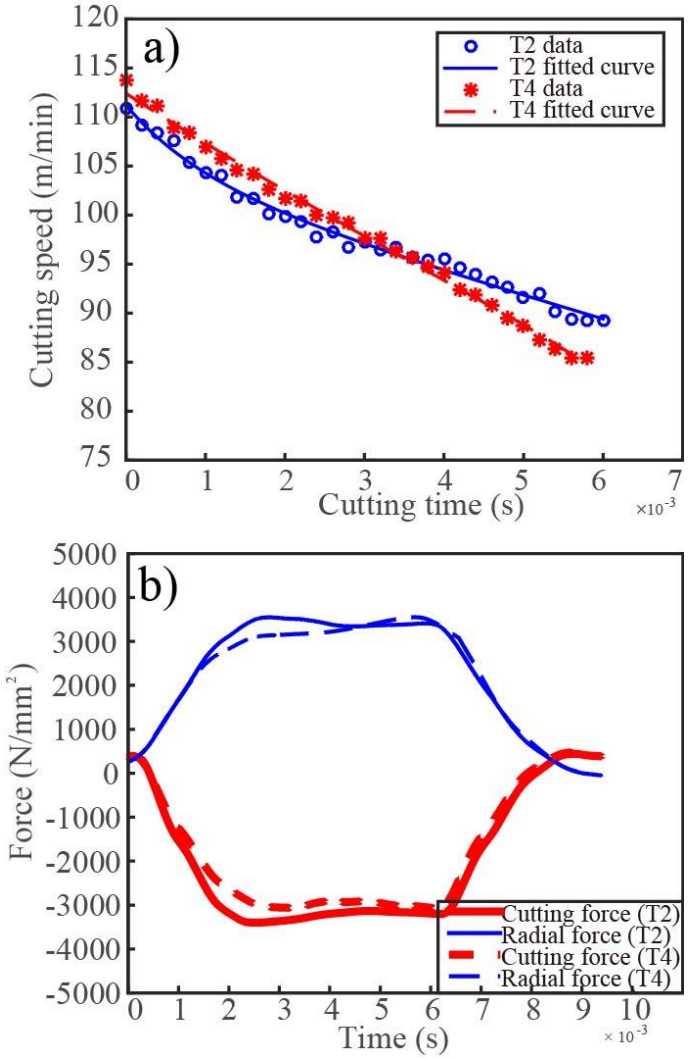



Fig.5-15 Cutting force and speeds for worn tools group Case 2. a) Cutting speeds; b) Specific cutting force.

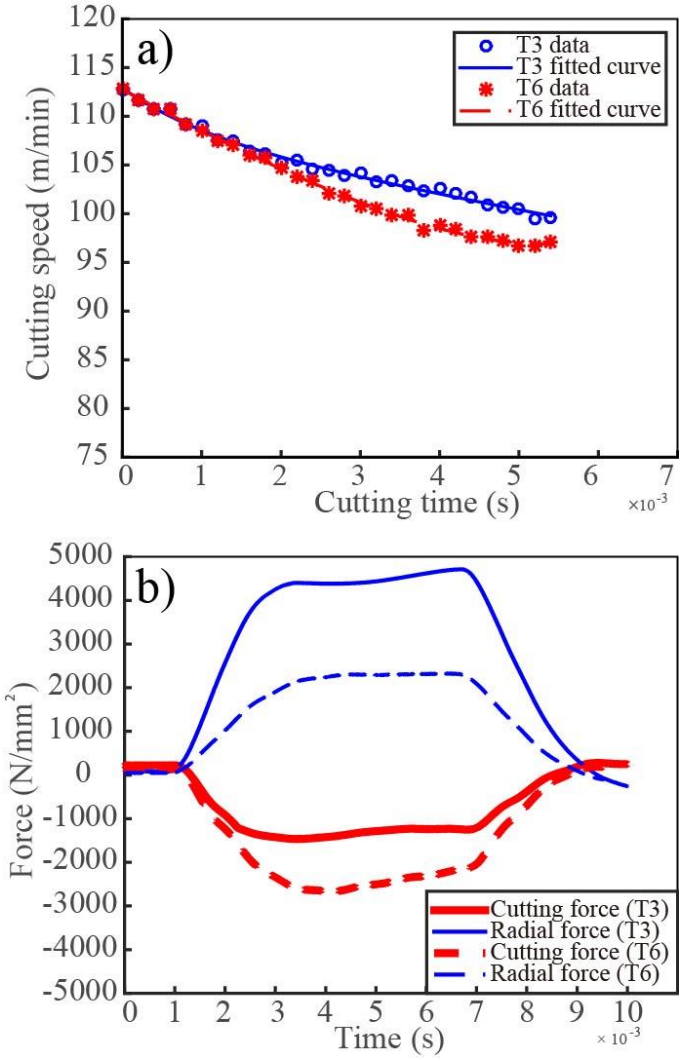



Fig.5-16 Cutting force and speeds for worn tools group Case 3. a) Cutting speeds; b) Specific cutting force.

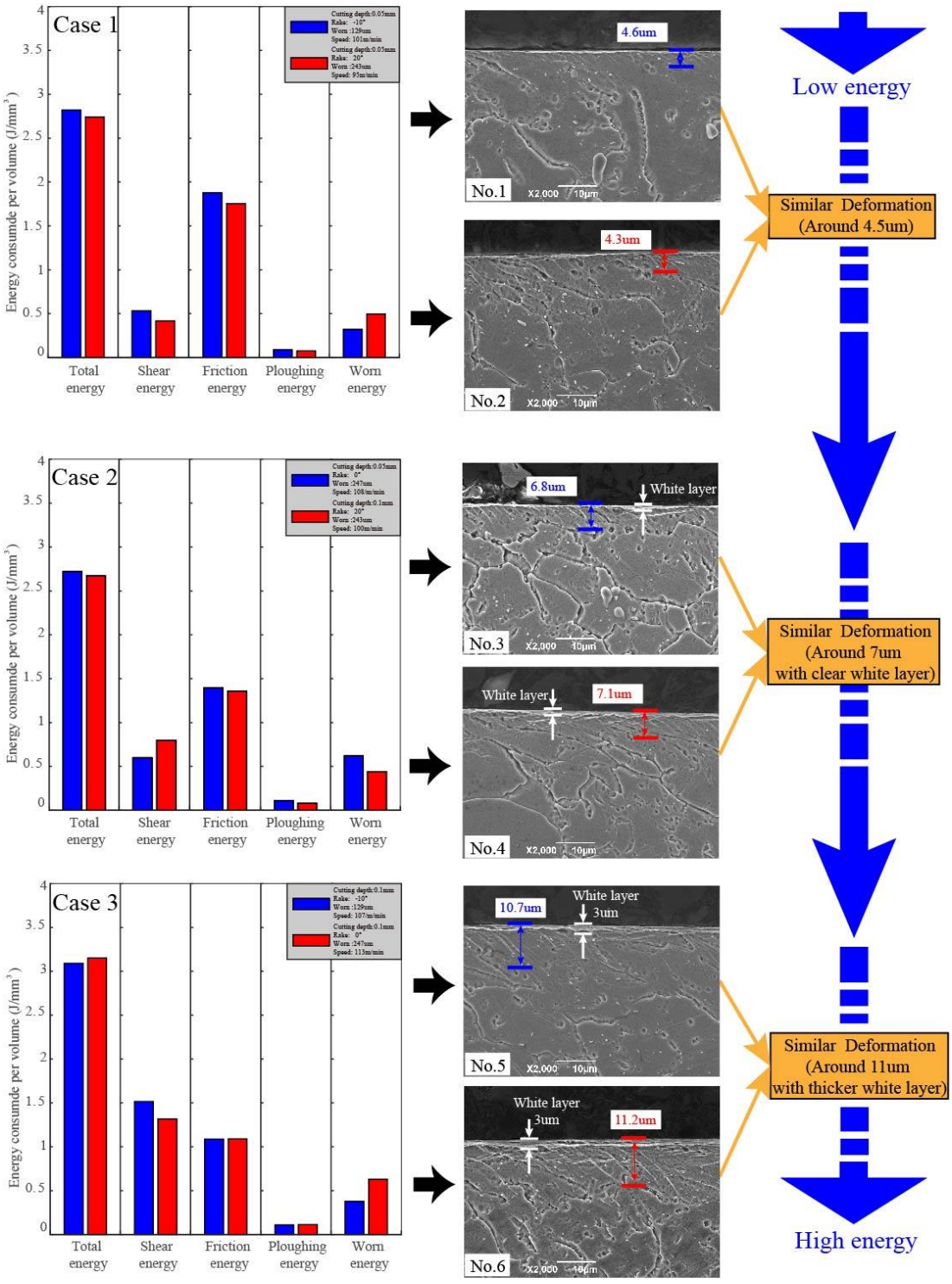



Fig.5-17 Energy distribution and corresponding machined surface for worn tools tests.

A comparison for these three cutting Cases for worn tools is carried out and shown in Fig.5-17. Seen from the energy consumed in different cases, the total energy has a slight increase from Case1 to Case3 while there is a clear increase in the part of shear energy. The ploughing and worn energy do not show large changes

and the friction energy does not contribute to the formation of machined surface. This means that the shear energy plays a significant role in determining the quality of the machined surface and its increase will increase the deformation depth of the machined surface while the other parts do not change too much. But the worn energy does contributes to the formation of white layer. The white layer is easier to be generated with the worn energy included compared with the fresh tool which has no worn energy at all. The blue arrow flow direction in Fig.5-17 gives an illustration of the machined surface integrity changing with the energy distribution variation. It shows that a white layer will be generated while the input energy similar to the energy distribution in Case 2 and a worse surface will be found if the energy goes higher in shear part.

### 5.5.4 Energy threshold for workpiece damage

The above research leads to the open question if the inverse relationship is valid: given cutting parameters that yield the same input energy, do they result in the same level of surface damage? If this is valid, it will open the possibility to define energy thresholds for ensuring that particular levels of surface damage are not exceeded; hence, no need to test various cutting parameters to attain this goal. Seen from above, tests that result in three levels of input $E_{con}$ ($E_1$, $E_2$, $E_3$ – Fig.5-18), each of them with two different combinations of cutting parameters (Test A and Test B (Fig.5-18a)), have been carried out. For example, in Scenario 1, we compare Test A (γ=neutral, $v_c$=150m/min) and test B ($\gamma$=negative, $v_c$=50m/min), similar energy partitions (Fig.5-18b) and surface deformation depth (11μm for Test A and 10.5μm for Test B) are obtained. Comparable results have been found presented for different levels of energy for the other two scenarios (scenario 2 and scenario 3) which result in same level of surface damage respectively.

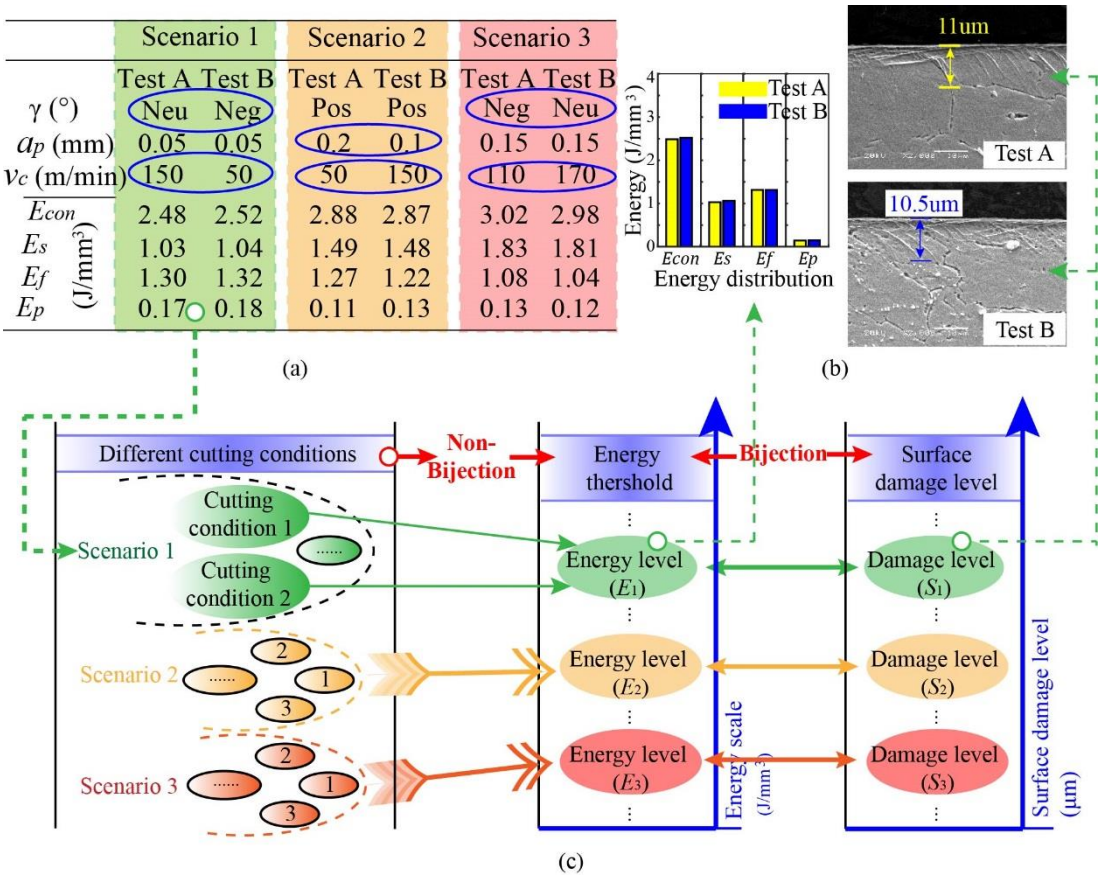



Fig. 5-18 Energy threshold for surface damage. a)Validation data sheet; b) Energy partition for scenario 1; c) Energy threshold evaluation

In other words, as seen in Fig.5-18c, both cutting conditions (Test A and B) in Scenario 1 (green colour) yield the same energy level $E_1$ in cutting areas, which leads to an equivalent level of surface damage $S_1$. The relationship between cutting conditions and energy level is identified as non-bijection, which means that various combinations of cutting parameters can lead to the same input energy level. While the bijective relationship is fixed between surface damage levels and input energy level ($E_s$, $E_p$), showing that each certain level of surface damage (e.g. $S_1$) will correspond to one energy level (e.g. $E_1$) with the inverse relationship also being true. Examples for other energy levels (yellow colour for $E_2$ and red colour for $E_3$ – see Fig. 5-18c) follow similar dependencies. This gives the perspective that a specific surface damage level could be controlled as long as the level of input energy remains "constant" irrespective of the cutting parameters combination used. Thus, an energy threshold for a specific surface damage level can be identified with this proposed method.

This approach introduces a huge advantage for optimization and selection of cutting parameters resulting in specific surface integrity by studying the input

energy levels during the cutting process rather than performing extensive machining trails with various cutting parameter combinations blindly.

## 5.6 Conclusions

In this chapter, the proposed quick and effective method to carry out cutting tests has been discussed. The main findings and advantages of this paper could be summarised as follows:

1) A novel PBCT machine has been designed and validated, to allow performing orthogonal cutting tests without CNC machine tools in different conditions, by use of small volume of sample material. This would allow the ability to test the materials which are in the development stage, and have no massive volume. Traditionally, it is difficult to carry out practical cutting tests and obtain comprehensive understanding of the cutting performance for a small volumes of materials. However this method will save lots of time and money to understand the surface integrity related machinability of specific materials and it will greatly facilitate the material developing progress
2) The surface integrity of machined surface is highly correlated with the energy consumed during the cutting process and the energy distribution in different cutting areas (shear, friction, ploughing and worn). With different energy distribution and input during cutting, different surface integrity will be generated.
3) It is found that if the energy input and distribution is similar during the cutting process, similar surface integrity could be obtained even when the cutting condition is completely different. This means that, the surface integrity could be evaluated based on the energy consumed and distribution during cutting.
4) The energy input increase in the cutting process leads to the changing of surface integrity. Shear and worn energy play significant roles in determining surface integrity, and unacceptable (white layer) machined surface will be generated once the input energy goes over the energy threshold.

The method proposed above has been demonstrated to be capable of achieving successful testing of a variety of different case-scenarios for different cutting conditions. The advantages of the method compared to conventional testing (e.g. reduce the need for testing material samples), as well as the possibility of testing surface integrity related machinability by use of an energy conservation approach,

which leads to a completely new method to study the surface integrity of machined surfaces. The energetic approach in the description of the process dynamics, considers the surface integrity evaluation in a novel. A custom made PBCT testing rig has been presented and used to validate the process in In718, with significant success. As this method does not depend on specific material, it can be used to study the cutting performance of other metals, composites, ceramics and plastic etc., further expanding its applicability range. Further improvement of the system, such as the use of ultra-high speed capturing and monitoring systems, could be included to further expand the range of possible testing conditions (e.g. high speed cutting). By simple adaptation of the system and respective modifications, grinding and milling can also be simulated.

# Chapter 6

# A novel method to continuously map the surface integrity and cutting performance transition in various cutting conditions

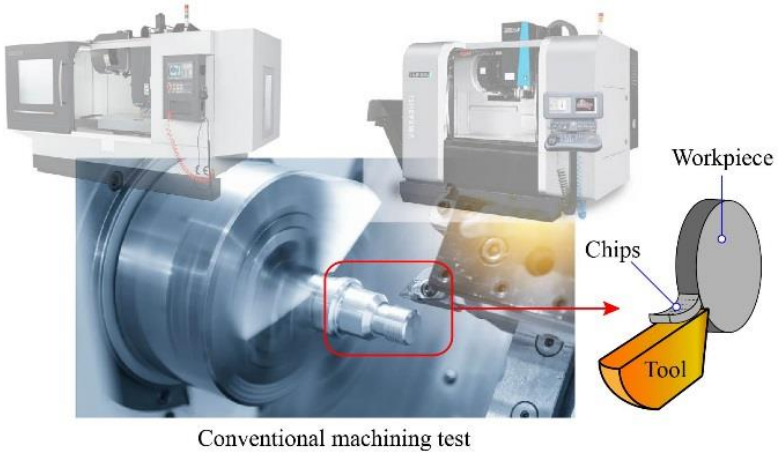
Resourceful methods (e.g. massive machining tests on machine tools) are used to study the cutting performance of materials and surface integrity of machined workpiece, which obstruct the comprehensive understanding of these properties. To change the current situation, this work proposes an innovative concept, which is able to generate machined surfaces that cover a large range of cutting speeds on very limited geometry samples in single tests, to study the machined surface integrity of a Ni-based superalloy based on the developed pendulum based cutting test (PBCT) machine. This presented an obvious chip morphology variation, i.e. serrated chips at start and smooth chips at the end, following the cutting speed decrease during the cutting process while the cutting process was monitored. An energy-based surface integrity evaluation method was applied whereby the consumed energy in different cutting areas (shear, friction and ploughing) at different cutting speeds could be calculated and correlated with the corresponding surface integrity. Electron Back Scattering Diffraction (EBSD) techniques were used to quantitatively study the plastic deformation of acquired machined surfaces while the residual stresses and Nano-hardness were measured beneath machined surfaces with X-ray Diffraction (XRD) and Nano-indentation respectively. The experimental results showed that the machined surface integrity under different cutting conditions could be revealed quickly at one time with the proposed method. In addition, this work may introduce the foundation of a revolutionary way to carry out the surface integrity investigation of materials effectively and contribute to the surface integrity quantitative technique as well.

## 6.1 Introduction

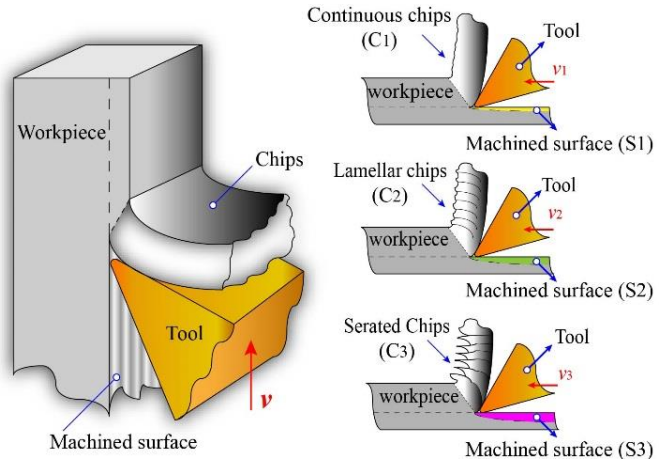
As known, superalloys, with their superior properties, e.g. high strength and corrosion resistance at high temperature, have been widely employed for harsh operational environmental applications such as aerospace, nuclear, medical and marine, which bring more difficulties for the machining of these materials [79]. Strict surface integrity checks are especially issued on these machined safety critical components as they are directly related to the service performance of the generated products [2]. Thus, studies on the cutting performance of these specific materials and their surface integrity were considerably reported [80]–[83].

However, the state-of-art adopted methods are either resourceful or time consuming (e.g. massive tests on machine tools) or lack of practical machined workpiece (e.g. FE simulation, mathematic models). This is therefore the motive of this work to develop an efficient and practical method to carry out material surface integrity related machinability tests and surface integrity evaluation rapidly.

Currently, machinability is normally evaluated based on the analysis of different cutting results (cutting force, tool wear, chip formation, temperature etc.) [81], [82], [88], [91]–[93], [95]–[97] which are extracted from the machining tests with varying cutting parameter combinations. It is evident that countless part sectioning of the sample followed by surface and superficial observation [97], [135], [136] will be needed to study the corresponding surface integrity comprehensively. Moreover, the cutting processes are traditionally implemented on the machine tools to acquire the sample and data followed by a series of surface integrity analyses [137], while generally only one specific combination of cutting parameters could be achieved and consequently a single corresponding machined surface could be acquired on one sample each time. For instance, as shown in Fig.6-1, various cutting tests should be carried out separately and individually on different samples to collect the data (e.g. cutting force, chips and machined surface) that are needed for different cutting speeds (e.g. $v_1$, $v_2$ or $v_3$) , which will be huge challenges when considering the massive cutting parameters needed to be covered and evaluated. Undoubtedly this process will cost lots of resource (material, time, labour etc.) to get even limited understanding of a specific kind of material while normally large amount of tested bulk materials will be scraped after these kinds of tests. More importantly, it will be even harder to study the machining properties of the materials in small volumes while this is a common phenomenon during the materials developing period.




a)




b)

Fig.6-1 Traditional cutting test method whereby a massive cutting tests and a large number of resources are needed for evaluating the machinability of the materials. a) Cutting tests with conventional machine tools, and b) Cutting illustration at different cutting conditions

In the framework of machining, this problem has been clearly noted as a significant challenge to rapidly identify the cutting performance of materials and the surface integrity on corresponding components. Therefore, researchers have tried to study the material machinability in alternative ways instead of carrying out massive practical machine tests on traditional machine tools. The Split-Hopkinson Pressure Bar machine had been employed to estimate the flow stress of materials by generating chips on specific designed samples and the results were input to analytical models to simulate the chip formation [118], but no machinability and surface integrity was discussed. Stefan et.al. had tried to study the cutting process with a modified charpy machine, but it was just used as quick stop rig [138]–[140]

to investigate the tool wear [123] or dead zone in the cutting process while no in-depth discussion about material cutting performance were included either. Another popular non-traditional method to study the cutting performance is FE simulation and analytical model calculation [141][142][143]. However the problems for these methods are that practical machined surface could not be acquired for successive analysis (e.g. superficial layer observation) and it is difficult to define the simulation conditions due to the hypothesis of uncertain parameters, simplification of boundaries and lack of practical machined workpiece etc. [144], [145]. Meanwhile, the indirect evaluation method such as energy consumption [146]–[148] were used to study the machining cutting process, but most of them focus on the energy consumed by machine tools rather than considering the particular energy that is consumed in the cutting area for formation of chip and surface.

Regarding the surface metallurgy as another aspect to evaluate surface integrity[149], it has been studied by using optical scope (Microscope), Scanning electron microscope (SEM) or Transmission electron microscopy (TEM) results to study the deformation on the sub-surface of the machined samples [135]. Several researchers had tried to study the deformation depth based on the EBSD test [69], [70], [150] and XRD results [151], [152]. However most of these research methods mentioned are qualitative based, which could not give a general standard evaluation of surface integrity quantitatively. Therefore, this study will study the machined surface integrity quantitatively as well. In addition, normally these kinds of measurement methods were not compared and correlated together, therefore this research builds their relationships and correlates them with the partitioned energy during the cutting process.

Regarding to chapter 4 relating to present research proposed an innovative concept to evaluate energy threshold for specific surface integrity with the help of designed pendulum based cutting test (PBCT) method. It brought a certain advantage that qualified the ability to study the material cutting process with limited materials and carry out cutting tests rapidly, however multiple experiments are still necessary for covering a variety of cutting parameter combinations.

To considerably reduce the resources needed to obtain comprehensive understanding of the material cutting performance, a new concept to capture the cutting process covering a continuous varying cutting speed range is proposed by employing the PBCT machine. Then the influence of cutting speed variation on the energy partition during cutting process and chips formation could be revealed in a

single sample. Accordingly continuous surface integrity variation caused by the cutting speed changing is investigated and quantified with different study techniques (SEM, EBSD, XRD and Nano-indentation) and correlated with the input energy. In this way, the cutting performance of materials with different cutting parameter combinations could be studied while the corresponding surface integrity could be acquired and quantified on a single sample. This will significantly simplify the surface integrity related machinability evaluation process of both mature and developing materials.

## 6.2 Research methodology and experiment details

### 6.2.1 Proposed concept

In this study a modified pendulum based cutting test machine (Fig.6-2a) was employed to carry out material surface integrity related machinability investigation based on chapter 5. It is of advantages for performing orthogonal cutting tests on limited geometry materials with the ability to evaluate surface integrity using energy aspects. To fill in the gap that massive cutting tests need to be implemented for different cutting parameters combinations, new designs and configurations giving us the ability to acquire a larger speed variation range during the cutting process, are proposed in which the cutting speed decreases from the start to the end during the whole cutting process because of the energy loss. Therefore, a 20mm length sample is used (Fig.6-2a), and the cutting depth is kept constant at $t_c$. Following the cutting tool advancing in the cutting process (Fig.6-2b), the cutting speed is declining leading to cutting conditions changing, thus generating different machined surfaces and cutting chips. As supposed, the generated single sample contains a surface machined at continuous changing speeds which will help us to understand the surface integrity at different cutting conditions (Fig.6-2b). It is worth mentioning that the morphology variation of chips (serrated, lamellar or continuous etc.) caused by speed changing should be visible as well, which cannot be done on the conventional machine tools. In addition, the consumed energy in different partitions (Fig.6-2a) is calculated and related to chip morphology to help to understand the shear phenomenon variation of materials depending on the input energy and cutting speeds. Also, it is convenient to study the continuous deformation variation on machined surfaces on the single sample with different detection techniques and the quantification method is also presented.

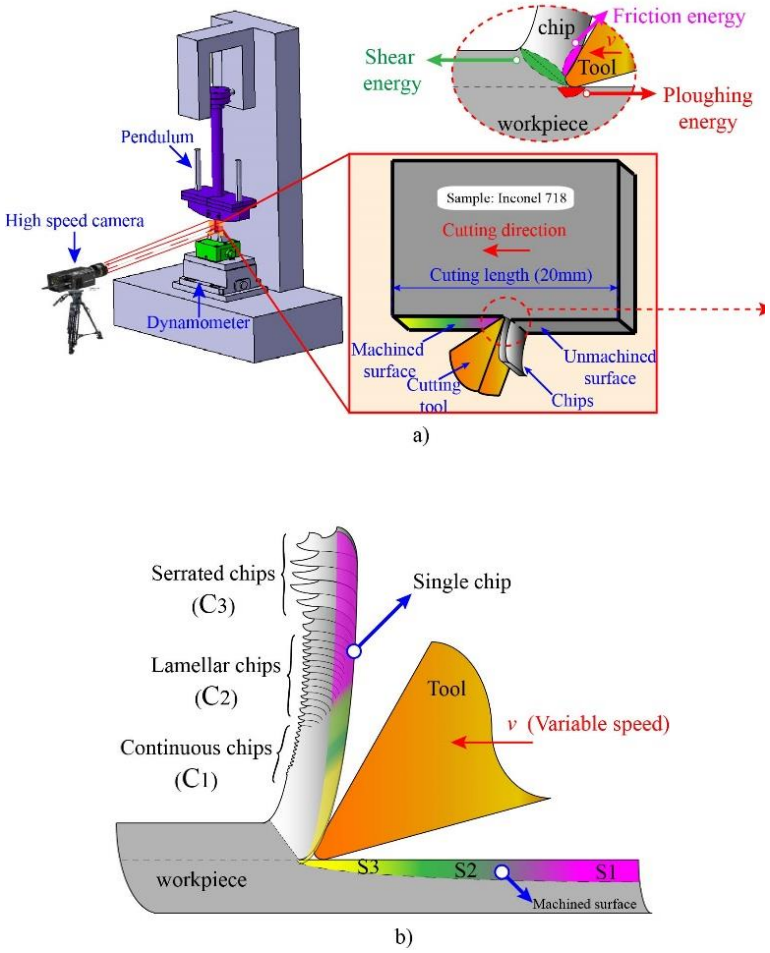



Fig.6-2 Proposed test concept with PBCT. a) Proposed PBCT test method and b) Morphology continuous variation chip

### 6.2.2 Experiment setup

The sample used in this paper is Inconel 718 with the dimension of 1mm×20mm×25mm and detailed cutting conditions and parameters used in this study are summarized in Table 6-1. Cutting depth ($a_p$) and width ($b$) are kept constant at 0.1mm and 1mm respectively, while the cutting length ($l$) is 20mm as described above. A customized solid carbide cutting tool with large tool radius and neutral rake angle is employed.

Table 6-1: Cutting condition

| Start cutting speed $v$ (m/min) | Cutting depth $a_p$ (mm) | Rake angle $\gamma$ (°) | Tool radius $R$ (μm) | Cutting length $l$ (mm) | Cutting width $b$ (mm) |
|---|---|---|---|---|---|

| | | | | | |
|---|---|---|---|---|---|
| 150 | 0.1 | 0 | 50 | 20 | 1 |

The machined surface integrity investigation of workpiece was conducted following the speed variation at the cutting direction. SEM (JEOL 6490LV) and EBSD (JEOL 7100F) techniques were employed to evaluate the superficial microstructure deformation of polished workpieces caused by material removal. The corresponding EBSD measurements were analysed by applying Channel-5 software from HKL technology and self-build calculation algorithm model [153] to quantify the deformation. Mechanical properties of the superficial surface, including residual stress and Nano-hardness, were analysed to compare with the corresponding microstructure change. A Proto iXRD machine with a 1mm diameter aperture and 12.5kV voltage was employed for the residual stress measurement of the machined surface. With the help of electrical polishing, the profile of measurement depth to 300μm under the machined surface was acquired. Nano-hardness was carried out on a Nanotest Platform 3 instrument from MicroMaterials Ltd with a diamond Berkovich indenter.

## 6.3 Results and discussion

### 6.3.1 Continuous varying cutting speeds in single test

By employing the high speed camera, the cutting process implemented on PBCT (Fig.6-3) with customized tool (Fig.6-4) could be properly monitored for checking the cutting evolution. Track points are set on the cutting sample thus the real time movement of the sample could be acquired (Fig.6-5a and b). Based on the displacement deviation of marked points between each frame, the cutting speeds at each captured picture could be calculated and derived from the Motion Studio x64 software. This allows the tracking of cutting speeds, then the position of corresponding chips and machined surface could be located to analyse the cutting performance of materials at different cutting conditions.

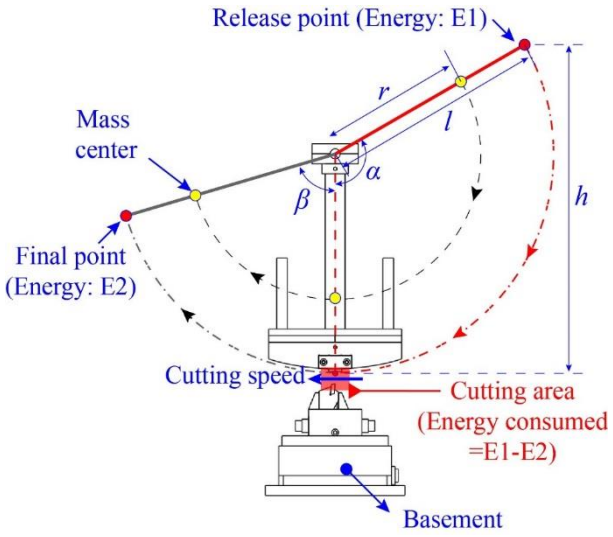



Fig.6-3 Illustration of cutting tests process in single test (Principle of PBCT test)

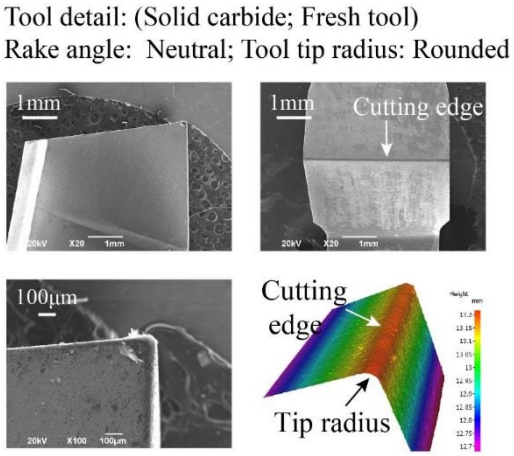



Fig.6-4 Geometry of the customized tool. (Rake angle:0°; Tool radius: 50μm)

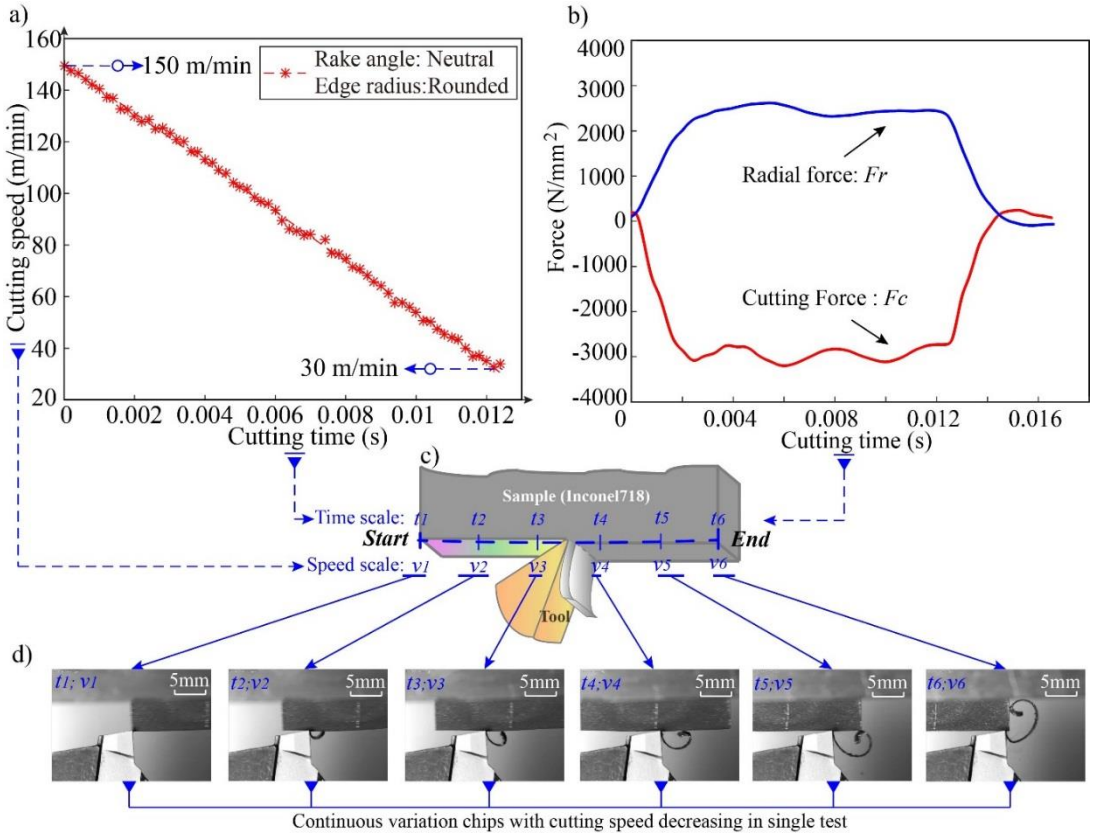



Fig.6-5 Illustration of cutting tests process in single test. a) Continuous decreasing cutting speeds; b) Corresponding cutting force; c) Illustration of cutting process; d) Snaps of monitored cutting process with a decrease of cutting speed

Fig.6-5c explains the evolution of the cutting process and interaction between the machined samples and the cutting tool, indicating that different cutting speeds could be correlated to corresponding tracked points at time scale. The tracked cutting process for the conducted test could be found in Fig.6-5d while the snapshot at several individual times (e.g. t1, t2, t3…) were presented to show the instantaneous cutting scenarios (v1, v2, v3…). A continuous decreasing cutting speed (starting from around 150m/min to 30m/min) on the single sample could be found (Fig.6-5a), validating the proposed concept. Corresponding continuous cutting and radial force following the cutting speed variation were monitored and presented (Fig.6-5b), while there is a good correlation between cutting force and tracked speeds in time scale that the cutting process lasts for around 0.012s. At the same time, the machined surface at these speeds could be found on the sample, which gives us enough information to investigate the cutting performance of the material at this large speed range in only one sample. Although it has been reported that the cutting forces reduced with the increase of cutting speed due to

a reduction in the increased cutting temperature which softens the metal aiding grain boundary dislocation [37-38], no noticeable difference was found here which is likely because the accumulated cutting temperature is not high enough to influence the material deformation process in such a short cutting time in this experiment.

The achieved continuous descending cutting speed indicates the ability of the PBCT based method for acquiring a certain range of cutting speeds rapidly. The example instantaneous pictures show that the whole cutting process is properly monitored and it could be used to analyse any involved speed.

### 6.3.2 Energy consumption during cutting process

An energy based surface integrity evaluation method has been proposed in chapter 3, whereby an energy threshold could be evaluated for a specific level of surface damage. The consumed energy in different cutting regions (shear energy $E_s$, friction energy $E_f$ and ploughing energy $E_p$) was calculated with the built energy model. Both the varying cutting speeds and forces have been acquired at one time while the chips were collected as well, thus the variation of consumed energy caused by the changing of cutting speed could be obtained (Fig.6-6). It can be seen (Fig.6-6b) that the consumed total energy (shear energy + ploughing energy + friction energy), which is basically determined by the cutting force, is slightly decreased following the cutting condition change and formed corresponding surface, showing a similar tendency with the acquired force (Fig.6-5b). The shear energy ($E_s$), as a significant factor on determining surface damage, decreased significantly with the declining of cutting speed when the other cutting parameters were kept constant. This is because the variation of cutting speed leads to the changing of shear angles, thereby the chip formation and shear energy will be influenced to affect the energy partition. An increasing trend is found for friction energy which shows a contrary tendency of shear energy. However the friction energy is considered to have no effect on the surface integrity because it mainly reflects the interaction between the chips and tool rake face. While the ploughing energy maintains a stable level at the whole process which is believed to be because the ploughing phenomenon remains almost constant for the same tool even for different cutting speeds.

The distance ($L$) from start point of the sample to the target position where the studied cutting speed is used could be acquired based on equation (6-1). Therefore the position of corresponding machined surface could be located (Fig.6-6a) for analysis.

$$L = \int_0^t v(t)dt \tag{6-1}$$

where *t* is the time when the target cutting speed achieved.

Several cutting speed points are chosen and the corresponding energy consumed at these individual positions are shown in Table 6-2 and bar charts (Fig.6-6 c). It shows the comparison of consumed energy in different cutting areas at specific cutting speeds and their variation between different cutting speeds. Evidently the cutting speed is found to have significant influence on the shear energy and friction energy variation while the total energy and ploughing energy are not affected so much.

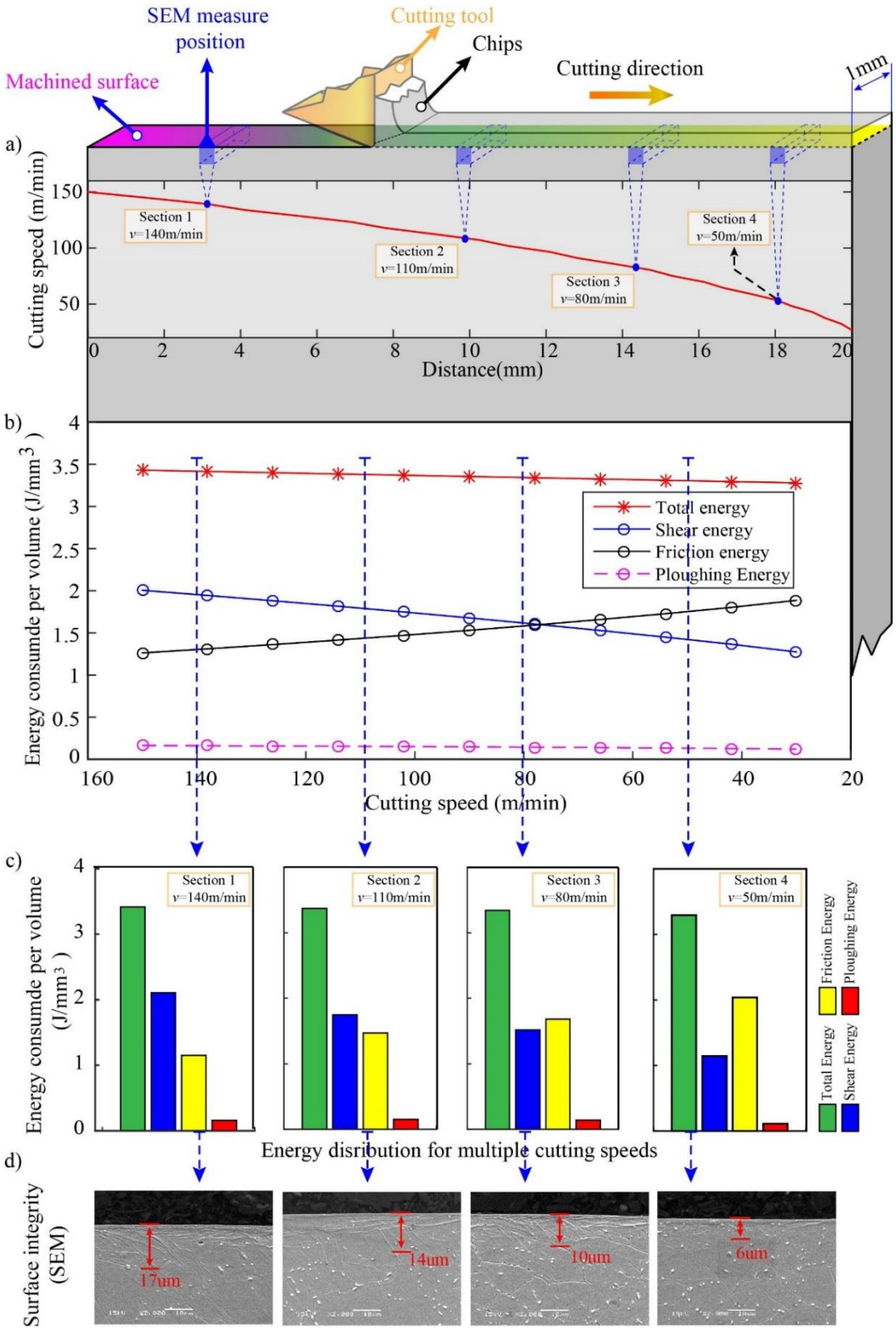



Fig. 6-6 Schematic and test results for different speeds in one single test. a) The position of corresponding speed on machined surface; b) Continuous energy changing with cutting speed varying; 3) Energy distribution at selected cutting speeds; 4) Corresponding machined surface of selected cutting speeds.

Table 6-2 Test results and consumed energy for selected cutting speeds

| Cutting speed (m/min) | Cutting force ($N/mm^2$) | Radial force ($N/mm^2$) | Total energy | Shear energy | Friction energy | Ploughing energy |
|---|---|---|---|---|---|---|
| 140 | 3418 | 2930 | 3.42 | 1.94 | 1.31 | 0.160 |
| 110 | 3389 | 3088 | 3.38 | 1.81 | 1.41 | 0.154 |
| 80 | 3335 | 2976 | 3.33 | 1.60 | 1.59 | 0.143 |
| 50 | 3274 | 3260 | 3.26 | 1.36 | 1.80 | 0.127 |

The corresponding machined surface integrity for these cutting speeds was preliminarily observed by using SEM on the properly polished sample. The grain deformation depth is regarded as the indicator to describe the superficial surface quality (Fig.6-6d) and correlated to the consumed energy. For example, the deformation depth is around 23μm at the speed of 150m/min ($t\approx5\times10^{-4}s$) and decreases to around 6.2μm (($t\approx1.1\times10^{-2}s$)) when the speed is around 50m/min, while seen from the energy aspect there is a clear shear energy decrease but the total energy and ploughing energy show little variation. As already described that the friction energy (interaction between chips and tool rake face) has no direct contribution to surface integrity, the shear energy is certainly the one that greatly relates to the surface quality and its decrease will lead to a better subsurface quality (lower deformation depth), which had been validated as well in chapter 5. The continuous varying energy distribution following the speed change shows that the cutting speed change will have a great effect on surface integrity and the machined surface at different cutting speeds could be located and analysed on a single sample in this test.

### 6.3.3 Chip morphology variation for different cutting speeds in single test

A significant variation chip (Fig.6-7a), where a clear serrated morphology appears at the start area when the cutting speed is high (e.g. 140m/min) and the chip shape becomes smooth at the end where the speed becomes low (e.g. 40m/min), is found and collected from the test. As known the chip morphology is interdependent on the cutting parameters [156] and higher cutting speeds will produce saw-tooth shape chips [157].

The cross-sectional images of the chip shows a continuous transformation from the heavily serrated chips to near uniformly deformed smooth chips. As seen (Fig.6-7b), the chip morphology at around 60m/min was still in saw-tooth shape

but naturally transited to a continuous one when the cutting speed decreased to around 50m/min. The influence of cutting speeds variation on the chip morphology is clearly presented on the collected chip from this single cutting test.

Also, the chip morphology was analysed with parameters defined (Fig.6-7) such as the chip thickness $h_p$ (peak-back surface distance), shear deformation $h_v$ (valley-back surface distance), and $\varphi$ (shear angle) were measured. For example, the corresponding parameters of chip morphology at around 140m/min ($t \approx 5\times10^{-4}$s) is illustrated (Fig.6-7c) and another three selected speeds (110m/min, 80m/min and 50m/min) are also shown in Fig.6-7d, e and f. Based on the measured data of chip morphology at different cutting speeds (from 150m/min to 30m/min), it could be seen (Fig.6-8a) that the shear angle is located at the range from 30° to 45°, and has an increasing tendency following the cutting speeds change from high speed to low, which has a good coherence with what are known [158].

The consumed energy that relates to the chips formation (shear energy and friction energy) was correlated with the chip morphology variation as well. It could be seen that the shear angle shows a converse trend with shear energy $E_s$ following the cutting speed decrease. Moreover, the relationship between the consumed shear energy and corresponding shear angle was built (Fig.6-8b), expressing that less shear energy $E_s$ is consumed when the shear angle is at a larger level. For example, the consumed shear energy $E_s$ was around $1.4\times10^9$ J/mm$^3$ when the shear angle was around 43°, but it became $1.9\times10^9$ J/mm$^3$ after the shear angle increased to 33°. It could be explained (Fig.6-9) that when the cutting depth remains constant ($t_c$), a larger shear angle ($\varphi_2$) corresponds to a smaller shear plane area ($A_2$) while the shear angle ($\varphi_1$) is correspond to the shear plane area ($A_1$). It is evident that more shear energy $E_{s1}$ will be needed to shear the materials in a larger area $A_1$ compared with area $A_2$. Therefore, a bigger shear angle means less shear energy is needed to remove the material, which explains the phenomenon found in Fig.6b that the shear energy is increasing following the shear angles decreasing.

In addition, an index value $S$ (equation (3)) is introduced to describe the height of the serrated part of the chips, and its variation was presented with the cutting speed changing and correlated energy (Fig.6-8c). The teeth height ($S$) starts from around 100μm (significantly serrated chips) and decreases to almost 0μm (smooth chips) with the cutting speed decreasing (shear angle increasing), clearly showing the effect of cutting speeds on chip morphology in another view. To clearly study

the influence of consumed energy (both $E_s$ and $E_f$) on chip morphology, they were presented as a function of $S$ (equation 6-2) in Fig.6d. When the shear energy $E_s$ is increasing, a larger $S$ is found and at the same time the friction energy $E_f$ have a negative relationship with $S$. It could be explained that a larger shear energy will increase the deformation of the material in the shear area to a larger $S$, while less friction energy $E_f$ means the deformed material by shearing effect were affected less by the interaction between chip and tool rake face.

$$S = h_p - h_v \tag{6-2}$$

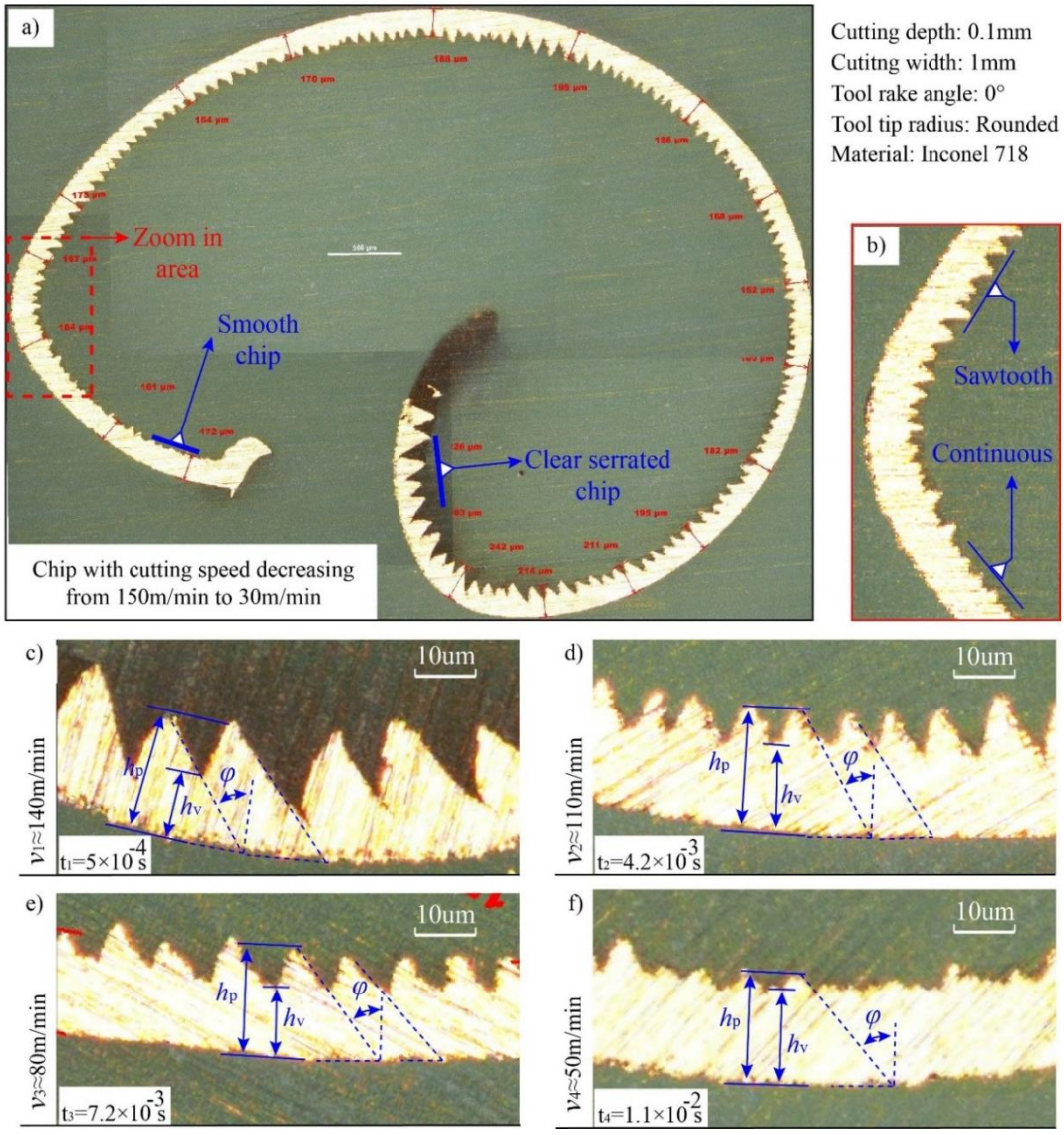



Fig.6-7 Chip morphology variation in single test. a) Chip morphology collected from single test; b) Zoom in area of chip morphology shape transformation; c) Chip morphology at $v$=140m/min; d) Chip morphology at $v$=110m/min; e) Chip morphology at $v$=80m/min; f) Chip morphology at $v$=50m/min;

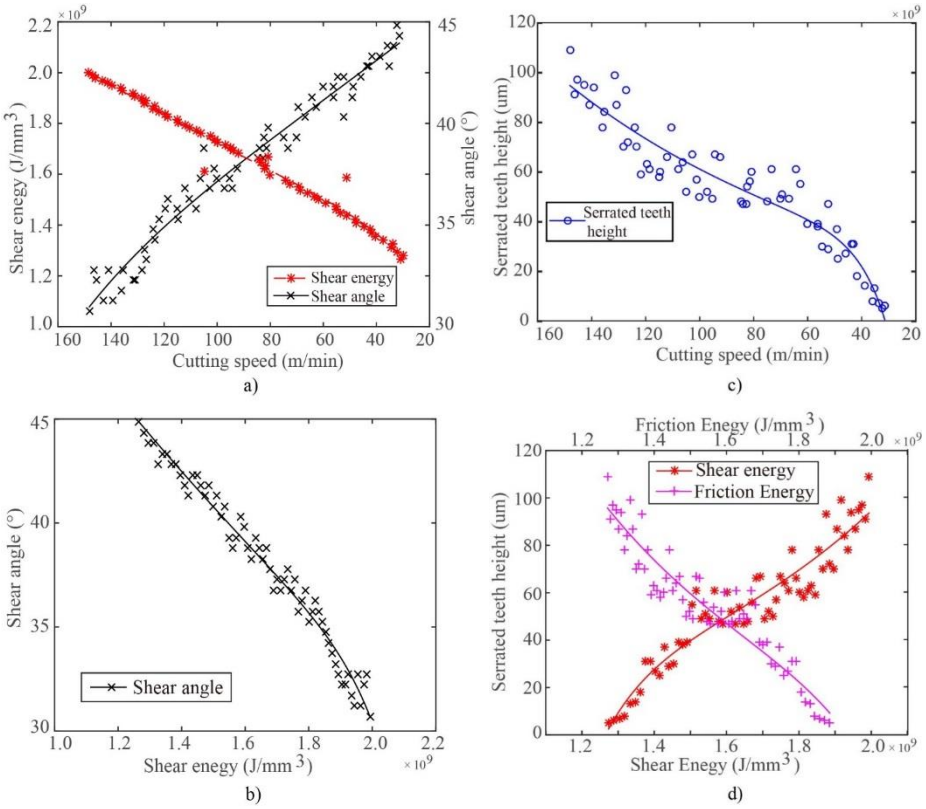



Fig.6-8 Relationship among chip morphology, consumed energy and cutting conditions. a) Relationship between shear angle and cutting speeds; b) The effect of shear energy on shear; c) The effect of cutting speeds of serrated teeth height *S*; d) Relationship between *S* and both of shear energy and friction energy

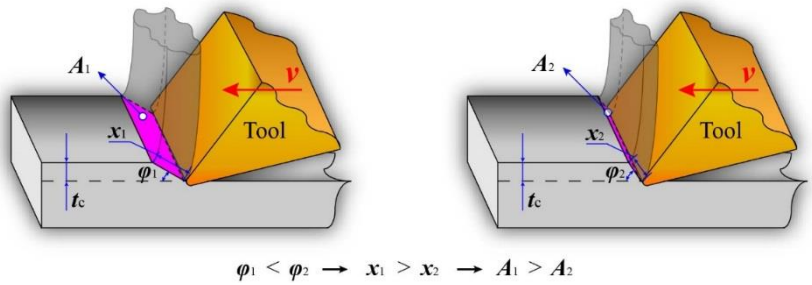



Fig.6-9 Comparison of shear plan at different shear angles

### 6.3.4 Surface integrity investigation with EBSD

EBSD, providing grain orientation and the information of intragranular misorientations [159], is an advanced technique that can be used to study the machining surface integrity by measuring the superficial surface layer. The EBSD analysis of the superficial machined surface layer at selected cutting speeds (around 140m/min, 110m/min, 80m/min and 50m/min) were carried out with

employing line scanning mode on an area of 90μm×65μm stretching from machined surface into the sample and using 0.08μm micrometre resolution.

The representative inverse pole figure colour map with band contrast maps overlaid (Fig.6-10a) show the intragranular misorientation and plastic activity of the superficial surface at different cutting speeds. It is quite obvious that the near machined surface region (A) is severely deformed while the grain crystalline level (lattice rotation) in region B is less and it continues decreasing towards the bulk materials (C). Also, it is noticed that the extent of overall deformation zone for high speed (e.g. $v$=140m/min) is higher compared with the low speed one (e.g. $v$=50m/min) and it has a decreasing tendency following the speed decreasing.

The extent of plastic deformation strain in the superficial layer of the machined surface is presented as strain contouring (SC) mapping [70] by calculating the orientation changes within each grain and weighted by grain size (Fig.6-10b). For example, in Fig.6-10b-I, the near surface area is denoted by green colour indicating increasing strain regions and low strain area (blue colour) is distinguished approaching the bulk materials area. It is worth saying that the appearance of black areas or bonds in the map is due to the grain size being too small (in Nano-scale) to be identified at the current chosen resolution. Evidently the high SC area (green) in the subsurface for low cutting speed is noticeable less than the corresponding higher speed ones. An average intragranular misorientation (AMIS) value is used to study the extent of plastic deformation quantitatively. With measuring $N$ points in a line across $M$ grains, the AMIS figures could be calculated by following Eq. (6-3), where $\theta_{jk}$ is the misorientation between points $j$ and $k$ within grain $i$.

$$AMIS = \frac{\sum_{i=1}^{M}\left(\frac{2\sum_{j=2}^{N}\sum_{k=1}^{j}\theta_{jk}}{N_i(N_i-1)}\right)_{grain(i)}}{M} \tag{6-3}$$

The AMIS profiles (Fig.6-10c) also describe the deformation level as a function of depth from the machined surface down to the bulk materials and a decreasing phenomenon of its value is accordingly found in this direction. It is not surprising that the AMIS profile for the surface generated by a higher cutting speed remains larger than those acquired from lower speeds, which shows good correlation with the above SC results. For example, the AMIS value remains around 4° until 40μm under the machined surface for at cutting speed of 140m/min, but it is only 2.5° even in the maximum level at 30μm for the cutting condition with 50m/min. Finally

all of the AMIS values reached to the stable level (less than 1°), but at different superficial surface depths.

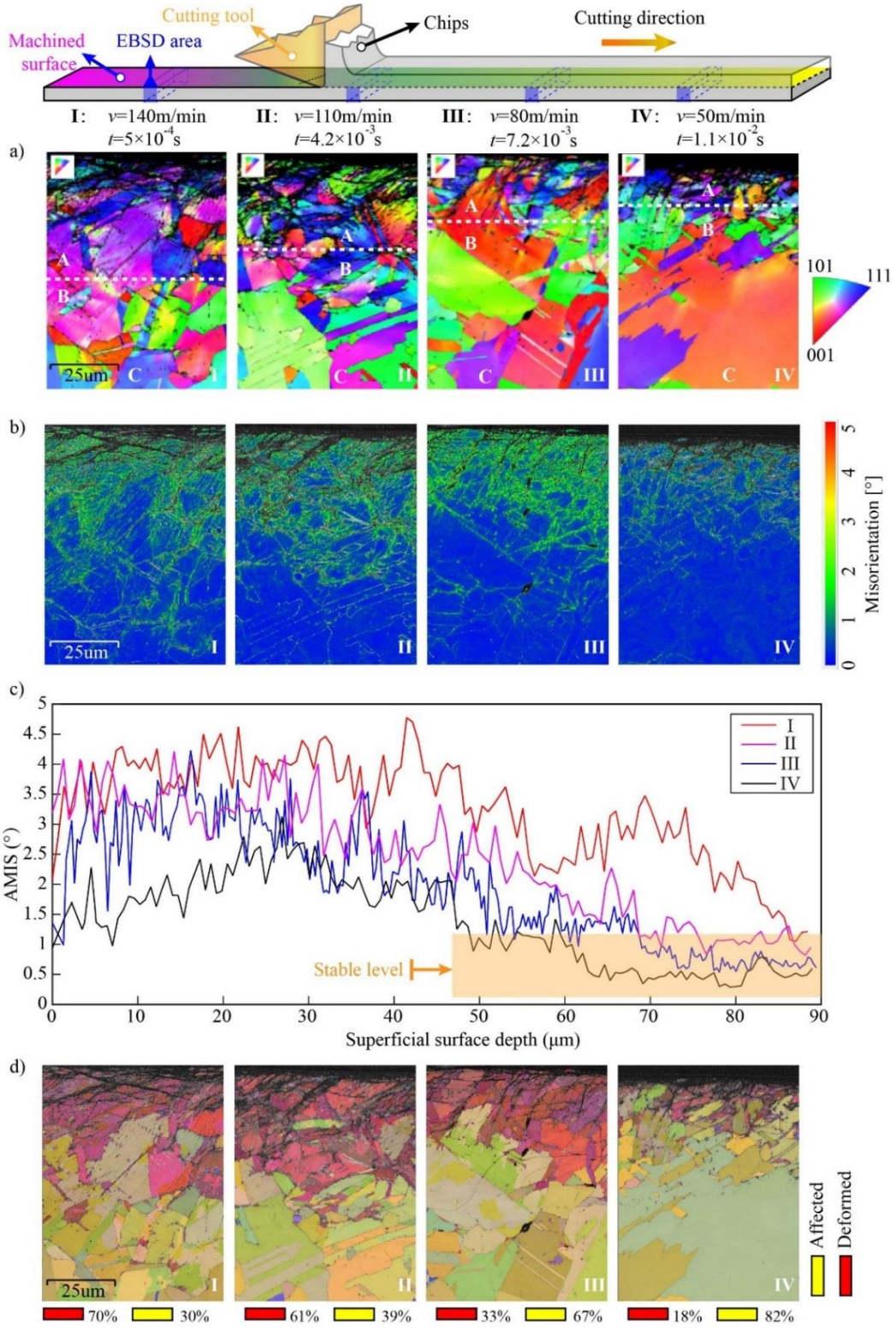



Fig.6-10 EBSD results for single sample at different cutting speeds. a) Inverse pole figure of selected cutting speeds; b) Subsurface strain contour map; c)

Corresponding AMIS variation in depth direction under machined surface; d) Proportion of affected grain distribution by machining at different cutting speeds

As seen, the grain misorientation beneath the machined surface is decreasing from the top (grain severely deformed) to bulk materials (free of deformation), while the machining affected region could be divided into heavy deformation layer (deformed), partially deformed layer (affected) and no deformation area (bulk materials). Normally the grains in the heavy deformed areas could be observed in SEM pictures as they were elongated or tended to bend towards the cutting direction. The distribution of grains in the affected regions for the above measured and analysed areas were shown in Fig.6-10 d. A large amount of grains were deformed beneath the machined surface with higher cutting speeds (70% at 140m/min) while it was 18% at 50m/min, but almost of all of the rest grains in the measured areas were affected by the machining process which is not visible with only SEM techniques.

To conclude, the EBSD study techniques reveal the machined surface integrity in a deeper level, which gives more information on machined induced deformation in the grain level and could quantify the surface integrity in grain misorientation. The results show that the grain deformation level is more obvious near the machined surface and decreases to no deformation until bulk materials. It is, however, worth underlining that the deformed layer is more pronounced under the cutting conditions with higher cutting speeds compared to those with lower cutting speeds. While correlating with the consumed energy as presented above, the grain deformation depth has a positive relationship with the consumed shear energy, which means that the shear energy has a dominant role in determining the grain misorientation as the ploughing energy shows little variation during this process.

### 6.3.5 Residual stress analysis of machined surface integrity

The subsurface damage induced by machining consisted of not only deformed grains (studied by EBSD techniques presented above), the residual stress left on the machined surface which is highly related to the work performance and service life of the product is worth investigating as well.

The residual stress on the machined sample was measured at four different positions (corresponding to former selected cutting speeds) as illustrated in Fig.6-11a. With the help of Electrolytic Polisher, the residual stress in each position was measured from surface to bulk materials layer by layer in the depth direction. For example, in the first position (2.5mm from start), different measured depths ($d_1$,

$d_2$, $d_3$…) are illustrated (Fig.6-11b) after material was removed by electric polishing. A non-linear phenomenon that a higher slope is found at the start area (Fig.6-11b zoom in) while the slope tend to slow down following the depth goes deeper. This is because the contact area of polish liquid and workpiece is smaller when the polished depth is small (e.g.10μm) therefore less material is needed to be remove to achieve the target depth while more material is need to be removed for a deeper depth (150μm).

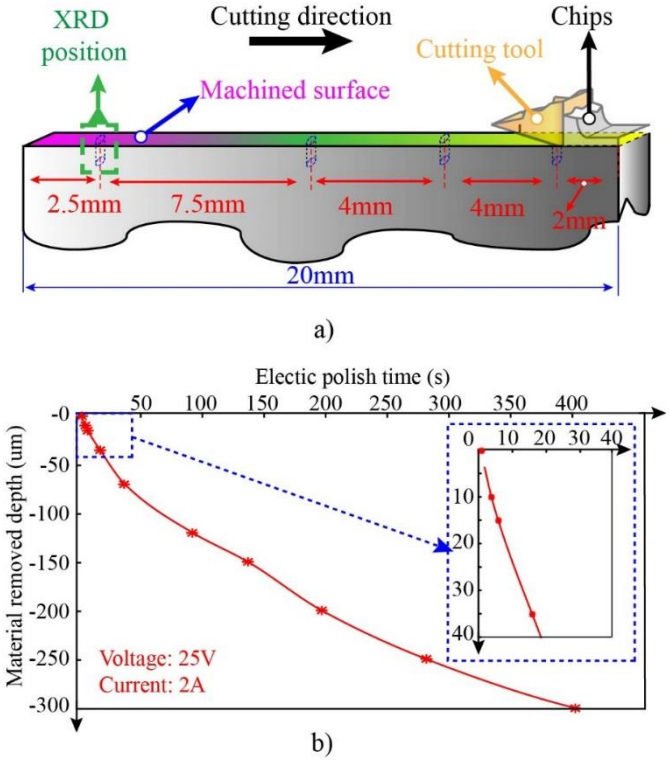



Fig.6-11 Residual stress measurement of machined sample at different positions. a) XRD measurement position and b) The relationship of polishing depth versus polishing imposed time

As a function of the depth under the machined surface and cutting length, the residual stress acquired at different subsurface depths and cutting speeds were fitted as a surface (Fig.6-12a). It could be seen that the highest point (largest stress) is found approaching the start area of the cutting when the cutting speeds is at high level (e.g. 140m/min). Then the stress starts to go down following the superficial surface depth and cutting length increasing (speed decreasing). It is true for the residual stress in both cutting direction and orthogonal direction, therefore it is chosen to present and discuss only cutting direction stresses in this work. Seen from the X-Z view of the 3D map in Fig.6-12a, the residual stress was presented as the function of depth under the surface (shown in Fig.6-12b) and the profile was tensile at the surface position with values ranging from around 370MPa

to 1400MPa depending on the different cutting speeds employed. However, the stress value drops rapidly following the increasing of superficial surface depth and reaches compressive levels (within 50μm) quickly before it slowly goes back to non-affected level (deeper than around 250μm).

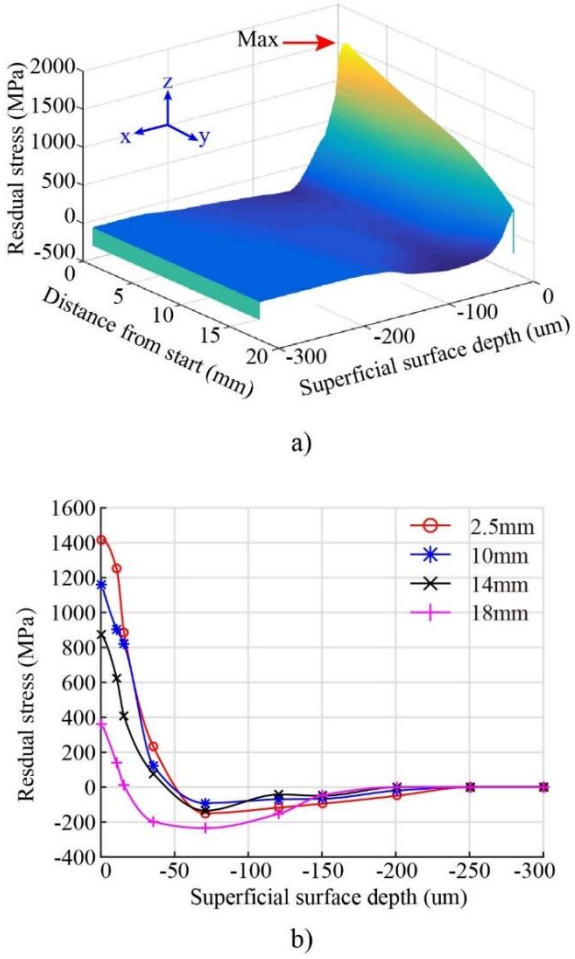



Fig.6-12 Residual stress results at different depth and position. a) Continuous residual stress profile versus depth and cutting length, and b) Residual stress distribution at different position and depth

Fig.6-13b also shows the in-depth investigation of the peak-half width value for these measurements. The maximal peak half-width values ($LC_{max}$), determined on the workpiece surface and giving the information on the work-hardening state of the surface, show a significant difference on surface work-hardening for different cutting conditions. Highest $LC_{max}$ is found when $v$=150m/min and the minimum is located at $v$=50m/min, which is reasonable and has a good correlation with the acquired residual stress profile. The relationship between input shear energy and residual stress left on the machined surface is presented in Fig.6-13a. It could be found that the variation of them are sharing the same tendency that the residual stress on the surface (0μm) is decreasing following the consumed shear energy

reducing. This indicates that the shear energy input into the cutting area has an important relationship on the residual stress left on the machined surface, which is backing the conclusion above that the shear energy significantly determines the machined surface integrity. It could be concluded that a higher cutting speed will lead to a higher surface tensile stress at the surface and superficial layer of the workpiece, which could be found in [160] as well. The biggest compressive stress (around -200MPa) is found at the end of the machined surface when the cutting speed has slowed down (e.g. 50m/min). It could be explained that at this cutting speed the temperature effect is relatively small in such a small sample and short cutting time, thus the mechanical effects dominate, resulting in more compressive stress.

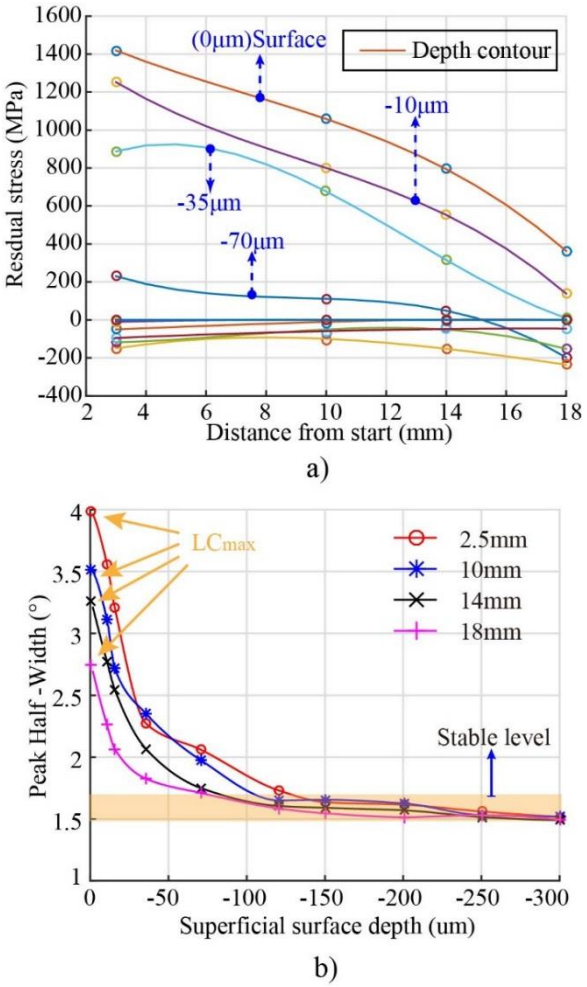



Fig.6-13 Residual stress results at different depth and position. a) Residual stress contour at different position, and b) Peak half-width values for measured residual stress

### 6.3.6 Superficial surface Nano-hardness investigation

The superficial surface work-hardening of machined workpieces is still considered as a significant negative factor to evaluate surface integrity of Ni-based superalloy, resulting tool wear and low service life etc. [161]. To investigate the mechanical properties of the sub-surface layer, Nano-hardness profiles were obtained by applying Nano-indentation measurements on the acquired sample (Fig.6-14). Four series of Nano-indentations, each consisting of 9 indentations, were performed at different positions along a line perpendicular to the machined surface and in the direction from superficial surface to bulk materials. It is worth noting that a space of 3μm between two neighbouring indent points in each series indentation was set and the first measurement started at about 1.5μm under the machined surface to avoid edge softening effect (Fig.6-15a). A Berkovich indenter with a 120° tip is used and the indented marks are shown in Fig.6-15b.

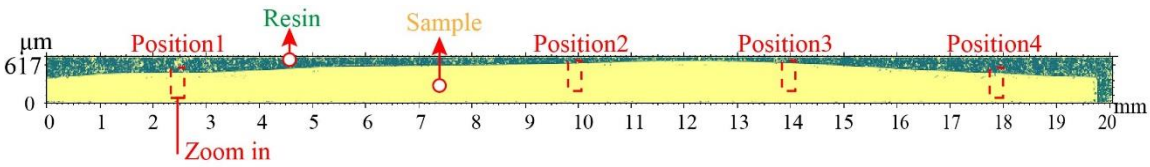



Fig.6-14 Illustration of the positions of Nano-Hardness measurement on the machined sample

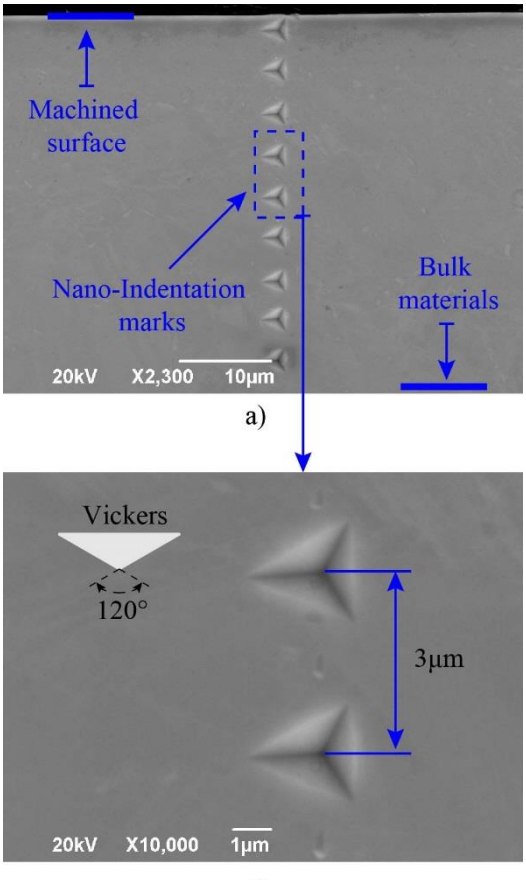
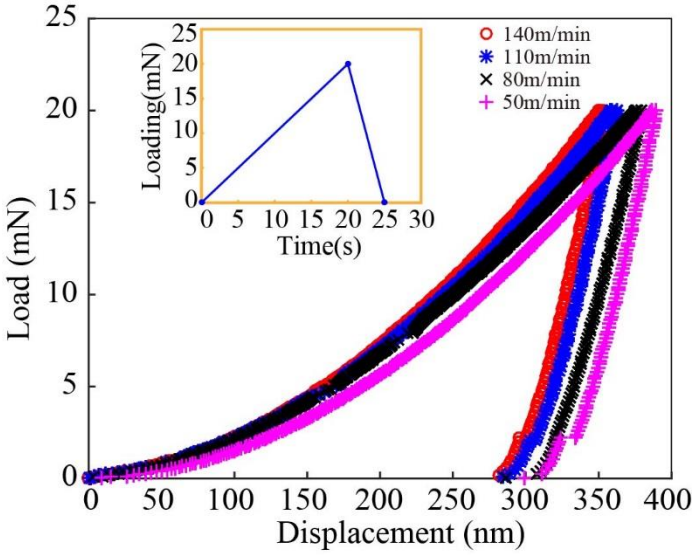
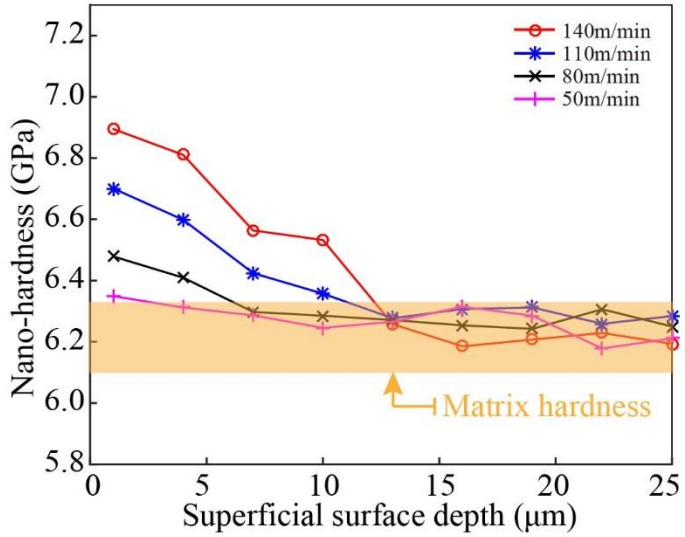


Fig.6-15 Nano-Hardness measurement marks in superficial surface. a) Example of one serial measurement, and b) magnification of two neighbouring indentations




a)




b)

Fig.6-16 Results for nano-hardness measurement. a) Load-displacement curves at different measurement positions, and b) Nano-hardness comparison at different positions

Fig.6-16 a shows the typical load-displacement curves from the measurements for the first point of each test series (the nearest point to the machined surface) while each indentation was implemented with a loading cycle and unloading. Evidently the response of each of the four positions was different such that the smallest displacement (indentation depth) was found for the area acquired from cutting

speed at 140m/min and the largest one was for 50m/min. From the described data, the hardness of corresponding points could be calculated (Fig.6-16b) while the bulk material hardness were also obtained from Inconel 718 matrix for reference.

The Nano-hardness distribution across the measured area illustrated a marked difference among the subsurface acquired from different cutting speeds, that the hardness for cutting condition of speed at 50m/min shows little variations across the distributions, while a noticeable increased Nano-hardness can be found for a higher speed (e.g.140m/min). A continuous hardness decreasing could be observed on the surface with cutting speed decreasing, for example the hardness of nearest surface position decreased from 6.88GPa to 6.35GPa while the corresponding cutting speed changes from 140m/min to 50m/min. All of the hardness decreased to matrix level from the very near surface region to bulk material, which is somehow expected when it is correlated with the sub-surface plastic deformation (Fig.6-10) which introduces work-hardened phenomenon. In addition, no significant difference in hardness over repeated tests was seen.

## 6.4 Conclusions

The findings and conclusion in this chapter could be drawn as follow:

1) With the help of proposed and modified PBCT machine, a properly monitored cutting process with continuous cutting speeds changing (from 150m/min to 30m/min) were carried out on a limited geometry (20mmlength) Inconel 718 sample in single test. It validates the ability of this method to rapidly obtain machined surface integrity of materials at different cutting conditions in a one-go test rather than resourceful tests on traditional machine tools.

2) The chip morphology variation caused by cutting speed changing is demonstrated by the continuous variation chip that serrated at the start (150m/min) and nearly uniformed at the end (30m/min). The collected chip from one single test were analysed by measuring the defined parameters and it validated the conclusion that the shear angle increasing with cutting speed decrease.

3) Energy consumed in different cutting areas during the variation of cutting speeds changes is studied as well and it gives the information that the shear energy is decreases following a decrease in the cutting speeding, and the corresponding surface deformation depth decreasing.

4) The EBSD study, including inverse pole figure and strain contouring, gives an in-depth investigation on the grain deformation and misorientation of the superficial surface layer. The AIMS value and grain deformation distribution percentage enable the quantification of the surface integrity.

5) Measured residual stress results with XRD shows that a higher residual stress was located when the cutting speed is relatively high and Nano-hardness results show that high cutting speed will lead to a higher surface hardness, while both of them validate the former analysis results and have good correlation with published results.

To conclude, this study reports the innovative method of testing materials cutting performance with limited resource required and gives the potential to study cutting performance and surface integrity in a game changing way.

# Chapter 7

# Discussion, conclusion and future Work

In this Chapter, the research and analysis conducted in the previous chapters will be summarised. The discussion will combine the research findings together with the aims of this PhD research project, and the advantages of this method to carry out wet cutting tests will be discussed. The findings and suggestions about surface integrity evaluation and methods to prevent surface anomalies will be presented and discussed. Then a discussion of the potential improvement of this work will be given as well as concluding the possible future topics and applications for both academic and industrial purposes.

## 7.1 Discussions

The research carried out in this thesis was based on the surface related machinability investigation of material used in aero-engines regarding the high strength and stability requirements. This follows orthogonal cutting on the target materials, taking Inconel 718 as an example, with different cutting parameters acquired. It investigated the conventional method used for material machinability study and discussed their advantages and disadvantages. To fill in the gaps that the state-of-art method is not good enough for studying the materials in relative small volumes and could not investigate the cutting performance transition in different cutting conditions continuously, a new method which is able to rapidly capture the machined surface of materials is proposed. With this method, a designed pendulum is used to hold the target material and released at a specific angle, thereby an anticipated cutting speed will be achieved when the pendulum is in the lowest point where the target sample will come across the fixed cutting tools. Then the orthogonal cutting process could be carried out, while the dynamometer is used to acquire the cutting force during this time and a high speed camera is used to monitor the cutting process as the cutting time is short (in the level of $10^{-3}$ s while considering the cutting length at maximum 20mm). The cutting process in the designed pendulum machine could be acquired and compared with the conventional machining in machine tools. The sample used in the test is in the dimension of 25mmx25mmx1mm, which is quite small compared with the ones used in machine tools. In addition, the cutting conditions with multiple cutting speeds could be acquired in this small sample in a single test as shown in Chapter 6. This is a huge advantage when considering the massive cutting tests needed for conventional cutting tests.

Apart from this, conventionally different cutting conditions needed to be tested for selecting appropriate cutting parameters and the results would be useless if any of the parameters have been changed. This means that no transferable results could be applied with the conventional evaluation methods for cutting performance. An energy-based evaluation method for surface integrity related machinability, dividing the energy for removing materials into shear, friction, ploughing and worn energy (energy consumed between tool flank face and machine surface because of the tool wear), was built. In this case, the consumed energy was regarded as the factor that governs the deformation process and generation of the machined surface. It is worth mentioning that the energy evaluation method is not restricted to specific cutting conditions or parameters. Therefore it could be used to evaluate the cutting process from the basic material removal process. Regardless of the cutting parameters used in the cutting process, as long as the energy input into the cutting areas are determined, the machined surface integrity could be revealed. In other words, the energy thresholds for specific surface damage level could be determined with the energy evaluation methods. Therefore, the energy consumed in different cutting areas as stated in the previous chapters was calculated and studied to build the relationships with surface integrity.

It should be underlined that these very complex relationships are encountered mainly when the surface integrity is a key output measure, for example, in the situation that is of more interest for high added value industries such as aerospace, nuclear and defence manufacturing sectors. The literature review in Chapter 2 shows that the current cutting performance evaluations, include conventional machined tool cutting tests with massive trials and parameters, analytical and simulation methods that are using assumptions, and the evaluation method from the view of consumed electrical power etc.

To overcome the drawbacks of huge test requirements for material cutting performance evaluation, a PBCT machine was proposed and the detailed design was presented in Chapter 3. To evaluate the machined surface integrity in an effective way, an energy model is proposed and associated with the PBCT method for surface integrity related machinability investigation, and the detailed information for built energy models and theory could be found in Chapter 3 as well. With the combination of these two proposed concepts, the surfaces integrity of machined surface could be quickly acquired and the consumed energy for specific surface damage level could be calculated. The validation results of these concepts could be found in Chapter 5 and 6, where multiple cutting tests were carried out and the corresponding consumed energy and surface integrity were analysed.

In Fig.7-1, an illustration of the detailed surface integrity related machinability evaluation process for Inconel 718 with the proposed PBCT energy method was presented. The PBCT machine is designed and validated at first, then the desired cutting tests can be carried out on it. There are two main test objectives here and one of them is to build the relationship between consumed energy with the machined surface integrity (damage level). In this case, the concept is that the consumed energy in the cutting areas could be correlated to the machined surface integrity. Another objective is to investigate the possibility that the machined surface at multiple cutting speeds could be acquired in a single test, which will show another advantage of this method that it could hugely reduce the amount of cutting tests. The cutting forces, monitored videos (speed could be decomposed from the video) and cutting chips could be collected for above mentioned cutting tests.

At the same time, the energy model for calculating energy distribution in different cutting areas could be built based on the known basic formulations. With the cutting data (including force, chips, speed) acquired in the cutting tests, the energy consumed for these corresponding areas during the cutting process could be calculated. As the machined sample will be sectioned and subsurface deformation will be observed for each test, the surface integrity and energy consumed to generate these surfaces could be correlated together. Based on the analysis and the relationships found in the results, the surface related machinability of the target materials could be revealed, while the energy thresholds for specific surface damage level can be identified.

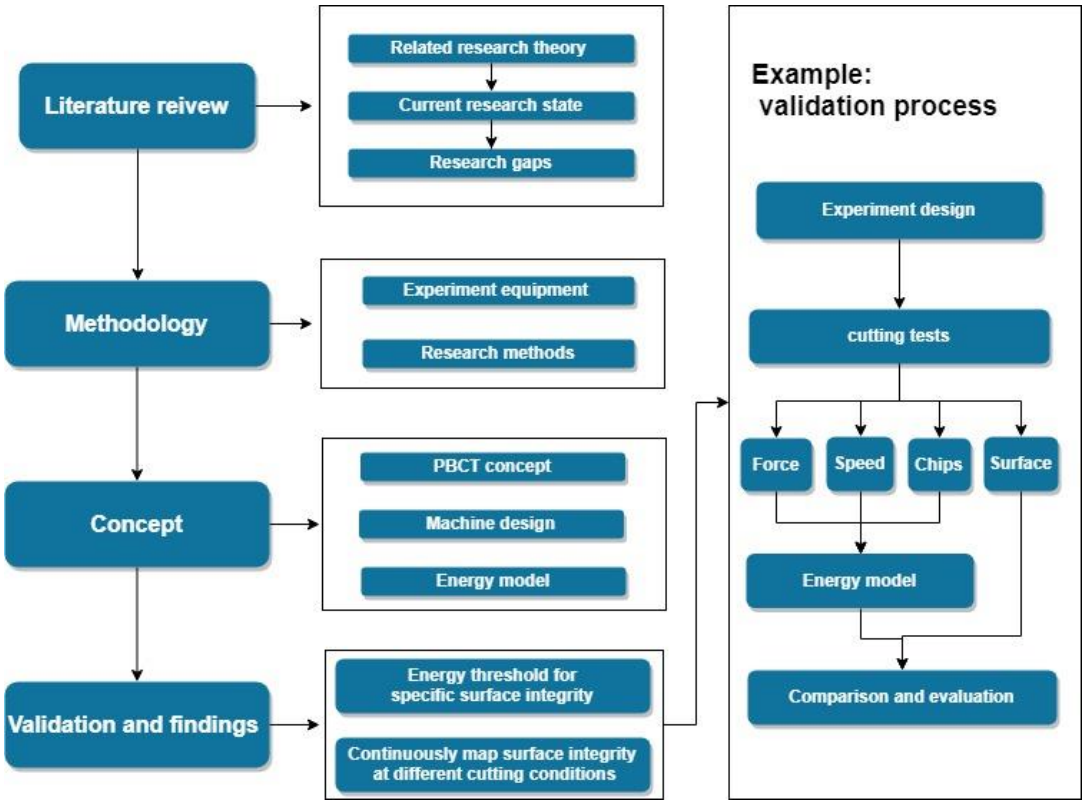



Fig. 7-1 Surface integrity related machinability evaluation process with PBCT energy method

To prove the above proposed ideas, the validation of the concept that the energy consumed in the cutting areas can be linked to the machined surface and used for evaluating materials' properties was carried out at first in Chapter 5. It shows that the studied energy has significant influence on the generated surface integrity as supposed. Both fresh tools and worn tools are included into the tests to prove the robustness of the proposed concept. Furthermore, it was found that similar deformation surfaces could be acquired if the input energy distributions in the cutting areas are similar irrespective of the cutting parameters being different. This means that desired surface integrity could be achieved by controlling the energy level input into the cutting areas rather than controlling the cutting parameters.

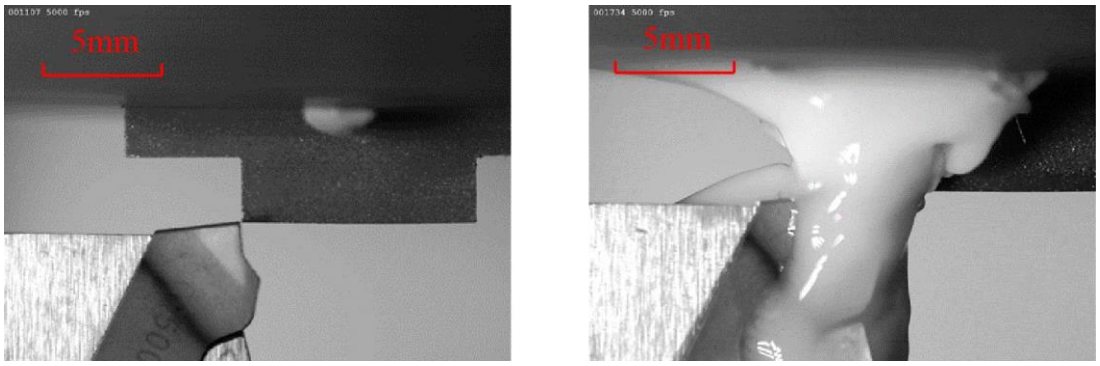
While considering the characteristic of the PBCT method that the cutting speed continues decreasing during the cutting process, validating the concept to obtain machined surfaces at multiple cutting speeds in single test was carried out in Chapter 6. A new designed sample with a long cutting length is used to cover a larger range of cutting speeds (150m/min to 30m/min). Corresponding morphology variation chips and machined surface following the speed changing were acquired. Therefore the surface integrity at the above range of cutting speed

variation could be inspected on the single sample which significantly reduces the work needed with conventional methods. Several measurement methods including EBSD, XRD, Nano-indentation etc. have been employed to study the material deformation, while quantitative methods for deformation depths of the machined surface have been provided as well.

By analysing the validation test results, the roles of energy in different areas during the cutting process could be concluded. It is found that the shear energy has direct relationship with the machined surface integrity (material drag depth as an indenter here) and it plays the dominant roles. The friction energy consumed in the interaction between the generated chips and tool rake face has no direct contribution to the surface integrity. The ploughing energy is mainly influenced by the radius of the tools rather than the cutting parameters variation. The worn energy caused by the tool wear at the flank face of tool and consumed in the cutting process has a significant influence on the surface deformation and white layer generation as well. In terms of the chips generated, the morphology has been found to be related to the energy consumed and varied following the speed variation. Continuous shear angle variation was found from the collected chips in the single test while the energy variation has a good correlation with them. This enables the study the chip formation phenomenon on different cutting speeds in a single test.

As mentioned in this thesis, there are wet cutting conditions considered during the design of the PBCT machine. To preliminarily validate the wet cutting application of PBCT, several trial tests have been carried out with fabricated wet cutting rigs. The coolant liquid used is ROCOL V-CUT MP cutting fluid with a proportion of 1:10 to water. An illustration of the comparison of tests carried out in dry and wet cutting conditions is presented in Fig.7-2. The whole cutting area is covered by the cutting fluid which proves that the cutting process is in a wet cutting condition.

The cutting sample with a 10mm cutting length and 1mm cutting width is used, and fresh cutting tools with neutral (0°) rake angle is used. Detailed cutting parameters are listed table 7-1.




a) b)

Fig.7-2 Comparison of PBCT tests in dry and wet cutting conditions

Table.7-1 Cutting parameters of dry and wet cutting tests for Inconel 718

| Number | Cutting depth (mm) | Rake angle (°) | Cutting condition | Tool condition | Cutting length (mm) | Cutting width (mm) |
|---|---|---|---|---|---|---|
| 1 | 0.05 | 0 | Dry | Fresh Tool | 10 | 1 |
| 2 | 0.05 | 0 | Wet | | | |

The cutting force for wet cutting during the cutting process were captured and presented in Fig.7-3. It could be seen that cutting force slightly decreased after the coolant is introduced into the cutting process. Correspondingly the cutting speed variations during the cutting process are presented in Fig.7-4. The cutting speeds decreased from the start to the end during the cutting process for both dry and wet cutting. However, the speed decline rate is different, because the energy consumed for dry and wet cutting conditions is different during the cutting process. The cutting speeds at 105m/min and corresponding cutting forces were selected. Then the energy consumed during the cutting process were calculated based on the acquired cutting force and cutting speeds and they are presented in Fig.7-5. As seen the energy consumed at each aspect (total, shear, friction and ploughing) decreased after the wet cutting is used.

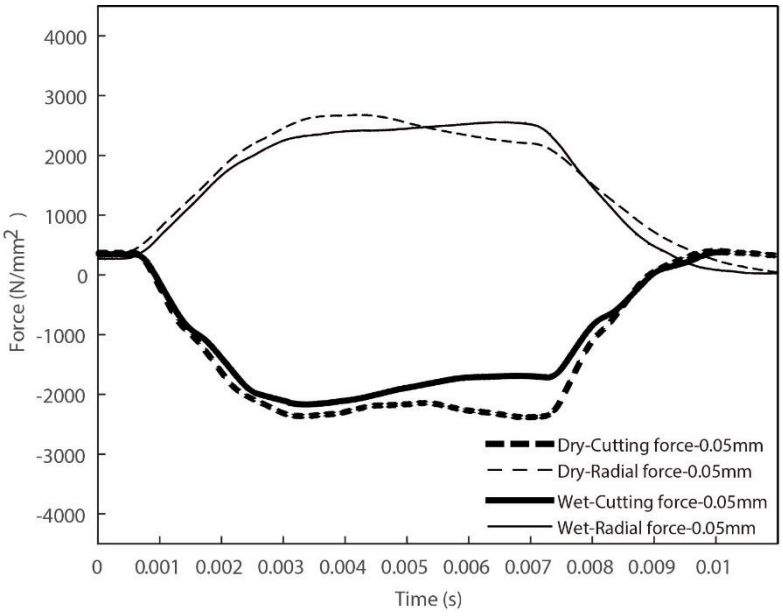



Fig.7-3 Cutting force comparison for wet and dry cutting

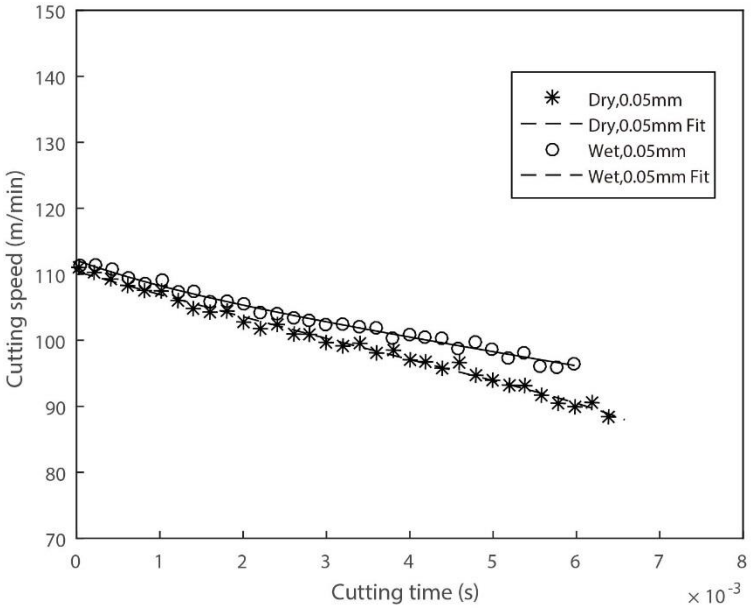



Fig.7-4 Speed variation for tools in dry and wet cutting condition

The superficial surface integrity of machined samples for above mentioned cutting tests are shown in Fig.7-6. Seen from the energy distribution bar, the energy consumed during the dry cutting condition is higher than the corresponding wet cutting condition. This could be reflected on the machined surface deformation depth where the dry cutting conditions (7um) naturally is higher than those in wet cutting conditions (3um).

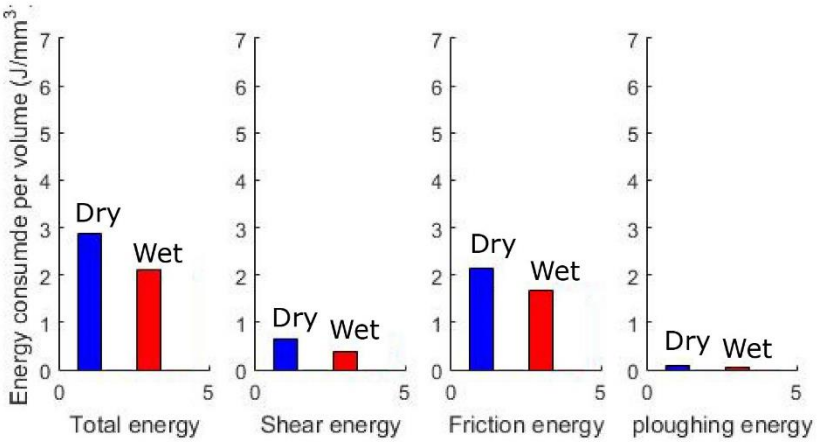



Fig.7-5 Energy distribution for cutting in both wet and dry cutting condition

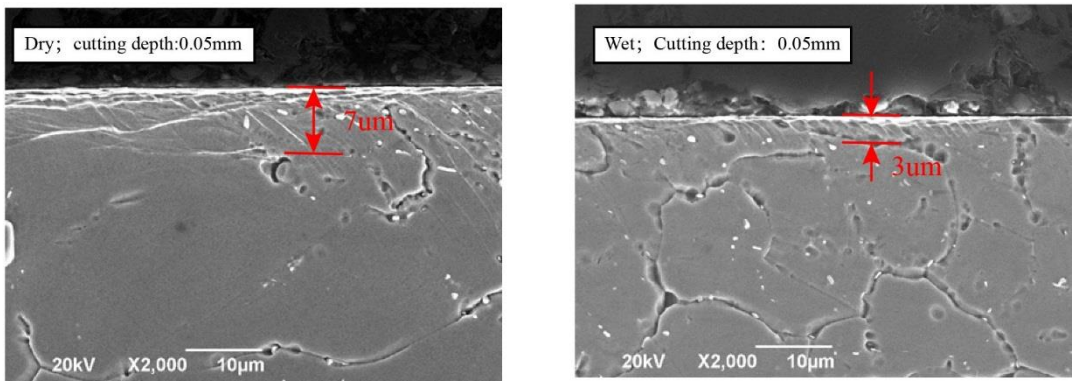



Fig.7-6 Surface integrity comparison of machined surface in dry and wet cutting condition

The validation tests and comparison between dry and wet cutting conditions indicate that this PBCT method is applicable to study the cutting process in wet cutting conditions and the corresponding machined surface integrity could be evaluated from the acquired samples. Also, the difference in comparison between dry and wet cutting condition shows that there are thermal effects existing in the cutting process even in the short cutting time and they have affected the machined surface integrity. However, how much heat has been generated and built-up, and how high the temperature could reach in the cutting process are still unclear. Therefore, more research effort needs to be put into this area in the future.

## 7.2 Recommendation for Surface integrity related machinability evaluation

In the above mentioned methods including test and energy based analysis for material surface related machinability evaluation, the proposed PBCT method is

proved to be an adequate method to capture the cutting process on small volume materials. Also, it is proved to be able to acquire the machined surface and cutting results at multiple cutting conditions at one time. This will again hugely reduce the work load for carrying out cutting tests regarding the resource aspect.

The energy based method for surface integrity evaluation directly treats the energy consumed by chips formation and new surface generation as the factors to study in the cutting process. Energy thresholds for specific surface damage levels could be determined, which work as an agent to deliver the surface integrity state. It brings the possibility to understand the surface integrity via the energy consumed from the calculation based cutting monitored results, while no sectioning and metallurgy observation will be needed to check the surface. Combining with the PBCT test method, this evaluation concept could extensively decrease the resource required for the evaluation of cutting performance of materials.

1) Machining test method

As discussed currently the majority of the methods to test the cutting performance of materials are based on the practical cutting tests on machine tools with lots of materials and massive different cutting conditions. This is quite resourceful for testing materials in small volume comprehensively. Therefore, this thesis provides a possible alternative method to accomplish the above goals.

It indicates that as long as the relative movement between material and tools could be achieved, the cutting process could be implemented, therefore it is not restricted to specific machine tools or machines. As found in the literatures, the Split-Hopkinson pressure bar (SHPB) test has been tried to study the chip formation phenomenon and gather initial parameters for cutting process simulation to improve the accuracy. However, it was not used to study the cutting process itself comprehensively. The suggestion is that, this machine maybe able to be modified to simulate the high speed cutting process during cutting with small amount of materials as well because it does have the possibility to increase the relative movement speed between two items (sample and tool). However, proper design, including the force measurement, speed tracking, cutting process monitoring and fixture are needed before it could be used to study the cutting process independently.

Apart from this, the linear motor which obviously has the ability to generate the required speed for cutting is also possible to be employed for carrying out cutting tests. The sample could be fixed on the motor and keep a variable distance from

the cutting tool to adjust the cutting depth, while the other cutting parameters could be designed accordingly. This will also give the possibility to avoid using machine tools to carry out cutting tests. The accessory equipment for having a proper monitoring process should be designed to give enough information for studying the cutting process.

Therefore, although this proposed PBCT method is able to carry out the cutting tests quickly, it is still worth exploring other potential methods to enhance the ability (such as high speed) of evaluating the cutting process without utilizing machine tools.

2) Surface integrity evaluation

Surface integrity has been paid a lot attention in this research to validate the concept of evaluating materials machinability as it is the most important aspect for the component manufacturers especially for those in safety critical industries. The energy based evaluation method mentioned in this thesis proposed a way to study the material deformation and surface generation directly in an energy view, where the cutting parameters combination are not limited to specific groups. The energy in different cutting areas (shear, plough, friction and ploughing energy) has been considered and correlated to the material drag depth of the machined surface.

Regarding the evaluation techniques for the surface, it is recommended to investigate the deformation status with EBSD as well, which will be able to tell the difference of deformation in grain levels quantitatively rather than the empirical evaluation methods such as SEM and microscope. With this technique, the benchmark of specific damage depth of surface could be built and correlated to the current surface inspection method. This will help the manufacturers to understand the quality of the components deeply and have a better prediction of its service performance.

### 7.3 Conclusion and key findings

The investigation of pendulum based cutting test and energy based surface integrity evaluation method prove the concept of rapidly evaluate materials machinability in small volumes without using machine tools. It has brought huge advantages compared with current machinability assessment methods. Energy thresholds for specific surface damage level were found and established to validate the effectiveness of the proposed methods. In addition, the surface integrity was

evaluated with different techniques and a quantitative method was presented. Based on the results from this work, the following conclusions are drawn:

1) Machining experiment in small volume materials with pendulum based cutting tests

With the trend of advanced materials (e.g. Ni-based superalloy) used in harsh working conditions increasing, it becomes more pronounced to understand the machined surface integrity and cutting performance of these materials at different cutting conditions, especially for those new developed ones. This presented work introduced a novel pendulum based cutting test method to capture the material surface related machinability properties in limited geometry samples. The PBCT machine is designed and accessories are used to carry out an orthogonal cutting process. Various cutting tests including both fresh tools and worn tools were used to carry out tests to validate the proposed method. Corresponding cutting force, videos of the cutting process, generated chips and surfaces are acquired.

These results proved that this method has the ability to test the materials in small volumes especially those under development period that have no massive volume. Traditionally, it is difficult to carry out practical cutting tests and obtain comprehensive understanding of the cutting performance for these kinds of materials. However this method has not only given the possibility to test surface integrity related machinability, it also saves lots of time and money to understand the machinability of a specific material and it will greatly facilitate the material developing progress. To conclude, the PBCT method is verified as an applicable method to carry out machining tests on small batch materials to study their cutting performance.

2) Surface integrity investigation with energy based evaluation method

Apart from the experimental method mentioned above, this research also provides a novel method to evaluate the surface integrity in energy aspects. To study the cutting process in energy view, an energy model to calculate the energy consumed and distributed in different cutting areas during the cutting process is proposed. Collected cutting force, speeds and measured chips from the PBCT experiment were used to calculate the corresponding energy in the cutting areas with an energy model which refers to basic machining mechanisms. The energy distributed in the cutting areas was divided into shear energy (governing the material shear deformation during ahead of the cutting tools), friction energy (representing the interaction between generated chips and tool rake face), ploughing energy (the phenomenon caused by the interaction between tool radius and machine

workpiece) and worn energy (the energy consumed because of the contact between worn tool flank face ad machined surface), while the last one is only applicable for worn tools.

The comparison between machined surface integrity, material drag depth studied by SEM, and consumed energy shows that the surface integrity of machined surface is highly correlated to the energy consumed during the cutting process and the energy distribution in different cutting areas (shear, friction, ploughing and worn). With different energy distribution and input during cutting, a different surface integrity will be generated. Therefore, the energy consumed and its distribution in the cutting areas could be used as an indicator to evaluate the surface.

3) Energy threshold identification for specific surface damage level

Inspired by the above finds that the level of surface damage could be related by the input energy (Es, Ep), this leads to the open question if the inverse relationship is valid: Given cutting parameters that yield the same input energy do they result in the same level of surface damage? This opens the possibility to define energy thresholds for ensuring that particular levels of surface damage are not exceeded; hence, no need to test various cutting parameters to attain this goal. Several testing groups were carried out and it is also found that if the energy input and distribution are similar during the cutting process, similar surface integrity could be obtained even when the cutting condition is completely different. This means that the surface integrity could be alternatively evaluated based on the energy consumed and distribution during cutting. The energy input increase in the cutting process leads to the changing of surface integrity. Shear and worn energy (energy consumed between tool flank face and machine surface because of the tool wear) plays a significant role in determining surface integrity, and unacceptable (white layer) machined surface will be generated once the input energy goes over the energy threshold. An example to validate this conclusion is presented in Chapter 5 on the workpiece of Inconel 718. The energy consumed for different surface damage levels is identified and the corresponding energy threshold was discussed for both fresh and worn tools.

4) Continuous mapping of cutting condition transition in a single test

As present, resourceful methods (e.g. massive machining tests on machine tools) are used to study the surface integrity related cutting performance of materials, which obstruct the comprehensive understanding of these properties. Also, the current cutting performance investigations of materials focus on specific cutting

parameter combination individually, therefore the continuous cutting mechanism transaction between different cutting conditions has not been revealed and discussed yet. To fill in the gaps, this research proposed an innovative concept, which is able to generate machined surfaces that cover a large range of cutting speeds continuously on very limited geometry samples in a single test, to study the machined surface integrity of Ni-based superalloy based on the developed pendulum based cutting test (PBCT) machine. It presents an obvious chip morphology variation, i.e. serrated shape at the start area and smooth chips at the end of the chip, following the cutting speed decreasing during the cutting process while the cutting process was properly monitored. Coupled with the energy-based surface integrity evaluation method, the consumed energy in different cutting areas (shear, friction and ploughing) at different cutting speeds could be calculated and correlated with the continuous cutting mechanism transition between different cutting conditions. It validates the ability of this method to rapidly obtain machined surface integrity of materials at different cutting conditions in a one-go test rather than resourceful tests on traditional machine tools. The collected chips from one single test were analysed by measuring the defined parameters and the continuous cutting mechanism transition could be mapped.

5) Machined surface integrity quantification technique

The above research shows that energy consumed in different cutting areas during the variation of cutting speeds changing gives the information that the shear energy decreases following cutting speed decreasing, as well as that the corresponding surface deformation depth is decreasing. To investigate the surface integrity, EBSD techniques, including inverse pole figure and strain contouring, give an in-depth investigation on the grain deformation and misorientation of the superficial surface layer. Different from the previous research with EBSD that qualitatively investigate the subsurface deformation, the AIMS value and grain deformation distribution percentage attempt to quantify the surface integrity. Measured residual stress results with XRD shows that a higher residual stress was located when the cutting speed is relatively high and Nano-hardness results conclude that high cutting speed will lead to a higher surface hardness, while both of them validate the former analysis results and have good correlation with published literature. Obtained results including collected chips and sample surface integrity were analysed in-depth with different techniques, such as EBSD, XRD, and Nano-indentation. The experimental results showed that this research introduces the foundation of a revolutionary way to carry out the surface integrity

investigation of materials effectively and contribute to the surface integrity quantifying technique as well.

### 7.4 Completion of work from initial aims and objectives

One of the main challenges was to find an alternative way to carry out machining tests properly without using machine tools, thereby hugely reduce the working load for evaluating surface integrity related material machinability as highlighted in Chapter1. Therefore, a novelty PBCT method has been developed to test the cutting performance of materials instead of using conventional machine tools, while the surface integrity was evaluated with the proposed energy based method by considering the energy consumed in different cutting areas during the cutting process. Regarding the initial proposed tasks for the PhD project, all of the aims and objectives were achieved as listed below:

1) Current research status of materials machinability evaluation methods has been revealed in Chiapter2 and the research gaps were presented. As the objective to sort out the research goals, (Section 4.1) the PBCT method was proposed for cutting performance evaluation, with which the machining tests could be carried out rapidly on limited geometry samples. The validation of this method has been implemented on Inconel 718 (Chapter5 and 6), where several cutting tests were applied. At the same time, the cutting process was monitored properly which gives the possibility to capture the detailed information of the cutting process, thereby deeper investigation.

2) In section 3.2, an alternative method for surface integrity evaluation with built energy model was presented. It treats the energy directly consumed in different cutting areas as the factor to evaluate the surface integrity (e.g. material drag depth) which built the relationship between cutting energy and machined surface integrity as shown in Section 5.5. Also, it was found that similar surface integrity could be achieved as long as the energy input into the cutting areas was kept similar regardless of the variation of cutting conditions. Accordingly the energy threshold for a specific surface damage level has been proved and discussed for both fresh and worn tools in Chapter 5.

3) The work presented in chapter 6 was aimed to continuously map the machining mechanism variation between different cutting conditions. The results in Section6.3 showed that cutting conditions covering a large range of cutting speeds were captured in single test on one sample, while continuous chips with varying morphology caused by cutting condition changes were shown in Section 6.3.3. More importantly, machined surfaces at continuous decreasing cutting speeds

were collected (Section 6.3.4), which provided the opportunity to study the cutting mechanism variation in different cutting conditions continuously and correlated to the consumed energy. The relationship between energy consumed and the chip characteristic and surface deformation were analysed in Chapter 6.3.

4) As another outcome of this thesis, the surface integrity was paid lots of attention as shown in Section 2.3, Section 5.5 and Section 6.3. Different techniques (SEM, XRD, EBSD and neon-indentation etc.) were adopted to obtain an in-depth understanding of the superficial surface damage. Specifically, the quantified method for surface integrity evaluation was presented in Section 6.3.4, which contributes to the establishing of standards for surface integrity evaluation quantitatively rather than qualitatively. Other inspection methods were used to prove the method.

## 7.5 Future works

Regarding the initial aims and objectives of this project supported by Rolls Royce, SECO Tool and European Marie Curie Project, they have been well achieved in this thesis. But based on the experience obtained during the research and the results, several questions and topics that could be further explored have been raised.

1）This thesis reports the innovative method to carry out the surface integrity related machinability test with limited resource required and gives the potential to study cutting performance and surface integrity in a game changing way. Also, it is worth saying that this method is suitable to test not only metal, but also composite, ceramic, plastic etc. as well as tribology, scratch and grinding tests which can be carried out with appropriate minor modification. Therefore, dissemination of this method to a broader areas is a promising opportunity for application. For example, colleagues in our group has started to test the grinding performance of the grit on specific materials with this proposed PBCT method. It will provide alternative tools for the material properties and cutting performance investigation.

2) As seen in this thesis, the PBCT method is able to carry out material cutting tests rapidly and validated in the widely used superalloy, Inconel718. It is clear that the cutting time is quite short (in the level of $10^{-2}$s) during the tests. Therefore, the cutting temperature built-up phenomenon is not obvious compared with the conventional long time cutting tests, which means that the cutting temperature will be not implemented on the practical cutting process. To fill in this gap, a high temperature module which could heat up both the cutting tools and sample to the test target temperature before the cutting test needs to be developed. In this case,

this machine could capture almost all of the practical cutting scenarios including dry cutting, wet cutting and high temperature cutting.

3) Similar to above point, the thermal influence for surface integrity evaluation has not been included into the energy evaluation model. As present, the thermal influence were not significant because the temperature built-up phenomenon is not obvious in such a short cutting time. However, it does need to be considered after the high temperature model is introduced into the tests. Therefore, energy investigation including the effect of thermal investigation for surface integrity should be carried out to improve the accuracy of this method.

4) In this thesis, the energy model divided into shear, friction, ploughing and worn energy (energy consumed between tool flank face and machine surface because of the tool wear) has been correlated to the cutting areas and used to evaluate the cutting performance, which gives new views of surface integrity evaluation. However, the detail information of how these divided energy contribute the cutting performance and how they influence the material deformation and surface generation is not clear. Therefore, in-depth research are necessary to cover this topic to provide more information about optimizing the cutting process and predict surface integrity after machining from acquired data and calculated energy.

5) Regarding the surface integrity inspection method, a quantitative method with EBSD techniques has been proposed and presented in the thesis, while XRD, nano-hardness were used to validate the quantitative method. Apart from this, other quantitative method should be explored as well. With quantitative method, the standards for machined surface properties could be built accurately rather than the empirical evaluation with qualitative method. The superficial surface grain deformation and stress distribution could be derived from the acquired EBSD results which will be helpful for building corresponding standards, thereby improve the quantitative method for surface integrity.

6) This proposed method gives access to monitor the cutting process properly as shown in this thesis while cutting force, material removal process were captured as well. Another possible topic with this technique is to improve the magnification of the high speed lens which may provide the detail information of material deformation in grain level. This actually had been preliminarily validated by the author but not in this thesis. At the same time, the monitored data could be input into a crystal plasticity model to simulate the cutting process in crystal level, which will give the detail deformation information for specific grains. It will open the gate to correlate the cutting process in micro level with macro level.

To conclude, this method does need to be improved in the future, for example oblique cutting and high speed cutting could be included. Apart from turning tests, grinding, milling could also can be simulated with appropriate modification. Better monitoring and analysis equipment can be used to improve the study of the cutting process. However, this method still brings lots of advantages and leads to a completely new method to study the surface integrity of machined surfaces. The energy view considers the surface integrity evaluation in a novel and well-adapted way. Developed PBCT machine shows great advantage as this method does not depend on a specific material, it could be used to study the cutting performance of other metals, composites, ceramics and plastic etc., which means that this method has a broad application prospect. The researcher will continue to carry out studies on this method to make it more powerful and applicable in the future.

# Chapter 8

## Reference

[1] P. Spittle, "Gas turbine technology," *Phys. Educ.*, vol. 38, no. 6, p. 504, 2003.

[2] S. J. Findlay and N. D. Harrison, "Why aircraft fail," *Mater. today*, vol. 5, no. 11, pp. 18–25, 2002.

[3] M. Rauch and E. Roos, "Life assessment of multiaxially cyclic loaded turbine components," *Fatigue Fract. Eng. Mater. Struct.*, vol. 31, no. 6, pp. 441–451, 2008.

[4] L. Witek, "Failure analysis of turbine disc of an aero engine," *Eng. Fail. Anal.*, vol. 13, no. 1, pp. 9–17, 2006.

[5] M. R. Khajavi and M. H. Shariat, "Failure of first stage gas turbine blades," *Eng. Fail. Anal.*, vol. 11, no. 4, pp. 589–597, 2004.

[6] D. Novovic, R. C. Dewes, D. K. Aspinwall, W. Voice, and P. Bowen, "The effect of machined topography and integrity on fatigue life," *Int. J. Mach. Tools Manuf.*, vol. 44, no. 2–3, pp. 125–134, 2004.

[7] Wikipedia, "Rolls-Royce Trent 800." [Online]. Available: https://en.wikipedia.org/wiki/Rolls-Royce_Trent_800.

[8] D. R. Muzyka, C. T. Sims, and W. C. Hagel, "The metallurgy of nickel-iron alloys," *Superalloys, Wiley, New York*, pp. 113–143, 1972.

[9] V. P. Astakhov, *Metal cutting mechanics*. CRC press, 1998.

[10] T. J. Drozda, *Tool and manufacturing engineers handbook: machining*, vol. 1. Society of Manufacturing Engineers, 1983.

[11] D. A. Stephenson and J. S. Agapiou, *Metal cutting theory and practice*. CRC press, 2016.

[12] M. C. Shaw, *Metal cutting principles*,Edition 2. Oxford university press New York, 2005.

[13] A. YE, *Manufacturing Automation: Metal Cutting Mechanics, Maching Tool Vibrations and CNC design*. Cabmridge University Press, 2000.

[14] K. Nakayama, "Basic Rules on the Form of Chip Metal Cutting," *CIRP Ann.*, vol. 27, no. 1, p. 17, 1978.

[15] A. Ã. Moufki, A. Devillez, D. Dudzinski, and A. Molinari, "Thermomechanical modelling of oblique cutting and experimental validation," vol. 44, pp. 971–989, 2004.

[16] M. E. Merchant, "Mechanics of the metal cutting process. II. Plasticity conditions in orthogonal cutting," *J. Appl. Phys.*, vol. 16, no. 6, pp. 318–324, 1945.

[17] Production Engineering, "Theory of metal cutting," 2015, Mechanical Department (Module 1),MG University.

[18] *International Standard ISO 3002−1 Basic quantities in cutting and grinding. Part 1: Geometry of the active part of cutting tools - general terms, reference systems, tool and working angles, chip breakers*. 1982.

[19] *American National Standard ANSI B94.50−1975 Basic nomenclature and definitions for single-point cutting tools*. 1975.

[20] V. Astakhov, *Tribology of metal cutting*. London: Elsevier, 2006.

[21] C. Chong, "Cutting tools with different rake angles," 2017.

[22] G. Boothroyd, *Fundamentals of metal machining and machine tools*, Crc Press, 1988.

[23] M. Kronenberg, *Machining Science and Application: Theory and Practice for Operation and Development of Machining Processes*. Pergamon, 1966.

[24] G. E. Dieter, *Mechanical metallurgy*. London: McGraw-Hill Book Company, 1961.

[25] Z. D. Jastrzebski and R. Komanduri, "The Nature and Properties of Engineering Materials." American Society of Mechanical Engineers, 1988.

[26] S. Everitt, M. J. Starink, H. T. Pang, I. M. Wilcock, M. B. Henderson, and P. A. S. Reed, "A comparison of high temperature fatigue crack propagation in various subsolvus heat treated turbine disc alloys," *Mater. Sci. Technol.*, vol. 23, no. 12, pp. 1419–1423, 2007.

[27] B. Ekmekci, "Residual stresses and white layer in electric discharge

machining (EDM)," *Appl. Surf. Sci.*, vol. 253, no. 23, pp. 9234–9240, 2007.

[28] Technical staff of the machinability data center, *Machining data handbook*, 3 ed. OH 45209: United States of America:Metcut reserach associates Inc, 1980.

[29] G. T. Smith, *Industrial metrology: surfaces and roundness*. Springer Science & Business Media, 2002.

[30] A. R. C. Sharman, A. Amarasinghe, and K. Ridgway, "Tool life and surface integrity aspects when drilling and hole making in Inconel 718," *J. Mater. Process. Technol.*, vol. 200, no. 1–3, pp. 424–432, 2008.

[31] W. N. Thomas, "The effect of scratches and of various workshop finishes upon the fatigue strength of steel," University of Oxford, 1923.

[32] G. C. Noll and G. C. Erickson, "Allowable stresses for steel members of finite life," *Proc. Soc. Expert. Stress Anal.*, vol. 5, no. 2, pp. 132–143, 1948.

[33] P. G. Fluck, "The influence of surface roughness on the fatigue life and scatter of test results of 2 steels", Proceedings american society for testing and materials, 1951, vol. 51, pp. 584–592.

[34] D. A. Axinte and P. Andrews, "Some considerations on tool wear and workpiece surface quality of holes finished by reaming or milling in a nickel base superalloy," *Proc. Inst. Mech. Eng. Part B J. Eng. Manuf.*, vol. 221, no. 4, pp. 591–603, 2007.

[35] M. P. Jackson and R. C. Reed, "Heat treatment of UDIMET 720Li: the effect of microstructure on properties," *Mater. Sci. Eng. A*, vol. 259, no. 1, pp. 85–97, 1999.

[36] and T. L. J. Breadmore, P., R.G. Davies, "On temperature dependence of flow stress of nickel-base alloys," *Metall. Soc. AIME-Transacation*, vol. 245, no. 7, pp. 1537–1545, 1969.

[37] Rolls-Royce plc., "CME 5043 Section 1," Derby, United Kingdom, 2007.

[38] D. Axinte, F. Boud, J. Penny, N. Gindy, and D. J. Williams, "Broaching of Ti-6-4--Detection of workpiece surface anomalies on dovetail slots through

process monitoring," *CIRP Ann.*, vol. 54, no. 1, pp. 87–90, 2005.

[39] S. and D. S. C. Reichman, "Powder metallurgy," in *Superalloys II*, New York: John Wiley & Sons, 1987.

[40] B. L. Ferguson, "Aerospace applications," in *ASM Handbook*, A. International, Ed. OH: Materials Park, 1997.

[41] H. E. Exner, "Qualitative and quantitative surface microscopy," *Phys. Metall.*, 1996.

[42] "Nikon Eclipse E200 Microscope Cutaway Diagram," 2003. [Online]. Available: https://micro.magnet.fsu.edu/primer/anatomy/nikone200cutaway.html.

[43] T. E. Everhart and R. F. M. Thornley, "Wide-band detector for micro-microampere low-energy electron currents," *J. Sci. Instrum.*, vol. 37, no. 7, p. 246, 1960.

[44] A. Javidi, U. Rieger, and W. Eichlseder, "The effect of machining on the surface integrity and fatigue life," *Int. J. Fatigue*, vol. 30, no. 10–11, pp. 2050–2055, 2008.

[45] R. L. Barrie *et al.*, "Effectiveness of shot peening in suppressing fatigue cracking at non-metallic inclusions in Udimet®720," *Mater. Sci. Eng. A*, vol. 474, no. 1–2, pp. 71–81, 2008.

[46] M. A. S. Torres and H. J. C. Voorwald, "An evaluation of shot peening, residual stress and stress relaxation on the fatigue life of AISI 4340 steel," *Int. J. Fatigue*, vol. 24, no. 8, pp. 877–886, 2002.

[47] G. E. Dieter and D. J. Bacon, *Mechanical metallurgy*, vol. 3. McGraw-hill New York, 1986.

[48] A. Taylor, *X-ray metallography*. New York: John Willey & Sons, 1961.

[49] F. A. Kandil, D. J. Lord, A. T. Fry, and P. V Grant, "A review of residual stress measurement methods: a guide to technique selection," 2001.

[50] P. S. Prevey and others, "X-ray diffraction residual stress techniques," *ASM Int. ASM Handbook.*, vol. 10, pp. 380–392, 1986.

[51] P. J. Withers and H. Bhadeshia, "Residual stress. Part 1--measurement

techniques," *Mater. Sci. Technol.*, vol. 17, no. 4, pp. 355–365, 2001.

[52] B. A. X.-R. Solutions, "Diffrac Plus - Residual stress determination user's manual."

[53] M. Ravi Shankar *et al.*, "Severe plastic deformation of difficult-to-deform materials at near-ambient temperatures," *Metall. Mater. Trans. A*, vol. 38, no. 9, pp. 1899–1905, 2007.

[54] E. O. Ezugwu, J. Bonney, D. A. Fadare, and W. F. Sales, "Machining of nickel-base, Inconel 718, alloy with ceramic tools under finishing conditions with various coolant supply pressures," *J. Mater. Process. Technol.*, vol. 162, pp. 609–614, 2005.

[55] E. Brinksmeier, J. T. Cammett, W. Konig, P. Leskovar, J. Peters, and H. K. Tönshoff, "Residual stresses measurement and causes in machining processes," *Cirp Ann.*, vol. 31, no. 2, pp. 491–510, 1982.

[56] T. Kitagawa, A. Kubo, and K. Maekawa, "Temperature and wear of cutting tools in high-speed machining of Inconel 718 and Ti? 6Al? 6V? 2Sn," *Wear*, vol. 202, no. 2, pp. 142–148, 1997.

[57] E. F. Smart and E. M. Trent, "Temperature distribution in tools used for cutting iron, titanium and nickel," *Int. J. Prod. Res.*, vol. 13, no. 3, pp. 265–290, 1975.

[58] G. Parrish, "Influence of microstructure on the properties of case-carbusied components," *Heat Treat. Met.*, vol. 4, no. 4, pp. 107–116, 1977.

[59] A. R. C. Sharman, J. I. Hughes, and K. Ridgway, "An analysis of the residual stresses generated in Inconel 718 when turning," *J. Mater. Process. Technol.*, vol. 173, no. 3, pp. 359–367, 2006.

[60] M. M. El-Khabeery and M. Fattouh, "Residual stress distribution caused by milling," *Int. J. Mach. Tools Manuf.*, vol. 29, no. 3, pp. 391–401, 1989.

[61] H. Ishigami, K. Matsui, Y. Jin, and K. Ando, "Study on stress, reflection and double shot peening to increase fatigue limit," *Proc. ICRS6*, vol. 1, pp. 667–673, 2000.

[62] P. Juijerm, I. Altenberger, and B. Scholtes, "Fatigue and residual stress

relaxation of deep rolled differently aged aluminium alloy AA6110," *Mater. Sci. Eng. A*, vol. 426, no. 1–2, pp. 4–10, 2006.

[63] K. Neailey, "Surface integrity of machined components: microstructural aspects," *Met. Mater.*, vol. 4, no. 2, pp. 93–96, 1988.

[64] V. Randle and O. Engler, *Introduction to texture analysis: macrotexture, microtexture and orientation mapping*. CRC press, 2014.

[65] K. Dicks, "Introduction to EBSD," *Oxford Instruments Analytical*, 2003. [Online]. Available: www.EBSD.com.

[66] B. Mouawad, X. Boulnat, D. Fabrègue, M. Perez, and Y. De Carlan, "Tailoring the microstructure and the mechanical properties of ultrafine grained high strength ferritic steels by powder metallurgy," *J. Nucl. Mater.*, vol. 465, pp. 54–62, 2015.

[67] S. To, W. B. Lee, and C. Y. Chan, "Effect of machining velocity on the crystallographic textures in a diamond turned aluminium single crystal," *Texture, Stress. Microstruct.*, vol. 31, no. 4, pp. 249–261, 1999.

[68] A. Yamamoto, T. Yamada, S. Nakahigashi, L. Liu, M. Terasawa, and H. Tsubakino, "Effects of surface grinding on hardness distribution and residual stress in low carbon austenitic stainless steel SUS316L," *ISIJ Int.*, vol. 44, no. 10, pp. 1780–1782, 2004.

[69] R. M'Saoubi and L. Ryde, "Application of the EBSD technique for the characterisation of deformation zones in metal cutting," *Mater. Sci. Eng. A*, vol. 405, no. 1–2, pp. 339–349, 2005.

[70] R. M'Saoubi *et al.*, "Surface integrity analysis of machined Inconel 718 over multiple length scales," *CIRP Ann. Technol.*, vol. 61, no. 1, pp. 99–102, 2012.

[71] S. B. and R. U. K. H.M. Ismaeel, M.A. Khattak, M.N. Tamin, M.S. Khan, N.iQBAL, S.Kazi, "Energy Absorption Ability of Thin-Walled Square Hollow Section of Low Carbon Sheet Metals under Quasi-Static Axial Compression," *J. Adv. Res. Appl. Mech.*, vol. 18, no. 1, pp. 1–14, 2016.

[72] W. C. Oliver and G. M. Pharr, "Measurement of hardness and elastic modulus by instrumented indentation: Advances in understanding and refinements to methodology," *J. Mater. Res.*, vol. 19, no. 1, pp. 3–20,

2004.

[73] H. Couvy, D. Lahiri, J. Chen, A. Agarwal, and G. Sen, "Nanohardness and Youngs modulus of nanopolycrystalline diamond," *Scr. Mater.*, vol. 64, no. 11, pp. 1019–1022, 2011.

[74] W. C. Oliver and G. M. Pharr, "An improved technique for determining hardness and elastic modulus using load and displacement sensing indentation experiments," *J. Mater. Res.*, vol. 7, no. 6, pp. 1564–1583, 1992.

[75] Y. B. Guo and J. Sahni, "A comparative study of the white layer by hard turning versus grinding," *Int. J. Mach. Tools Manuf.*, vol. 44, pp. 135–145, 2004.

[76] F. Hashimoto, Y. B. Guo, and A. W. Warren, "Surface integrity difference between hard turned and ground surfaces and its impact on fatigue life," *CIRP Ann.*, vol. 55, no. 1, pp. 81–84, 2006.

[77] L. Chen, A. Ahadi, J. Zhou, and J.-E. Ståhl, "Modeling effect of surface roughness on nanoindentation tests," *Procedia CIRP*, vol. 8, pp. 334–339, 2013.

[78] S. H. R. Sanei and R. S. Fertig III, "Length-scale dependence of variability in epoxy modulus extracted from composite prepreg," *Polym. Test.*, vol. 50, pp. 297–300, 2016.

[79] R. M'Saoubi *et al.*, "High performance cutting of advanced aerospace alloys and composite materials," *CIRP Ann. Technol.*, vol. 64, no. 2, pp. 557–580, 2015.

[80] A. Devillez, F. Schneider, S. Dominiak, D. Dudzinski, and D. Larrouquere, "Cutting forces and wear in dry machining of Inconel 718 with coated carbide tools," *Wear*, vol. 262, no. 7, pp. 931–942, 2007.

[81] K. Shintani, H. Kato, Y. Fujimura, A. Yamamoto, and T. Maeda, "Cutting performance of CBN tools in machining of nickel based superalloy," *Seimitsu Kogaku Kaishi*, vol. 58, no. 10, pp. 1685–1690, 1992.

[82] V. Bushlya, J. Zhou, and J.-E. Ståhl, "Effect of cutting conditions on machinability of superalloy Inconel 718 during high speed turning with coated and uncoated PCBN tools," *Procedia CIRP*, vol. 3, pp. 370–375,

2012.

[83] N. Fang and Q. Wu, "A comparative study of the cutting forces in high speed machining of Ti--6Al--4V and Inconel 718 with a round cutting edge tool," *J. Mater. Process. Technol.*, vol. 209, no. 9, pp. 4385–4389, 2009.

[84] E. P. DeGarmo, J. T. Black, R. A. Kohser, and B. E. Klamecki, *Materials and process in manufacturing*. Prentice Hall, 1997.

[85] E. O. Ezugwu, J. Bonney, and Y. Yamane, "An overview of the machinability of aeroengine alloys," *J. Mater. Process. Technol.*, vol. 134, no. 2, pp. 233–253, 2003.

[86] E. O. Ezugwu, Z. M. Wang, and A. R. Machado, "The machinability of nickel-based alloys: a review," *J. Mater. Process. Technol.*, vol. 86, no. 1–3, pp. 1–16, 1999.

[87] C. T. Sims and W. C. Hagel, *The Superalloys-vital high temperature gas turbine materials for aerospace and industrial power*, no. BOOK. John Wiley & Sons, 1972.

[88] M. Nouari and H. Makich, "Experimental investigation on the effect of the material microstructure on tool wear when machining hard titanium alloys: Ti--6Al--4V and Ti-555," *Int. J. Refract. Met. Hard Mater.*, vol. 41, pp. 259–269, 2013.

[89] B. M. Kramer, "On tool materials for high speed machining," *J. Eng. Ind.*, vol. 109, no. 2, pp. 87–91, 1987.

[90] E. A. Almond, "Towards improved tests based on fundamental properties," in *Proceedings of the International Conference on Improved Performance of Tool Materials, The National Laboratory and the Metals Society, Teddington, Middlesex*, 1981, pp. 161–169.

[91] E. O. Ezugwu, "Key improvements in the machining of difficult-to-cut aerospace superalloys," *Int. J. Mach. Tools Manuf.*, vol. 45, no. 12, pp. 1353–1367, 2005.

[92] P.-J. Arrazola, A. Garay, L.-M. Iriarte, M. Armendia, S. Marya, and F. Le Maitre, "Machinability of titanium alloys (Ti6Al4V and Ti555. 3)," *J. Mater. Process. Technol.*, vol. 209, no. 5, pp. 2223–2230, 2009.

[93] I. S. Jawahir *et al.*, "Surface integrity in material removal processes: Recent advances," *CIRP Ann. Technol.*, vol. 60, no. 2, pp. 603–626, 2011.

[94] L. Settineri, P. C. Priarone, M. Arft, D. Lung, and T. Stoyanov, "An evaluative approach to correlate machinability, microstructures, and material properties of gamma titanium aluminides," *CIRP Ann. Technol.*, vol. 63, no. 1, pp. 57–60, 2014.

[95] M. A. Xavior, M. Patil, A. Maiti, M. Raj, and N. Lohia, "Machinability studies on INCONEL 718," in *IOP Conference Series: Materials Science and Engineering*, 2016, vol. 149, no. 1, p. 12019.

[96] C. R. Dandekar, Y. C. Shin, and J. Barnes, "Machinability improvement of titanium alloy (Ti--6Al--4V) via LAM and hybrid machining," *Int. J. Mach. Tools Manuf.*, vol. 50, no. 2, pp. 174–182, 2010.

[97] D. Ulutan and T. Ozel, "Machining induced surface integrity in titanium and nickel alloys: a review," *Int. J. Mach. Tools Manuf.*, vol. 51, no. 3, pp. 250–280, 2011.

[98] T. Gutowski, J. Dahmus, and A. Thiriez, "Electrical energy requirements for manufacturing processes," in *13th CIRP international conference on life cycle engineering*, 2006, vol. 31, pp. 623–638.

[99] V. A. Balogun and P. T. Mativenga, "Modelling of direct energy requirements in mechanical machining processes," *J. Clean. Prod.*, vol. 41, pp. 179–186, 2013.

[100] M. P. Sealy, Z. Y. Liu, Y. B. Guo, and Z. Q. Liu, "Energy based process signature for surface integrity in hard milling," *J. Mater. Process. Technol.*, vol. 238, pp. 284–289, 2016.

[101] M. Sarwar, M. Persson, H. Hellbergh, and J. Haider, "Measurement of specific cutting energy for evaluating the efficiency of bandsawing different workpiece materials," *Int. J. Mach. Tools Manuf.*, vol. 49, no. 12, pp. 958–965, 2009.

[102] M. Yurdakul and H. Akdas, "Prediction of specific cutting energy for large diameter circular saws during natural stone cutting," *Int. J. Rock Mech. Min. Sci.*, vol. 53, pp. 38–44, 2012.

[103] W. Polini and S. Turchetta, "Force and specific energy in stone cutting by

diamond mill," *Int. J. Mach. Tools Manuf.*, vol. 44, no. 11, pp. 1189–1196, 2004.

[104] F. Jafarian, M. I. Ciaran, D. Umbrello, P. J. Arrazola, L. Filice, and H. Amirabadi, "Finite element simulation of machining Inconel 718 alloy including microstructure changes," *Int. J. Mech. Sci.*, vol. 88, pp. 110–121, 2014.

[105] G. Rotella, O. W. Dillon Jr, D. Umbrello, L. Settineri, and I. S. Jawahir, "Finite element modeling of microstructural changes in turning of AA7075-T651 alloy," *J. Manuf. Process.*, vol. 15, no. 1, pp. 87–95, 2013.

[106] D. Umbrello, R. M saoubi, and J. C. Outeiro, "The influence of Johnson--Cook material constants on finite element simulation of machining of AISI 316L steel," *Int. J. Mach. Tools Manuf.*, vol. 47, no. 3–4, pp. 462–470, 2007.

[107] J. J. DeMange, V. Prakash, and J. M. Pereira, "Effects of material microstructure on blunt projectile penetration of a nickel-based super alloy," *Int. J. Impact Eng.*, vol. 36, no. 8, pp. 1027–1043, 2009.

[108] X. Wang, C. Huang, B. Zou, H. Liu, H. Zhu, and J. Wang, "Dynamic behavior and a modified Johnson--Cook constitutive model of Inconel 718 at high strain rate and elevated temperature," *Mater. Sci. Eng. A*, vol. 580, pp. 385–390, 2013.

[109] F. Klocke, D. Lung, and S. Buchkremer, "Inverse identification of the constitutive equation of Inconel 718 and AISI 1045 from FE machining simulations," *Procedia Cirp*, vol. 8, pp. 212–217, 2013.

[110] S. Issler, "Development of a Concept for Life Prediction of Blade-Disc-Connections of Gasturbines (originally in German)," PhD Dissertation, University of Stuttgart, German, 2002.

[111] J. M. Pereira and B. A. Lerch, "Effects of heat treatment on the ballistic impact properties of Inconel 718 for jet engine fan containment applications," *Int. J. Impact Eng.*, vol. 25, no. 8, pp. 715–733, 2001.

[112] A. V Mitrofanov, V. I. Babitsky, and V. V Silberschmidt, "Thermomechanical finite element simulations of ultrasonically assisted turning," *Comput. Mater. Sci.*, vol. 32, no. 3–4, pp. 463–471, 2005.

[113] J. Lorentzon, N. Järvstråt, and B. L. Josefson, "Modelling chip formation of alloy 718," *J. Mater. Process. Technol.*, vol. 209, no. 10, pp. 4645–4653, 2009.

[114] R. Sievert, A. H. Hamann, D. Noack, P. Löwe, K. N. Singh, and G. Künecke, "Simulation of thermal softening, damage and chip segmentation in a nickel super-alloy," *HK Tönshoff, F. Hollmann Hochgeschwindigkeitspannen, Wiley-vch*, pp. 446–469, 2005.

[115] T. Ozel, I. Llanos, J. Soriano, and P.-J. Arrazola, "3D finite element modelling of chip formation process for machining Inconel 718: comparison of FE software predictions," *Mach. Sci. Technol.*, vol. 15, no. 1, pp. 21–46, 2011.

[116] A. Malakizadi, S. Cedergren, K. B. Surreddi, and L. Nyborg, "A methodology to evaluate the machinability of Alloy 718 by means of FE simulation," in *International Conference on Advanced Manufacturing Engineering and Technologies. Stockholm: NEWTECH*, 2013, pp. 95–106.

[117] A. Del Prete, L. Filice, and D. Umbrello, "Numerical simulation of machining nickel-based alloys," *Procedia CIRP*, vol. 8, pp. 540–545, 2013.

[118] H. Chandrasekaran, R. M'saoubi, and H. Chazal, "Modelling of material flow stress in chip formation process from orthogonal milling and split Hopkinson bar tests," *Mach. Sci. Technol.*, vol. 9, no. 1, pp. 131–145, 2005.

[119] R. Pfeiffer, R. Collet, L. Denaud, and G. Fromentin, "Analysis of chip formation mechanisms and modelling of slabber process," *Wood Sci. Technol.*, pp. 1–18, 2014.

[120] F. Eyma, P.-J. Méausoone, P. Larricq, and R. Marchal, "Utilization of a dynamometric pendulum to estimate cutting forces involved during routing. Comparison with actual calculated values," *Ann. For. Sci.*, vol. 62, no. 5, pp. 441–447, 2005.

[121] A. Chardin, "Utilisation du pendule dynamométrique dans les recherches sur le sciage des bois," *Bois Forêts des Trop. Tech. For. Trop.*, vol. 58, pp. 49–61, 1958.

[122] O. Vingsbo, "Experimental studies of shear zones during chip formation in

metal cutting," *Le J. Phys. Colloq.*, vol. 46, no. C5, pp. C5--371, 1985.

[123] F. Bergman and S. Jacobson, "Tool wear mechanisms in intermittent cutting of metal matrix composites," *Wear*, vol. 179, no. 1–2, pp. 89–93, 1994.

[124] A. R. Rodrigues and R. T. Coelho, "An investigation of specific energy on the chip formation process using an instrumented Charpy test machine," *CEP*, vol. 13, p. 590, 2009.

[125] S. Schuldt *et al.*, "High-speed cutting of foods: Development of a special testing device," *J. Food Eng.*, vol. 216, pp. 36–41, 2018.

[126] T. Muro, Y. Takegaki, and K. Yoshikawa, "Impact cutting property of rock material using a point attack bit," *J. terramechanics*, vol. 34, no. 2, pp. 83–108, 1997.

[127] E. O. Ezugwu and J. Bonney, "Effect of high-pressure coolant supply when machining nickel-base, Inconel 718, alloy with coated carbide tools," *J. Mater. Process. Technol.*, vol. 153, pp. 1045–1050, 2004.

[128] D. K. Aspinwall, R. C. Dewes, E. Ng, C. Sage, and S. L. Soo, "The influence of cutter orientation and workpiece angle on machinability when high-speed milling Inconel 718 under finishing conditions," vol. 47, pp. 1839–1846, 2007.

[129] D. Axinte, M. Axinte, and J. D. T. Tannock, "A multicriteria model for cutting ¯ uid evaluation," vol. 217, pp. 1341–1353, 2003.

[130] and J. V. Zerrouki, V., G. Perrin, C. Colin, "Effect of drilling anomalies on low cycle fatigue behaviour of superalloy IN718," in *7th CIRP International Workshop on Modeling of Machining Operations*, 2004.

[131] K. Hussain, D. S. Wilkinson, and J. D. Embury, "Effect of surface finish on high temperature fatigue of a nickel based super alloy," *Int. J. Fatigue*, vol. 31, no. 4, pp. 743–750, 2009.

[132] I. Repository, "Institutional Repository Plastic behaviour of microstructural constituents of cortical bone tissue : a nanoindentation study This item was submitted to Loughborough ' s Institutional Repository ( https://dspace.lboro.ac.uk/) by the author and is made available under the," vol. 2, no. 2, pp. 136–157, 2013.

[133] E. Budak, E. Ozlu, H. Bakioglu, and Z. Barzegar, "Thermo-mechanical modeling of the third deformation zone in machining for prediction of cutting forces," *CIRP Ann. Technol.*, vol. 65, no. 1, pp. 121–124, 2016.

[134] Y. Huang and S. Y. Liang, "Modeling of cutting forces under hard turning conditions considering tool wear effect," *Trans. ASME-B-Journal Manuf. Sci. Eng.*, vol. 127, no. 2, pp. 262–270, 2005.

[135] R. M'Saoubi, D. Axinte, C. Herbert, M. Hardy, and P. Salmon, "Surface integrity of nickel-based alloys subjected to severe plastic deformation by abusive drilling," *CIRP Ann. Technol.*, vol. 63, no. 1, pp. 61–64, 2014.

[136] S. L. Soo, R. Hood, D. K. Aspinwall, W. E. Voice, and C. Sage, "Machinability and surface integrity of RR1000 nickel based superalloy," *CIRP Ann. Technol.*, vol. 60, no. 1, pp. 89–92, 2011.

[137] I. A. Choudhury and M. A. El-Baradie, "Machinability of nickel-base super alloys: a general review," *J. Mater. Process. Technol.*, vol. 77, no. 1, pp. 278–284, 1998.

[138] S. Jacobson and P. Wallén, "A new classification system for dead zones in metal cutting," *Int. J. Mach. Tools Manuf.*, vol. 28, no. 4, pp. 529–538, 1988.

[139] P. Wallen, S. Jacobson, and S. Hogmark, "An experimental method for studies of intermittent cutting at small cutting depths," *Int. J. Mach. Tools Manuf.*, vol. 28, no. 4, pp. 539–550, 1988.

[140] P. Wallén, S. Jacobson, and S. Hogmark, "Intermittent metal cutting at small cutting depths. Dead zone phenomena and surface finish," *Int. J. Mach. Tools Manuf.*, vol. 28, no. 4, pp. 515–528, 1988.

[141] D. Raabe, "Simulation of rolling textures of bcc metals considering grain interactions and crystallographic slip on ${$110$}$,${$112$}$ and ${$123$}$ planes," *Mater. Sci. Eng. A*, vol. 197, no. 1, pp. 31–37, 1995.

[142] D. Biermann, R. Amuth, S. Hess, and M. Tiffe, "Simulation based analysis and optimisation of the cutting edge micro shape for machining of nickel-base alloys," *Procedia CIRP*, vol. 67, pp. 284–289, 2018.

[143] E. Uhlmann, M. G. von der Schulenburg, and R. Zettier, "Finite element modeling and cutting simulation of Inconel 718," *CIRP Ann. Technol.*, vol.

56, no. 1, pp. 61–64, 2007.

[144] J. Weng, K. Zhuang, C. Hu, D. Zhu, S. Guo, and H. Ding, "A novel approach to thermal modeling based on three-dimensional analysis in turning Inconel 718 with round insert," *J. Mater. Process. Technol.*, 2018.

[145] M. Lotfi, M. Jahanbakhsh, and A. A. Farid, "Wear estimation of ceramic and coated carbide tools in turning of Inconel 625: 3D FE analysis," *Tribol. Int.*, vol. 99, pp. 107–116, 2016.

[146] M. Mori, M. Fujishima, Y. Inamasu, and Y. Oda, "A study on energy efficiency improvement for machine tools," *CIRP Ann. Technol.*, vol. 60, no. 1, pp. 145–148, 2011.

[147] K. S. Sangwan and G. Kant, "Optimization of machining parameters for improving energy efficiency using integrated response surface methodology and genetic algorithm approach," *Procedia CIRP*, vol. 61, pp. 517–522, 2017.

[148] S. Kara and W. Li, "Unit process energy consumption models for material removal processes," *CIRP Ann. Technol.*, vol. 60, no. 1, pp. 37–40, 2011.

[149] A. Thakur and S. Gangopadhyay, "State-of-the-art in surface integrity in machining of nickel-based super alloys," *Int. J. Mach. Tools Manuf.*, vol. 100, pp. 25–54, 2016.

[150] M. Imran, P. T. Mativenga, A. Gholinia, and P. J. Withers, "Comparison of tool wear mechanisms and surface integrity for dry and wet micro-drilling of nickel-base superalloys," *Int. J. Mach. Tools Manuf.*, vol. 76, pp. 49–60, 2014.

[151] J. Du, S. Lv, and others, "Deformation-phase transformation coupling mechanism of white layer formation in high speed machining of FGH95 Ni-based superalloy," *Appl. Surf. Sci.*, vol. 292, pp. 197–203, 2014.

[152] A. Devillez, G. Le Coz, S. Dominiak, and D. Dudzinski, "Dry machining of Inconel 718, workpiece surface integrity," *J. Mater. Process. Technol.*, vol. 211, no. 10, pp. 1590–1598, 2011.

[153] Z. Liao, D. Axinte, M. Mieszala, R. M Saoubi, J. Michler, and M. Hardy, "On the influence of gamma prime upon machining of advanced nickel based superalloy," *CIRP Ann.*, 2018.

[154] A. B. Sadat and M. Y. Reddy, "Surface integrity of inconel-718 nickel-base superalloy using controlled and natural contact length tools. Part I: Lubricated," *Exp. Mech.*, vol. 32, no. 3, pp. 282–288, 1992.

[155] R. M. Arunachalam, M. A. Mannan, and A. C. Spowage, "Residual stress and surface roughness when facing age hardened Inconel 718 with CBN and ceramic cutting tools," *Int. J. Mach. Tools Manuf.*, vol. 44, no. 9, pp. 879–887, 2004.

[156] R. F. Recht, "A dynamic analysis of high-speed machining," *J. Eng. Ind.*, vol. 107, no. 4, pp. 309–315, 1985.

[157] J. J. J. Wang and M. Y. Zheng, "On the machining characteristics of H13 tool steel in different hardness states in ball end milling," *Int. J. Adv. Manuf. Technol.*, vol. 22, no. 11–12, pp. 855–863, 2003.

[158] C. Wang, Y. Xie, L. Zheng, Z. Qin, D. Tang, and Y. Song, "Research on the chip formation mechanism during the high-speed milling of hardened steel," *Int. J. Mach. Tools Manuf.*, vol. 79, pp. 31–48, 2014.

[159] J. M. Zhou, V. Bushlya, R. L. Peng, S. Johansson, P. Avdovic, and J. E. Stahl, "Effects of tool wear on subsurface deformation of nickel-based superalloy," *Procedia Eng.*, vol. 19, pp. 407–413, 2011.

[160] C. Schlauer and M. Odén, "Residual stress evolution and near-surface microstructure after turning of the nickel-based superalloy Inconel 718," *Zeitschrift für Met.*, vol. 96, no. 4, pp. 385–392, 2005.

[161] M. Aramesh, S. Montazeri, and S. C. Veldhuis, "A novel treatment for cutting tools for reducing the chipping and improving tool life during machining of Inconel 718," *Wear*, vol. 414, pp. 79–88, 2018.